Dark interactions beyond the Lambda-CDM model

MA van der Westhuizen

orcid.org/0000-0001-5027-8762

Dissertation accepted in partial fulfilment of the requirements for the degree *Master of Science in Astrophysical Sciences* at the North-West University

Supervisor: Prof AA Gidelew

Graduation May 2022

25269917

Acknowledgements

I would firstly like to thank both the National Astrophysics and Space Science Program (NASSP), and the National Research Foundation (NRF) for funding this work. This extends to the North-West University's Centre for Space Research (CSR), which always did more than was expected to help students cross any bureaucratic or financial boundaries. Without this financial support, I would not have been able to pursue my goals of doing research and contemplating life, the universe and everything.

Secondly, I want to thank my supervisor, Prof Amare Abebe, for all his guidance and support over the last two years. Not only was he always patient and supportive when my research took an unplanned detour from our original topics, but he actively encouraged me to pursue new directions that I found exciting. This dissertation is largely a product of these unplanned detours.

I am also grateful to my friend and colleague Renier Hough, who helped me adapt the MCMC simulation that he developed to our cosmological models. This collaboration resulted in chapter 4 of this dissertation and will hopefully continue to produce interesting results in the future. He acted as a co-supervisor in all but name.

I am greatly indebted to my friends and family for all their emotional support and superhuman tolerance against all my unsolicited lectures and ramblings on the expansion of the universe and the nature of dark energy. But most importantly, I would like to thank both my mom and my girlfriend. As they both always believed in me, even when I didn't believe in myself. This work is dedicated to both of you.

Declaration

I, Marcel van der Westhuizen (25269917), declare that this dissertation titled, 'Dark interactions beyond the Lambda-CDM model' has not been submitted to this or any other university for any degree or examination, that the work presented in it is my own and that all the sources I have used or quoted have been acknowledged by complete reference.

Chapters 3 and 4 of this dissertation are based on the following publication:

- M A van der Westhuizen and A Abebe, 'Dark coupling: cosmological implications of interacting dark energy and dark matter fluids', SA Inst. Phys. Proceedings SAIP2021 (Accepted).

Signature: 

Marcel van der Westhuizen

Date: 10 November 2021

Abstract

In this study, cosmological models are considered, where dark matter and dark energy are coupled and may exchange energy through non-gravitational interactions with one other. These interacting dark energy (IDE) models are introduced to address problems with the standard ΛCDM model of cosmology, in which dark energy is assumed to be a cosmological constant. The central problem addressed in this study is the cosmic coincidence problem (regarding the presently measured coincidental ratio of dark matter to dark energy). Assuming two different linear dark energy couplings, $Q_1 = \delta H \rho_{\rm dm}$ and $Q_2 = \delta H \rho_{\rm de}$, we find that interacting dark energy models may alleviate and even solve the cosmic coincidence problem by stabilising the ratio of dark matter to dark energy in both the past and future. Furthermore, we examine how these dark interactions affect crucial events in the expansion history of the universe. These events include the big bang and cosmic acceleration, as well as the radiation-matter and matter-dark energy equality.

Besides studying the cosmological consequences of an interaction between the dark sectors, we also investigate the viability of IDE models on both theoretical and observational grounds. For both models considered, we find that negative energy densities are inevitable if energy flows from dark matter to dark energy and that consequently we should only seriously consider models where energy flows from dark energy to dark matter. To additionally ensure that these models are free from early time instabilities, we need to require that dark energy is in the 'phantom' ($\omega < -1$) regime. This has the consequence that model $Q_1 = \delta H \rho_{\rm dm}$ will end with a future big rip singularity, while $Q_2 = \delta H \rho_{\rm de}$ may avoid this fate with the right choice of cosmological parameters. Cosmological parameters for these models are obtained from type-Ia supernovae data using a previously developed Markov Chain Monte-Carlo (MCMC) simulation. The predicted expansion history from these models are then statistically compared to the supernovae data and the ΛCDM model, where we find that $Q_1 = \delta H \rho_{\rm dm}$ is statistically rejected, while $Q_2 = \delta H \rho_{\rm de}$ may be considered viable.

Keywords: cosmology, cosmic acceleration, ΛCDM model, dark energy, dark matter, interacting dark energy, cosmic coincidence problem, big rip, type Ia supernova, MCMC simulation

Contents

List of Figures

List of Tables

CHAPTER 1

General relativity and the cosmological field equations

1.1 A brief history of cosmology

As long as we humans have been around, we have looked up at the stars and pondered nature's greatest mysteries. Where do we come from? What is this world around us? What will be our ultimate fate? Countless answers to these questions have been suggested from countless cultures and philosophical systems and are encapsulated in the rich mythological stories, and creation myths found the world over. These answers have varied widely but have tended to invoke supernatural forces and are commonly teleological, meaning everything was designed with a purpose; usually, one centred around human beings [5].

This anthropocentric view started to fade with the discovery of a heliocentric universe in the 16th century by Copernicus, Galileo and Kepler, showing that the location of earth is not special, but just another planet orbiting the sun [5]. This was complemented by the publication of Newton's *Principia* in 1687, in which he showed that the dynamics of objects on earth and the heavens above are dictated by the same set of observable natural laws. Furthermore, in the 19th century, the geologist Charles Lyell advocated in his *Principles of Geology* that the key to understanding geological phenomena is by way of gradual natural processes that can still be directly observed today [6]. Since these processes are slow, he also concluded that the earth (and the universe) must be much older than the commonly believed 6000 years. Lyell's view, in turn, inspired Charles Darwin to write his 1859 book *On the Origin of Species* which formed the foundation of evolutionary biology [6]. Darwin showed us how the great diversity of life may arise from natural processes which are

still observable today, but more significant questions remained. How did the universe evolve to its current form? What observable natural laws guide its evolution? Did the universe have a beginning, and how will it end? Answering these more significant questions with explanations based on natural observable processes may be seen as the primary goal of the field of cosmology.

Cosmology in its modern scientific form can be said to have begun with the publication of Einstein's theory of general relativity in 1915 [7–11]. This theory suggested that what we experience as gravity is actually the effect of energy bending spacetime itself and successfully explained the precession of the perihelion of mercury and predicted the gravitational lensing of light, both of which Newton's gravity failed to do [8, 9]. This theory also predicted an expanding universe, as was shown independently by the Russian mathematician Alexander Friedmann in 1922 and the Belgian priest George Lemaître in 1927, both by solving The Einstein field equations [12]. Einstein himself was aware of Friedmann's work but believed it to be mathematical speculation with no physical basis [12]. Einstein instead was so convinced that the universe must be static that he modified his theory by adding the notorious cosmological constant Λ into his equations to balance the effect of gravity [13, 14] (The relevance of the cosmological constant is still a matter of debate today and will be a central point discussed in this dissertation). Einstein's static universe which was eternal and had no beginning or end, was held as the standard model by most of the scientific community of the early twentieth century as no observations indicated otherwise.

At this time, Lemaître believed that if the universe is expanding, that distant stars and galaxies should be receding away from us and that their electromagnetic radiation should be Doppler shifted to longer wavelengths at the 'redder' end of the spectrum [12]. The groundbreaking work of both Friedmann and Lemaître remained obscure and unknown. This changed in 1929 when Edwin Hubble measured the redshift of distant galaxies and found that these galaxies are receding away from us with a relative velocity v proportional to their distance d from the earth [15]:

$$v = H_0 d \quad \rightarrow \quad H_0 = \frac{v}{d}, \tag{1.1}$$

with H_0 a proportionality constant known as the Hubble constant (with units kilometres per second per megaparsec km $s^{-1}Mpc^{-1}$) indicating how the recessional velocity v (in km s^{-1}) of any object increases with every megaparsec in distance d. This is known as the Hubble-Lemaître law since Hubble made the empirical discovery, but the interpretation and prediction that such redshift should be indicative of an expanding universe was made by Lemaître [12]. Since the universe was expanding, it could be inferred that at some time in the distant past, all galaxies must have been at the same point in space, the singularity (called the 'primeval atom' by Lemaître [12]) from which the universe was born. Thus, the first evidence for the big bang model was discovered.

Additional evidence for the big bang was found by Alpher and Gamow in 1948 by considering the

formation of light elements in the universe (primordial helium from hydrogen in a hot big bang) by a process known as big bang nucleosynthesis [16]. In this same paper, it was predicted that from the conditions needed for successful nucleosynthesis, radiation should have been released when the early universe transitioned from opaque plasma to a more neutral state which was transparent to radiation. This radiation was predicted to be observable in the present as isotropic blackbody radiation with a temperature of a few Kelvin [17]. This prediction became direct evidence for the big bang model with the discovery of the cosmic microwave background radiation (CMB) by Penzias and Wilson in 1965 [18]. A more recent analysis of the CMB by the Planck telescope in 2018 has given our most accurate measurements of the Cosmological parameters [4].

After discovering the Hubble-Lemaître law and the CMB, static models and the cosmological constant were mostly abandoned. It was widely accepted that the universe was expanding and was born during the big bang. Friedmann and Lemaître cosmological models became standard, where the expansion is decelerating due to the attractive force of gravity. Another paradigm shift occurred in 1998 with the discovery of Cosmic acceleration from observational evidence of Type Ia supernovae [19–22]. This discovery reintroduced the cosmological constant Λ for the wider class of models called Dark energy as a reference to the earlier discovery of a mysterious form of non-luminous dark Matter by Zwicky and Rubin in the 1930's and 1970's [23, 24].

After these discoveries, the current model of cosmology was in place, The ΛCDM model (Λ cold dark matter). This model considered the universe to start with a big bang, followed by a short period of rapid expansion called inflation, after which the universe expands and cools to its current state. This expansion is predicted to accelerate and continue indefinitely into the future.

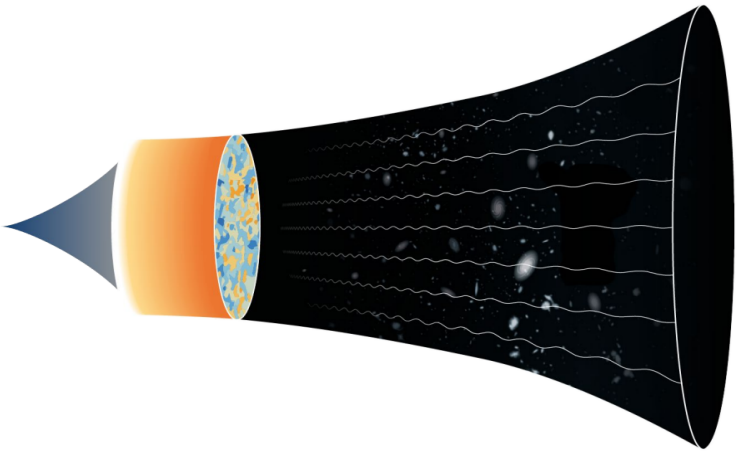

Figure 1.1: *Expansion of the Universe from the Big Bang [1]*

However, Problems with the ΛCDM model still remain, especially regarding the nature of dark matter and dark energy. Investigating the viability of Interacting dark energy models that may solve these problems will be the main goal of this dissertation. Before doing this, we will first consider general relativity and the cosmological field equations from which all cosmology flows.

1.2 The Einstein field equations

The Einstein field equations (EFE) are the most fundamental equations in general relativity, which relate the curvature of spacetime to its stress-energy content. These equations also describe which path energy will take through a curved spacetime [8, 9]. This path may thus be obtained by applying the principle of least action $\delta S = 0$ to the full Einstein-Hilbert action S, which includes terms for the cosmological constant Λ, as well as the Lagrangian L_M of the matter fields [11]:

$$\delta S = \delta \int \sqrt{-g} \left[\frac{1}{2\kappa} (R - 2\Lambda) + L_M \right] dx^4 = 0, \tag{1.2}$$

where $g = \det(g_{\alpha\beta})$ is the determinant of the metric, R the Ricci scalar and $\kappa = \frac{8\pi G}{c^4}$ is the Einstein gravitational constant (with G the universal gravitational constant and c the speed of light). The presence of dx^4 indicates that integration takes place over all four dimensions of spacetime. From this variational principle one may derive the Einstein field equations as[1] [8, 9, 11]

$$G_{\alpha\beta} + \Lambda g_{\alpha\beta} = \frac{8\pi G}{c^4} T_{\alpha\beta} \quad ; \quad \text{where} \quad G_{\alpha\beta} \equiv R_{\alpha\beta} - \frac{1}{2} R g_{\alpha\beta}. \tag{1.3}$$

With $G_{\alpha\beta}$ the Einstein tensor, Λ is the cosmological constant (which is discussed in detail in sections 2.1.3, 2.2, 2.5.1 and 2.6), $g_{\alpha\beta}$ the metric tensor, G the universal gravitational constant, c the speed of light, $T_{\alpha\beta}$ the stress-energy tensor, $R_{\alpha\beta}$ the Ricci curvature tensor and R the scalar curvature. This equation (without Λ , as originally formulated) may be understood intuitively by comparing it to Newton's equation for gravitation:

$$G_{\alpha\beta} = \frac{8\pi G}{c^4} T_{\alpha\beta} \quad ; \quad F = \frac{G m_1 m_2}{r^2}. \tag{1.4}$$

In Newton's equation, there is mass m on the R.H.S., which creates a gravitational force F on the L.H.S. of the equation. Conversely, in the Einstein field equations, there is the stress-energy tensor $T_{\alpha\beta}$ (which describes the mass-energy content of the system) on the R.H.S., which creates the curvature of spacetime as described by the Einstein tensor $G_{\alpha\beta}$ on the L.H.S. Thus, the matter and energy of any system will create the curvature within it, which in turn determines the path taken by the matter and energy. This idea can be encapsulated by the famous quote from John Wheeler: *Spacetime tells matter how to move; matter tells spacetime how to curve* [25]

From the equivalence principle, the local properties of spacetime at small distances should be indistinguishable from the flat spacetime of special relativity [8–11]. Overall curvature is still taken into account, such that the metric tensor $g_{\alpha\beta}$ describes the geometry of the spacetime considered. Solving the Einstein field equations with the correct metric, leads to the Friedmann equations.

[1] The full derivation of the Einsteil field equations from the Einstein-Hilbert action; as well as the derivation of the Friedmann equations, with all calculations shown, can be found in the Google drive folder https://drive.google.com/drive/folders/1Y3MhWzDrRC5v4D9jSCsAv_2X1QDwf7PW?usp=sharing

1.3 Derivation of the cosmological field equations

1.3.1 The Friedmann-Lemaître-Robertson-Walker metric

The cosmological field equations, also known as the Friedmann equations, are the most important equations in all of cosmology and was first derived in 1922 from general relativity by Russian physicist and mathematician Alexander Friedmann [26].

Friedmann's equations were based on two basic assumptions. Firstly, that the universe on a large scale looks more or less uniform and symmetric in all directions (isotropy), for which the isotropic nature of the CMB may be taken as evidence [9, 18]. The second assumption is the Copernican principle that there is nothing special about our location, and there is no preferred direction or centre of the universe [10]. Taking this assumption alongside the first assumption of isotropy implies homogeneity [9]. The assumptions of isotropy and homogeneity may be taken together as the cosmological principle [9–11]. Discussions and recent observational tests of this principle can be found in [27–30]. Cosmological models exist which violate the cosmological principle and may be inhomogeneous models, such as the Lemaître -Tolman-Bondi model [31, 32] or anisotropic models such as the Bianchi type models [33, 34].

Taking the cosmological principle into account, we can start solving the EFE (1.3) by determining the metric tensor $g_{\alpha\beta}$, which describes the geometry of the expanding universe. The size of the universe will be given by the dimensionless scale factor $a(t)$, which indicates the size of the universe relative to the present day. There are three different metrics which correspond to an expanding isotropic and homogeneous geometry, these are flat, closed (spherical) and open (hyperbolic) geometries [8–11]. From homogeneity, the spatial curvature must be the same at each point in these geometries. A flat geometry will have zero spatial curvature everywhere, while for the closed and open cases there is a constant positive or negative spatial curvature respectively. These three metrics may be combined into a single metric by using a change of coordinates, yielding [8–11]

$$ds^2 = -dt^2 + \frac{a^2(t)}{1-kr^2}dr^2 + a^2(t)r^2 d\theta^2 + a^2(t)r^2\sin^2\theta d\phi^2, \tag{1.5}$$

where the $k = +1, 0, -1$ is the curvature constant corresponding to a closed (spherical), flat or open (hyperbolic) universe respectively (see Geometry of the universe for more on curvature). This is known as the FriedmannLemaître RobertsonWalker (FLRW) metric. In tensor form this is

$$g_{\alpha\beta} = \begin{pmatrix} -1 & 0 & 0 & 0 \\ 0 & \frac{a^2(t)}{1-kr^2} & 0 & 0 \\ 0 & 0 & a^2(t)r^2 & 0 \\ 0 & 0 & 0 & a^2(t)r^2\sin^2\theta \end{pmatrix}. \tag{1.6}$$

This metric is given in spherical coordinates (t, r, θ and ϕ) and can be seen to be isotropic because it only has diagonal entries and therefore has no preferred direction in space and time. It is also homogeneous since the spatial part of this metric has the same form as a 3-sphere in four-dimensional Euclidean space, while reducing to a three-dimensional Euclidean space at small scales when curvature becomes negligible (as in the case $k = 0$ and $a(t) = 1$) [9]. Evaluating the Einstein field equations (1.3) with this metric gives the Friedmann equation. For this derivation, we will be working in normalized $c = 1$ units.

1.3.2 Calculating the Christoffel symbols

In order to calculate the various components of the Einstein field equations for the FLRW metric (1.6), the non-zero Christoffel symbols for this metric will first be needed. This will be used to determine the components of the Ricci curvature tensor $R_{\alpha\beta}$ (1.10) as well as the scalar curvature R (1.12). From here onwards, the time dependence of the scale factor will be implicit ($a(t) = a$).

The general expression for the Christoffel symbols $\Gamma^{\alpha}_{\beta\gamma}$ is given by [8]:

$$\Gamma^{\delta}_{\beta\gamma} = \frac{1}{2} g^{\alpha\delta} \left(\frac{\partial g_{\alpha\beta}}{\partial x^{\gamma}} + \frac{\partial g_{\alpha\gamma}}{\partial x^{\beta}} - \frac{\partial g_{\beta\gamma}}{\partial x^{\alpha}} \right) \quad \rightarrow \quad \Gamma^{\alpha}_{\beta\gamma} = \frac{1}{2} g^{\alpha\alpha} \left(\frac{\partial g_{\alpha\beta}}{\partial x^{\gamma}} + \frac{\partial g_{\alpha\gamma}}{\partial x^{\beta}} - \frac{\partial g_{\beta\gamma}}{\partial x^{\alpha}} \right). \tag{1.7}$$

Since there are no cross-terms in the FLRW metric (due to isotropy), (1.7) was simplified by setting $\delta = \alpha$. Here $g^{\alpha\delta}$ is the contravariant form of the FLRW metric tensor (1.6) such that:

$$g^{\alpha\delta} = \begin{pmatrix} -1 & 0 & 0 & 0 \\ 0 & \frac{1-kr^2}{a^2} & 0 & 0 \\ 0 & 0 & \frac{1}{a^2 r^2} & 0 \\ 0 & 0 & 0 & \frac{1}{a^2 r^2 \sin^2\theta} \end{pmatrix}. \tag{1.8}$$

Equations (1.7), (1.8) and (1.6) are used to determine all the non-zero Christoffel symbols:

$$\begin{aligned} \Gamma^{1}_{33} &= -r \sin^2\theta \left(1 - kr^2\right) && ; && \Gamma^{0}_{11} = \frac{a\dot{a}}{1-kr^2} \\ \Gamma^{1}_{01} = \Gamma^{1}_{10} = \Gamma^{2}_{02} = \Gamma^{2}_{20} = \Gamma^{3}_{03} = \Gamma^{3}_{30} &= \frac{\dot{a}}{a} && ; && \Gamma^{0}_{22} = a\dot{a}r^2 \\ \Gamma^{2}_{33} &= -\sin(\theta)\cos\theta && ; && \Gamma^{0}_{33} = a\dot{a}r^2 \sin^2\theta \\ \Gamma^{2}_{12} = \Gamma^{2}_{21} = \Gamma^{3}_{13} = \Gamma^{3}_{31} &= \frac{1}{r} && ; && \Gamma^{1}_{11} = \frac{kr}{1-kr^2} \\ \Gamma^{3}_{32} &= \Gamma^{3}_{23} = \cot\theta && ; && \Gamma^{1}_{22} = -r\left(1 - kr^2\right), \end{aligned} \tag{1.9}$$

where $0, 1, 2$ and 3 in the spherical coordinates being used correspond to t, r, θ and ϕ.

1.3.3 Calculating the Ricci curvature tensor

Now that all the non-zero Christoffel symbols have been determined (1.9), the Ricci curvature can be expressed directly in terms of Christoffel symbols by:

$$R_{\alpha\beta} = \frac{\partial \Gamma^{\gamma}_{\alpha\beta}}{\partial x^{\gamma}} - \frac{\partial \Gamma^{\gamma}_{\alpha\gamma}}{\partial x^{\beta}} + \Gamma^{\gamma}_{\alpha\beta}\Gamma^{\delta}_{\gamma\delta} - \Gamma^{\gamma}_{\alpha\delta}\Gamma^{\delta}_{\beta\gamma}. \tag{1.10}$$

The non-zero components of the Ricci curvature tensor are the diagonal elements R_{00}, R_{11}, R_{22} and R_{33}, which are calculated and given in tensor form as:

$$R_{\alpha\beta} = \begin{pmatrix} -3\left(\frac{\ddot{a}}{a}\right) & 0 & 0 & 0 \\ 0 & \frac{a\ddot{a}+2\dot{a}^2+2k}{1-kr^2} & 0 & 0 \\ 0 & 0 & \left(a\ddot{a}+2\dot{a}^2+2k\right) r^2 & 0 \\ 0 & 0 & 0 & \left(a\ddot{a}+2\dot{a}^2+2k\right) r^2 \sin^2\theta \end{pmatrix}. \tag{1.11}$$

1.3.4 Calculating the scalar curvature

The scalar curvature R may now be calculated from the Ricci curvature $R_{\alpha\beta}$ in (1.11) and the contravariant of the FRLW metric $g^{\alpha\beta}$ in (1.8) such that:

$$R = R_{\alpha\beta} g^{\alpha\beta}. \tag{1.12}$$

Repeated indices indicate summation, considering only the non-zero components:

$$R = R_{00} g^{00} + R_{11} g^{11} + R_{22} g^{22} + R_{33} g^{33}. \tag{1.13}$$

Substituting the components from (1.11) and (1.8) into (1.14) and simplifying gives:

$$R = 6\left[\left(\frac{\ddot{a}}{a}\right) + \left(\frac{\dot{a}}{a}\right)^2 + \frac{k}{a^2}\right]. \tag{1.14}$$

1.3.5 Calculating the stress-energy tensor

The FLRW metric, which is isotropic and homogeneous, is a perfect fluid solution. The perfect fluid stress-energy tensor $T^{\alpha\beta}$ (from which its contravariant form $T_{\alpha\beta}$ may be obtained) is given by [9]:

$$T^{\alpha\beta} = (\rho + P)\, u^{\alpha} u^{\beta} + P g^{\alpha\beta} \quad \rightarrow \quad T_{\alpha\beta} = (\rho + P)\, u_{\alpha} u_{\beta} + P g_{\alpha\beta}, \tag{1.15}$$

where ρ is the energy density, P is the pressure of the fluid and u is the four velocity. We will only be using contravariant form $T_{\alpha\beta}$.

Since the universe model is considered to be a totally isotropic and homogeneous fluid, the velocity of the fluid should have no preffered direction and therefore only a temporal component. In the frame of an observer at rest w.r.t. the fluid (which has constant density and pressure and is not flowing around), the observer will then have a four velocity:

$$u^{\alpha} = \begin{pmatrix} 1 & 0 & 0 & 0 \end{pmatrix} \tag{1.16}$$

1.3.6 Obtaining the 1st Friedmann equation

The first Friedmann equation can now be obtained by considering the temporal part $\alpha = \beta = 0$ of the Einstein field equations in (1.3) with $c = 1$:

$$G_{00} + \Lambda g_{00} = 8\pi G T_{00} \qquad ; \qquad \text{where} \quad G_{00} = R_{00} - \frac{1}{2} R g_{00}. \tag{1.17}$$

Substituting into G_{00} the corresponding components from (1.11), (1.14) and (1.6) gives:

$$G_{00} = R_{00} - \frac{1}{2} R g_{00} = -3\left(\frac{\ddot{a}}{a}\right) - \frac{1}{2}\left\{6\left[\left(\frac{\ddot{a}}{a}\right) + \left(\frac{\dot{a}}{a}\right)^2 + \frac{k}{a^2}\right]\right\}(-1) = 3\left[\left(\frac{\dot{a}}{a}\right)^2 + \frac{k}{a^2}\right]. \tag{1.18}$$

Furthermore, the temporal component of the stress-energy tensor is given by (1.15), while substituting in the corresponding components from (1.16) and (1.6) gives:

$$T_{00} = (\rho + P)\, u_0 u_0 + P g_{00} = (\rho + P)\,(1)(1) + P(-1) = \rho. \tag{1.19}$$

Substituting (1.18), (1.19) and (1.6) into (1.17) gives:

$$\begin{aligned} 3\left[\left(\frac{\dot{a}}{a}\right)^2 + \frac{k}{a^2}\right] + \Lambda(-1) &= 8\pi G\rho \\ \left(\frac{\dot{a}}{a}\right)^2 &= \frac{8\pi G\rho}{3} - \frac{k}{a^2} + \frac{\Lambda}{3}. \end{aligned} \tag{1.20}$$

From considerations of dimensionality, the speed of light c can be put back into (1.20). The L.H.S. has dimensions of time^{-2}, and both k and Λ have dimensions of length^{-2}, needing only a c^2 to be dimensionally consistent with the R.H.S.. Thus, the Friedmann equation becomes:

$$\rightarrow H^2 = \left(\frac{\dot{a}}{a}\right)^2 = \frac{8\pi G\rho}{3} - \frac{kc^2}{a^2} + \frac{\Lambda c^2}{3}, \tag{1.21}$$

where $H = \dot{a}/a$ is the time dependent Hubble parameter that indicates the rate of expansion. At present this is equal to the Hubble constant H_0 which corresponds with (1.1), if $v = \dot{a}$ and $d = a$.

1.3.7 Obtaining the 2nd Friedmann equation

The 2nd Friedmann equation, which is also known as the Raychaudhuri equation, is obtained by considering the spatial part $\alpha = \beta = 1$ (for each spatial component, the same equation is reached) of the Einstein field equations in (1.3) with $c = 1$:

$$G_{11} + \Lambda g_{11} = 8\pi G T_{11} \qquad ; \qquad \text{where} \quad G_{11} = R_{11} - \frac{1}{2} R g_{11}. \tag{1.22}$$

Here the Ricci curvature component R_{11} from (1.11) may be written as function of g_{11} from (1.6):

$$R_{11} = \frac{a\ddot{a} + 2\dot{a}^2 + 2k}{1 - kr^2} = \frac{1}{a^2}\left(a\ddot{a} + 2\dot{a}^2 + 2k\right)\left(\frac{a^2}{1 - kr^2}\right) = \frac{1}{a^2}\left(a\ddot{a} + 2\dot{a}^2 + 2k\right) g_{11}. \tag{1.23}$$

Furthermore, the stress-energy tensor is given by the spatial components of (1.15) with the corresponding four velocity components from (1.16), giving:

$$T_{11} = (\rho + P)\, u_1 u_1 + P g_{11} = (\rho + P)\,(0)(0) + P g_{11} = P g_{11}. \tag{1.24}$$

Substituting (1.23), (1.24) and (1.14) into (1.22) gives:

$$\frac{1}{a^2}\left(a\ddot{a} + 2\dot{a}^2 + 2k\right) g_{11} - \frac{1}{2}\left\{6\left[\left(\frac{\ddot{a}}{a}\right) + \left(\frac{\dot{a}}{a}\right)^2 + \frac{k}{a^2}\right]\right\} g_{11} + \Lambda g_{11} = 8\pi G P g_{11}. \tag{1.25}$$

Dividing both sides of (1.25) by $(-g_{11})$ and simplifying gives:

$$\left(\frac{\ddot{a}}{a}\right) + \frac{1}{2}\left(\frac{\dot{a}}{a}\right)^2 = -4\pi G P - \frac{k}{2a^2} + \frac{\Lambda}{2}. \tag{1.26}$$

The first Friedmann equation (1.20) can be substituted into (1.26) to obtain the second one:

$$\begin{aligned} \left(\frac{\ddot{a}}{a}\right) + \frac{1}{2}\left(\frac{8\pi G\rho}{3} - \frac{k}{a^2} + \frac{\Lambda}{3}\right) &= -4\pi G P - \frac{k}{2a^2} + \frac{\Lambda}{2} \\ \left(\frac{\ddot{a}}{a}\right) &= -\frac{4\pi G}{3}(\rho + 3P) + \frac{\Lambda}{3}. \end{aligned} \tag{1.27}$$

Taking considerations of dimensionality into account, the speed of light c can be put back into the equation by dividing the pressure P by c^2 and multiplying Λ by c^2. Thus, the second Friedmann equation (or Raychaudhuri equation) is:

$$\rightarrow \left(\frac{\ddot{a}}{a}\right) = -\frac{4\pi G}{3}\left(\rho + \frac{3P}{c^2}\right) + \frac{\Lambda c^2}{3}. \tag{1.28}$$

The two Friedmann equations (1.21) and (1.28) relate the expansion of the universe to the energy density ρ and pressure P of the Components of the universe and will be used as the basis for all cosmological models considered from here on forward.

1.4 Geometry of the universe

From The Einstein field equations it is known that mass-energy curves the fabric of spacetime itself. The large-scale geometry of the universe is thus determined by its energy density. The curvature constant k which was introduced in the FLRW metric (1.5) (which has the dimensions of length^{-2}) is constant in both time and space and therefore it has a fixed value in an expanding universe. This value is determined by the total amount of mass-energy created in the Big Bang and stays the same throughout the evolution of the universe. The universe can have any of three possible shapes depending on the value of k. The curvature may either be positive ($k = +1$), there may be no curvature ($k = 0$), or it may be negative ($k = -1$). These three scenarios lead to a universe having either a closed, flat or open geometry respectively [11]. From the Friedmann equation (1.21) (with Λ included in the energy density ρ as will be shown in (2.7)), it may be seen that a critical energy density ρ_c, which leads to a flat universe ($k = 0$), may be obtained:

$$\begin{aligned} H^2 = \frac{8}{3}\pi G\rho - \frac{kc^2}{a^2} = \frac{8}{3}\pi G\rho_c \quad ; \quad (k = 0 \text{ when } \rho = \rho_c) \\ \rightarrow \rho_c = \frac{3}{8\pi G}H^2. \end{aligned} \tag{1.29}$$

The present critical density $\rho_{(c,0)}$ may be determined by using $G = 6.67 \times 10^{-11}$ m^{3}kg^{-1}s^{-2} and the present Hubble parameter $H_0 = 67.4$ km s^{-1} Mpc^{-1} $= 2.18 \times 10^{-18}$ s^{-1} (which has been converted to units s^{-1}) as measured by the Planck telescope [4]. Using these constants, the present critical density needed to obtain a flat universe is approximately:

$$\rho_{(c,0)} = \frac{3}{8\pi G}H_0^2 = \frac{3(2.18 \times 10^{-18} \text{ s}^{-1})^2}{8\pi(6.67 \times 10^{-11} \text{ m}^3\text{kg}^{-1}\text{s}^{-2})} \approx 8.53 \times 10^{-27} \text{ kg m}^{-3}. \tag{1.30}$$

Thus, if the current total energy density of the universe is greater than or less than $\rho_{(c,0)}$, the universe will either be closed or open respectively. This may be further simplified by introducing another new quantity called the density parameter Ω, which is a fractional density that describes the ratio of energy density ρ to the critical density ρ_c:

$$\Omega = \frac{\rho}{\rho_c} = \frac{8\pi G\rho}{3H^2}. \tag{1.31}$$

For any for any fluid x, (1.31) leads to the following useful relations between the density parameter Ω_x and the energy density ρ_x (with $\Omega_{(x,0)}$ and $\rho_{(x,0)}$ the present values), such that:

$$\begin{aligned} \Omega_x = \frac{8\pi G}{3H^2}\rho_x \quad ; \quad \Omega_{(x,0)} = \frac{8\pi G}{3H_0^2}\rho_{(x,0)}, \\ \rho_x = \frac{3H^2}{8\pi G}\Omega_x \quad ; \quad \rho_{(x,0)} = \frac{3H_0^2}{8\pi G}\Omega_{(x,0)}. \end{aligned} \tag{1.32}$$

This may be substituted into the Friedmann equation and yields the relation:

$$
\begin{aligned}
H^2 &= \frac{8\pi G\rho}{3} - \frac{kc^2}{a^2} \\
1 &= \frac{8\pi G\rho}{3H^2} - \frac{kc^2}{a^2H^2} \\
1 &= \Omega + \Omega_{\mathrm{k}} \\
1 - \Omega = \Omega_{\mathrm{k}} &= -\frac{kc^2}{a^2H^2} \qquad \left(\text{where at present } \Omega_{(\mathrm{k},0)} = -\frac{kc^2}{H_0^2}\right),
\end{aligned}
\tag{1.33}
$$

with Ω_{k} as the newly defined curvature parameter. From the curvature constant k, the density parameter Ω and curvature parameter Ω_{k} we have :

$$
\begin{aligned}
k = +1 \;\; ; \;\; \rho > \rho_c \;\; ; \;\; \Omega > 1 \;\; ; \;\; \Omega_{\mathrm{k}} < 0 \quad &\text{(Closed Universe)}, \\
k = \;\; 0 \;\; ; \;\; \rho = \rho_c \;\; ; \;\; \Omega = 1 \;\; ; \;\; \Omega_{\mathrm{k}} = 0 \quad &\text{(Flat Universe)}, \\
k = -1 \;\; ; \;\; \rho < \rho_c \;\; ; \;\; \Omega < 1 \;\; ; \;\; \Omega_{\mathrm{k}} > 0 \quad &\text{(Open Universe)}.
\end{aligned}
\tag{1.34}
$$

The geometry of the universe is therefore determined by its total energy density. This geometry may be measured directly from the CMB, since a light beam will follow a straight path (null geodesic) on a curved surface, such that lines converge on a sphere (closed universe), remain straight on a flat surface (flat universe) and diverge on a saddle (open universe) [8]. Different geometries predict different sizes of the CMB anisotropies as shown in Figure 1.2.

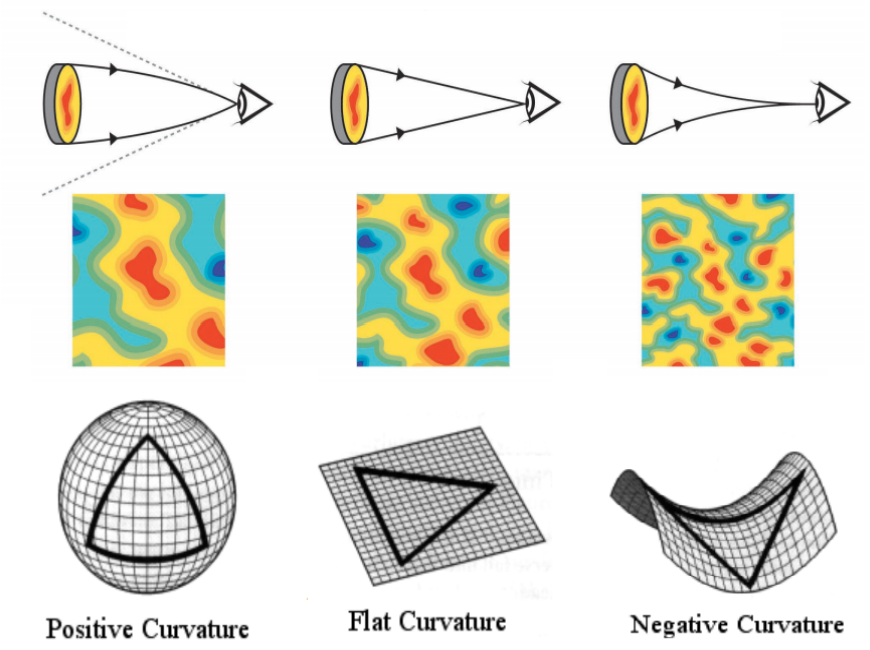

Figure 1.2: *Curvature of the Universe [1]*

The geometry as measured by the Planck collaboration is discussed in Cosmological parameters. The geometry of the universe also dictates its evolution, as may be seen in Tables 2.1 and 2.2.

1.5 The conservation equation

The conservation equation, also known as the fluid equation, describes the evolution of the energy densities of fluids contained in the universe. This equation can be derived from applying the first law of thermodynamics to the universe as a whole [10]. The law states that the total energy in an isolated system is constant:

$$\dot{E} = Q - W, \tag{1.35}$$

where $\dot{E}$ is the change in the internal energy of the system, Q is the heat flow out of the system, and W is the work done by the system. The work is equal to the product of the pressure P of the system and its change in volume $\dot{V}$ [35]. The work done on the system is therefore

$$W = P\dot{V}. \tag{1.36}$$

It is assumed that the universe is homogeneous and that its expansion is adiabatic, such that there is a transfer of energy as work but not as heat. Since there is no heat flow, we have

$$Q = 0. \tag{1.37}$$

Substituting (1.37) and (1.36) into (1.35) gives:

$$\dot{E} + P\dot{V} = 0. \tag{1.38}$$

If a sphere with a radius equivalent to the scale factor a is considered, then the change in the volume of the sphere is:

$$\dot{V} = \frac{d}{dt}\left(\frac{4}{3}\pi a^3\right) = \frac{4}{3}\pi(3)a^2\dot{a} = 3\left(\frac{4}{3}\pi a^3\right)\left(\frac{\dot{a}}{a}\right) = 3VH, \tag{1.39}$$

with H the Hubble parameter. From mass-energy equivalence (while noting that the mass m may be written in terms of energy density ρ and the volume V), the energy contained in the sphere is:

$$E = mc^2 = V\rho c^2. \tag{1.40}$$

The change in this energy is:

$$\dot{E} = V\dot{\rho}c^2 + \dot{V}\rho c^2. \tag{1.41}$$

Substituting $\dot{V}$ from (1.39) into (1.41) gives:

$$\dot{E} = V\dot{\rho}c^2 + 3VH\rho c^2 = Vc^2\left(\dot{\rho} + 3H\rho\right). \tag{1.42}$$

The change in energy and volume can now be substituted back into the first law of thermodynamics. So substituting (1.39) and (1.42) into (1.38) gives:

$$\begin{aligned} \dot{E} + P\dot{V} &= 0 \\ Vc^2\left(\dot{\rho} + 3H\rho\right) + P\left(3VH\right) &= 0 \\ \dot{\rho} + 3H\left(\rho + \frac{P}{c^2}\right) &= 0. \end{aligned} \tag{1.43}$$

This is the conservation for any fluid in the universe model. Note that the pressure and density have the same value everywhere in our universe models due to the assumptions of homogeneity made for the FLRW metric. The conservation equation may be simplified by introducing the equation of state ω, which relates the pressure of a cosmological fluid to its energy density:

$$\begin{aligned} \omega &= \frac{P}{\rho c^2} \\ P &= \omega\rho c^2. \end{aligned} \tag{1.44}$$

Substituting (1.44) into the conservation of energy equation (1.43) gives:

$$\begin{aligned} \dot{\rho} + 3H\left(\rho + \frac{\omega\rho c^2}{c^2}\right) &= 0 \\ \dot{\rho} + 3H\rho(1+\omega) &= 0. \end{aligned} \tag{1.45}$$

This differential equation may be solved to tell us how the energy density ρ of any fluid which is conserved with an equation of state ω evolves with the scale factor:

$$\begin{aligned} \int\left(\frac{1}{\rho}\right)d\rho &= -3(1+\omega)\int\left(\frac{1}{a}\right)da \\ \ln\rho &= -3(1+\omega)\ln a + d \\ \rho_{\mathrm{x}} &= \rho_{(\mathrm{x},0)}a^{-3(1+\omega_{\mathrm{x}})}, \end{aligned} \tag{1.46}$$

where the subscript denotes some fluid x, and $\rho_{(\mathrm{x},0)}$ is the present energy density of the fluid considered. From (1.46) it can be seen that the equation of state of a fluid ω_{x} determines the rate at which its energy density ρ_{x} dilutes with increasing a as the universe expands. Using the relations from (1.33) alongside (1.46), we obtain the following useful equations regarding the evolution of the energy density ρ_{x} and density parameter Ω_x:

$$\begin{aligned} \rho_{\mathrm{x}} &= \frac{3H_0^2}{8\pi G}\Omega_{(\mathrm{x},0)}a^{-3(1+\omega_{\mathrm{x}})}, \\ \Omega_{\mathrm{x}} &= \frac{8\pi G}{3H^2}\rho_{\mathrm{x}} = \frac{H_0^2}{H^2}\Omega_{(\mathrm{x},0)}a^{-3(1+\omega_{\mathrm{x}})}. \end{aligned} \tag{1.47}$$

It is worthwhile to note that in general relativity, the energy density ρ and pressure P of these fluids have different energy conditions of varying importance to consider.

1.6 Energy conditions

In general relativity, the main energy conditions are given by [36–39]:

$$\text{Strong Energy Condition (SEC):} \quad \rho + P \geq 0 \quad \text{and} \quad \rho + 3P \geq 0 \quad \rightarrow \quad \omega \geq -\frac{1}{3} \tag{1.48}$$

$$\text{Weak Energy Condition (WEC):} \quad \rho + P \geq 0 \quad \text{and} \quad \rho \geq 0 \quad \rightarrow \quad \omega \geq -1 \tag{1.49}$$

$$\text{Dominant Energy Condition (DEC):} \quad \rho \geq 0 \quad \text{and} \quad \rho \geq |P| \quad \rightarrow \quad \omega \geq -1 \tag{1.50}$$

$$\text{Null Energy Condition (NEC):} \quad \rho + P \geq 0 \quad \rightarrow \quad \omega \geq -1 \tag{1.51}$$

It may be seen that if some of these conditions are violated, others will be as well, for instance if the NEC is violated, then the WEC and SEC will also not be satisfied. The least restraining of these conditions is the SEC.

One consequence of the SEC is that the active gravitational potential is always positive [40]. This can be clearly seen from the Raychaudhuri equation (2.15) (with Λ is grouped in the ρ term). Any fluid with an equation of state $\omega > -1/3$ will therefore decelerate the expansion of the universe (since the R.H.S. of (2.15) will be negative). The opposite holds as well; in order to produce accelerated expansion, the SEC must be violated $\omega < -1/3$. This violation of the SEC is not regarded as too exotic in cosmology due to the currently observed Cosmic acceleration at late times, as well as the proposed early time accelerating expansion during the inflationary epoch [38]. The SEC has also been used alongside the WEC to produce the Hawking-Penrose singularity theorems [36, 37].

The DEC was in turn used by Hawking and Ellis to develop their conservation theorem [36], which results in energy-momentum not being able to appear from nowhere. The DEC, therefore, guarantees a system's stability from vacuum decay, a process in which the vacuum decays into positive and negative particles [41]. Any model in which the universe decays before the present age should be theoretically ruled out. It should be noted that the violation of the DEC does not necessarily imply vacuum decay but is dependent on the details of the model (see [41] for a discussion on this).

The NEC has the consequence that inertial mass density is always positive, as well as prohibiting time travel and wormholes [38, 42]. Another consequence of violating the NEC is that fields can appear which have negative kinetic energy. These fields are known as ghosts and would preferably be avoided in a realistic cosmological model. [43]. It should further be noted that violating NEC does not necessarily imply negative energy densities ($\rho < 0$). It may mean that the pressure is amply negative $P < 0$ so that $\rho + P < 0$ holds, while energy density is still positive ($\rho > 0$) [44].

As a minimum requirement, all valid cosmological models we consider need to have energy densities that remain positive throughout the past and predicted future expansion histories.

CHAPTER 2

ΛCDM and other non-interacting models

2.1 Components of the universe

The nature of any cosmological model is determined by the cosmological field equations (1.21) and (1.28). These, in turn, depend on the constituents of the model, specifically their energy density ρ and pressure P. Most cosmological models consist of different combinations of three fluids, which are broadly grouped as radiation, matter, and dark energy [9–11]. In this section, we will assume each of the three fluids to only interact gravitationally with one another and therefore be separately conserved and uncoupled to each other.

2.1.1 Radiation

Radiation refers to ultra-relativistic particles with small or zero rest mass, which principally include photons and neutrinos [11]. Neutrinos are neutral leptons that are divided into three groups or 'flavours' depending on their mass, namely the electron neutrino, muon neutrino and tau neutrino [10].

The energy density of particles in a fluid x for any model may be written as $\rho_x = nE$, where E is the mean energy of the particles and n is the number density. The number density of both relativistic and non-relativistic particles have the dependence $n \propto a^3$, due to these particles diluting with the expansion of the universe. This dependency holds as long as the energy of the fluid is conserved [10]. Furthermore, the energy E of relativistic particles (which we assume to be massless)

is given by the Planck-Einstein relation $E = hc/\lambda$, with λ the wavelength of the particle. This wavelength λ_e will be linearly stretched with the scale factor a as the universe expands, such that any observed photons have a cosmological redshift z [8]:

$$1 + z = \frac{\lambda_0}{\lambda_e} = \frac{a_0}{a} = \frac{1}{a}, \tag{2.1}$$

with λ_0 and λ_e the observed and emitted wavelengths of the photons. The energy of radiation therefore has the dependence $E \propto \lambda^{-1} \propto a^{-1}$. Thus, taking the density dilution and cosmological redshift into account, the energy density of radiation has the dependence $\rho_r = nE = n(hc/\lambda) \propto a^{-3}a^{-1} \propto a^{-4}$ [10]. This coincides with the pressure P and energy density ρ of radiation being related to an equation of state ω equal to $P = 1/3\rho \rightarrow \omega_r = 1/3$, such that the energy evolves according to the conservation equation (1.46):

$$\rho_r = \rho_r a^{-3(1+\omega_r)} = \rho_{(r,0)} a^{-3(1+1/3)} = \rho_{(r,0)} a^{-4}. \tag{2.2}$$

From (1.47) and (2.1), we may also obtain the following useful relations:

$$\begin{aligned} \rho_r &= \frac{3H_0^2}{8\pi G}\Omega_{(r,0)} a^{-4} \quad ; \quad \rho_r = \frac{3H_0^2}{8\pi G}\Omega_{(r,0)}(1+z)^4, \\ \Omega_r &= \frac{H_0^2}{H^2}\Omega_{(r,0)} a^4 \quad ; \quad \Omega_r = \frac{H_0^2}{H^2}\Omega_{(r,0)}(1+z)^4. \end{aligned} \tag{2.3}$$

2.1.2 Matter

The first hints of dark matter were obtained from observations of galaxy clusters (by Fritz Zwicky during the 1930s [23]) and studies of the rotation curves of galaxies (made by Vera Rubin during the 1970s [24]) [45]. If the rotation of stars in a galaxy behave similar to the Keplerian motion of planets in our solar system, then it would be expected that the centripetal force $F_c = mv(r)^2/r$ of the stars would be balanced by the Newtonian gravitational force F_G (1.4) such that :

$$\frac{mv(r)^2}{r} = \frac{GM(r)m}{r^2} \rightarrow v(r) = \sqrt{\frac{GM(r)}{r}}, \tag{2.4}$$

with $v(r)$ the rotational speed of the object at radius r, m the mass of the object and $M(r)$ the mass contained within the radius r. This implies that the rotational velocity of stars should decrease with distance r from the center $v(r) \propto 1/\sqrt{r}$, but observations of spiral galaxies by Rubin showed that rotational velocities instead increase with radial distance from the galaxy center [24]. From this, she concluded that this phenomenon could be best explained by a spherical halo of non-luminous matter extending beyond the visible galactic disk [24]. Newer observations since have supported her claims and shown that these rotational velocity curves are typically flat with increasing distance [2, 46–48], as seen in Figure 2.1. An early candidate to explain this behaviour was baryonic dark matter or Massive Compact Halo Objects (MaCHO's), which would include brown dwarfs and

other dark stellar remnants. This theory has since become less popular as data from gravitational lensing, CMB anisotropies, large scale structure, and the behaviour of the bullet cluster has been found to be consistent with non-baryonic dark matter [2–4, 46–50].

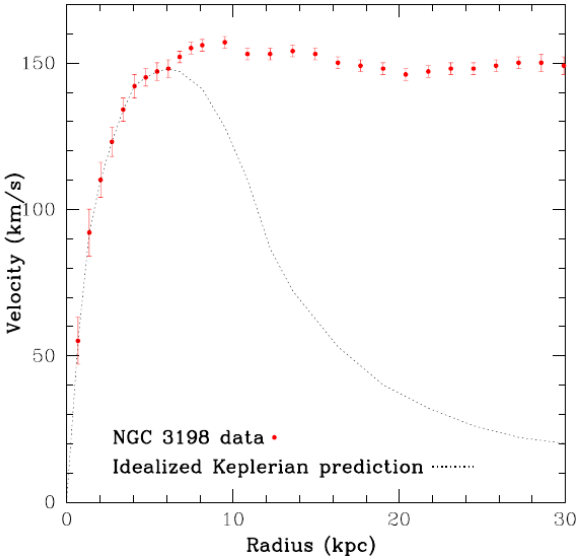

Figure 2.1: *Rotational velocities of hydrogen (HI regions) in NGC 3198 [2]*

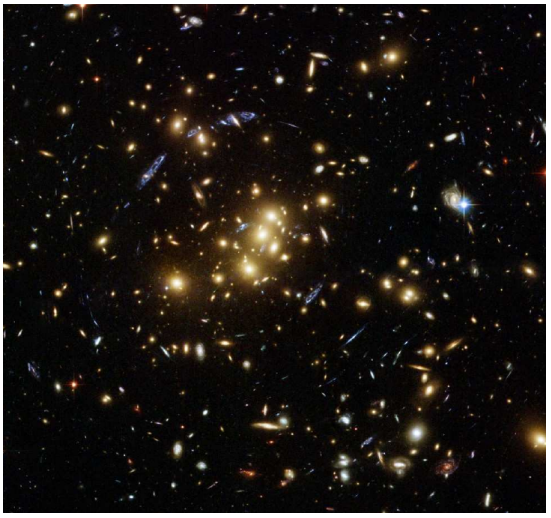

Figure 2.2: *Strong gravitational lensing from dark matter around galaxy cluster CL0024+17 [3].*

Besides being non-baryonic, we also know dark matter should be electromagnetically neutral since it does not seem to interact with radiation or baryonic matter in any non-gravitational way. Furthermore, from the structure of dark matter halos and the bullet cluster, we know that it cannot interact too strongly with itself [2, 47, 50, 51]. Due to these constraints, a possible dark matter candidate has been proposed, called a Weakly Interacting Massive Particle (WIMP) [52]. Different WIMPs have been proposed but have thus far remained elusive and have never been directly detected [53]. Other popular candidates include axions, sterile neutrinos and primordial black holes [54–58]. It has also been proposed that dark matter is an illusion and that the mass discrepancies for which it was introduced can be explained away by modifying Newtonian dynamics at low accelerations. These theories are broadly called Modified Newtonian Dynamics (MOND) [59, 60].

For our purposes, we only need to assume dark matter to be cold (non-relativistic), as opposed to relativistic hot dark matter (HDM [61]). The matter component thus consists of baryonic matter and cold dark matter, which is pressureless. The energy density will thus dilute with the expansion of the universe as $\rho_{\mathrm{m}} = nE = n(mc^2) \propto a^{-3}$. This coincides with a pressureless equation of state equal $P = 0 \rightarrow \omega_{\mathrm{m}} = 0$ [11] which evolves according to the conservation equation (1.45) as:

$$\rho_{\mathrm{m}} = \rho_{(\mathrm{m},0)} a^{-3(1+\omega_{\mathrm{m}})} = \rho_{(\mathrm{m},0)} a^{-3(1+0)} = \rho_{(\mathrm{m},0)} a^{-3}. \tag{2.5}$$

From (1.47), we may also obtain the following useful relations:

$$\begin{aligned} \rho_{\mathrm{m}} &= \frac{3H_0^2}{8\pi G}\Omega_{(\mathrm{m},0)}a^{-3} \quad ; \quad \rho_{\mathrm{m}} = \frac{3H_0^2}{8\pi G}\Omega_{(\mathrm{m},0)}(1+z)^3 \\ \Omega_{\mathrm{m}} &= \frac{H_0^2}{H^2}\Omega_{(\mathrm{m},0)}a^{3} \quad ; \quad \Omega_{\mathrm{m}} = \frac{H_0^2}{H^2}\Omega_{(\mathrm{m},0)}(1+z)^3. \end{aligned} \tag{2.6}$$

2.1.3 Dark energy

Dark energy refers to a wide class of models that describe an energy source with a negative pressure that causes a long-range repulsive force to counteract the force of gravity (see [62] for a taxonomy of dark energy models, as well as [63–66] for reviews and recent developments on some of these dark energy models). Later we will discuss Quintessence and phantom dark energy, where dark energy is dynamical and considered to be a scalar field with $\omega \neq -1$. We will first consider the first dark energy model.

The simplest and most common dark energy model is vacuum energy, which refers to a cosmological constant Λ that pervades all of space with a constant density [67]. We introduced this cosmological constant into the Einstein-Hilbert action (1.2) to produce the Einstein field equations (1.3) and in turn the cosmological field equations (1.21, 1.28). From these field equations (1.21, 1.28), we may see that the constant Λ may be interpreted as a fluid with an energy density ρ_Λ that can be grouped with the energy density term ρ if it has the form:

$$\rho_\Lambda = \frac{\Lambda c^2}{8\pi G} \tag{2.7}$$

The source of this vacuum energy is hypothesised to be quantum fluctuations in the vacuum [67, 68], which we explore in some detail in section 2.6.1. These quantum fluctuations supposedly create a negative pressure $P = -\rho c^2$ that results in an equation of state $\omega_\Lambda = -1$. From the conservation equation (1.45), this implies that vacuum energy evolves with scale factor as:

$$\rho_\Lambda = \rho_{(\Lambda,0)}a^{-3(1+\omega_\Lambda)} = \rho_\Lambda a^{-3(1+-1)} = \rho_{(\Lambda,0)}. \tag{2.8}$$

Thus, the energy density of the vacuum always has the same constant value. This is expected, as the vacuum itself cannot be diluted. From (1.47), we may also obtain the following useful relations:

$$\rho_\Lambda = \frac{3H_0^2}{8\pi G}\Omega_{(\Lambda,0)} \quad ; \quad \Omega_\Lambda = \frac{H_0^2}{H^2}\Omega_{(\Lambda,0)} \quad ; \quad \Lambda = \frac{3H_0^2}{c^2}\Omega_{(\Lambda,0)}, \tag{2.9}$$

where the last relation is obtained by equating ρ_Λ in (2.7) and (2.9). The importance of vacuum energy for cosmological models is presently mostly associated with Cosmic acceleration, but we will first discuss the reason for its initial introduction. This will brings us to the first modern cosmological model, Einstein's static universe.

2.2 Einstein's static universe

When Einstein first solved his field equations (1.3) for an isotropic and homogeneous universe he found that there were no static solutions ($\ddot{a} = \dot{a} = 0$; $a = a_0$) [9, 14, 67]. This can be seen by considering the Raychaudhuri equation (1.28) for a static model without the Λ term:

$$\left(\frac{\ddot{a}}{a}\right) = 0 = -\frac{4\pi G}{3}\left(\rho + \frac{3P}{c^2}\right) \quad \rightarrow \quad (\text{L.H.S} = 0 \; ; \; \text{R.H.S} < 0)\,. \tag{2.10}$$

This contradiction is true as long as the strong energy condition ($\rho + \frac{3P}{c^2} > 0$) holds, which has the consequence of gravitational attraction always being positive [14]. Since Einstein believed the universe to be static (as the data at the time suggested), he added a positive Λ term to balance out the gravitational force of matter (which is pressureless $P_{\mathrm{m}} = 0$, with $\rho_{\mathrm{m}} = \rho_{(\mathrm{m},0)}$ for a static case), such that (2.10) becomes:

$$\begin{aligned} 0 &= -\frac{4\pi G}{3}\left(\rho_{(\mathrm{m},0)} + \frac{3P_{\mathrm{m}}}{c^2}\right) + \frac{\Lambda c^2}{3} \\ \rho_{(\mathrm{m},0)} &= \frac{\Lambda c^2}{4\pi G} = 2\rho_{(\Lambda,0)}, \end{aligned} \tag{2.11}$$

where the last equality follows from (2.7). Substituting (2.11) into a static Friedmann equation (1.21) with $\dot{a} = 0$, we can see that this model must have a closed geometry :

$$\begin{aligned} \left(\frac{\dot{a}}{a}\right)^2 = 0 &= \frac{8\pi G\rho_{(\mathrm{m},0)}}{3} + \frac{\Lambda c^2}{3} - \frac{kc^2}{a_0^2} \\ 0 &= \frac{8\pi G\rho_{(\mathrm{m},0)}}{3} + \frac{4\pi G\rho_{(\mathrm{m},0)}}{3} - kc^2 \\ \rho_{(\mathrm{m},0)} &= \frac{kc^2}{4\pi G} \rightarrow \Lambda = k. \end{aligned} \tag{2.12}$$

Thus $k = +1$, since $\Lambda > 0$. This was Einstein's first cosmological model, which he published in 1917 [13], but was later dropped when the Hubble expansion was discovered. Besides this contradicting observation, the static model is also unstable. From (2.11), it can be seen that the cosmological constant has to be fine-tuned to exactly match the matter density of the universe. If a single proton is added or removed, or if any matter decays into radiation, this fine balance will be upset, and the universe will start contracting or expanding [9].

Einstein later dropped the cosmological constant (which he may have called his 'biggest blunder' [69])and the idea of a static universe [14]. Later he proposed a dynamic universe alongside de Sitter, a flat matter-only universe which expands while decelerating (Einstein-de Sitter universe [70]). Cosmological models from here onwards were dynamic. The cosmological constant might have been discarded alongside static universe models, but it would be resurrected once more to describe late-time acceleration in The ΛCDM model.

2.3 Hubble and deceleration parameters

We can now consider a more useful form of the Friedmann equation for dynamical models containing matter, radiation and/or dark energy. This can be done by rewriting (1.21), with Λ (2.7) part of the energy density ρ which is distributed between radiation ρ_{r}, matter ρ_{m} and dark energy ρ_{Λ}:

$$\left(\frac{\dot{a}}{a}\right)^2 = \frac{8\pi G}{3}\left(\rho_{\mathrm{r}} + \rho_{\mathrm{m}} + \rho_{\Lambda}\right) - \frac{kc^2}{a^2}. \tag{2.13}$$

This can now be written in terms of the density parameter relations Ω_{r} ,Ω_{m}, Ω_{Λ} and Ω_{k} from (2.3), (2.6), (2.3) (2.9) and (1.33) respectively, such that:

$$\begin{aligned}\left(\frac{\dot{a}}{a}\right)^2 &= \frac{8\pi G}{3}\left(\frac{3H_0^2}{8\pi G}\right)\left(\Omega_{(\mathrm{r},0)}a^{-4} + \Omega_{(\mathrm{m},0)}a^{-3} + \Omega_{(\Lambda,0)}\right) + H_0\Omega_{(\mathrm{k},0)}a^{-2} \\ H^2 = \left(\frac{\dot{a}}{a}\right)^2 &= H_0^2\left(\Omega_{(\mathrm{r},0)}a^{-4} + \Omega_{(\mathrm{m},0)}a^{-3} + \Omega_{(\Lambda,0)} + \Omega_{(\mathrm{k},0)}a^{-2}\right).\end{aligned} \tag{2.14}$$

The deceleration may be described by introducing the dimensionless deceleration parameter $q = -\left(\ddot{a}a/\dot{a}\right)$. An expression for q may be obtained by first rewriting the Raychaudhuri equation (with Λ grouped with the energy ρ (2.7)) in terms of the equation of state ω (1.44) a:

$$\begin{aligned}\left(\frac{\ddot{a}}{a}\right) &= -\frac{4\pi G}{3}\left(\rho + \frac{3P}{c^2}\right) \\ \left(\frac{\ddot{a}}{a}\right) &= -\frac{4\pi G}{3}\sum \rho_{\mathrm{x}}\left(1 + 3\omega_{\mathrm{x}}\right),\end{aligned} \tag{2.15}$$

where summation is used since each fluid will have a different equation of state. We now substitute in the density parameter $\rho_{\mathrm{x}} = \frac{3H^2}{8\pi G}\Omega_{\mathrm{x}}$ with $H = \dot{a}/a$ from (1.47):

$$\begin{aligned}\left(\frac{\ddot{a}}{a}\right) &= -\frac{4\pi G}{3}\sum\left(\frac{3}{8\pi G}\left(\frac{\dot{a}}{a}\right)^2\Omega_{\mathrm{x}}\right)\left(1 + 3\omega_{\mathrm{x}}\right) \\ q = -\left(\frac{\ddot{a}a}{\dot{a}^2}\right) &= \frac{1}{2}\sum \Omega_{\mathrm{x}}\left(1 + 3\omega\right).\end{aligned} \tag{2.16}$$

From which we see $q > 0$ (deceleration) if $\omega > -1/3$. Thus radiation ($\omega = 1/3$) and matter ($\omega = 0$) decelerate, while a cosmological constant ($\omega = -1$) accelerates expansion. Substituting in each of the density parameters in redshift space z and their corresponding equations of state ω give:

$$q = \Omega_{\mathrm{r}} + \frac{1}{2}\Omega_{\mathrm{m}} - \Omega_{\Lambda} = \frac{H_0^2\left[\Omega_{\mathrm{r}}(1+z)^4 + \frac{1}{2}\Omega_{\mathrm{m}}(1+z)^3 - \Omega_{\Lambda}\right]}{H^2}. \tag{2.17}$$

Substituting in the Hubble parameter (2.14) yields:

$$q = \frac{\Omega_{(\mathrm{r},0)}(1+z)^4 + \frac{1}{2}\Omega_{(\mathrm{m},0)}(1+z)^3 - \Omega_{(\Lambda,0)}}{\Omega_{(\mathrm{r},0)}(1+z)^4 + \Omega_{(\mathrm{m},0)}(1+z)^3 + \Omega_{(\Lambda,0)} + \Omega_{(\mathrm{k},0)}(1+z)^2}. \tag{2.18}$$

2.4 Single-fluid cosmological models

2.4.1 Friedmann and Lemaître cosmological models

To get an intuitive understanding of how each of the fluids (and their density) affects the dynamics of the universe, we will first consider some simplified cosmological models which only have a single fluid. Due to the simplicity of these models, the Friedmann equation may be analytically solved, which is usually very difficult for multi-fluid models. The dynamics of these models may therefore be described by solving the Friedmann equation (2.14):

$$\begin{aligned}\left(\frac{\dot{a}}{a}\right)^2 &= H_0^2(\Omega_{(\mathrm{r},0)}a^{-4} + \Omega_{(\mathrm{m},0)}a^{-3} + \Omega_{(\Lambda,0)} + \Omega_{(\mathrm{k},0)}a^{-2}) \\ \dot{a} &= H_0\sqrt{\Omega_{(\mathrm{r},0)}a^{-2} + \Omega_{(\mathrm{m},0)}a^{-1} + \Omega_{(\Lambda,0)}a^2 + \Omega_{(\mathrm{k},0)}}.\end{aligned} \tag{2.19}$$

These models may be divided into two main classes. The first group are Friedmann models, which have matter or radiation, but no cosmological constant $\Omega_{(\mathrm{r},0)} \neq 0$ or $\Omega_{(\mathrm{m},0)} \neq 0$ and $\Omega_{(\Lambda,0)} = 0$. The second group is Lemaître models where there is a non-zero cosmological constant, but we will only be considering single-fluid models so we have $\Omega_{(\mathrm{r},0)} = \Omega_{(\mathrm{m},0)} = 0$ and $\Omega_{(\Lambda,0)} \neq 0$ [9–11].

The Friedmann models consist only of radiation or matter, which both decelerate the expansion of the universe (2.16). This leads to the curve for $a(t)$ being convex everywhere, implying that $a(t)$ will always become zero in the past, leading to a big bang singularity. If the universe had a constant expansion rate, it would have an age $t_0 = 1/H_0$, but since the expansion for Friedmann models was faster in the past, it must have taken less time for the universe to reach its current size such that $t_0 < \frac{1}{H_0}$. The future evolution of these models may be seen from their Friedmann equation:

$$\dot{a} = H_0\sqrt{\Omega_{(\mathrm{r},0)}a^{-2} + \Omega_{(\mathrm{m},0)}a^{-1} + \Omega_{(\mathrm{k},0)}} \approx H_0\sqrt{\Omega_{(\mathrm{k},0)}} = H_0\sqrt{1 - \left(\Omega_{(\mathrm{r},0)} + \Omega_{(\mathrm{m},0)}\right)}. \tag{2.20}$$

From (2.20) it can be seen that as the universe expands ($a \gg 1$) the first two terms will approach zero (as a has a negative exponent) and the $\Omega_{(\mathrm{k},0)} = 1 - \left(\Omega_{(\mathrm{r},0)} + \Omega_{(\mathrm{m},0)}\right)$ term will dominate the equation. The density $\Omega_{(\mathrm{r},0)} + \Omega_{(\mathrm{m},0)}$ will therefore determine the destiny of these models [9, 10]:

Table 2.1: *Ultimate fate of Friedmann models ($t \to \infty$)*

Curvature	$\ddot{a}$	$\dot{a}$	a	Ultimate fate
Open ($\Omega_{(\mathrm{r},0)} + \Omega_{(\mathrm{m},0)} < 1$)	–	+constant	∞	Big chill (Heat death)
Flat ($\Omega_{(\mathrm{r},0)} + \Omega_{(\mathrm{m},0)} = 1$)	–	0	∞	Big chill (Heat death)
Closed ($\Omega_{(\mathrm{r},0)} + \Omega_{(\mathrm{m},0)} > 0$)	–	0 at $a_{\max}$	0	Big crunch/bounce

The big chill or heat death refers to the universe expanding forever ($a \to \infty$) and cooling over an infinite amount of time until the universe reaches maximum entropy. These models will decelerate and approach a constant velocity (Open case) or approach a static state ($\dot{a} = 0$) over an infinite time (Flat case) but will never re-collapse. For closed models, the universe stops expanding $\dot{a} = 0$ when it reaches a maximum size ($a_{\max}$). Since it is still decelerating ($\ddot{a} < 0$), the universe will finally re-collapse into a singularity at the big crunch ($a \to 0$). Depending on the solution of a, the universe may start expanding again after the big crunch (in what is known as a big bounce) until it collapses again. This cycle may be repeated indefinitely.

The Lemaître models include a cosmological constant that always accelerates the expansion of the universe (2.16). The curve of $a(t)$ is thus concave everywhere, and the scale factor will always become infinite in the future, leading to a big chill or heat death. The different past expansion histories of these models may be seen from the Friedmann equation:

$$\dot{a} = H_0\sqrt{\Omega_{(\Lambda,0)}a^2 + \Omega_{(\mathrm{k},0)}} \to H_0\sqrt{\Omega_{(\mathrm{k},0)}} = H_0\sqrt{1 - \Omega_{(\Lambda,0)}}. \tag{2.21}$$

From (2.21) it can be seen that at early times when the universe was smaller ($a \ll 1$), the first term will approach zero and the $\Omega_{(\mathrm{k},0)} = 1 - \Omega_{(\Lambda,0)}$ term will dominate the equation. The density $\Omega_{(\Lambda,0)}$ will therefore determine the past and origin of these models.

Table 2.2: *Distant past of Lemaître models ($t \to -\infty$)*

Curvature	$\ddot{a}$	$\dot{a}$	a	Distant past / Origin
Open ($\Omega_{(\Lambda,0)} < 1$)	+	+constant	0	Big bang
Flat ($\Omega_{(\Lambda,0)} = 1$)	+	0	$\to 0$	No big bang singularity
Closed ($\Omega_{(\Lambda,0)} > 1$)	+	0 at $a_{\min}$	∞	Non-singular big bounce

For these models, $\dot{a} > 0$ means that the universe will expand into the future and contract into the past. Thus, an open universe with $\dot{a} > 0$ in the distant past will contract into a big bang singularity $a \to 0$. Conversely, a flat universe will contract infinitely into the past as it becomes smaller and approaches a static state ($\dot{a} = 0$) but never reaches a big bang singularity. A closed universe will stop contracting ($\dot{a} = 0$) in the past when it reaches a minimum size ($a_{\min}$). Since the curve of $a(t)$ is concave everywhere due to the accelerating expansion ($\ddot{a} > 0$), this must be a saddle point where the scale factor increases further into the past and approaches $a \to \infty$. This is known as a non-singular big bounce, as the universe bounces without a singularity (as in the closed Friedmann model) [43].

To mathematically support these arguments, we will analytically solve the Friedmann equation for models containing only radiation, matter or a cosmological constant, with each of the three geometries. The full calculations of these solutions are found in Appendix A.

2.4.2 Solutions for radiation-dominated Friedmann models

The Friedmann equation has been analytically solved for radiation-dominated Friedmann models to obtain expressions for the evolution of the scale factor $a(t)$, the time t and the age of the universe model t_0. Here the phase $\theta = H_0\sqrt{\Omega_{(\mathrm{r},0)} - 1}\eta$ and $\phi = H_0\sqrt{1 - \Omega_{(\mathrm{r},0)}}\eta$, with η conformal time as defined in (A.52). For closed and open geometries, the age of the universe is obtained at $t_0 = t(\theta_0)$ and $t(\phi_0)$ respectively. The Hubble constant used is $H_0 = 67.4$ km s^{-1}Mpc^{-1} ≈ 0.069 Gyr^{-1}.

Table 2.3: *Friedmann equation solutions for radiation-dominated universes (Friedmann Models)*

Curvature	Scale Factor (a)	Time (t)	Age (t_0)
Open ($\Omega_{(\mathrm{r},0)} < 1$)	$\sqrt{\frac{\Omega_{(\mathrm{r},0)}}{1-\Omega_{(\mathrm{r},0)}}}\sinh(\phi)$	$\frac{\sqrt{\Omega_{(\mathrm{r},0)}}}{H_0(1-\Omega_{(\mathrm{r},0)})}[\cosh(\phi) - 1]$	$\phi_0 = \sinh^{-1}\sqrt{\frac{1-\Omega_{(\mathrm{r},0)}}{\Omega_{(\mathrm{r},0)}}}$
Flat ($\Omega_{(\mathrm{r},0)} = 1$)	$\sqrt{2H_0 t}$	-	$t_0 = \frac{1}{2H_0}$
Closed ($\Omega_{(\mathrm{r},0)} > 1$)	$\sqrt{\frac{\Omega_{(\mathrm{r},0)}}{\Omega_{(\mathrm{r},0)}-1}}\sin(\theta)$	$\frac{\sqrt{\Omega_{(\mathrm{r},0)}}}{H_0(\Omega_{(\mathrm{r},0)}-1)}[1 - \cos(\theta)]$	$\theta_0 = \sin^{-1}\sqrt{\frac{\Omega_{(\mathrm{r},0)}-1}{\Omega_{(\mathrm{r},0)}}}$

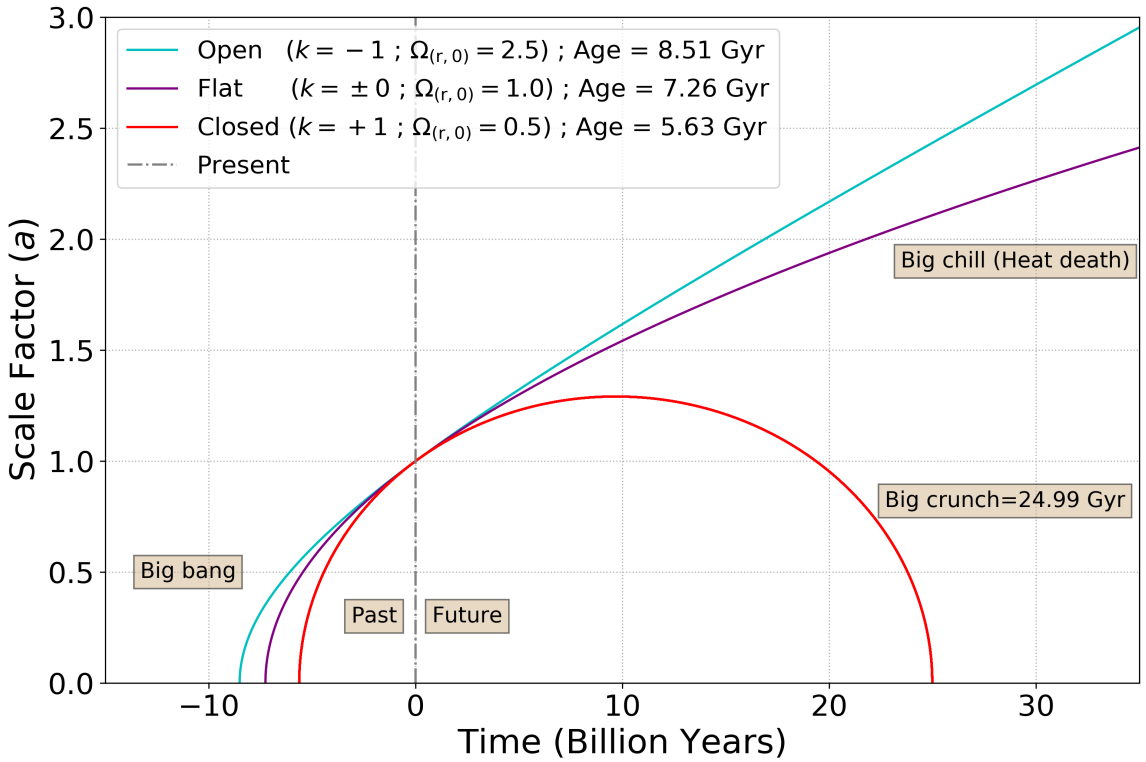

Figure 2.3: *Evolution of radiation-dominated Friedmann models*

In Figure 2.3 it can be seen that the analytical solutions show the same behaviour predicted in table 2.1. All models begin with a big bang (with $t_0 < 1/H_0$)), from which the expansion decelerates. The model will either expand forever (heat death) or re-collapse (big crunch), depending on whether the density is less ($\Omega_{(\mathrm{r},0)} < 1$ open) or more ($\Omega_{(\mathrm{r},0)} > 1$ closed) than the critical density ($\Omega_{(\mathrm{r},0)} = 1$), which corresponds to a flat geometry. The density, therefore, predicts the destiny of the system.

2.4.3 Solutions for matter-dominated Friedmann models

The Friedmann equation has been analytically solved for matter-dominated Friedmann models to obtain expressions for the evolution of the scale factor $a(t)$, the time t and either the age t_0 of the universe model or the time of a single bouncing cycle t_b. The phase $\theta = H_0\sqrt{\Omega_{(\mathrm{m},0)} - 1}\eta$ and $\phi = H_0\sqrt{1 - \Omega_{(\mathrm{m},0)}}\eta$. For the open geometry, the age of the universe model is $t_0 = t(\phi_0)$.

Table 2.4: *Friedmann equation solutions for matter-dominated universes (Friedmann Models)*

k	Scale Factor (a)	Time (t)	Age (t_0) / Bounce cycle (t_b)
Open	$\frac{\Omega_{(\mathrm{m},0)}}{2\left(1-\Omega_{(\mathrm{m},0)}\right)}\left(\cosh(\phi) - 1\right)$	$\frac{\Omega_{(\mathrm{m},0)}}{2H_0\left(1-\Omega_{(\mathrm{m},0)}\right)^{3/2}}\left[\sinh(\phi) - \phi\right]$	$\phi_0 = \cosh^{-1}\left(1 + \frac{2\left(1-\Omega_{(\mathrm{m},0)}\right)}{\Omega_{(\mathrm{m},0)}}\right)$
Flat	$\left(\frac{3}{2}H_0 t\right)^{2/3}$	-	$t_0 = \frac{2}{3H_0}$
Closed	$\frac{\Omega_{(\mathrm{m},0)}}{2\left(\Omega_{(\mathrm{m},0)}-1\right)}\left(1 - \cos(\theta)\right)$	$\frac{\Omega_{(\mathrm{m},0)}}{2H_0\left(\Omega_{(\mathrm{m},0)}-1\right)^{3/2}}\left[\theta - \sin(\theta)\right]$	$t_b = \frac{\pi}{H_0}\frac{\Omega_{(\mathrm{m},0)}}{\left(\Omega_{(\mathrm{m},0)}-1\right)^{3/2}}$

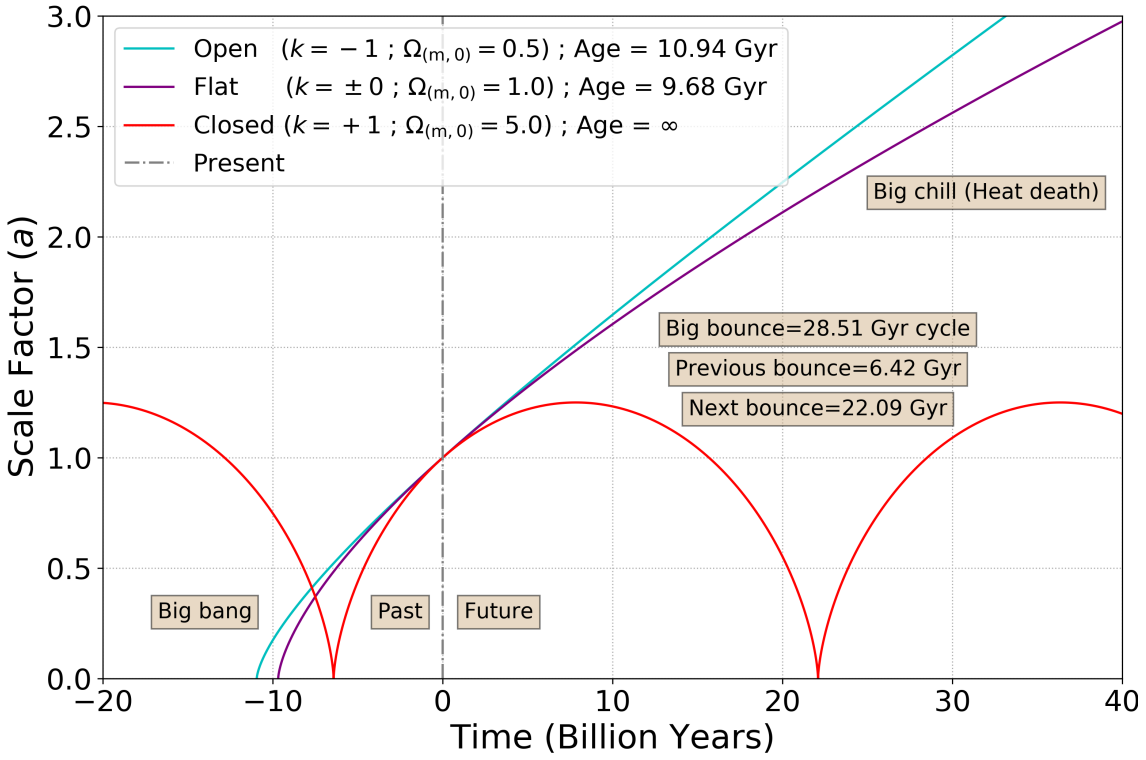

Figure 2.4: *Evolution of matter-dominated Friedmann models*

In Figure 2.4 the behaviour is the same as predicted in table 2.1. The flat (also known as the Einstein-de Sitter model [70]) and open cases behave qualitatively similar to the radiation-dominated models in Figure 2.3. Conversely, the closed model is a cycloid with an infinite cycle of expansion and re-collapse followed by a big bounce. This model will therefore have an infinite age and continue bouncing indefinitely into the future. The time from the previous bounce and to the next bounce is also calculated in Appendix A.

2.4.4 Solutions for cosmological constant-dominated Lemaître models

The Friedmann equation has been analytically solved for cosmological constant-dominated Lemaître models to obtain expressions for the evolution of the scale factor $a(t)$, the time t and either the age t_0 of the universe model or the time since the non-singular bounce t_b. The phase $\varphi = H_0\sqrt{1-\Omega_{(\Lambda,0)}}t$ and $\psi = H_0\sqrt{\Omega_{(\Lambda,0)}-1}t$.

Table 2.5: *Friedmann equation solutions for Λ dominated universes (Lemaître Models)*

Curvature	Scale Factor (a)	Time (t)	Age (t_0) / Bounce time (t_b)
Open ($\Omega_{(\Lambda,0)} < 1$)	$\sqrt{\frac{1-\Omega_{(\Lambda,0)}}{\Omega_{(\Lambda,0)}}}\sinh(\varphi)$	-	$t_0 = \frac{1}{H_0\sqrt{1-\Omega_{(\Lambda,0)}}}\sinh^{-1}\left(\sqrt{\frac{\Omega_{(\Lambda,0)}}{1-\Omega_{(\Lambda,0)}}}\right)$
Flat ($\Omega_{(\Lambda,0)} = 1$)	$e^{H_0 t}$	-	∞
Closed ($\Omega_{(\Lambda,0)} > 1$)	$\sqrt{\frac{\Omega_{(\Lambda,0)}-1}{\Omega_{(\Lambda,0)}}}\cosh(\psi)$	-	$t_b = \frac{1}{H_0\sqrt{\Omega_{(\Lambda,0)}-1}}\cosh^{-1}\left(\sqrt{\frac{\Omega_{(\Lambda,0)}}{\Omega_{(\Lambda,0)}-1}}\right)$

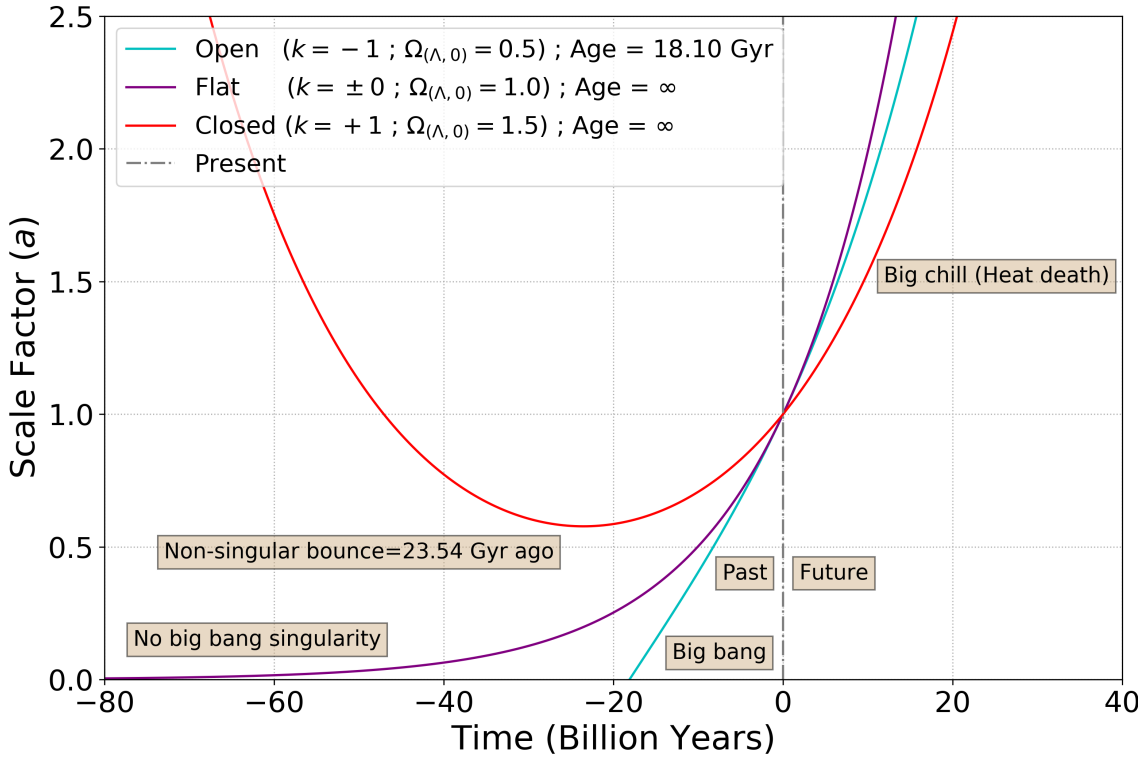

Figure 2.5: *Evolution of cosmological constant-dominated Lemaître models*

In Figure 2.5 the behaviour is the same as predicted in table 2.2. All models have an accelerated expansion which ends with a heat death. The density of the cosmological constant determines the origin of the model. The model will either have a big bang ($\Omega_{(\Lambda,0)} < 1$ Open) or will have a non-singular bounce ($\Omega_{(\Lambda,0)} > 1$ closed) at a minimum size a_{min}. The critical density ($\Omega_{(\Lambda,0)} = 1$ flat geometry) is known as a de Sitter model and has no big bang singularity in the past and is infinitely old. This model has particular interest due to its similarity to inflation models [9].

2.5 The ΛCDM model

2.5.1 Cosmic acceleration

From our daily experience, we know that the universe contains matter and at least some radiation. Therefore, most of the single-fluid models can immediately be discarded as an accurate description of our universe. For many years matter-dominated universes (See Figure 2.4) were considered the most probable models, and from (2.16), we know that these matter-dominated universes should be decelerating. A complete paradigm shift occurred in 1998 when both the Supernova Cosmology Project and the High-z Supernova Search Team from observations of Standard candles and type Ia supernovae independently discovered that the expansion of the universe is not slowing down as expected, but instead speeding up [19–22]. Since this discovery of the accelerating expansion (which from (2.16) requires $\omega < -1/3$), the cosmological constant Λ (with $\omega = -1$) made an immediate return as an obvious candidate for this unexpected observation. These developments led to a new model which contains radiation, baryonic and dark matter and a cosmological constant Λ. This is called the ΛCDM (Lambda cold dark matter) model and is the standard model of cosmology.

2.5.2 Cosmological parameters

To determine how the ΛCDM model evolves and which predictions it makes, the values of the cosmological parameters ($\Omega_{\mathrm{r},0}$, $\Omega_{\mathrm{m},0}$, $\Omega_{\Lambda,0}$) need to be known. These parameters will tell us how the energy of the universe is distributed between radiation, matter and the cosmological constant, as well as tell us what geometry the universe has. All measurements are obtained from the CMB.

The present radiation density $\Omega_{(\mathrm{r},0)}$ consists of photons, which is dominated by CMB photons $\Omega_{(\mathrm{CMB},0)}$ and neutrinos $\Omega_{(\nu,0)}$. The energy density of the CMB photons is calculated using the Stefan Boltzmann-law ($\rho_{\mathrm{CMB}} = \alpha T_{CMB}^4$ with α the reduced Stefan Boltzman constant) with the temperature measured directly from the blackbody radiation of the CMB [9, 10, 71]. This temperature is measured by the WMAP telescope as $T_{\mathrm{CMB}} = 2.7255$ K [72]. Therefore, the CMB density parameter is obtained from the ratio of the energy density of CMB photons ρ_{CMB} to the critical density ρ_{c} (1.30) and has the value:

$$\Omega_{(\mathrm{CMB},0)} = \frac{\rho_{CMB}}{\rho_c} = \left(\alpha T_{CMB}^4\right)\left(\frac{8\pi G}{3H_0^2}\right) = \frac{\left(8.41\times10^{-33}\ \mathrm{kg\ m^{-3}K^{-4}}\right)\left(2.7255\ \mathrm{K}\right)^4}{8.53\times10^{-27}\ \mathrm{kg.m^{-3}}} \approx 5.44\times10^{-5}. \tag{2.22}$$

The energy density of neutrinos should be comparable to those of CMB photons. A detailed calculation shows that each neutrino flavour should have an energy of 0.277 $\Omega_{(\mathrm{CMB},0)}$. Since there are three neutrino flavours we have $\Omega_{(\nu,0)} = 3(0.277\Omega_{(\mathrm{CMB},0))} = 0.681\Omega_{(\mathrm{CMB},0)} \approx 3.70\times10^{-5}$ [10].

The present radiation density parameter is then:

$$\Omega_{(\mathrm{r},0)} = \Omega_{(\mathrm{CMB},0)} + \Omega_{(\nu,0)} \approx 9 \times 10^{-5}. \tag{2.23}$$

The other cosmological parameters may be obtained from measurements of the temperature anisotropies in the CMB, which were made by the Planck Telescope in 2018 [4].

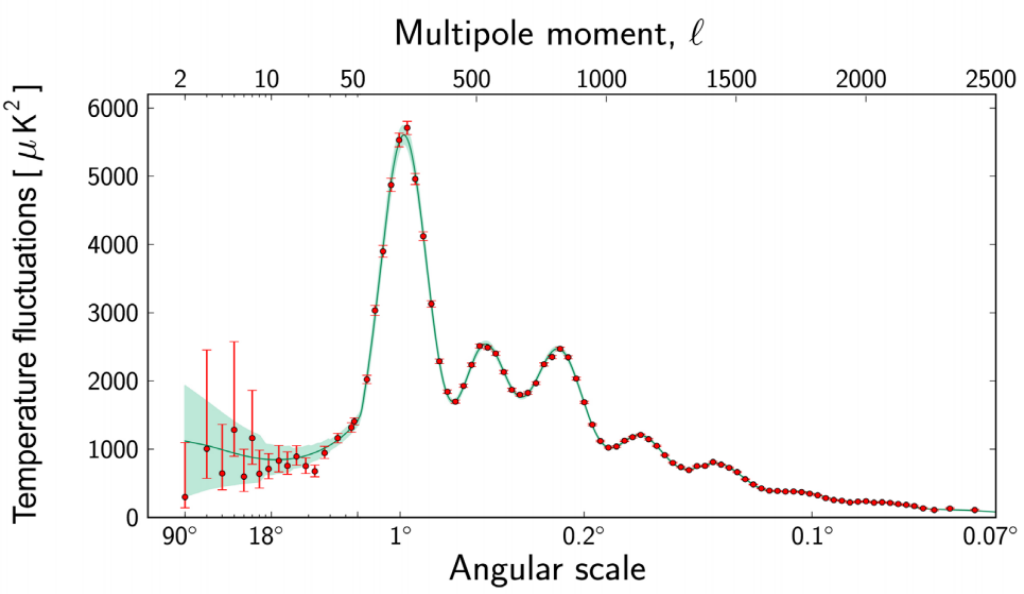

Figure 2.6: *Temperature anisotropies of the CMB [1]*

From these measurements it was determined that the universe has an almost perfectly flat geometry such that $\Omega_{(\mathrm{k},0)} = 0.001 \pm 0.002$. The density of matter has also been determined to be $\Omega_{(\mathrm{m},0)} = 0.315 \pm 0.007$, of which about 85% consists of cold dark matter $\Omega_{(\mathrm{dm},0)} = 0.266$ and only about 15% is baryonic matter $\Omega_{(\mathrm{bm},0)} = 0.049$ [4]. Using these parameters, the dark energy density $\Omega_{(\Lambda,0)}$ may be determined using equation (1.33):

$$\begin{aligned} 1 &= \Omega_{(\mathrm{r},0)} + \Omega_{(\mathrm{m},0)} + \Omega_{(\Lambda,0)} + \Omega_{(\mathrm{k},0)} \\ \rightarrow \Omega_{(\Lambda,0)} &= 1 - \Omega_{(\mathrm{r},0)} - \Omega_{(\mathrm{m},0)} - \Omega_{(\mathrm{k},0)} = 1 - 9 \times 10^{-5} - 0.315 - 0.001 \approx 0.685. \end{aligned} \tag{2.24}$$

Taking the sum of the dark matter and dark energy parameters $\Omega_{(\mathrm{dm},0)} + \Omega_{(\Lambda,0)} = 0.685 + 0.266 = 0.951$ we see that 95% of the energy budget of the universe is distributed between the dark sectors. Finally, the Planck telescope also measured the Hubble constant to be $H_0 = 67.4$ km s^{-1}Mpcs^{-1} [4]. The following cosmological parameters will thus be used throughout, unless stated otherwise:

$$\Omega_{(\mathrm{r},0)} = 9 \times 10^{-5} \quad ; \quad \Omega_{(\mathrm{m},0)} = 0.315 \quad ; \quad \Omega_{(\Lambda,0)} = 0.685 \quad ; \quad H_0 = 67.4 \text{ km s}^{-1}\text{Mpcs}^{-1}. \tag{2.25}$$

It should be noted that there are many other probes to measure these cosmological parameters. For a review of the different measurements of cosmological parameters at the end of 2019, see [73].

2.5.3 Radiation, matter and dark energy dominated epochs

The ΛCDM model is a multi-fluid model, with each of the fluids evolving independently of the others. Since the energy densities of radiation, matter and the cosmological constant dilute at different rates as the universe expands ($\propto a^{-4}$, $\propto a^{-3}$ and $\propto a^{0}$ respectively), each species will dominate at different times in the history of the universe. This can be seen by plotting the energy densities ρ and density parameters Ω for radiation (2.3), matter (2.6) and dark energy (2.9) against redshift $(1+z)$, using the cosmological parameters (2.25) as the present initial conditions.

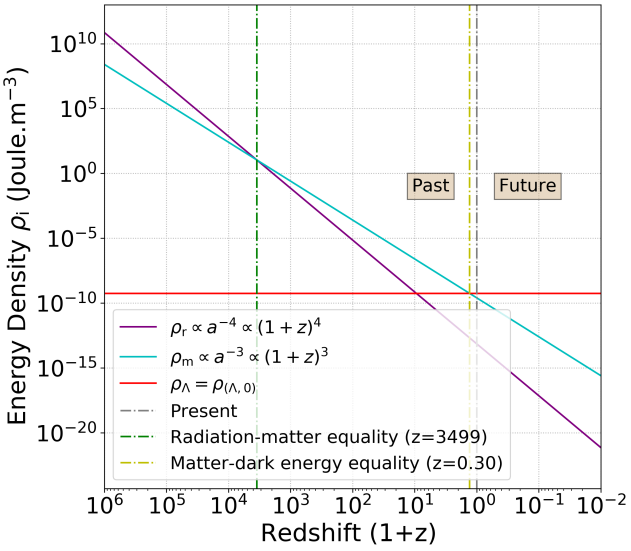

Figure 2.7: *Evolution of energy densities ρ with redshift $(1+z)$ (ΛCDM)*

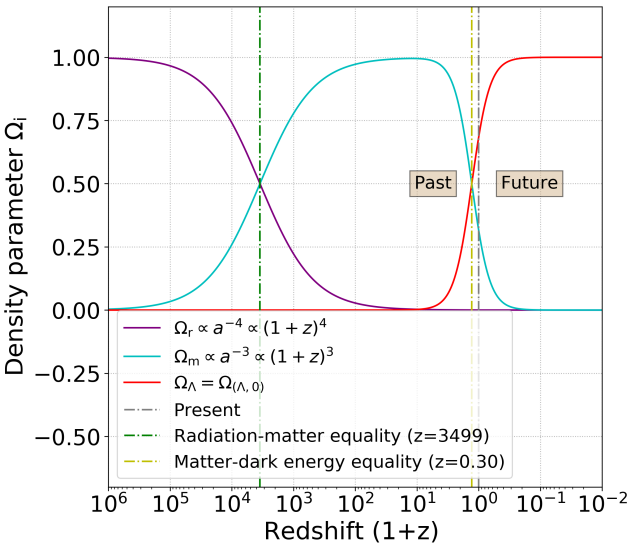

Figure 2.8: *Evolution of density parameters Ω with redshift $(1+z)$ (ΛCDM)*

From Figures 2.7 and 2.8 we can see that there was an early period (a large redshift z equates to small a, and thus the distant past) of radiation domination, which was followed by periods of matter and dark energy domination respectively. The exact redshift where the radiation-matter equality $z_{\mathrm{r=m}}$ and the matter-dark energy equality $z_{\mathrm{m=\Lambda}}$ happens is calculated in Appendix D.1 as:

$$\begin{aligned} z_{\mathrm{r=m}} &= \frac{\Omega_{(\mathrm{m},0)}}{\Omega_{(\mathrm{r},0)}} - 1 = \frac{0.315}{9\times10^{-5}} - 1 = 3499 \quad (\text{when } \rho_{\mathrm{r}} = \rho_{\mathrm{m}} \approx 10.93 \text{ Joule m}^{-3}), \\ z_{\mathrm{m=\Lambda}} &= \left(\frac{\Omega_{(\Lambda,0)}}{\Omega_{(\mathrm{m},0)}}\right)^{1/3} - 1 = \left(\frac{0.685}{0.315}\right)^{1/3} - 1 = 0.3 \quad (\text{when } \rho_{\mathrm{m}} = \rho_{\Lambda} \approx 5.54\times10^{-10} \text{ Joule m}^{-3}). \end{aligned} \tag{2.26}$$

The radiation, matter and dark energy dominated epochs will each leave their mark on the expansion history of this model. This can be seen by considering the three fluids in the model as a single fluid with a dynamical effective equation of state ω^{eff}. This effective equation of state is given by the ratio of the sum of each fluid's pressure P_{tot} over the total energy densities ρ_{tot}:

$$\omega^{\mathrm{eff}} = \frac{P_{\mathrm{tot}}}{\rho_{\mathrm{tot}}} = \frac{P_{\mathrm{r}} + P_{\mathrm{m}} + P_{\Lambda}}{\rho_{\mathrm{r}} + \rho_{\mathrm{m}} + \rho_{\Lambda}} = \frac{\omega_{\mathrm{r}}\rho_{\mathrm{r}} + \omega_{\mathrm{m}}\rho_{\mathrm{m}} + \omega_{\Lambda}\rho_{\Lambda}}{\rho_{\mathrm{r}} + \rho_{\mathrm{m}} + \rho_{\Lambda}} = \frac{\frac{1}{3}\rho_{\mathrm{r}} - \rho_{\Lambda}}{\rho_{\mathrm{r}} + \rho_{\mathrm{m}} + \rho_{\Lambda}} = \frac{\frac{1}{3}\Omega_{\mathrm{r}} - \Omega_{\Lambda}}{\Omega_{\mathrm{r}} + \Omega_{\mathrm{m}} + \Omega_{\Lambda}}. \tag{2.27}$$

Substituting the density parameters for radiation (2.3), matter (2.6) and dark energy (2.9) gives:

$$\omega^{\text{eff}} = \frac{\frac{1}{3}\Omega_{(\text{r},0)}(1+z)^4 - \Omega_{(\Lambda,0)}}{\Omega_{(\text{r},0)}(1+z)^4 + \Omega_{(\text{m},0)}(1+z)^3 + \Omega_{(\Lambda,0)}}. \tag{2.28}$$

This effective equation of state ω^{eff} may be used alongside the deceleration parameter (2.18) with parameters (2.25) to see the different phases of the expansion history.

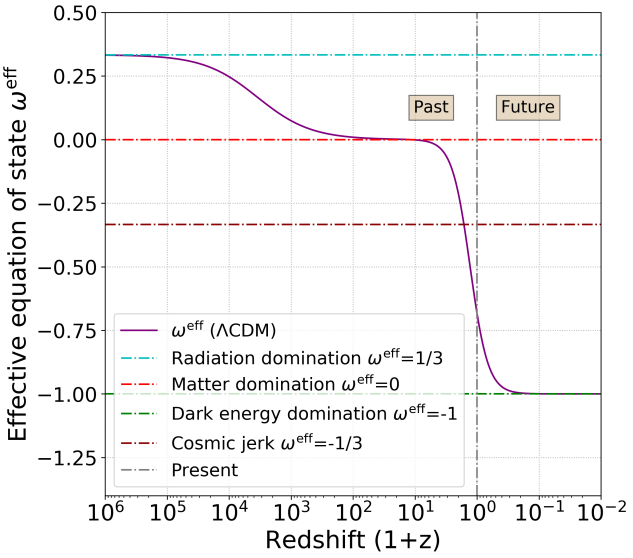

Figure 2.9: *Evolution of the effective equation of state ω^{eff} with redshift $(1+z)$ (ΛCDM)*

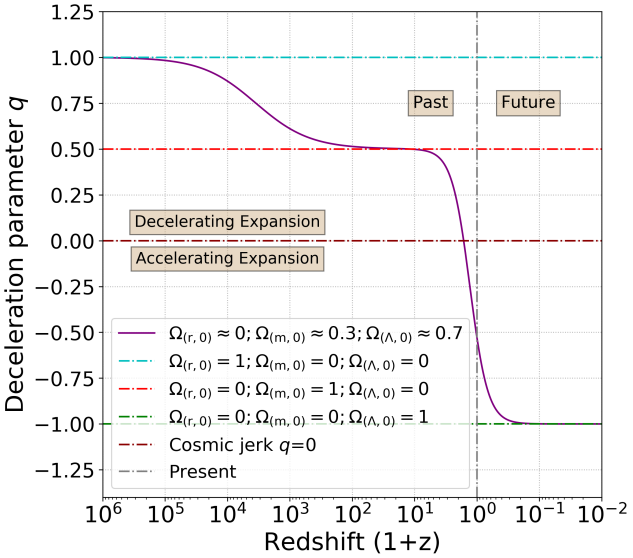

Figure 2.10: *Evolution of deceleration parameter q with redshift $(1+z)$ (ΛCDM)*

From Figure 2.9 it can be seen that the ΛCDM model mimics the behaviour of radiation fluid in the distant past, since the effective equation of state is equal to that of radiation $\omega^{\text{eff}} = \omega_{\text{r}} = 1/3$. This behaviour coincides with the deceleration parameter $q \approx 1$ in the distant past in Figure 2.10, mimicking that of a flat radiation-dominated universe (which is indicated by the blue dashed line). Similarly, as the universe expands it later mimics matter fluid $\omega^{\text{eff}} = \omega_{\text{m}} = 0$ and finally a cosmological constant $\omega^{\text{eff}} = \omega_{\Lambda} = -1$. These epochs, in turn, have a deceleration parameter $q = 0.5$ and $q = -1$, which mimic a flat matter (Einstein-de Sitter indicated by the dashed red line) and flat cosmological constant (de Sitter indicated by the dashed green line) universe, respectively. It can thus be seen that the expansion of the ΛCDM model decelerates during radiation and matter domination before accelerating when dark energy becomes dominant enough. This transition from deceleration to acceleration (called a cosmic jerk) occurs when $q = 0$, which happens if $\Omega_{\text{dm}} \approx 2\Omega_{\Lambda}$ D.8 or the effective equation of state is $\omega^{\text{eff}} = 1/3$. The exact transition redshift z_{t} where this cosmic jerk occurs is calculated in Appendix D.1, giving:

$$z_{\text{t}} = \left(\frac{2\Omega_{(\Lambda,0)}}{\Omega_{(\text{m},0)}}\right)^{1/3} - 1 = \left(\frac{2(0.685)}{0.315}\right)^{1/3} - 1 = 0.63. \tag{2.29}$$

Direct evidence from Type Ia supernovae for this cosmic jerk was discovered by one of the teams who first discovered the cosmic acceleration [74, 75].

2.5.4 Origin, evolution and fate of ΛCDM model

As seen in the previous section, the ΛCDM model should initially have a period of decelerating expansion followed by accelerated expansion. This should be reflected in the way the scale factor evolves with time. The Friedmann equation for the ΛCDM model (2.19) cannot be solved analytically in any simple manner and therefore numerical methods will be resorted to instead. The 4th order Runge-Kutta method was adopted [76] which is generally recommended for numerical integration of first-order differential equations (This method is described in Appendix A.4). To ensure the numerical integration works for the ΛCDM model, we will also use the numerical method to reproduce some of the previous analytical solutions from Figures 2.3, 2.4 and 2.5.

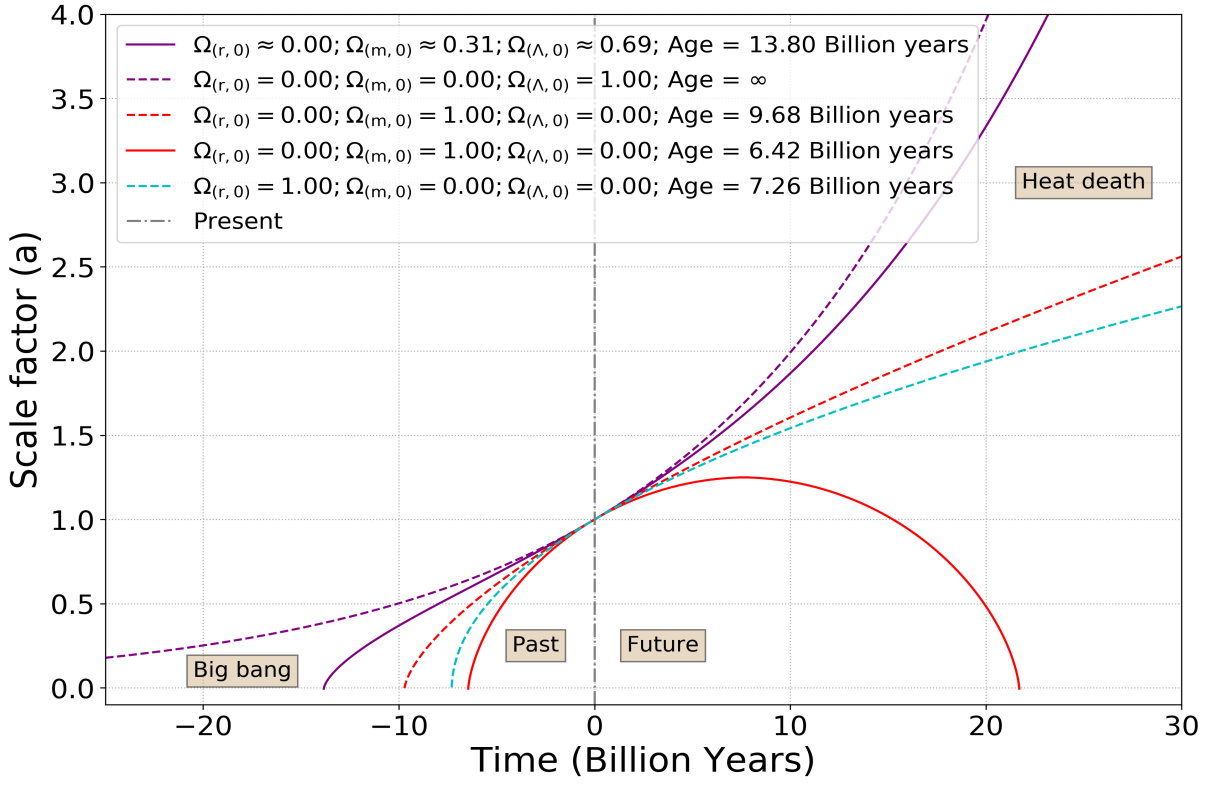

Figure 2.11: *Origin, evolution and fate of ΛCDM model*

From Figure 2.11 the expansion history of the ΛCDM model (solid purple line) can be seen, alongside that of a de-Sitter universe (dashed purple line), Einstein-de Sitter universe (dashed red line), closed matter-dominated universe (solid red line) and a flat radiation-dominated universe (dashed blue line). The age of each model is calculated by numerical integration of the Friedmann equation (2.19), which may be rewritten as [9]:

$$\int_0^t dt = \int_0^a \frac{1}{H(a)} da = \int_0^a \frac{1}{H_0 \sqrt{(\Omega_{(r,0)} a^{-2} + \Omega_{(m,0)} a^{-1} + \Omega_{(\Lambda,0)} a^2 + \Omega_{(k,0)})}} da. \tag{2.30}$$

The resulting plots and ages of each of the single-fluid models can be seen to coincide with the analytical solutions obtained in Figures 2.3, 2.4 and 2.5. Therefore, we may conclude that the numerical method is an accurate approximation of the true behaviour of the ΛCDM model.

It may therefore be seen that the ΛCDM model started from a big bang approximately 13.80 billion years ago [4]. The universe then started with an initial period of decelerating expansion (where the plot is convex), followed by a recent period of accelerating expansion (where the plot is concave), which should continue indefinitely into the future. This behaviour coincides with Figures 2.7, 2.8, 2.9 and 2.10, where there is an initial period of deceleration $q > 0$ during radiation and matter domination, followed by an infinite period of accelerating expansion $q < 0$ during the final era of dark energy domination. It can thus be seen that the ΛCDM model behaves qualitatively similar to an Einstein-de Sitter universe in the distant past while behaving like a de-Sitter universe at later times. It may also be seen that the Hubble parameter converges to a constant value as $a \to \infty$ which corresponds to $(1 + z) \to 0$, thus from equation (2.14) we have:

$$H = H_0\sqrt{\Omega_{(r,0)}(0)^4 + \Omega_{(d,0)}(0)^3 + \Omega_{(\Lambda,0)} + \Omega_{(k,0)}(0)^2} = H_0\sqrt{\Omega_{(\Lambda,0)}} \approx 56 \text{ km/s/Mpc}. \tag{2.31}$$

Since we now know how the scale factor evolves with time, and since the scale factor is related to redshift by the relation $a = 1/(1 + z)$, we can determine at which redshift z and time t important cosmic events in the ΛCDM model happened. Using the equations which relate energy density to redshift (2.3, 2.6 and 2.9), we may also find the energy density of radiation ρ_{r}, matter ρ_{m} and dark energy ρ_Λ at these events. These events include the big bang, the radiation-matter and matter-dark energy equalities (2.26) as well as acceleration at the cosmic jerk (2.29). These results are summarised in Table 2.6 below.

Table 2.6: *Important events in the ΛCDM model (using CMB data [4])*

Event	Redshift z	Time (Gyr)	ρ_{r}	ρ_{m}	ρ_Λ (J/m^3)
Big bang singularity	∞	13.80	∞	∞	∞
Radiation-matter equality	3499	13.80	10.9	10.9	5.5e-10
Cosmic jerk ($q = 0$)	0.63	6.12	5.2e-13	1.2e-9	5.5e-10
Matter-dark energy equality	0.30	3.50	2.1e-13	1.1e-9	5.5e-10

with $\Lambda \approx 1.09 \times 10^{-53}$ m^{-2} from (2.9). From Table 2.6 it is seen that the radiation-matter equality occurred soon after the big bang, leading to a period of matter domination that lasted approximately 10 billion years before dark energy became dominant. The universe then started accelerating at approximately half its present age, when $\rho_{\text{m}} \approx 2\rho_\Lambda$. This accelerated expansion then continues indefinitely until the universe cools with a slow heat death over billions of years.

These conclusions and observations all rely on the ΛCDM model being an accurate description of the universe we live in. To know if this is the case, we should also consider it's shortcomings.

2.6 Problems with the ΛCDM model

The ΛCDM model has proven to be very successful [4], but crucial problems with the ΛCDM model remain. These include the well-known flatness (fine-tuning needed to produce flat curvature we observe today), horizon (the universe being highly homogeneous, though distant regions are causally disconnected) and magnetic monopole (lack of predicted magnetic monopoles at high energies) problems for which early time accelerated expansion in the form of inflation was introduced by Alan Guth [8–11, 77–80]. We will only briefly mention these, as we will be primarily concerned with problems associated with the nature of the dark sectors, which make up 95% of the universe's energy budget. We will explore three of these problems in some detail.

2.6.1 The cosmological constant problem

The cosmological constant problem or vacuum catastrophe refers to the measured energy density of the vacuum being over 120 orders of magnitude smaller than the theoretical prediction [9, 68]. A simplified way to show how this result is obtained is by calculating the amount of energy that a quantum vacuum fluctuation can contribute within a Planck volume [68, 81]. To do this, first consider the Heinsenberg uncertainty principle:

$$\Delta E \Delta t \geq \frac{\hbar}{2}, \tag{2.32}$$

with ΔE and Δt the uncertainties in energy and time, respectively. The vacuum cannot have zero energy, as this would imply a zero uncertainty in the value of the energy $\Delta E = 0$, which would violate Heisenberg's uncertainty principle. Therefore, the vacuum must have energy in the form of quantum fluctuations created by the need for a non-zero uncertainty in energy ΔE. Furthermore, these quantum energy fluctuations ΔE cannot take on any value but are constrained by how long the fluctuation lasts Δt. Thus, the energy of a quantum fluctuation is obtained by rewriting (2.32):

$$\Delta E \geq \frac{\hbar}{2\Delta t}. \tag{2.33}$$

The maximum amount of energy that a vacuum fluctuation can have may only exist in the minimum amount of time. From (2.33), it can be seen that energy would become infinite in the limit of zero time as $\Delta t \to 0$ causes $\Delta E \to \infty$. This can be avoided by noting that the smallest scale our current physical theories can probe is the Planck scale, which implies a lower limit to both space and time. This is denoted by the Planck length l_{Planck} and the Planck time t_{Planck}, which are constructed from the fundamental constants: Planck's constant $\hbar$, the universal gravitational constant G and the speed of light c. The Planck length is the minimum length that can be meaningfully studied while the Planck time is the time it takes light to travel one Planck length. The Planck length

l_{Planck} and the time t_{Planck} are thus mathematically defined as [8, 10]:

$$l_{\text{Planck}} = \sqrt{\frac{\hbar G}{c^3}} = 1.616 \times 10^{-35} \text{ m}, \tag{2.34}$$

$$t_{\text{Planck}} = \frac{l_{\text{Planck}}}{c} = \sqrt{\frac{\hbar G}{c^5}} = 5.319 \times 10^{-44} \text{ s}. \tag{2.35}$$

This Planck time acts as a temporal limit to the Heisenberg uncertainty principle. The largest energy fluctuation must therefore occur within the Planck time and can be defined as the Planck energy E_{Planck}. This is obtained by substituting the Planck time (2.35) into the Heisenberg uncertainty principle (2.33:

$$E_{\text{Planck}} \sim \frac{\hbar}{\Delta t} = \hbar\sqrt{\frac{c^5}{\hbar G}} = \sqrt{\frac{\hbar c^5}{G}} = 1.96 \times 10^{9} \text{ Joule}. \tag{2.36}$$

This may be used to determine the maximum energy density due to vacuum fluctuations. This should occur at the minimum volume, which is just the cube of the Planck length and is known as the Planck volume v_{Planck}:

$$v_{\text{Planck}} = (l_{\text{Planck}})^3 = \left(\sqrt{\frac{\hbar G}{c^3}}\right)^3 = \sqrt{\frac{\hbar^3 G^3}{c^9}} = 4.222 \times 10^{-105} \text{ m}^3. \tag{2.37}$$

The predicted vacuum energy density ρ_Λ is thus obtained by dividing the Planck energy E_{Planck} (2.36) by the Planck volume v_{Planck} (2.37):

$$\rho_{(\Lambda,\text{predicted})} = \frac{E_{\text{Planck}}}{v_{\text{Planck}}} = \sqrt{\frac{\hbar c^5}{G}\frac{c^9}{\hbar^3 G^3}} = \sqrt{\frac{c^{14}}{G^4\hbar^2}} = \frac{c^7}{G^2\hbar} \sim 10^{114} \text{ Joule.m}^{-3}. \tag{2.38}$$

This is an enormously large energy density. Conversely, the current measured value of the vacuum energy is much smaller and given by:

$$\rho_{(\Lambda,\text{measured})} = \frac{3H_0^2}{8\pi G}\Omega_{(\Lambda,0)} \sim 10^{-10} \text{ Joule.m}^{-3}. \tag{2.39}$$

The magnitude of the difference between the theoretical predicted vacuum energy $\rho_{(\Lambda,\text{predicted}}$ and the measured vacuum energy density is $(\rho_{(\Lambda,\text{measured})})$ is:

$$\frac{\rho_{(\Lambda,\text{predicted})}}{\rho_{(\Lambda,\text{measured})}} = \frac{10^{114} \text{ Joule.m}^{-3}}{10^{-10} \text{ Joule.m}^{-3}} \sim 10^{-10} \text{ Joule.m}^{-3} \sim 10^{124}. \tag{2.40}$$

Thus, the predicted energy density of the vacuum from quantum mechanics is over 120 orders of magnitude larger than the cosmologically measured value. This is also known as the vacuum catastrophe and has been referred to as the worst prediction in the history of physics [9]. The cosmological constant problem, therefore, casts doubt on dark energy being a cosmological constant, motivating research into alternative dark energy models [82].

2.6.2 The cosmic coincidence problem

The cosmic coincidence problem states that the dark matter and dark energy densities have the same order of magnitude at the present moment of cosmic history while differing with many orders of magnitude in the past and predicted future [83]. This is due to dark matter scaling as $\rho_{\text{dm}} \propto a^{-3}$ (2.5), while cosmological constant scales as $\rho_\Lambda \propto a^0$. This causes ρ_{dm} to vary greatly with time while ρ_Λ stays constant (as shown in Figure 2.7). Therefore, the distant past is completely dominated by dark matter ($\rho_{\text{dm}} \gg \rho_\Lambda$), while the distant future is dominated by dark energy ($\rho_\Lambda \gg \rho_{\text{dm}}$), but we happen to be observing the universe when the dark matter to dark energy ratio is approximately one to two. This coincidence seems unlikely, and a possible explanation to this problem would add more viability to any cosmological model [84].

The magnitude of this problem is indicated by the ratio $r = \frac{\rho_{\text{dm}}}{\rho_{\text{de}}}$. For conserved fluids (where $\rho_{\text{dm/de}}$ evolves according to (1.46)), as well as for the special ΛCDM case, this ratio is:

$$r = \frac{\rho_{\text{dm}}}{\rho_{\text{de}}} = \frac{\rho_{(\text{dm},0)} a^{-3(1+\omega_{\text{dm}})}}{\rho_{(\text{de},0)} a^{-3(1+\omega_{\text{de}})}} = r_0 a^{-3(\omega_{\text{dm}}-\omega_{\text{de}})} \quad ; \quad r_{\Lambda\text{CDM}} = \frac{\rho_{\text{dm}}}{\rho_\Lambda} = \frac{\rho_{(\text{dm},0)} a^{-3}}{\rho_{(\Lambda,0)}} = r_0 a^{-3}, \tag{2.41}$$

where $r_0 = \left(\rho_{(\text{dm},0)}/\rho_{(\text{de},0)}\right) = \left(\Omega_{(\text{dm},0)}/\Omega_{(\text{de},0)}\right)$ is the present ratio of dark matter to dark energy. To understand the order of magnitude of this problem, it is informative to calculate r at the Planck scale as an indicator of the amount of fine-tuning the ΛCDM model needs from initial conditions [82]. This may be done by considering that the cosmic microwave background (CMB) temperature scales as $T = T_0 a^{-1} \rightarrow a = \frac{T_0}{T}$ [9]. This ratio can then give the scale factor at the Planck scale:

$$a_{\text{Planck}} = \frac{T_0}{T_{\text{Planck}}}. \tag{2.42}$$

The current temperature of the CMB is $T_0 = 2.725\text{K}$ [72] and the temperature at the Planck scale is $T_{\text{Planck}} = \sqrt{\frac{\hbar c^5}{G k_B}} = 1.416 \times 10^{32}\text{K}$ [85]. Substituting (2.42) into (2.41) for the ΛCDM case ($\omega = -1; \Omega_{\text{dm}} = 0.266; \Omega_{\text{de}} = 0.685$), gives the size of the coincidence problem at the Planck scale:

$$r_{\text{Planck}} = r_0 a_{\text{Planck}}^{-3} = r_0 \left(\frac{T_0}{T_{\text{Planck}}}\right)^{-3} = \frac{0.266}{0.685} \left(\frac{2.725\text{K}}{1.416 \times 10^{32}\text{K}}\right)^{-3} = 5.1 \times 10^{94} \approx 10^{95}. \tag{2.43}$$

This indicates that the initial conditions of dark matter and dark energy should be fine-tuned to about 95 orders of magnitude to produce a universe where the two densities nearly coincide today, approximately 14 billion years later [86]. The magnitude of this problem for any specific model can be denoted by the constant ζ, which is defined from the relation:

$$r \propto r_0 a^{-\zeta}. \tag{2.44}$$

If $\zeta = 0$, then r is a constant throughout cosmic evolution, and the coincidence problem is solved. The magnitude of the deviation from $\zeta = 0$, indicates the magnitude of the coincidence problem (used from here on forward to denote cosmic coincidence problem) [82–84]. Thus for the ΛCDM case (2.41), the value of this constant is $\zeta_{\Lambda\text{CDM}} = 3$. Therefore, any model which has $\zeta > 3$ will worsen the coincidence problem, while $\zeta < 3$ alleviates the problem (relative to the ΛCDM model).

$$\zeta_{\Lambda\text{CDM}} = 3 \rightarrow \begin{cases} \zeta > 3 & \textit{worsens} \text{ the coincidence problem} \\ \zeta < 3 & \textit{alleviates} \text{ the coincidence problem} \\ \zeta = 0 & \textit{solves} \text{ the coincidence problem} \end{cases} \tag{2.45}$$

Furthmore, from the first equation in (2.41), we see that for the general case $\zeta = 3\,(\omega_{\text{dm}} - \omega_{\text{de}})$. This shows that the magnitude of the coinicidence problem is determined by the difference in the equation of state of dark matter ω_{dm} and dark energy ω_{de}, which causes the fluids to redshift and dilute at different rates. The coincidence problem would also be solved if $\zeta = 0$, which happens when $\omega_{\text{dm}} = \omega_{\text{de}}$. This may also be obtained if some exotic interaction causes dark matter and dark energy to redshift at the same rate, causing similar Effective equations of state, such that $\omega_{\text{dm}}^{\text{eff}} = \omega_{\text{de}}^{\text{eff}}$. Finally, if dark matter is pressureless $\omega_{\text{dm}} = 0$, then $\zeta = -3\omega_{\text{de}}$. This implies that models where $\omega_{\text{de}} > -1$ alleviate, while $\omega_{\text{de}} < -1$ worsen the coincidence problem. These models are known as Quintessence and phantom dark energy respectively and will be discussed shortly.

Therefore, the coincidence problem motivates research into dark matter and dark energy models that maintain a small or constant ratio r in either the past or future expansion.

2.6.3 The Hubble tension

The Hubble tension concerns the 4.4σ level discrepancy between values of the Hubble constant H_0, that the ΛCDM model predicts using data either from early time probes (mainly the Cosmic Microwave Background) and late time determinations using redshift and distances (mostly from Type Ia Supernovae using a calibrated local distance ladder) [87–89].

As we have mentioned, the Planck collaboration has measured the Hubble constant to be approximately $H_0 = 67.4 \pm 0.5\text{km s}^{-1}\text{Mpcs}^{-1}$ [4]. Conversely, recent measurements of Type Ia supernovae (calibrated with Cepheid variables) have obtained a best estimate for Hubble constant of $H_0 = 74.03 \pm 1.42\text{km s}^{-1}\text{Mpcs}^{-1}$ [90] in 2019 and more recently $H_0 = 73.0 \pm 1.4\text{km s}^{-1}\text{Mpcs}^{-1}$ in 2021 [91]. As measurements have become more accurate, this tension has only become greater. This discrepancy has hinted at new physics beyond the standard model. This problem has become one of the most relevant issues in all of cosmology. This may be seen from a recent review article on the problem and its possible solutions [88], which include over 1000 references while concluding that no specific proposal makes a strong case for solving this tension.

2.7 Quintessence and phantom dark energy

Due to these problems associated with the ΛCDM model, it has been proposed that dark energy might not be the cosmological constant Λ, but some other dynamical dark energy with $\omega \neq -1$. Due to the observed Cosmic acceleration, we still require $\omega < -1/3$. However, the equation of state may either be greater or smaller than $\omega = -1$, dividing these models broadly into either the quintessence or phantom regimes, respectively. For discussions on quintessence and phantom dark energy see [92–96]. This leads to a proposed fluid (usually in the form of a scalar field) with an energy density ρ_{de}, which evolves according to the conservation equation (1.46), such that:

$$\rho_{\text{de}} = \rho_{(\text{de},0)} a^{-3(1+\omega)} \begin{cases} -3(1+\omega) < 0 & \text{if} \quad -1 < \omega < -1/3 \quad \text{(quintessence)} \\ -3(1+\omega) > 0 & \text{if} \quad \omega < -1 \quad \text{(phantom).} \end{cases} \tag{2.46}$$

From (2.46), it can be seen that ρ_{de} decreases with expansion in the quintessence regime, while increasing in the phantom regime. Since ρ_{dm} decreases with expansion, quintessence alleviates, whilst phantom dark energy worsens The cosmic coincidence problem. Only measurements of the dark energy equation of state will tell us which regime is the best description of our universe (for recent observations, see [97, 98]). To understand the cosmological consequences of dynamical dark energy, it is worthwhile first to discuss some horizons in cosmology.

2.7.1 Particle horizon and Hubble distance

The largest physical distance that anything could have travelled since the big bang is limited by the speed of light, and that maximum travel radius is known as the particle horizon [8–11]. The physical distance to this horizon as measured by an observer at any time, is given by D_{horiz} [8]. A closely related phenomenon is the Hubble distance D_H, which defines the largest physical distance over which physical processes can operate coherently in the universe at any time [9].

$$D_{\text{horiz}} = c \int \frac{dt'}{a(t')} \qquad ; \qquad D_H = \frac{c}{H}. \tag{2.47}$$

This Hubble distance is in the same order as the particle horizon (proper distance to particle horizon D_p is approximately $D_p(t) \sim ct \sim cH^{-1} \sim D_H$) and may be called the horizon size [9]. The horizon size may denote the area which is causally connected in the universe[9]. Using the Friedmann equation (2.13) for a flat FLRW universe, as well as the relationship between energy density and the scale factor (1.46), we may determine a proportionality relationship between the horizon size H^{-1} and the scale factor:

$$H^2 \propto \rho \propto a^{-3(1+\omega)} \quad \rightarrow \quad H^{-1} \propto a^{3/2(1+\omega)} \quad \rightarrow \quad D_H \propto a^{\epsilon} \qquad \text{where } \epsilon = \frac{3}{2}(1+\omega) \tag{2.48}$$

This relationship may be used to determine how the horizon size evolved with the expansion history of the universe, such that:

$$D_H \propto a^{\epsilon} \begin{cases} \text{if} & \omega > -\frac{1}{3} \rightarrow & \epsilon > 1 & : & \text{Horizon size grows faster than scale factor} \\ \text{if} & -1 < \omega < -\frac{1}{3} \rightarrow & 0 < \epsilon < 1 & : & \text{Horizon size grows slower than scale factor} \\ \text{if} & \omega = -1 \rightarrow & \epsilon = 0 & : & \text{Horizon size constant as scale factor grows} \\ \text{if} & \omega < -1 \rightarrow & \epsilon < 0 & : & \text{Horizon size decreases as scale factor grows} \end{cases} \tag{2.49}$$

For the radiation ($\omega = 1/3 \rightarrow \epsilon = 2$) and matter ($\omega = 0 \rightarrow \epsilon = 3/2$) dominated eras, which constitute most of the expansion history of the universe, $\epsilon > 1$, which implies an exponential increase of horizon size with time. This has the physical consequence that the number of visible galaxies will grow as more galaxies enter the horizon [9, 95]. Contrary to this, during dark energy domination (in the quintessence regime $-1 < \omega < -1/3 \rightarrow 0 < \epsilon < 1$ and for a cosmological constant $\omega = -1 \rightarrow \epsilon = 1$) the horizon either stays constant or grows slower than the scale factor, causing distant galaxies to disappear beyond the cosmic horizon over time and become unobservable to us. Only gravitationally bound objects (such as the Milky Way and our local galactic cluster) will remain causally connected and observable in the distant future [95].

2.7.2 Big rip

A more dramatic consequence awaits phantom dark energy. This can be seen by considering how the Hubble distance d_H evolves for phantom energy. From (2.49) it is seen that during phantom dark energy domination ($\omega < -1 \rightarrow \epsilon < 0$), the horizon size decreases as the scale factor and expansion rate keeps growing. The disappearance of galaxies beyond the horizon will therefore be accelerated as the horizon closes in on us [95]. Since the horizon indicates the largest distance over which physical processes operate [9], the shrinking of the horizon will dissociate the structure of bound objects. As this horizon grows smaller and approaches the Planck scale, all gravitationally bound objects will be stripped apart. Eventually, even individual molecules and atoms will be ripped apart; effectively making all communication between any two parts impossible. This scenario is called the "big rip" singularity [94, 95]. The big rip is also characterised by both the energy density of dark energy and the scale factor becoming infinite $\rho_{\text{de}} \rightarrow \infty$; $a \rightarrow \infty$ in a finite amount of time t_{rip}, which indicates a late time singularity [10, 95]. The evolution of the scale factor and the time of the big rip singularity t_{rip} is calculated in Appendix E.1 and found to be:

$$t_{\text{rip}} \approx -\frac{2}{3H_0(1+\omega)\sqrt{1-\Omega_{(m,0)}}}. \tag{2.50}$$

This coincides with what was found by [95]. This rip behaviour can be seen by plotting the evolution of the scale factor and energy density against time; for models containing either a cosmological

constant; quintessence or phantom dark energy. All cosmological parameters are the same as in (2.25), except the dark energy equation of state ω. These are used to calculate the time of the big rip and the age for each model.

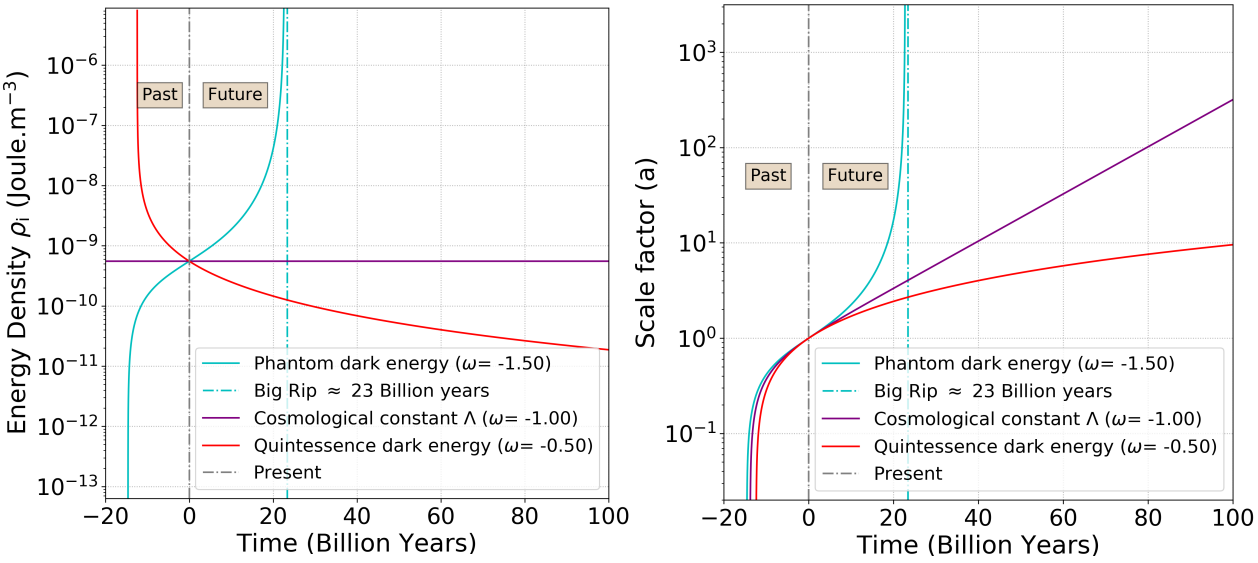

Figure 2.12: *Evolution of energy density and scale factor for quintessence and phantom dark energy universes (big rip)*

From the left panel in Figure 2.12 it can be seen that while a cosmological constant has a constant density with expansion, quintessence and phantom dark energy are dynamical instead. In the quintessence regime, the dark energy density has an exponential decay with expansion. Quintessence models will still have an accelerated expansion, but the acceleration rate will decrease with time, relative to a cosmological constant. Conversely, in the phantom model, the energy density increases exponentially with time, resulting in an increase of the rate of the accelerated expansion. This continues until both the energy density and the scale factor becomes infinite at time $t_{\text{rip}} \approx 23$ billion years, which coincides with the rip age for $\omega = -1.5$, calculated in [95]. It can also be seen from the right panel in Figure 2.12 that quintessence models predict a younger age for the universe (age $\approx$ 12.4 billion years), while the phantom model predicts an older age (age $\approx$ 14.6 billion years), relative to the ΛCDM model (age $\approx$ 13.8 billion years).

It should be noted that if the validity of phantom dark energy models is considered, special attention should be paid to how these models violate the Energy conditions of general relativity and the consequences of doing so [41].

Quintessence and phantom dark energy models open up an entirely new world of possibilities for what dark energy could be, beyond the cosmological constant Λ. For our purposes, we will now consider a specific set of dynamical dark energy models which could alleviate and even solve The cosmic coincidence problem, while being a potential candidate for addressing the The Hubble tension. These models have a non-gravitational interaction between dark matter and dark energy.

CHAPTER 3

Interacting dark energy models

3.1 Interactions between dark matter and dark energy

Thus far, we have assumed that the various Components of the universe are separately conserved and only interact gravitationally with each other on cosmological scales. This assumption is especially reasonable in the case of baryonic matter, for which strong constraints have been imposed on a 'fifth-force' beyond gravity, electromagnetism and the strong and weak nuclear forces [99]. Furthermore, a new significant interaction with photons would probably cause deviations from photons following a geodesic path, contradicting measurements from solar eclipses [82]. This leaves us with the possibility of non-gravitational interactions between the two dark sectors, which dominate the energy density of the universe; dark matter (DM) and dark energy (DE) [83, 100].

The properties of both dark matter and dark energy are not well constrained, so it is not unreasonable to assume that they might have, as of yet, undiscovered interactions amongst themselves. If there is an interaction in the dark sector, it cannot be too strong since the ΛCDM has no interaction and is incredibly successful [4, 82]. The nature of any such interaction might be hinted at from the Problems with the ΛCDM model, especially The cosmic coincidence problem. This problem could be addressed by proposing a coupling between dark matter and dark energy, which could stabilise the ratio of the two throughout expansion history.

A coupling between dark matter and dark energy may be proposed in which dark matter and dark energy are not separately conserved, but the energy (and momentum) of the total dark sector

is conserved. These are known as interacting dark energy models (IDE). This conservation of the dark sector is expressed mathematically from the conservation equation (1.46) for both fluids:

$$\dot{\rho}_{\rm dm} + \dot{\rho}_{\rm de} + 3H\left(\rho_{\rm dm} + \rho_{\rm de} + P_{\rm dm} + P_{\rm de}\right) = 0. \tag{3.1}$$

This total conservation equation may be decoupled into separate equations for dark matter and dark energy by assuming an arbitrary interaction equation Q. This creates a mechanism where the components can exchange energy (or momentum) in a non-gravitational way, such that dark matter and dark energy have the following separate conservation equations [82, 84, 87, 101–109]:

$$\dot{\rho}_{\rm dm} + 3H\left(\rho_{\rm dm} + P_{\rm dm}\right) = Q \qquad ; \qquad \dot{\rho}_{\rm de} + 3H\left(\rho_{\rm de} + P_{\rm de}\right) = -Q. \tag{3.2}$$

We will still assume pressure-less dark matter ($P_{\rm dm} = 0 \rightarrow \omega_{\rm dm} = 0$), and note that baryonic matter $\omega_{\rm bm} = 0$ and radiation $\omega_{\rm r} = 1/3$ are uncoupled $Q = 0$, as in the ΛCDM model. We thus have the following conservation equations for interacting dark energy models:

$$\begin{aligned} \dot{\rho}_{\rm dm} + 3H\rho_{\rm dm} = Q \qquad &; \qquad \dot{\rho}_{\rm de} + 3H\rho_{\rm de}(1+\omega) = -Q, \\ \dot{\rho}_{\rm bm} + 3H\rho_{\rm bm} = 0 \qquad &; \qquad \dot{\rho}_{\rm r} + 3H\rho_{\rm r}(1+1/3) = 0. \end{aligned} \tag{3.3}$$

The dark energy equation of state ($\omega_{\rm de} = \omega$ from here onwards) is left as a free variable, since the dark energy may be either vacuum energy ($\omega = -1$), in the quintessence ($-1 < \omega < -1/3$) or phantom ($\omega < -1$) regime. Here Q is an arbitrary coupling function whose sign determines how energy (or momentum) is transferred between dark energy and dark matter. If $Q > 0$, then the energy (or momentum) is transferred from dark energy to dark matter and vice versa for $Q < 0$, such that [82, 84, 87, 101–109]:

$$Q = \begin{cases} > 0 & \text{Dark Energy} \rightarrow \text{Dark Matter (iDEDM regime)} \\ < 0 & \text{Dark Matter} \rightarrow \text{Dark Energy (iDMDE regime)} \\ = 0 & \text{No interaction.} \end{cases} \tag{3.4}$$

Here we have denoted the interacting case where energy flows from dark energy to dark matter ($Q > 0$) as the interacting Dark Energy Dark Matter regime (iDEDM), and vice versa as the interacting Dark Matter Dark Energy regime (iDMDE) [109]. Since there is currently no fundamental theory for the coupling equation Q, the coupling in most works is purely phenomenologically motivated; and must be tested against observations [82, 84, 87, 101–106, 108, 109]. The coupling is thus freely chosen, but we will only consider models where the coupling function Q is either proportional to the dark matter or the dark energy density, which could have a strong field theoretical ground [110]. The core publications we considered for these types of models are [101, 103, 104]. For recent developments and observational constraints see [87, 105–110]; and for comprehensive review articles on interacting dark energy, see [82, 84]. Before examining any specific models, we will discuss some general features that hold for interaction function Q.

3.2 Properties of interacting dark energy models

3.2.1 Effective equations of state

An informative approach to understanding the effect of a coupling in the dark sector, is to define a dynamical effective equation of state parameter $\omega_{\rm dm}^{\rm eff}$ and $\omega_{\rm de}^{\rm eff}$, for dark matter and dark energy respectively. These effective equations of state may be used to describe the background equations which are equivalent to (3.3) for the uncoupled case ($Q = 0$), such that [84, 101–103]:

$$\dot{\rho}_{\rm dm} + 3H\rho_{\rm dm}(1 + \omega_{\rm dm}^{\rm eff}) = 0 \qquad ; \qquad \dot{\rho}_{\rm de} + 3H\rho_{\rm de}(1 + \omega_{\rm de}^{\rm eff}) = 0. \tag{3.5}$$

The energy densities $\rho_{\rm dm/de}$ should thus evolve according to (1.46) with $\omega = \omega_{\rm dm/de}^{\rm eff}$:

$$\rho_{\rm dm} = \rho_{\rm (dm,0)} a^{-3(1+\omega_{\rm dm}^{\rm eff})} \qquad ; \qquad \rho_{\rm de} = \rho_{\rm (de,0)} a^{-3(1+\omega_{\rm de}^{\rm eff})} \tag{3.6}$$

It can therefore be seen that the effective equations of state will determine the rate at which the fluids redshift. Rewriting (3.5) and substituting in (3.3), gives an expression for the $\omega_{\rm dm}^{\rm eff}$ in terms of the interaction term Q:

$$\begin{aligned} \dot{\rho}_{\rm dm} + 3H\rho_{\rm dm} + 3H\rho_{\rm dm}\omega_{\rm dm}^{\rm eff} &= 0 \\ Q + 3H\rho_{\rm dm}\omega_{\rm dm}^{\rm eff} &= 0 \\ \rightarrow \omega_{\rm dm}^{\rm eff} &= -\frac{Q}{3H\rho_{\rm dm}}. \end{aligned} \tag{3.7}$$

Similarly, for dark energy, we first rewrite (3.3)

$$\dot{\rho}_{\rm de} + 3H\rho_{\rm de} = -Q - 3H\rho_{\rm de}\omega_{\rm de}. \tag{3.8}$$

Rewriting (3.5) and substituting (3.8) in, gives an expression for the $\omega_{\rm de}^{\rm eff}$ in terms of the interaction term Q, such that:

$$\begin{aligned} \dot{\rho}_{\rm de} + 3H\rho_{\rm de} + 3H\rho_{\rm de}\omega_{\rm de}^{\rm eff} &= 0 \\ -Q - 3H\rho_{\rm de}\omega_{\rm de} + 3H\rho_{\rm de}\omega_{\rm de}^{\rm eff} &= 0 \\ \rightarrow \omega_{\rm de}^{\rm eff} &= \omega_{\rm de} + \frac{Q}{3H\rho_{\rm de}}. \end{aligned} \tag{3.9}$$

Comparing (3.6) and (3.8) to the uncoupled equations of state (noting $\omega_{\rm dm} = 0$), the effects of an interaction may be understood to imply that if [84, 102, 103]:

$$Q > 0 \text{ (iDEDM)} \begin{cases} \omega_{\text{dm}}^{\text{eff}} < 0 & \text{Dark matter redshifts } \textit{slower} \text{ than } \text{a}^{-3} \text{ (less DM in past)}, \\ \omega_{\text{de}}^{\text{eff}} > \omega_{\text{de}} & \text{Dark energy has } \textit{less} \text{ accelerating pressure}, \end{cases} \tag{3.10}$$

$$Q < 0 \text{ (iDMDE)} \begin{cases} \omega_{\text{dm}}^{\text{eff}} > 0 & \text{Dark matter redshifts } \textit{faster} \text{ than } \text{a}^{-3} \text{ (more DM in past)}, \\ \omega_{\text{de}}^{\text{eff}} < \omega_{\text{de}} & \text{Dark energy has } \textit{more} \text{ accelerating pressure}. \end{cases} \tag{3.11}$$

This implies that even if $\omega_{\text{de}} = -1$, when $Q < 0$ or $Q > 0$, then the dark energy may behave like either uncoupled quintessence $\omega_{\text{de}}^{\text{eff}} > -1$ or uncoupled phantom $\omega_{\text{de}}^{\text{eff}} < -1$ dark energy respectively. If there is no interaction between dark matter and dark energy ($Q = 0$), the effective equations of state reduces back to the uncoupled model, such that $\omega_{\text{dm}}^{\text{eff}} = \omega_{\text{dm}} = 0$ and $\omega_{\text{de}}^{\text{eff}} = \omega_{\text{de}}$.

3.2.2 Addressing the coincidence problem

These effective equations of state allow us to make predictions regarding the consequences of a dark coupling; and why it is introduced to address The cosmic coincidence problem. This can be seen by considering the ratio r_{IDE} of ρ_{dm} to ρ_{de} from (3.6) for interacting dark energy models:

$$r_{\text{IDE}} = \frac{\rho_{\text{dm}}}{\rho_{\text{de}}} = \frac{\rho_{(\text{dm},0)} a^{-3(1+\omega_{\text{dm}}^{\text{eff}})}}{\rho_{(\text{de},0)} a^{-3(1+\omega_{\text{de}}^{\text{eff}})}} = r_0 a^{-\zeta_{\text{IDE}}} \quad ; \quad \text{with} \quad \zeta_{\text{IDE}} = 3\left(\omega_{\text{dm}}^{\text{eff}} - \omega_{\text{de}}^{\text{eff}}\right), \tag{3.12}$$

with ζ indicating the magnitude of the coincidence problem as introduced in (2.44). Thus, from (3.13) and (3.12), we see that the smaller the difference between $\omega_{\text{dm}}^{\text{eff}}$ and $\omega_{\text{de}}^{\text{eff}}$ the more the coincidence problem will be alleviated, while being solved if $\zeta = 0$, which happens when $\omega_{\text{dm}}^{\text{eff}} = \omega_{\text{de}}^{\text{eff}}$. This can be achieved if dark matter redshifts slower $\omega_{\text{dm}}^{\text{eff}} < \omega_{\text{dm}}$ and dark energy redshifts faster $\omega_{\text{de}}^{\text{eff}} > \omega_{\text{de}}$, which coincides with the iDEDM ($Q > 0$) scenario.

In the iDEDM ($Q > 0$) scenario, energy flows away from DE, causing ρ_{de} to redshift faster $\omega_{\text{de}}^{\text{eff}} > \omega_{\text{de}}$ and decrease with expansion. The DM in turn receives this lost energy, which causes ρ_{dm} to redshift and dilute at a slower rate $\omega_{\text{dm}}^{\text{eff}} < \omega_{\text{dm}}$. Both fluids in this scenario dilute with expansion and redshift at a more similar rate, which is indicated by the smaller difference $(\omega_{\text{dm}}^{\text{eff}} - \omega_{\text{de}}^{\text{eff}})$, relative to the uncoupled case. This has the immediate consequence of alleviating the coincidence problem (3.12). Thus, in the extreme case when $\omega_{\text{dm}}^{\text{eff}} = \omega_{\text{de}}^{\text{eff}}$; DM and DE redshift at the same rate, fixing the ratio of DM to DE $r \propto a^0 \rightarrow \zeta = 0$, effectively solving the coincidence problem. The opposite holds for the iDMDE ($Q < 0$) scenario, where energy flows away from DM, causing DM to redshift and dilute at a faster rate. Conversely, DE receives energy and the density increases with expansion. This leads to an even bigger difference in the rate at which DM and DE redshifts, indicated by the larger difference in $(\omega_{\text{dm}}^{\text{eff}} - \omega_{\text{de}}^{\text{eff}})$. Thus, iDMDE models will worsen the coincidence problem.

From (3.10),(3.11) and (3.12), while noting that $\zeta_{\Lambda\text{CDM}} = 3$, we may conclude:

$$\zeta_{\text{IDE}} = 3\left(\omega_{\text{dm}}^{\text{eff}} - \omega_{\text{de}}^{\text{eff}}\right) \begin{cases} Q > 0 \text{ (iDEDM):} & \zeta_{\text{IDE}} < \zeta_{\Lambda\text{CDM}} \quad \textit{alleviates} \text{ coincidence problem,} \\ Q < 0 \text{ (iDMDE):} & \zeta_{\text{IDE}} > \zeta_{\Lambda\text{CDM}} \quad \textit{worsens} \text{ coincidence problem.} \end{cases} \tag{3.13}$$

3.2.3 Cosmological implications of a dark coupling

Besides addressing the coincidence problem, IDE models have other far reaching cosmological consequences. Since $\omega_{\text{dm}}^{\text{eff}} < 0$ for iDEDM, DM redshifts *slower*, which leads to *less* DM in the past and the radiation-matter equality happening *later* [103]. Similarly, $\omega_{\text{de}}^{\text{eff}} > \omega_{\text{de}}$, such that DE redshifts faster, causing *more* DE in the past. Less DM and more DE in the past, has the consequence that both the cosmic jerk and the matter-dark energy equality happens *earlier* in cosmic history. From the Friedmann equation (2.13), we can see that this overall suppression of dark matter density causes a lower value of the Hubble parameter at late times. This lower value of H_0, worsens the Hubble tension with regard to late time probes [109] (see [87, 105, 106, 108, 109] for how IDE models address the Hubble tension). Since the Hubble parameter; and therefore the expansion rate is lower, throughout most of expansion, the universe must have taken a longer time to reach its current size. Since more time was needed to reach current conditions, the universe should also be *older*. The opposite of this holds for iDMDE scenario. These various consequences of a coupling in the dark sector, is summarised in Table 3.1 below:

Table 3.1: *Consequences of interacting dark energy models (relative to uncoupled models)*

	$Q > 0$	$Q < 0$
Energy flow	DE $\rightarrow$ DM (iDEDM)	DM $\rightarrow$ DE (iDMDE)
Effective equations of state	$\omega_{\text{dm}}^{\text{eff}} < \omega_{\text{dm}}$; $\omega_{\text{de}}^{\text{eff}} > \omega_{\text{de}}$	$\omega_{\text{dm}}^{\text{eff}} > \omega_{\text{dm}}$; $\omega_{\text{de}}^{\text{eff}} < \omega_{\text{de}}$
Coincidence problem	Alleviates ($\zeta_{\text{IDE}} < \zeta_{\Lambda\text{CDM}}$)	Worsens ($\zeta_{\text{IDE}} > \zeta_{\Lambda\text{CDM}}$)
Hubble tension	Worsens	Alleviates
Age of universe	Older	Younger
Radiation-matter equality	Later ($z_{\text{IDE}} < z_{\Lambda\text{CDM}}$)	Earlier ($z_{\text{IDE}} > z_{\Lambda\text{CDM}}$)
Cosmic jerk ($q = 0$)	Earlier ($z_{\text{IDE}} > z_{\Lambda\text{CDM}}$)	Later ($z_{\text{IDE}} < z_{\Lambda\text{CDM}}$)
Matter-dark energy equality	Earlier ($z_{\text{IDE}} > z_{\Lambda\text{CDM}}$)	Later ($z_{\text{IDE}} < z_{\Lambda\text{CDM}}$)

These implications will only hold if the IDE model is viable. Any cosmological model may be considered unviable due to theoretical concerns, such as internal inconsistencies, instabilities, negative energy densities etc. A model that is free of these problems can only be deemed viable if it meets observational constraints, such as predicting an expansion history that coincides with cosmological data. This chapter will consider theoretical constraints before constraining our models with cosmological data in the next chapter.

3.2.4 Instabilities and the doom factor

The coupling between the dark sectors will influence the evolution of dark matter and dark energy perturbations. A complete perturbation analysis of these models is not within the scope of this study but can be found in [101] and [103]. For our purposes, we only want to know what combination of parameters may be used to avoid instabilities. This can be found in [103], by introducing the so-called doom factor **d**:

$$\mathbf{d} = \frac{Q}{3H\rho_{\rm de}(1+\omega)}. \tag{3.14}$$

This is called the doom factor since this factor is proportional to the coupling function Q and may induce non-adiabatic instabilities in the evolution of the dark energy perturbations [103]. The sign of **d** will determine if there is an early time instability. It was shown that if the doom factor is positive and large $\mathbf{d} > 1$; the dark energy perturbations will become dominated by the terms which are dependent on the coupling function Q, leading to a runaway; unstable growth regime [103]. As long as $\mathbf{d} < 0$, the model should be free of non-adiabatic instabilities at large scales. This doom factor can therefore provide the range of parameters that will give a priori stable universe, as is often done in literature [87, 103, 105, 106, 108, 109].

It should be noted that IDE models may often suffer from negative energy densities, depending on the interaction function Q and cosmological parameters chosen. We will consider models with negative energy densities as unphysical. To see whether IDE models can solve the coincidence problem while being physically viable, we need to investigate how the energy density of dark matter and dark energy evolves.

3.2.5 Evolution of energy densities and phase portraits

Since the coupling function Q is phenomenologically motivated, many different interaction functions exist, which could either be simple linear or complex non-linear interactions [82, 84]. This often leads to difficulties when trying to solve the coupled conservation equations (3.3) to obtain analytical expressions for how $\rho_{\rm dm}$ and $\rho_{\rm de}$ evolve. It is therefore informative to consider how the derivatives of the density parameters $\dot{\Omega}_{\rm x}$ evolve for any arbitrary coupling Q. This can be used to obtain phase portraits with flow lines in the ($\Omega_{\rm dm}$, $\Omega_{\rm de}$)-plane that has attractor and repulsor points. These attractor and repulsor points can tell us about how the ratio of DM to DE evolves and indicate whether the coupling solves the coincidence problem. Furthermore, these phase portraits can also tell us if the DM or DE energy densities become negative at any points, which indicates that the interaction Q is unphysical.

For this analysis, we will consider models which contain radiation $\Omega_{\rm r}$, baryonic matter $\Omega_{\rm bm}$, dark

matter$\Omega_{\rm dm}$ and dark energy $\Omega_{\rm de}$. This may be done by first considering how the density parameters evolve with time, which is done by taking the derivative of $\Omega_{\rm x}$ from (1.47), giving:

$$\dot{\Omega}_x = \left[\frac{8\pi\dot{G}}{3H^2}\rho_x\right] = \frac{8\pi G}{3}\left[\frac{\dot{\rho_x}}{H^2} - \rho\frac{2\dot{H}}{H^3}\right] = \frac{8\pi G}{3H^2}\left[\dot{\rho_x} - \rho\frac{2\dot{H}}{H}\right]. \tag{3.15}$$

From the conservation equations for interacting dark energy models (3.3) we have:

$$\dot{\rho}_{\rm x} = -3H\rho_{\rm x}(1+\omega_x) \pm Q, \tag{3.16}$$

where $\pm = +$ for $x =$dm and $\pm = -$ for $x =$de. Substituting (3.16) into (3.15) gives:

$$\begin{aligned}\dot{\Omega}_x &= \frac{8\pi G}{3H^2}\left[-3H\rho_{\rm x}(1+\omega_x) \pm Q - \rho_x\frac{2\dot{H}}{H}\right] \\ &= \frac{8\pi G}{3H^2}\rho_x H\left[-3(1+\omega_x) - \frac{2\dot{H}}{H^2}\right] \pm \frac{8\pi G}{3H^2}Q.\end{aligned} \tag{3.17}$$

Where we also have that:

$$\begin{aligned}\dot{H} &= \frac{d}{dt}\dot{a}a^{-1} = \frac{\ddot{a}}{a} - \left(\frac{\dot{a}}{a}\right)^2 \\ \rightarrow \frac{\dot{H}}{H^2} &= \frac{\ddot{a}a}{a^2} - 1 = -q - 1.\end{aligned} \tag{3.18}$$

Substituting (3.18) and $\rho_{\rm x} = \frac{3H^2}{8\pi G}\Omega_{\rm x}$ into (3.17) gives:

$$\begin{aligned}\dot{\Omega}_x &= \Omega_{\rm x}H\left[-3(1+\omega_x) + 2q + 1\right] \pm \frac{8\pi G}{3H^2}Q \\ &= \Omega_{\rm x}H\left[2q - 1 - 3\omega_x\right] \pm \frac{8\pi G}{3H^2}Q.\end{aligned} \tag{3.19}$$

Here we note that the deceleration parameter q for IDE models is obtained from (2.16), such that:

$$\begin{aligned}q &= \frac{1}{2}\left[\Omega_{\rm r}\left(1+3\omega_{\rm r}\right) + \Omega_{\rm bm}\left(1+3\omega_{\rm bm}\right) + \Omega_{\rm dm}\left(1+3\omega_{\rm dm}\right) + \Omega_{\rm de}\left(1+3\omega\right)\right] \\ q &= \frac{1}{2}\left[\Omega_{\rm r}\left(1+3\left(\frac{1}{3}\right)\right) + \Omega_{\rm bm}\left(1+3\left(0\right)\right) + \Omega_{\rm dm}\left(1+3\left(0\right)\right) + \Omega_{\rm de}\left(1+3\omega\right)\right] \\ q &= \Omega_{\rm r} + \frac{1}{2}\Omega_{\rm bm} + \frac{1}{2}\Omega_{\rm dm} + \frac{1}{2}\Omega_{\rm de}\left(1+3\omega\right).\end{aligned} \tag{3.20}$$

Substituting in the expression for the deceleration parameter q (3.20) gives:

$$\begin{aligned}\dot{\Omega}_x &= \Omega_{\rm x}H\left[2\left(\Omega_{\rm r} + \frac{1}{2}\Omega_{\rm bm} + \frac{1}{2}\Omega_{\rm dm} + \frac{1}{2}\Omega_{\rm de}\left(1+3\omega_{\rm de}\right)\right) - 1 - 3\omega_x\right] \pm \frac{8\pi G}{3H^2}Q \\ &= \Omega_{\rm x}H\left[2\Omega_{\rm r} + \Omega_{\rm bm} + \Omega_{\rm dm} + \Omega_{\rm de}\left(1+3\omega_{\rm de}\right) - 1 - 3\omega_x\right] \pm \frac{8\pi G}{3H^2}Q.\end{aligned} \tag{3.21}$$

This relation holds for either dark matter or dark energy, with any coupling function Q. If $Q = 0$, this reduces back to the same expression for the uncoupled case and may be used, not only for dark matter and dark energy, but for radiation ($\omega_r = 1/3$) and baryonic matter ($\omega_{\rm bm} = 0$) as well. For the different components one therefore has:

$$\begin{aligned}
\dot{\Omega}_{\rm de} &= \Omega_{\rm de} H \left[2\Omega_{\rm r} + \Omega_{\rm bm} + \Omega_{\rm dm} + \Omega_{\rm de}\left(1 + 3\omega_{\rm de}\right) - 1 - 3\omega_{\rm de}\right] - \frac{8\pi G}{3H^2} Q, \\
\dot{\Omega}_{\rm dm} &= \Omega_{\rm dm} H \left[2\Omega_{\rm r} + \Omega_{\rm bm} + \Omega_{\rm dm} + \Omega_{\rm de}\left(1 + 3\omega_{\rm de}\right) - 1\right] + \frac{8\pi G}{3H^2} Q, \\
\dot{\Omega}_{\rm bm} &= \Omega_{\rm bm} H \left[2\Omega_{\rm r} + \Omega_{\rm bm} + \Omega_{\rm dm} + \Omega_{\rm de}\left(1 + 3\omega_{\rm de}\right) - 1\right], \\
\dot{\Omega}_{\rm r} &= \Omega_{\rm r} H \left[2\Omega_{\rm r} + \Omega_{\rm bm} + \Omega_{\rm dm} + \Omega_{\rm de}\left(1 + 3\omega_{\rm de}\right) - 2\right].
\end{aligned} \tag{3.22}$$

Equation (3.21) reduces back to the ΛCDM case if $Q = 0$ and $\omega_{\rm de} = -1$, which can be found in [9]. For our purposes, we are interested in the parameter space of how dark matter and dark energy evolve with regard to each other. This can be obtained by dividing corresponding dark matter $\dot{\Omega}_{\rm dm}$ and dark energy $\dot{\Omega}_{\rm de}$ evolution equations (3.22) by each other, such that:

$$\frac{d\Omega_{\rm de}}{d\Omega_{\rm dm}} = \frac{\Omega_{\rm de} H \left[2\Omega_{\rm r} + \Omega_{\rm bm} + \Omega_{\rm dm} + \Omega_{\rm de}\left(1 + 3\omega_{\rm de}\right) - 1 - 3\omega_{\rm de}\right] - \frac{8\pi G}{3H^2} Q}{\Omega_{\rm dm} H \left[2\Omega_{\rm r} + \Omega_{\rm bm} + \Omega_{\rm dm} + \Omega_{\rm de}\left(1 + 3\omega_{\rm de}\right) - 1\right] + \frac{8\pi G}{3H^2} Q}. \tag{3.23}$$

This can be used to obtain a set of trajectories or flow lines in the ($\Omega_{\rm dm}$, $\Omega_{\rm de}$)-plane, which in turn have stable attractor and unstable repulsor points. These will be used to see if the ratio of dark matter to dark energy becomes fixed in the past or present, thus addressing the model's potential to solve the coincidence problem. Before considering any IDE models, we will first show how these phase portraits work for the ΛCDM model, as this will be the standard model to which we will compare our later results.

3.2.6 Phase portrait primer: ΛCDM model

For the ΛCDM case there is no coupling ($Q = 0$) and the dark energy is a cosmological constant ($\omega_{\rm de} = \omega_\Lambda = -1$), so (3.23) becomes:

$$\frac{d\Omega_\Lambda}{d\Omega_{\rm dm}} = \frac{\Omega_\Lambda \left[2\Omega_{\rm r} + \Omega_{\rm bm} + \Omega_{\rm dm} - 2\Omega_\Lambda + 2\right]}{\Omega_{\rm dm} \left[2\Omega_{\rm r} + \Omega_{\rm bm} + \Omega_{\rm dm} - 2\Omega_\Lambda - 1\right]}. \tag{3.24}$$

Noting that baryonic matter may be grouped with dark matter ($\Omega_{\rm bm} + \Omega_{\rm dm} = \Omega_m$) and assuming negligible radiation $\Omega_{\rm r} = 0$ (during matter and dark energy domination), the evolution of matter and dark energy with regard to one another can be analysed more clearly, thus (3.24) becomes:

$$\frac{d\Omega_\Lambda}{d\Omega_m} = \frac{\Omega_\Lambda \left[\Omega_m - 2\Omega_\Lambda + 2\right]}{\Omega_m \left[\Omega_m - 2\Omega_\Lambda - 1\right]}. \tag{3.25}$$

Using (3.25), the evolution of matter and dark energy may now be expressed with a phase portrait in the (Ω_m, Ω_Λ)-plane:

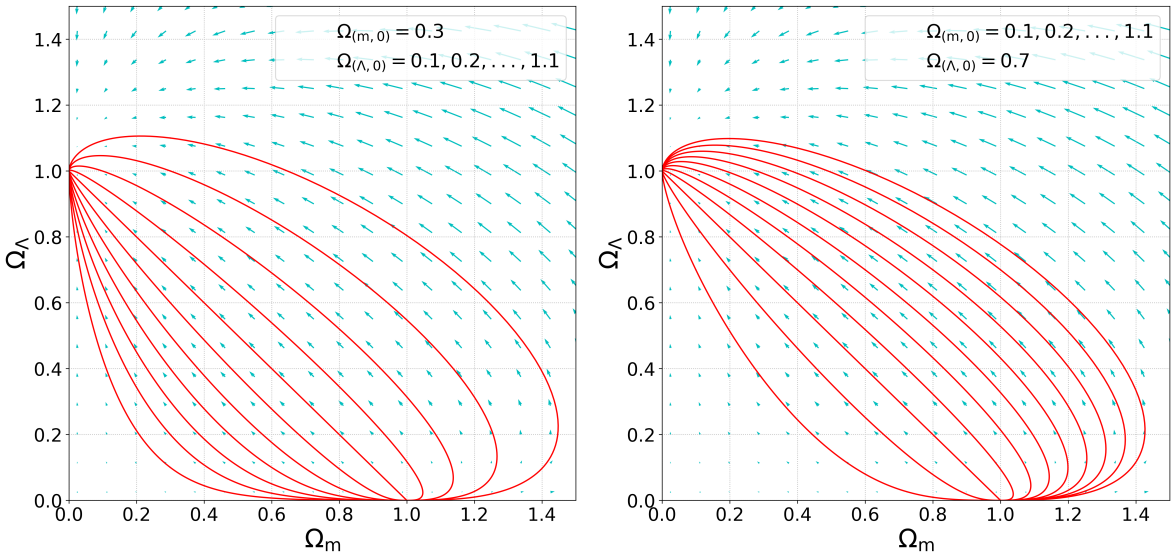

Figure 3.1: *Phase portraits for* $\Omega_{\rm dm}$ *and* $\Omega_{\rm de}$ *(*Λ*CDM)*

Every point on the plane defines a unique trajectory (as indicated by the blue arrows). However, for convenience, we have specified different trajectories (red lines) which pass through specific values for the present dark matter and dark energy densities. In the left hand panel of Figure 3.1, trajectories pass through the points $\Omega_{(\mathrm{m},0)} = 0.3$ and $\Omega_{(\Lambda,0)} = 0.1, 0.2, ..., 1.1$, while in the right hand panel the trajectories passes through $\Omega_{(\mathrm{m},0)} = 0.7$ and $\Omega_{(\mathrm{m},0)} = 0.1, 0.2, ..., 1.1$. These values have been chosen to reproduce the figures found in [9]. These various trajectories all have the same equilibrium points, which are calculated in Appendix B.1 as:

$$(\Omega_m, \Omega_\Lambda)_- = (1, 0) \qquad ; \qquad (\Omega_m, \Omega_\Lambda)_+ = (1, 0)\,. \tag{3.26}$$

From Figure 3.1, it can be seen that each of the trajectories start at $(1, 0)$, which is an unstable repulsor point from which all the trajectories diverge. Finally, these paths all converge again at the stable point $(0, 1)$, which is known as an attractor [9]. This implies that for a wide range of present cosmological parameters, each universe model starts with complete matter domination $(\Omega_\mathrm{m}, \Omega_\Lambda)_-$=$(1, 0)$ and evolves differently, but always ends up with complete dark energy domination $(\Omega_\mathrm{m}, \Omega_\Lambda)_+$=$(0, 1)$ [9]. This behaviour coincides with Figures 2.7, 2.8, 2.9, 2.10 and 2.11. These equilibrium points also highlight the coincidence problem, as the ratio of their coordinates indicate which value r tends to in the past r_- or the future r_+:

$$r_- = \frac{\Omega_{(\mathrm{m},-)}}{\Omega_{(\Lambda,-)}} = \frac{1}{0} \to \infty \qquad ; \qquad r_+ = \frac{\Omega_{(\mathrm{m},+)}}{\Omega_{(\Lambda,+)}} = \frac{0}{1} \to 0. \tag{3.27}$$

From (3.27), we can see that the ratio of DM to DE tends to $r_- \to \infty$ in the past, whilst approaching $r_+ \to 0$ in the future. This again indicates the magnitude of the coincidence problem for the ΛCDM model. IDE models that can find a constant non-zero or non-infinite value, for either r_- or r_+, should solve the coincidence problem in either the past or the future, respectively.

3.3 Interaction model 1: $Q_1 = \delta H \rho_{\rm dm}$

Now that the general properties of IDE models have been discussed, we will move on to two case studies. This will show that these properties hold for different coupling functions Q while highlighting significant differences between the couplings. First, we will consider two of the most common IDE models in literature, where we have a linear coupling function Q proportional to either the dark matter or dark energy density. These couplings will have the form:

$$Q_1 = \delta H \rho_{\rm dm} \quad ; \quad Q_2 = \delta H \rho_{\rm de}, \tag{3.28}$$

where H is the Hubble parameter and δ is a dimensionless coupling constant which determines the strength of the interaction between dark matter and dark energy [84, 103, 104]. It should be noted that the coupling constant δ is often indicated by α [101, 102] (which has an opposite sign to δ) or ξ in the literature [82, 87, 105, 106, 108, 109]. For these models we assume that $\delta < -3\omega$ (so that the coupling strength $|\delta|$ is not too strong [101]) This condition implies $(\delta < -3\omega) \rightarrow (\delta + 3\omega < 0)$. Furthermore, since we require that $H > 0$; $\rho_{\rm dm} > 0$; $\rho_{\rm de} > 0$ the sign of δ will determine the direction of energy flow. Therefore, $\delta > 0 \rightarrow Q > 0$ corresponds to the iDEDM regime and $\delta < 0 \rightarrow Q < 0$ to the iDMDE regime. The greatest qualitative difference between the two coupling functions, is that $Q_1 \propto \rho_{\rm dm}$ and $Q_2 \propto \rho_{\rm de}$, which implies that the effect of the coupling will be either most prominent during early dark matter domination, or later dark energy domination respectively. For all subsequent figures and calculations we use cosmological parameters (2.25), with $\delta = 0.25$ for (iDEDM) and $\delta = -0.25$ for (iDMDE), while temporarily choosing $\omega_{\rm de} = \omega = -1$, so that the coupling is the only variable that differs from the ΛCDM model, thus easing comparisons.

3.3.1 Phase portraits - $Q_1 = \delta H \rho_{\rm dm}$

We start by considering the phase portrait for Q_1, before moving onto analytical expressions for how the energy densities evolve. Assuming the coupling $Q_1 = \delta H \rho_{\rm dm}$, equation (3.22) becomes:

$$\begin{aligned} \frac{d\Omega_{\rm de}}{d\Omega_{\rm dm}} &= \frac{\Omega_{\rm de} H \left[2\Omega_{\rm r} + \Omega_{\rm bm} + \Omega_{\rm dm} + \Omega_{\rm de}\left(1 + 3\omega_{\rm de}\right) - 1 - 3\omega_{\rm de}\right] - \frac{8\pi G}{3H^2}\left(\delta H \rho_{\rm dm}\right)}{\Omega_{\rm dm} H \left[2\Omega_{\rm r} + \Omega_{\rm bm} + \Omega_{\rm dm} + \Omega_{\rm de}\left(1 + 3\omega_{\rm de}\right) - 1\right] + \frac{8\pi G}{3H^2}\left(\delta H \rho_{\rm dm}\right)} \\ &= \frac{\Omega_{\rm de}\left[2\Omega_{\rm r} + \Omega_{\rm bm} + \Omega_{\rm dm} + \Omega_{\rm de}\left(1 + 3\omega_{\rm de}\right) - 1 - 3\omega_{\rm de}\right] - \delta\Omega_{\rm dm}}{\Omega_{\rm dm}\left[2\Omega_{\rm r} + \Omega_{\rm bm} + \Omega_{\rm dm} + \Omega_{\rm de}\left(1 + 3\omega_{\rm de}\right) - 1 + \delta\right]}, \end{aligned} \tag{3.29}$$

where we have used the fact that $\frac{8\pi G}{3H^2}\rho_{\rm dm} = \Omega_{\rm dm}$. It can also be seen that the dependence on the Hubble parameter has been removed by this coupling. If we investigate the simple case where there is only dark matter and dark energy present ($\Omega_r = \Omega_{\rm bm} = 0$), (3.24) becomes:

$$\frac{d\Omega_{\rm de}}{d\Omega_{\rm dm}} = \frac{\Omega_{\rm de}\left[\Omega_{\rm dm} + \Omega_{\rm de}\left(1 + 3\omega_{\rm de}\right) - 1 - 3\omega_{\rm de}\right] - \delta\Omega_{\rm dm}}{\Omega_{\rm dm}\left[\Omega_{\rm dm} + \Omega_{\rm de}\left(1 + 3\omega_{\rm de}\right) - 1 + \delta\right]}. \tag{3.30}$$

Using (3.30), the evolution of coupled dark matter and dark energy may now be expressed with a phase portrait in the ($\Omega_{\rm dm}$, $\Omega_{\rm de}$)-plane:

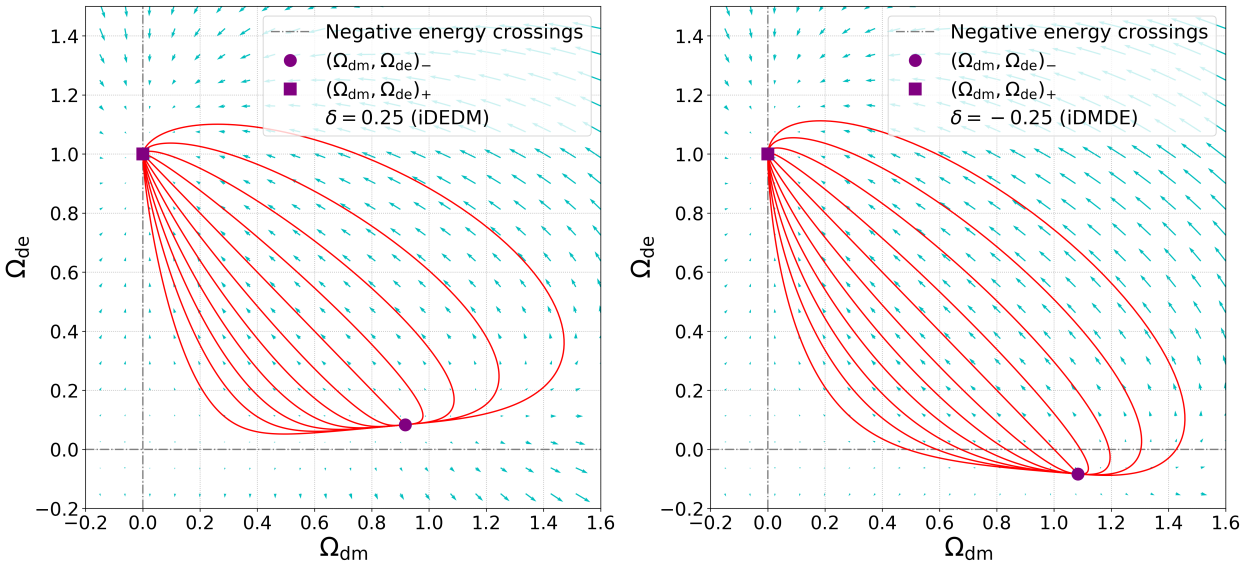

Figure 3.2: *Phase portraits for $\Omega_{\rm dm}$ and $\Omega_{\rm de}$ ($Q_1 = \delta H \rho_{\rm dm}$)*

In Figure 3.2, the left panel shows the phase portrait of a positive δ (iDEDM regime), while the right panel shows a negative δ (iDMDE regime). The arrows and red lines are as defined in Figure 3.1. The repulsor and attractor points are indicated by the purple circle and square on Figure 3.2 respectively, and are calculated in Appendix B.2 to have the following coordinates:

$$(\Omega_{\rm dm}, \Omega_{\rm de})_- = \left(1 + \frac{\delta}{3\omega}, -\frac{\delta}{3\omega}\right) \quad ; \quad (\Omega_{\rm dm}, \Omega_{\rm de})_+ = (0, 1)\,. \tag{3.31}$$

Similar to the ΛCDM model (Figure 3.1), there is a stable attractor endpoint at $(0, 1)$ for both couplings, but the unstable repulsor point has shifted. This change in the repulsor point can be seen to coincide with how this model solves the coincidence problem in the, past by fixing the ratio r of dark matter to dark energy at early times:

$$r_- = \frac{\Omega_{(\rm dm,-)}}{\Omega_{(de,-)}} = \frac{1 + \frac{\delta}{3\omega}}{-\frac{\delta}{3\omega}} \to -\frac{\delta + 3\omega}{\delta} \quad ; \quad r_+ = \frac{\Omega_{(\rm m,+)}}{\Omega_{(de,+)}} = \frac{0}{1} \to 0, \tag{3.32}$$

where we note the condition $\delta + 3\omega < 0$. This implies that if $\delta > 0$ (iDEDM) such that energy flows from DE to DM, that r_- becomes a positive constant and the coincidence problem should be solved in the past. Conversely, if $\delta < 0$ (iDMDE) and energy flows from DM to DE, then r_- becomes a negative constant. This implies that either DM or DE has a negative energy density, which makes the solution unphysical. From (3.31), we can see that the DE density parameter $\Omega_{\rm de,-} = -\frac{\delta}{3\omega}$ (with $\omega < 0$) must have been negative in the past if $\delta < 0$. This is shown in the right panel of Figure 3.2, where $\Omega_{\rm de}$ does indeed become negative. To obtain the exact conditions that lead to negative energy densities, as well as finding out how r evolves between r_- and r_+, we need to first find analytical solutions for how the energy densities of DM and DE evolve.

3.3.2 Background analytical equations - $Q_1 = \delta H \rho_{\text{dm}}$

To obtain analytical solutions for how the dark matter ρ_{dm} and dark energy ρ_{de} densities evolve, we need to solve the conservation equations (3.3) with $Q = \delta H \rho_{\text{dm}}$:

$$\dot{\rho}_{\text{dm}} + 3H\rho_{\text{dm}} = \delta H \rho_{\text{dm}} \quad ; \quad \dot{\rho}_{\text{de}} + 3H\rho_{\text{de}}(1+\omega) = -\delta H \rho_{\text{dm}}. \tag{3.33}$$

The differential equations (3.33) are solved in Appendix C.1, yielding expressions for ρ_{dm} and ρ_{de}:

$$\rho_{\text{dm}} = \rho_{(\text{dm},0)} a^{(\delta-3)}, \tag{3.34}$$

$$\rho_{\text{de}} = \left[\rho_{(\text{de},0)} + \rho_{(\text{dm},0)} \frac{\delta}{\delta + 3\omega}\left(1 - a^{\delta+3\omega}\right)\right] a^{-3(1+\omega)}. \tag{3.35}$$

The solutions (3.34) and (3.35) match with the energy densities found in [84, 101, 103]. The effective equation of states for this model can be obtained by substituting the coupling equation $Q_1 = \delta H \rho_{\text{dm}}$ into (3.7) and (3.9). Thus, the effective equation of state for dark matter $\omega_{\text{dm}}^{\text{eff}}$ is:

$$\omega_{\text{dm}}^{\text{eff}} = -\frac{Q}{3H\rho_{\text{dm}}} = -\frac{\delta H \rho_{\text{dm}}}{3H\rho_{\text{dm}}} = -\frac{\delta}{3}. \tag{3.36}$$

Similarly, the effective equation of state for dark energy $\omega_{\text{de}}^{\text{eff}}$ is then:

$$\omega_{\text{de}}^{\text{eff}} = \omega_{\text{de}} + \frac{Q}{3H\rho_{\text{de}}} = \omega_{\text{de}} + \frac{\delta H \rho_{\text{dm}}}{3H\rho_{\text{de}}} = \omega_{\text{de}} + \frac{\delta}{3} r, \tag{3.37}$$

which matches with [84, 101, 103]. It can be seen be seen that $\omega_{\text{dm}}^{\text{eff}}$ is constant throughout cosmic evolution, while $\omega_{\text{de}}^{\text{eff}}$ is dynamic with a dependence on the coincidence problem ratio $r = \rho_{\text{dm}}/\rho_{\text{de}}$. Equations (3.34), (3.35), (3.36) and (3.37) can be seen to reduce back to the ΛCDM model when $\delta = 0$ and $\omega = -1$. Using the relation $\rho_{(\text{x},0)} = \frac{3H_0^2}{8\pi G}\Omega_{(\text{x},0)}$ from (1.32) as well as the scalefactor redshift relation $a = (1+z)^{-1}$, we obtain useful relations for ρ_{dm} (3.34) and ρ_{de} (3.35):

$$\rho_{\text{dm}} = \frac{3H_0^2}{8\pi G}\Omega_{(\text{dm},0)}(1+z)^{-(\delta-3)}, \tag{3.38}$$

$$\rho_{\text{de}} = \frac{3H_0^2}{8\pi G}\left[\left(\Omega_{(\text{de},0)} + \Omega_{(\text{dm},0)}\frac{\delta}{\delta+3\omega}\left[1 - (1+z)^{-(\delta+3\omega)}\right]\right)(1+z)^{3(1+\omega)}\right]. \tag{3.39}$$

From the relation $\Omega_{\text{x}} = \frac{8\pi G}{3H^2}\rho_{\text{x}}$, we can obtain Ω_{dm} and Ω_{de} from (3.34) and (3.35) as:

$$\Omega_{\text{dm}} = \frac{H_0^2}{H^2}\Omega_{(\text{dm},0)}(1+z)^{-(\delta-3)}, \tag{3.40}$$

$$\Omega_{\text{de}} = \frac{H_0^2}{H^2}\left[\left(\Omega_{(\text{de},0)} + \Omega_{(\text{dm},0)}\frac{\delta}{\delta+3\omega}\left[1 - (1+z)^{-(\delta+3\omega)}\right]\right)(1+z)^{3(1+\omega)}\right]. \tag{3.41}$$

These analytical background equations can be used to explicitly show the consequences predicted in Table 3.1. Before doing this we should first determine the exact conditions to avoid the negative energy densities seen in Figure 3.2.

3.3.3 Positive energy conditions - $Q_1 = \delta H \rho_{\rm dm}$

From equation (3.34), it can be seen that the dark matter density $\rho_{\rm dm}$ is always positive, since $a^{(\delta-3)} > 0$ throughout the entire expansion history for all values of δ. Conversely, this is not necessarily the case for the dark energy density $\rho_{\rm de}$ (3.35), due to the presence of the negative term. To ensure that the dark energy density is always positive, we need to determine where the dark energy density crosses the zero density boundary and becomes negative so that conditions may be chosen to avoid this zero crossing. For this derivation, we follow a similar approach to [101]. This zero-crossing point can be found by setting the dark energy density (3.35) equal to zero:

$$\begin{aligned} 0 = \rho_{\rm de} &= \left[\rho_{(\rm de,0)} + \rho_{(\rm dm,0)} \frac{\delta}{\delta + 3\omega}\left(1 - a^{\delta+3\omega}\right)\right] a^{-3(1+\omega)} \\ 0 &= \rho_{(\rm de,0)} + \rho_{(\rm dm,0)} \frac{\delta}{\delta + 3\omega}\left(1 - a^{\delta+3\omega}\right) \\ -\rho_{(\rm dm,0)} \frac{\delta}{\delta + 3\omega}\left(1 - a^{\delta+3\omega}\right) &= \rho_{(\rm de,0)} \\ -1 + a^{\delta+3\omega} &= \frac{\rho_{(\rm de,0)}}{\rho_{(\rm dm,0)}} \frac{\delta + 3\omega}{\delta} \\ a^{\delta+3\omega} &= 1 + \frac{\rho_{(\rm de,0)}}{\rho_{(\rm dm,0)}} \frac{\delta + 3\omega}{\delta} \\ a^{\delta+3\omega} &= 1 + \frac{1}{r_0}\left(\frac{\delta + 3\omega}{\delta}\right), \end{aligned} \tag{3.42}$$

where $r_0 = \left(\rho_{(\rm dm,0)}/\rho_{(\rm de,0)}\right) = \left(\Omega_{(\rm dm,0)}/\Omega_{(\rm de,0)}\right)$. From this derived relation, we find that for the dark energy density to cross zero and become negative ($\rho_{\rm de} < 0$), there must be some solution to (3.42) for a within the domain of applicability. Using (3.42) and the relation $a = (1+z)^{-1}$, the zero crossing ($\rho_{\rm de} = 0$) happens at exactly redshift $z_{(\rm de=0)}$:

$$z_{(\rm de=0)} = \left[1 + \frac{1}{r_0}\left(\frac{\delta + 3\omega}{\delta}\right)\right]^{-\frac{1}{\delta+3\omega}} - 1. \tag{3.43}$$

Using (3.42), we may explore four scenarios (**(A)** - **(D)**) where the energy density may possibly cross zero and become negative. These scenarios will be either the iDMDE ($\delta < 0$) or iDEDM ($\delta > 0$) regime, for either the *past* or the *future*. This leads to:

$$a^{\delta+3\omega} = 1 + \frac{1}{r_0}\left(\frac{\delta + 3\omega}{\delta}\right) \qquad \text{where} \qquad (\delta + 3\omega < 0) \tag{3.44}$$

$$\delta < 0 \Rightarrow \begin{cases} \text{Past} & (a < 1) \quad \rightarrow \quad (\text{L.H.S.} > 1 \quad ; \quad \text{R.H.S.} > 1) & \textbf{(A)} \\ \text{Future} & (a > 1) \quad \rightarrow \quad (0 < \text{L.H.S.} < 1 \quad ; \quad \text{R.H.S.} > 1) & \textbf{(B)} \end{cases}$$

$$\delta > 0 \Rightarrow \begin{cases} \text{Past} & (a < 1) \quad \rightarrow \quad (\text{L.H.S.} > 1 \quad ; \quad \text{R.H.S.} < 1) & \textbf{(C)} \\ \text{Future} & (a > 1) \quad \rightarrow \quad (0 < \text{L.H.S.} < 1 \quad ; \quad \text{R.H.S.} < 1) & \textbf{(D)} \end{cases}$$

Here we can immediately see that for both **(B)** and **(C)** the L.H.S. and R.H.S. will never cross, which means that there will be no solution for (3.44) and thus the dark energy density will never cross zero and become negative. The energy density will therefore always remain positive for scenario's **(B)** (*Future* expansion with $\delta < 0$) and **(C)** (*Past* expansion with $\delta > 0$). Furthermore, scenario **(A)** will always have a solution, and the dark energy density will therefore always become negative in the *past*, which coincides with what was found in Figure 3.2. In scenario **(D)**, there will not be a solution or zero-crossing as long as the R.H.S.< 0. To ensure this, we may obtain the following condition by solving the R.H.S. of (3.44) for δ:

$$\begin{aligned} 1 + \frac{1}{r_0}\left(\frac{\delta + 3\omega}{\delta}\right) &< 0 \\ \delta + 3\omega &< -\delta r_0 \\ \delta\,(1 + r_0) &< -3\omega \\ \rightarrow \delta &< -\frac{3\omega}{(1 + r_0)}. \end{aligned} \tag{3.45}$$

Thus, if condition (3.45) is met, then scenario **(D)** (*Future* expansion with $\delta > 0$) will always have positive energy densities. Therefore, since both **(C)** and **(D)** will always have positive energy densities, the positive coupling $\delta > 0$ (with the necessary conditions met) may be seen as physical.

It may also be seen that if condition (3.45) holds, then the condition $\delta < -3\omega$ must necessarily hold as well. Finally putting all these conditions $(\delta > 0)\,;(\delta < -3\omega)\,;\left(\delta < -\frac{3\omega}{(1+r_0)}\right)$ together, we may obtain the following general condition to ensure that the energy densities will always remain positive for the coupling model $Q = \delta H \rho_{\rm dm}$. This condition is:

$$0 < \delta < -\frac{3\omega}{(1 + r_0)}. \tag{3.46}$$

The energy densities for all these conditions may be encapsulated in Table 3.2 below:

Conditions	$\rho_{\rm dm}$ (Past)	$\rho_{\rm dm}$ (Future)	$\rho_{\rm de}$ (Past)	$\rho_{\rm de}$ (Future)	Physical
$0 < \delta < -\frac{3\omega}{(1+r_0)}$	+	+	+	+	√
$\delta > 0\ ;\ \delta > -\frac{3\omega}{(1+r_0)}$	+	+	+	−	X
$\delta < 0$	+	+	−	+	X

Table 3.2: *Conditions for positive energy densities throughout cosmic evolution* ($Q_1 = \delta H \rho_{\rm dm}$)

Here (+) means that the energy densities will always remain positive, (−) means that the energy densities will always become negative somewhere in the cosmic evolution. Any scenario which could lead to negative energy densities should be considered *unphysical*. Thus, only systems that abide by the condition (3.46) may be considered *physical*. Therefore, for the coupling $Q_1 = \delta H \rho_{\rm dm}$, the iDMDE regime ($\delta < 0$) should be considered unphysical, while the iDEDM ($\delta < 0$) regime may be physical if condition (3.45) is met.

3.3.4 Cosmic coincidence problem - $Q_1 = \delta H \rho_{\rm dm}$

We have already seen in (3.32) that this model should be able to solve the coincidence problem in the past r_- for the iDEDM regime. We want to see if we can reproduce that result from the analytical expression for $\rho_{\rm dm}$ (3.34) and $\rho_{\rm de}$ (3.35). Furthermore, we are also interested in how r evolves from r_- to r_+. Thus we will obtain an expression for r:

$$\begin{aligned} r &= \frac{\rho_{\rm dm}}{\rho_{\rm de}} \\ &= \frac{\rho_{({\rm dm},0)} a^{(\delta-3)}}{\left[\rho_{({\rm de},0)} + \rho_{({\rm dm},0)} \frac{\delta}{\delta+3\omega}\left(1 - a^{\delta+3\omega}\right)\right] a^{-3(1+\omega)}} \\ &= \frac{\rho_{({\rm dm},0)} a^{(\delta-3)}}{\left[\frac{\rho_{({\rm de},0)}}{\rho_{(dm,0)}} + \frac{\delta}{\delta+3\omega}\left(1 - a^{\delta+3\omega}\right)\right] \rho_{({\rm dm},0)} a^{-3(1+\omega)}} \\ &= \frac{1}{\left[\frac{1}{r_0} + \frac{\delta}{\delta+3\omega}\left(1 - a^{\delta+3\omega}\right)\right] a^{-(\delta+3\omega)}} \\ &= \frac{1}{\left(\frac{1}{r_0} + \frac{\delta}{\delta+3\omega}\right) a^{-(\delta+3\omega)} - \frac{\delta}{\delta+3\omega}}. \end{aligned} \tag{3.47}$$

In terms of redshift z this becomes:

$$r(z) = \frac{1}{\left(\frac{1}{r_0} + \frac{\delta}{\delta+3\omega}\right)(1+z)^{(\delta+3\omega)} - \frac{\delta}{\delta+3\omega}}, \tag{3.48}$$

which matches [82]. From (3.47), it can be seen that r has the proportionality:

$$r \propto a^{(\delta+3\omega)} \qquad \rightarrow \qquad \zeta_{\rm Q_1} = -3\omega - \delta, \tag{3.49}$$

where ζ is defined as $r \propto r_0 a^{-\zeta}$ in (2.42). For the ΛCDM model $\zeta_{\Lambda{\rm CDM}} = 3$, while for a general uncoupled model $\zeta = -3\omega$, thus from (3.49) it can be seen that:

$$\zeta_{\rm Q_1} = -3\omega - \delta \rightarrow \begin{cases} \text{if } \delta > 0 \text{ (iDEDM)} & \rightarrow \quad \zeta_{\rm Q_1} < \zeta \quad \textit{alleviates} \text{ coincidence problem} \\ \text{if } \delta < 0 \text{ (iDMDE)} & \rightarrow \quad \zeta_{\rm Q_1} > \zeta \quad \textit{worsens} \text{ coincidence problem.} \end{cases} \tag{3.50}$$

This behaviour of iDEDM and iDMDE coincides with the previous analysis in (3.13). Furthermore, this behaviour becomes more extreme in both the distant past (at large redshifts $(1+z) \rightarrow \infty$) and the distant future (at redshifts $(1+z) \rightarrow 0$). This is seen by considering these limits for (3.48), while noting the condition $\delta + 3\omega < 0$, thus:

$$\lim_{(1+z)\rightarrow\infty} r_- \rightarrow -\frac{\delta+3\omega}{\delta}, \qquad ; \qquad \lim_{(1+z)\rightarrow 0} r_+ =\!\!\rightarrow 0. \tag{3.51}$$

This result exactly matches what was found from the phase portrait in Figure 3.2, with the repulsor point r_- and attractor point r_+ (3.32) being the same as the $(1+z) \rightarrow \infty$ and $(1+z) \rightarrow 0$ redshift

limits found for r in (3.51), respectively. Furthermore, in the distant past r has the proportionality:

$$\lim_{(1+z)\to 0} r_- \propto a^0 \quad \to \quad \zeta_{(Q_1,-)} = 0. \tag{3.52}$$

Since r is constant and $\zeta_{(Q_1,-)} = 0$, this model solves the coincidence problem for large redshifts during the distant past. This only holds for the $\delta > 0$ (iDEDM) regime, since $\delta < 0$ (iDMDE) will lead to a negative constant r_- due to ρ_{de} which becomes negative at $z_{(de=e0)}$ (3.43) as shown in Table 3.2, which is unphysical. Thus, for large redshifts in the distant past we have:

$$\lim_{(1+z)\to\infty} \zeta_{Q_1} = 0 \begin{cases} \text{if } \delta > 0 \to r_- = +\text{constant} & \textit{solves} \text{ coincidence problem} \\ \text{if } \delta < 0 \to r_- = -\text{constant} & \text{negative energy densities (unphysical).} \end{cases} \tag{3.53}$$

To understand why this model has this behaviour, we can consider how the effective equations of state ω^{eff} for IDE models can be used for Addressing the coincidence problem. To do this, we first need the explicit relation for ω^{eff}_{de}, which is obtained by substituting in r from (3.48) into (3.37):

$$\omega^{\text{eff}}_{de} = \omega_{de} + \frac{\delta}{3} r = \omega_{de} + \frac{\delta}{3} \frac{1}{\left(\frac{1}{r_0} + \frac{\delta}{\delta+3\omega}\right)(1+z)^{(\delta+3\omega)} - \frac{\delta}{\delta+3\omega}}. \tag{3.54}$$

In the distant past the ratio $r_- \to \frac{\delta+3\omega}{\delta}$, while in the distant future $r_+ \to 0$, as was seperately shown in both (3.32) and (3.51). Noting that $\omega^{\text{eff}}_{dm} = -\frac{\delta}{3}$ from (3.36), we can see how the dynamical effective equation of state ω^{eff}_{de} behaves in both the distant past and future:

$$\omega^{\text{eff}}_{de} = \omega_{de} + \frac{\delta}{3} r \begin{cases} \text{Distant past} \quad (r = r_-): & \omega^{\text{eff}}_{de} = \omega_{de} + \frac{\delta}{3}\left(-\frac{\delta+3\omega_{de}}{\delta}\right) = -\frac{\delta}{3} = \omega^{\text{eff}}_{dm} \\ \text{Distant future} \ (r = r_+): & \omega^{\text{eff}}_{de} = \omega_{de} + \frac{\delta}{3}(0) = \omega_{de}. \end{cases} \tag{3.55}$$

The effective equations of state for dark matter and dark energy is therefore the same in the distant past ($\omega^{\text{eff}}_{dm} = \omega^{\text{eff}}_{de}$). This shows that both dark matter and dark energy redshifts and dilutes at the same rate in the past, which effectively solves the coincidence problem for past expansion, as previously discussed with regards to (3.12) in section 3.2.2. This also explicitly shows that the limit where $r = +constant \to \zeta = 0$, corresponds with where $\omega^{\text{eff}}_{dm} = \omega^{\text{eff}}_{de}$

Furthermore, we can also see that in the distant future $\omega^{\text{eff}}_{de} = \omega_{de}$. The effect of the coupling on dark energy will thus become negligible in the future, effectively mimicking the behaviour of uncoupled dark energy. Therefore, we should expect the deviation of this model's behaviour from the ΛCDM model to be most prominent in the past, while approaching the ΛCDM model closer to the present and into the future. This behaviour will be seen in all subsequent figures for this model.

To more clearly see this close connection between the effective equations of state ω^{eff} and how this model addresses the coincidence problem, it is instructive to plot r (3.48) alongside both ω^{eff}_{dm} (3.54) and ω^{eff}_{de} (3.36).

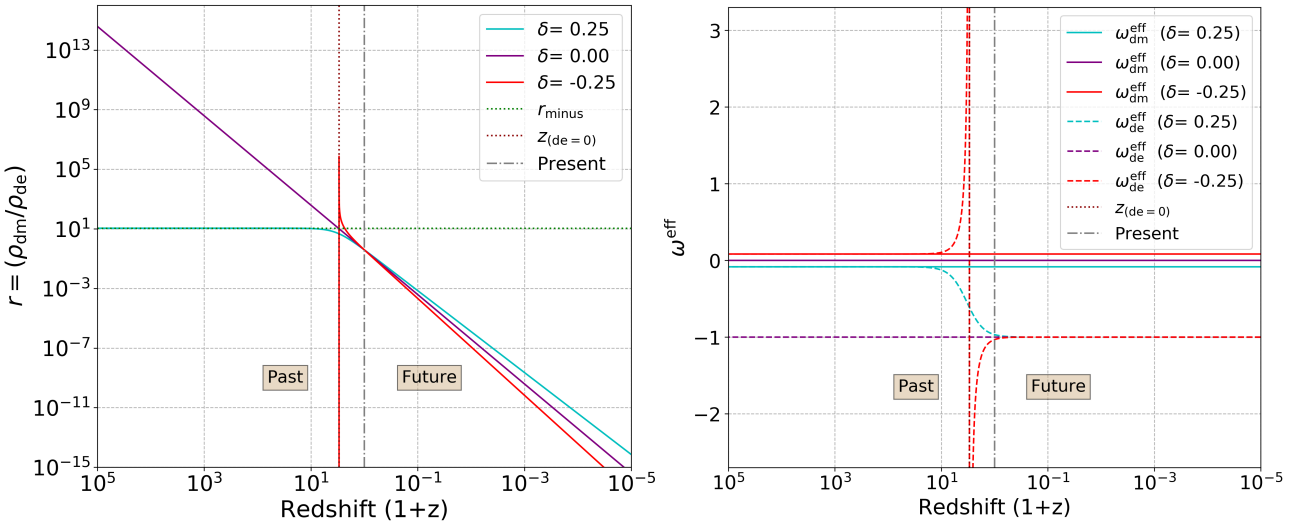

Figure 3.3: *Coincidence problem and effective equations of state ($Q_1 = \delta H \rho_{\mathrm{dm}}$)*

From the left panel in Figure 3.3 it can be seen that for the uncoupled case, r differs with many orders of magnitude in the past and future, indicating the coincidence that we live at a time when both ρ_{dm} to ρ_{de} has the same order of magnitude. For the coupled model with $\delta > 0$ (iDEDM), this coincidence problem is solved for the past expansion history, since r flattens and becomes constant $r \to r_-$ (indicated by the dashed green line) in the past, as predicted by (3.32) and (3.51). This coincides with the right panel where $\omega^{\mathrm{eff}}_{\mathrm{dm}} = \omega^{\mathrm{eff}}_{\mathrm{de}}$, as shown in (3.55). It may also be seen that the coincidence problem is alleviated for the future expansion, since the slope is smaller (as predicted by (3.50)), which coincides with $\omega^{\mathrm{eff}}_{\mathrm{dm}} < \omega_{\mathrm{dm}}$ from (3.12), causing a smaller difference $(\omega^{\mathrm{eff}}_{\mathrm{dm}} - \omega^{\mathrm{eff}}_{\mathrm{de}})$ relative to the uncoupled case.

Conversely, for $\delta < 0$ (iDEDM), we have $\omega^{\mathrm{eff}}_{\mathrm{dm}} > \omega_{\mathrm{dm}}$ which worsens the coincidence problem for the future expansion (since the slope is greater than the case $\delta = 0$). For the past expansion, it can also be seen that r approaches infinity before plummeting down, while $\omega^{\mathrm{eff}}_{\mathrm{de}}$ completely diverges. This is due to the dark energy density ρ_{de} which approaches zero and then becomes negative in the past at redshift $z_{(\mathrm{de}=0)}$ (indicated by red dotted line) from (3.43). Thus the results from (3.51), (3.50), (3.53) and (3.55) can clearly be seen in Figure 3.3 and may be generalised such that:

$$
\begin{aligned}
\delta > 0 \text{ (iDEDM)} \begin{cases} \text{Past expansion:} & \omega^{\mathrm{eff}}_{\mathrm{dm}} = \omega^{\mathrm{eff}}_{\mathrm{de}} \ (\zeta_{Q_1} = 0) & \textit{solves} \text{ coincidence problem} \\ \text{Future expansion:} & \omega^{\mathrm{eff}}_{\mathrm{dm}} < \omega_{\mathrm{dm}} \ (\zeta_{Q_1} < \zeta) & \textit{alleviates} \text{ coincidence problem,} \end{cases} \\
\delta < 0 \text{ (iDMDE)} \begin{cases} \text{Past expansion:} & \omega^{\mathrm{eff}}_{\mathrm{dm}} = \omega^{\mathrm{eff}}_{\mathrm{de}} \ (\rho_{\mathrm{de}} < 0) & \text{negative energy densities} \\ \text{Future expansion:} & \omega^{\mathrm{eff}}_{\mathrm{dm}} > \omega_{\mathrm{dm}} \ (\zeta_{Q_1} > \zeta) & \textit{worsens} \text{ coincidence problem.} \end{cases}
\end{aligned}
\tag{3.56}
$$

These results hold due to how energy flows between dark matter and dark energy, causing the fluids to redshift and dilute at different rates, as discussed in section 3.2.2. To explicitly see how this happens, we will consider how the energy densities of dark matter and dark energy evolve.

3.3.5 Evolution of energy densities and cosmic equalities - $Q_1 = \delta H \rho_{\text{dm}}$

As discussed in section 3.2.2, the energy exchange between the dark sectors causes these fluids to have a different effective equation of state, which in turn causes ρ_{dm} and ρ_{de} to redshift and dilute at different rates. This can be clearly seen by plotting ρ_{dm} (3.38) and ρ_{de} (3.39) against redshift:

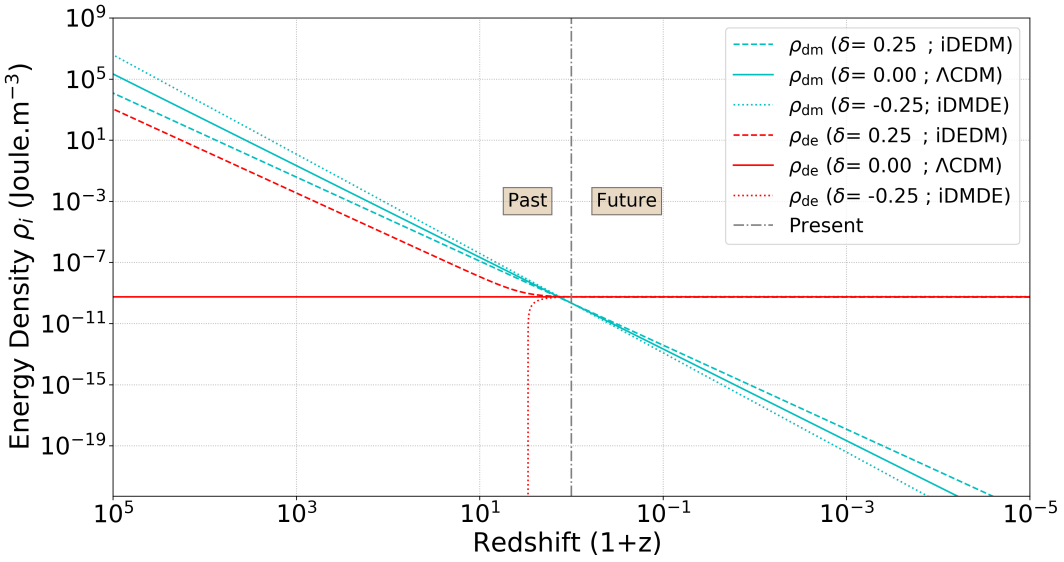

Figure 3.4: *Energy densities ρ vs redshift - ($Q_1 = \delta H \rho_{\text{dm}}$)*

In Figure 3.4, we can see that for the uncoupled case $\rho_{\text{dm}} \propto a^{-3}$ dilutes, while ρ_{de} stays constant with expansion, as was previously shown in Figure 2.7. This difference in the slope between how ρ_{dm} and ρ_{de} redshifts, is indicative of the coincidence problem. We can see that for $\delta > 0$ (iDEDM), dark energy loses energy and redshifts faster (greater slope), while dark matter receives energy and redshifts slower (smaller slope). This causes the slope at which ρ_{dm} and ρ_{de} redshift to be the same in the past, while being smaller in the future. This coincides with $\omega_{\text{dm}}^{\text{eff}} = \omega_{\text{de}}^{\text{eff}}$ and a constant value of r (solving the coincidence problem) for the past, while $\omega_{\text{dm}}^{\text{eff}} < \omega_{\text{dm}}$ which alleviates the coincidence problem in the future, as was shown in Figure 3.3 and summarised in (3.56).

The opposite of this holds for $\delta < 0$ (iDMDE). In this case, dark matter loses energy and redshifts even faster (greater slope), while dark energy receives energy, thus having a net increase in energy density over time and redshifts slower (smaller slope). This causes a greater difference in the slopes between how ρ_{dm} and ρ_{de} redshifts, coinciding with $\omega_{\text{dm}}^{\text{eff}} > \omega_{\text{dm}}$ which, worsens the coincidence problem as shown in (3.56). Since ρ_{de} increases with expansion, there was a time in the past when $\rho_{\text{de}} = 0$ at redshift $z_{(\text{de}=0)}$ (3.43), before which $\rho_{\text{de}} < 0$ and thus unphysical. This can clearly be seen in Figure 3.5, where the predicted redshift $z_{(\text{de}=0)}$ is indicated by the red marker.

A general point for both scenarios, is that the difference in the dark energy behaviour is only in the past, while being identical to the ΛCDM model in the future. This is due to $\omega_{\text{de}}^{\text{eff}}$ approximating that of the uncoupled scenario $\omega_{\text{de}}^{\text{eff}} = \omega_{\text{de}}$ in the future, as shown in (3.55).

The evolution of these energy densities may be further used to confirm some Cosmological implications of a dark coupling. This can be done by plotting the density parameters of dark matter Ω_{dm} (3.40), dark energy Ω_{de} (3.41), radiation Ω_{r} (2.3) and baryonic matter Ω_{bm} (2.6):

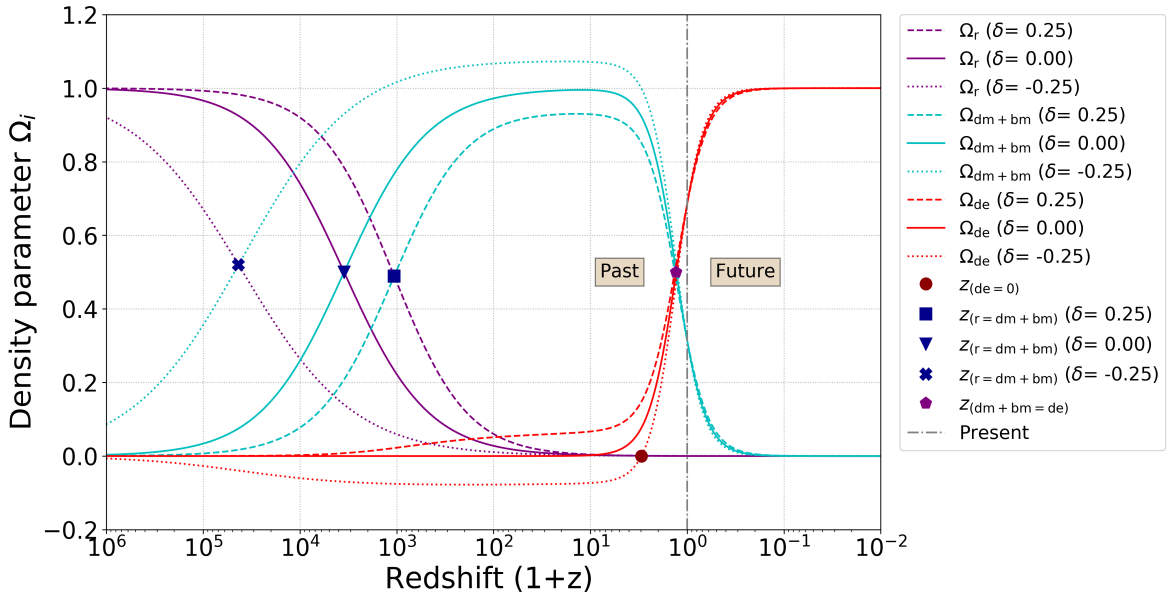

Figure 3.5: *Density parameters vs redshift - ($Q_1 = \delta H \rho_{\text{dm}}$)*

From Figures 3.4 and 3.5 it is seen that for $\delta > 0$ (iDEDM), there is *less* dark matter and *more* dark energy in the past, and vice versa for $\delta < 0$ (iDMDE). This has the effect that for $\delta > 0$ the radiation-matter equality happens *later* in cosmic history, while the matter-dark energy equality happens *earlier*, with the opposite holding for $\delta < 0$, which matches with [103]. The exact redshift where the radiation-matter $z_{(\text{r=dm+bm})}$ and matter-dark energy $z_{(\text{dm+bm=de})}$ equalities happen, is calculated in Appendix D.3 and given by equations (D.13) and (D.18) respectively. These equations were numerically solved with cosmological parameters (2.25), predicting the equalities indicated by the markers in Figure 3.5, which match with where the corresponding densities intersect. The matter-dark energy equality for all three cases is indicated by a single marker, as they happen at close redshifts. The exact redshift, cosmic time and energy density of each component at these equalities is found in Tables 3.5 and 3.6. These results confirm some predictions from Table 3.1:

$$\begin{aligned}
&\delta > 0 \text{ (iDEDM)} \begin{cases} \text{Radiation-matter equality:} & z_{\text{IDE}} < z_{\Lambda\text{CDM}} & \text{happens } \textit{later} \text{ than } \Lambda\text{CDM} \\ \text{Matter-dark energy equality:} & z_{\text{IDE}} > z_{\Lambda\text{CDM}} & \text{happens } \textit{earlier} \text{ than } \Lambda\text{CDM}, \end{cases} \\
&\delta < 0 \text{ (iDMDE)} \begin{cases} \text{Radiation-matter equality:} & z_{\text{IDE}} > z_{\Lambda\text{CDM}} & \text{happens } \textit{earlier} \text{ than } \Lambda\text{CDM} \\ \text{Matter-dark energy equality:} & z_{\text{IDE}} < z_{\Lambda\text{CDM}} & \text{happens } \textit{later} \text{ than } \Lambda\text{CDM}, \end{cases}
\end{aligned} \tag{3.57}$$

It may also be seen from Figure 3.4 that for the coupled models, dark matter never completely dominates $(\Omega_{\text{dm}}, \Omega_{\text{de}})_- = (1, 0)$ as in the ΛCDM case, but instead both dark matter and dark energy have the density parameters $(\Omega_{\text{dm}}, \Omega_{\text{de}})_- = \left(1 + \frac{\delta}{3\omega}, -\frac{\delta}{3\omega}\right)$ from repulsor point (3.31) during matter domination. During dark energy domination $(\Omega_{\text{dm}}, \Omega_{\text{de}})_+ = (0, 1)$, as in the ΛCDM case.

3.3.6 Evolution of deceleration parameter - $Q_1 = \delta H \rho_{\rm dm}$

This change in the value of the density parameters will influence how the deceleration parameter evolves for this model. This can be seen from the deceleration parameter for IDE models (3.20):

$$q = \Omega_{\rm r} + \frac{1}{2}\left(\Omega_{\rm bm} + \Omega_{\rm dm}\right) + \frac{1}{2}\Omega_{\rm de}\left(1 + 3\omega\right). \tag{3.58}$$

Furthermore, we have the effective equation of state for the total fluid in this model given by 2.27

$$\omega^{\rm eff} = \frac{P_{\rm tot}}{\rho_{\rm tot}} = \frac{\omega_{\rm r}\Omega_{\rm r} + \omega_{\rm bm}\Omega_{\rm bm} + \omega_{\rm dm}\Omega_{\rm dm} + \omega_{\rm de}\Omega_{\rm de}}{\Omega_{\rm r} + \Omega_{\rm bm} + \Omega_{\rm dm} + \Omega_{\rm de}} = \frac{\frac{1}{3}\Omega_{\rm r} + \omega_{\rm de}\Omega_{\rm de}}{\Omega_{\rm r} + \Omega_{\rm bm} + \Omega_{\rm dm} + \Omega_{\rm de}} \tag{3.59}$$

Plotting (3.58) and (3.59), with the density parameters of dark matter $\Omega_{\rm dm}$ (3.40), dark energy $\Omega_{\rm de}$ (3.41), radiation $\Omega_{\rm r}$ (2.3) and baryonic matter $\Omega_{\rm bm}$ (2.6), yields the following figures:

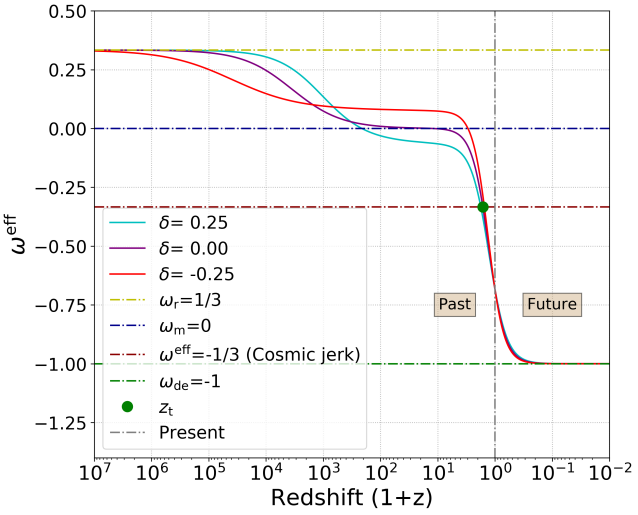

Figure 3.6: *Evolution of effective equation of state $\omega^{\rm eff}$ with redshift ($Q_1 = \delta H \rho_{\rm dm}$)*

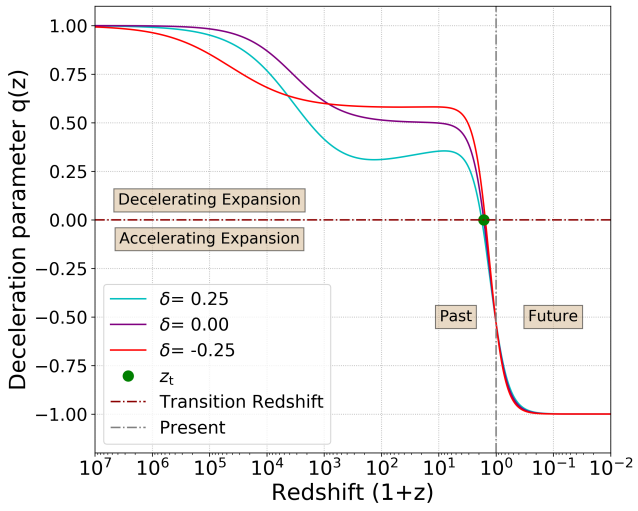

Figure 3.7: *Evolution of deceleration parameter q with redshift $(1+z)$ ($Q_1 = \delta H \rho_{\rm dm}$)*

It can be seen that both the deceleration parameter q and effective equation of state $\omega^{\rm eff}$ for IDE models follow the same qualitative evolution as the uncoupled case in Figures 2.9 and 2.10. Initially, the rate of expansion decelerates ($\omega^{\rm eff} > -1/3$; $q > 0$) before starting to accelerate ($\omega^{\rm eff} < -1/3$; $q < 0$) from the cosmic jerk onwards. This cosmic jerk occurs at the transition redshift $z_{\rm t}$, which is found by setting $q = 0$ in equation (3.59), which is calculated in Appendix D.2 and given by equation (D.24). Equation (D.24) was numerically solved and the predicted value for $z_{\rm t}$ is indicated on Figures 3.6 and 3.7 with a single marker, as the value of $z_{\rm t}$ is very close for all three models. The exact redshift of the cosmic jerk for each model is shown in Tables 3.5 and 3.6, from which we see that:

$$\text{Cosmic jerk } (z_{\rm t}) \begin{cases} \delta > 0 \text{ (iDEDM):} & z_{\rm IDE} > z_{\Lambda\rm CDM} \quad \text{happens } \textit{earlier} \text{ than } \Lambda\text{CDM}, \\ \delta < 0 \text{ (iDMDE):} & z_{\rm IDE} < z_{\Lambda\rm CDM} \quad \text{happens } \textit{later} \text{ than } \Lambda\text{CDM} \end{cases} \tag{3.60}$$

This confirms another prediction from Table 3.1. Furthermore, in section 2.5.3 we saw that during domination of a fluid x, such that $\Omega_{\rm x} = 1$, we have from (2.16) that $q = \frac{1}{2}(1 + 3\omega_{\rm x})$ and from (3.59) $\omega^{\rm eff} = \omega_{\rm x}$. It can thus be seen that this IDE model experiences radiation, matter and dark energy-domination as indicated by $\omega^{\rm eff}$ in Figure 3.6 that approaches $\omega_{\rm r}$, $\omega_{\rm m}$ and $\omega_{\rm de}$ respectively. $\omega^{\rm eff}$ and q converge to three different values that correspond to each terms in equation (3.58) and (3.59) dominating at different epochs. For radiation domination $(\Omega_{\rm r}, \Omega_{\rm dm+bm}, \Omega_{\rm de}) \approx (1, 0, 0) \rightarrow q = 1$; $\omega^{\rm eff} = 1/3$, and dark energy domination, $(\Omega_{\rm r}, \Omega_{\rm dm+bm}, \Omega_{\rm de}) \approx (0, 0, 1) \rightarrow q = -1$; $\omega^{\rm eff} = -1$, which matches with the ΛCDM model. Conversely, for matter-domination the density parameters are given by the repulsor point (3.31), such that $(\Omega_{\rm r}, \Omega_{\rm dm+bm}, \Omega_{\rm de}) \approx \left(0, 1 + \frac{\delta}{3\omega}, -\frac{\delta}{3\omega}\right)$. The deceleration parameter (3.58) then becomes:

$$\begin{aligned} q &= \Omega_{\rm r} + \frac{1}{2}\left(\Omega_{\rm bm} + \Omega_{\rm dm}\right) + \frac{1}{2}\Omega_{\rm de}\left(1 + 3\omega\right) = (0) + \frac{1}{2}\left(1 + \frac{\delta}{3\omega}\right) + \frac{1}{2}\left(-\frac{\delta}{3\omega}\right)(1 + 3\omega) \\ &= \frac{1}{2}\left(1 + \frac{\delta}{3\omega}\left[1 + (1 - 3\omega)\right]\right) = \frac{1}{2}\left(1 - \delta\right) = \frac{1}{2}\left(1 + 3\omega_{\rm dm}^{\rm eff}\right). \end{aligned} \tag{3.61}$$

For the effective equation of state (3.59) we have:

$$\omega^{\rm eff} = \frac{\frac{1}{3}\Omega_{\rm r} + \omega\Omega_{\rm de}}{\Omega_{\rm r} + \Omega_{\rm bm} + \Omega_{\rm dm} + \Omega_{\rm de}} = \frac{\frac{1}{3}(0) + \omega\left(-\frac{\delta}{3\omega}\right)}{(0) + \left(1 + \frac{\delta}{3\omega}\right) + \left(-\frac{\delta}{3\omega}\right)} = \frac{\left(-\frac{\delta}{3}\right)}{1} = -\frac{\delta}{3} = \omega_{\rm dm}^{\rm eff}, \tag{3.62}$$

where both (3.61) and (3.62) reduce back to the ΛCDM case when either $\delta = 0$ or $\omega_{\rm dm}^{\rm eff} = \omega_{\rm dm}$. We can calculate q and $\omega^{\rm eff}$ for the parameters used in Figures 3.6 and 3.7. Thus, for $\delta = 0.25$ (iDEDM) we have $q = \frac{1}{2}(1 - 0.25) = 0.375$; and $\omega^{\rm eff} = \left(-\frac{0.25}{3}\right) = -0.083$, while for $\delta = -0.25$ (iDMDE) we have $q = \frac{1}{2}(1 + 0.25) = 0.625$ and $\omega^{\rm eff} = \left(-\frac{-0.25}{3}\right) = 0.083$ for matter-domination. It should be noted that these are just approximations, as we assumed the absence of baryonic matter ($\Omega_{\rm bm} = 0$) in determining the repulsor point (3.31). These results can be seen to approximately match the values of q and $\omega^{\rm eff}$ in Figures 3.6 and 3.7 during matter-domination. This change in q and $\omega^{\rm eff}$ will directly affect the expansion rate and thus the age of the universe.

3.3.7 Hubble parameter and age of the universe - $Q_1 = \delta H \rho_{\rm dm}$

To determine how an interaction between dark matter and dark energy will affect the age of the universe (2.30), we consider the evolution of the scale factor from the Friedmann equation (2.13):

$$\int_0^t dt = \int_0^a \frac{1}{H(a)} da \qquad ; \quad H^2(a) = \left(\frac{\dot{a}}{a}\right)^2 = \frac{8\pi G}{3}\left(\rho_{\rm r} + \rho_{\rm bm} + \rho_{\rm dm} + \rho_{\rm de}\right) - \frac{kc^2}{a^2}, \tag{3.63}$$

where we use the energy densities $\rho_{\rm r}$ (2.3), $\rho_{\rm bm}$ (2.6), $\rho_{\rm dm}$ (3.38) and $\rho_{\rm de}$ (3.39) and $k = 0$. To see how a coupling changes the expansion rate throughout cosmic history, the Hubble parameter (2.13) relative to the non-interacting case ($H/H_{\delta=0}$), may be plotted for both a positive and negative coupling against redshift z. We also plot the evolution of the scale factor against time, by

numerically integrating (3.63) with the 4th order Runge Kutta method, as specified in Appendix A.4. We then obtain the following figures:

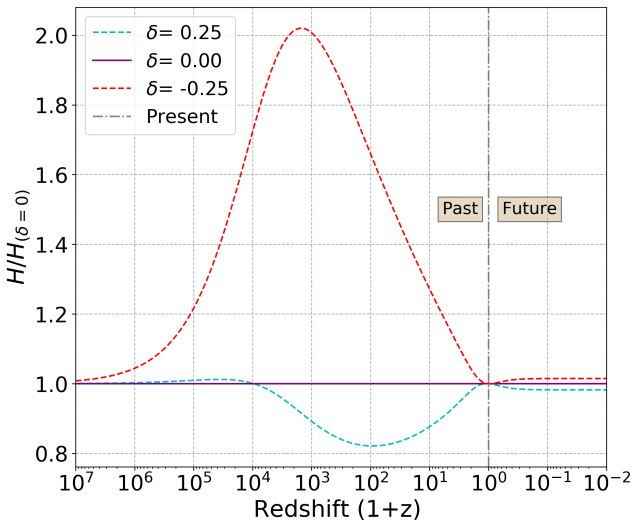

Figure 3.8: *Relative Hubble parameter* $(H/H_{\delta=0})$ *vs redshift* $(Q_1 = \delta H \rho_{\mathrm{dm}})$

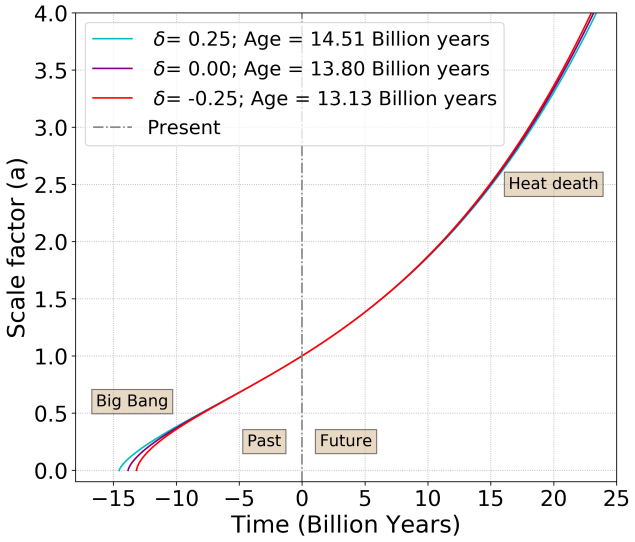

Figure 3.9: *Evolution of scale factor with time* $(Q_1 = \delta H \rho_{\mathrm{dm}})$

In Figure 3.8, whenever the relative Hubble factor is smaller than 1, then the expansion rate is slower than the uncoupled scenario ($H/H_{\delta=0} < 1 \rightarrow$ slower expansion rate). Conversely, when the relative Hubble factor is larger than 1, the expansion rate is faster than the uncoupled case ($H/H_{\delta=0} > 1 \rightarrow$ faster expansion rate). Therefore, it may be seen that throughout most of the past and future expansion history $\delta > 0$ (iDEDM) expands slower, while $\delta < 0$ (iDMDE) expands faster than the uncoupled case.

For $\delta > 0$ (iDEDM), this behaviour can be understood to be due to the overall suppression of dark matter and increase in dark energy density (Figures 3.4, 3.5), which in turn causes a lower value for the deceleration parameter q and effective equation of state ω^{eff} throughout most of the expansion history (Figures 3.6 and 3.7). When evolving the Friedmann equation backwards from present conditions, a lower deceleration parameter may be understood as causing the universe to decelerate slower from its current size $a = 1$ into the past singularity $a = 0$, thus causing a slower expansion rate. Due to $\delta > 0$ (iDEDM) having a slower expansion rate, more time is needed for the universe to evolve from a singularity ($a = 0$) to its current size ($a = 1$). This implies that $\delta > 0$ (iDEDM) should increase the calculated age of the universe, which can be seen to be the case in Figure 3.9. The opposite of this holds for $\delta < 0$ (iDMDE), such that the universe has a faster expansion rate which leads to a younger universe. Thus, we have:

$$\text{Age of universe } (t_0) \begin{cases} \delta > 0 \text{ (iDEDM):} & t_{(0,\mathrm{IDE})} > t_{(0,\Lambda\mathrm{CDM})} \quad \textit{Older} \text{ universe than } \Lambda\text{CDM}, \\ \delta < 0 \text{ (iDMDE):} & t_{(0,\mathrm{IDE})} < t_{(0,\Lambda\mathrm{CDM})} \quad \textit{Younger} \text{ universe than } \Lambda\text{CDM}. \end{cases} \tag{3.64}$$

It may also be noted that the earlier $H/H_{\delta=0}$ peak for $\delta = -0.25$ and later peak for $\delta = 0.25$ in Figure 3.8, corresponds to the earlier and later radiation-matter equality (and thus matter domination) respectively, which can be seen in Figure 3.5. Besides changing the universe's age, a coupling in the dark sector could lead to instabilities, which, if avoided, leads to a more dramatic end to the universe.

3.3.8 Doom factor and big rip - $Q_1 = \delta H \rho_{\rm dm}$

Thus far, we have assumed dark energy to have an equation of state $\omega = -1$, consistent with interacting vacuum energy. This was done to ease comparisons with the ΛCDM model, such that the interaction strength δ would be the only free parameter whose effect can be studied. Unfortunately, this is not realistic, as $\omega = -1$ causes the perturbation equations to diverge, causing gravitational instabilities [108, 109]. To know whetheher this IDE model is stable, we should consider the Instabilities and the doom factor for this model. We mentioned, if the doom factor $\mathbf{d} < 0$, the model should be free of non-adiabatic instabilities at large scales, providing the range of parameters that will give an a priori stable universe. Thus, for $Q_1 = \delta H \rho_{\rm dm}$ we have the doom factor (3.14):

$$\mathbf{d}_1 = \frac{Q_1}{3H\rho_{\rm de}(1+\omega)} = \frac{\delta H \rho_{\rm dm}}{3H\rho_{\rm de}(1+\omega)} = \frac{\delta}{3(1+\omega)}\frac{\rho_{\rm dm}}{\rho_{\rm de}}, \tag{3.65}$$

where we also apply the conditions that $\rho_{\rm dm} > 0$; $\rho_{\rm de} > 0$. Since we need $\mathbf{d} < 0$ to ensure a stable universe, we can see from (3.65) that this will only occur if δ and $(1+\omega)$ have opposite signs [103]. This then implies that:

$$\begin{aligned}
\mathbf{d}_1 < 0 &\begin{cases} \delta < 0 \quad ; \quad \omega > -1 & \text{(Quintessence regime)} \\ \delta > 0 \quad ; \quad \omega < -1 & \text{(Phantom regime)} \end{cases} && \rightarrow \text{No instabilities expected} \\
\mathbf{d}_1 > 0 &\begin{cases} \delta > 0 \quad ; \quad \omega > -1 & \text{(Quintessence regime)} \\ \delta < 0 \quad ; \quad \omega < -1 & \text{(Phantom regime)} \end{cases} && \rightarrow \text{Instabilities can develop if } \mathbf{d} > 1
\end{aligned} \tag{3.66}$$

These results should be combined with the positive energy condition $0 < \delta < -\frac{3\omega}{(1+r_0)}$ from (3.46) and Table 3.2. This implies that $\rho_{\rm de} < 0$ if $\delta < 0$ (iDMDE), which is unphysical and should be ruled out. The results from (3.65), (3.66) and (3.46) are taken together in the following table:

δ	Energy flow	ω	Dark energy	$\mathbf{d}$	a priori stable	$\rho_{\rm dm} > 0$	$\rho_{\rm de} > 0$	Viable
+	DE → DM	< -1	Phantom	-	√	√	√	√
+	DE → DM	> -1	Quintessence	+	X	√	√	X
-	DM → DE	< -1	Phantom	+	X	√	X	X
-	DM → DE	> -1	Quintessence	-	√	√	X	X

Table 3.3: *Stability and positive energy criteria ($Q_1 = \delta H \rho_{\rm dm}$)*

From Table 3.3, we see that the only scenario that is free from both negative energy densities and instabilities is phantom dark energy $\omega < -1$ in the $\delta > 0$ (iDEDM) regime. This has the consequence that these models will be plagued by the problems associated with phantom dark energy, violating the Energy conditions of general relativity; and the consequences of doing so [41]. Since $\omega_{\text{de}}^{\text{eff}} = \omega_{\text{de}}$ (3.55) in the future, an immediate consequence of dark energy being in the phantom regime, is that the universe model will experience a late time Big rip singularity as noted by [107].

An equivalent equation to (2.50) for the time of the big rip t_{rip} [10, 95] is derived for this IDE model in Appendix E.2 as:

$$t_{\text{rip}} \approx -\frac{2}{3H_0(1+\omega)\sqrt{1-\Omega_{(\text{bm},0)} - \left(1 - \frac{\delta}{\delta+3\omega}\right)\Omega_{(\text{dm},0)}}}, \tag{3.67}$$

which reduces back to (2.50) when $\delta = 0$. The predicted time of the big rip (3.67) is plotted alongside the evolution of the scale factor (3.63) in Figure 3.10:

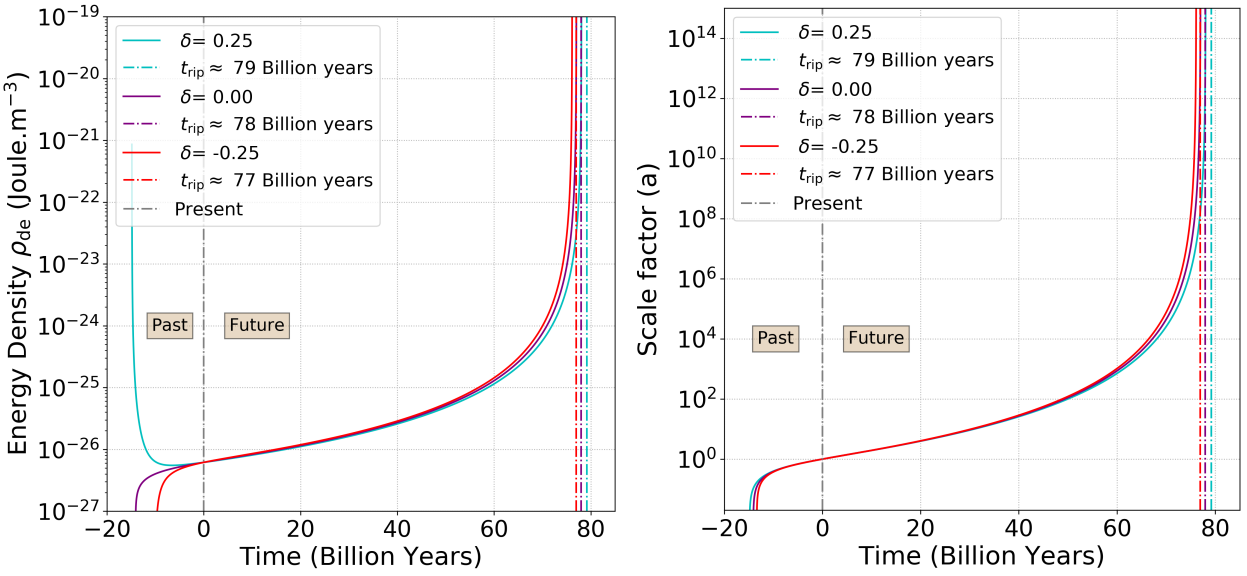

Figure 3.10: *Evolution of energy density, scale factor and the big rip for phantom ($\omega = -1.15$) IDE models - ($Q_1 = \delta H \rho_{\text{dm}}$)*

In Figure 3.10, we can see that both the $a \to \infty$; $\rho_{\text{de}} \to \infty$ at a finite time t_{rip}, as was previously also seen in Figure 2.12. For $\delta > 0$ (iDEDM), ρ_{de} dilutes similar to dark matter in the past (when $\omega_{\text{de}}^{\text{eff}} = \omega_{\text{dm}}$), after which it shows phantom behaviour by increasing in energy density with time (when $\omega_{\text{de}}^{\text{eff}} = \omega_{\text{de}}$). Furthermore, the coupling changes the time of the big rip such that:

$$\text{Big rip} \begin{cases} \delta > 0 \text{ (iDEDM)}: & t_{(\text{rip,IDE})} > t_{(\text{rip},\Lambda\text{CDM})} \quad \textit{Later} \text{ big rip than } \Lambda\text{CDM}, \\ \delta < 0 \text{ (iDMDE)}: & t_{(\text{rip,IDE})} < t_{(\text{rip},\Lambda\text{CDM})} \quad \textit{Earlier} \text{ big rip than } \Lambda\text{CDM}. \end{cases} \tag{3.68}$$

3.3.9 Concluding remarks on IDE model $Q_1 = \delta H \rho_{\rm dm}$

Thus far we have seen that all the Cosmological implications of a dark coupling predicted in Table 3.1 have held for the model $Q_1 = \delta H \rho_{\rm dm}$. We will now summarise these results.

For this model, we have derived the positive energy condition $0 < \delta < -\frac{3\omega}{(1+r_0)}$ (3.46), from which we see that the $\delta < 0$ (iDMDE) regime will always lead to $\rho_{\rm de} < 0$ during past expansion. This implies that only the $\delta > 0$ (iDMDE) regime should be taken seriously as a potential candidate for dark energy. For this $\delta > 0$ (iDMDE) regime, we have seen that this model can solve the coincidence problem in the past, whilst aleviating the problem for the future (3.56). This is due to dark energy deviating from the ΛCDM model in the past expansion $\omega_{\rm dm}^{\rm eff} = \omega_{\rm de}^{\rm eff}$, while mimicking the ΛCDM model in the future $\omega_{\rm de}^{\rm eff} = \omega_{\rm de}$ (3.55). Furthermore, this energy flow from DE to DM causes a *later* radiation-matter equality and both an *earlier* matter-dark energy equality (3.57) and cosmic jerk (3.68), while predicting an *older* age for the universe (3.68). The opposite holds for $\delta < 0$ (iDMDE). Using the cosmological parameters from (2.25), the exact redshift, cosmic time and energy densities during these important events, for the cases $\delta = 0$ (ΛCDM); $\delta = 0.25$ (iDEDM) and $\delta = -0.25$ (iDMDE), can be found in Tables 3.4, 3.5 and 3.6 respectively.

Table 3.4: *Important events in interacting dark energy model $\delta = 0.00$ (ΛCDM) - $Q_1 = \delta H \rho_{\rm dm}$*

Event	Redshift z	Time (Gyr)	$\rho_{\rm r}$	$\rho_{\rm m}$	ρ_Λ (J/m^3)
Big bang singularity	∞	13.80	∞	∞	∞
Radiation-matter equality	3499	13.80	10.9	10.9	5.5e-10
Cosmic jerk	0.63	6.12	5.2e-13	1.2e-9	5.5e-10
Matter-dark energy equality	0.30	3.50	2.1e-13	1.1e-9	5.5e-10

Table 3.5: *Important events in interacting dark energy model $\delta = 0.25$ (iDEDM) - $Q_1 = \delta H \rho_{\rm dm}$*

Event	Redshift z	Time (Gyr)	$\rho_{\rm r}$	$\rho_{\rm dm+bm}$	$\rho_{\rm de}$ (J/m^3)
Big bang singularity	∞	14.51	∞	∞	∞
Radiation-matter equality	1061	14.51	9.2e-2	9.2e-2	4.0e-3
Cosmic jerk	0.77	7.42	7.2e-13	1.3e-9	6.3e-10
Matter-dark energy equality	0.34	3.32	2.4e-13	5.8e-10	5.8e-10

Table 3.6: *Important events in interacting dark energy model $\delta = -0.25$ (iDMDE) - $Q_1 = \delta H \rho_{\rm dm}$*

Event	Redshift z	Time (Gyr)	$\rho_{\rm r}$	$\rho_{\rm dm+bm}$	$\rho_{\rm de}$ (J/m^3)
Big bang singularity	∞	13.13	∞	∞	∞
Radiation-matter equality	43 138	13.13	2.5e5	2.5e5	-1.9e-4
Cosmic jerk	0.53	5.43	4.0e-13	1.0e-9	5.0e-10
Matter-dark energy equality	0.26	3.14	1.8e-13	5.4e-10	5.4e-10

Finally, it should also be noted from Table 3.3 that the only viable regime for these models, to avoid both negative energy densities and gravitational instabilities, is phantom dark energy $\omega < -1$ in the $\delta > 0$ (iDEDM) regime. This has the direct consequence that these models will end with a big rip singularity after time $t_{\rm rip}$, for which we have derived expression (3.67).

3.4 Interaction model 2: $Q_2 = \delta H \rho_{\text{de}}$

We will now consider our second case study, where the interaction is proportional to the dark energy density $Q_2 \propto \rho_{\text{de}}$. The same analysis will be applied to this model that was done for Interaction model 1: $Q_1 = \delta H \rho_{\text{dm}}$ to show that many of the conclusions from section 3.3.9 hold in general for IDE models while noting key differences. The model $Q_2 = \delta H \rho_{\text{de}}$ is more common in the literature than the previous model considered. A possible explanation for this, is that in the iDMDE regime for $Q_1 = \delta H \rho_{\text{dm}}$ model, $\rho_{\text{de}} < 0$ in the past, as was pointed out in [103]. These authors then advocated for coupling $Q_2 \propto \rho_{\text{de}}$, since all energy densities remain positive throughout the past universe history, even in the iDMDE ($\delta < 0$) regime [103]. This result has often been taken at face value in the literature. However, we would like to focus attention to the fact that in the iDMDE ($\delta < 0$) regime, these models will **always** suffer from negative dark matter energy densities ($\rho_{\text{dm}} < 0$) during **future** expansion. This observation should render these models less favourable and should have been noted by many recent papers that have neglected to mention this problem [87, 105, 106, 108]. The exact conditions for positive energy densities will be calculated in section 3.4.3, but this result can immediately be seen from the phase portraits of these models.

3.4.1 Phase portraits - $Q_2 = \delta H \rho_{\text{de}}$

Assuming the coupling $Q_2 = \delta H \rho_{\text{de}}$, equation (3.22) becomes:

$$\begin{aligned}\frac{d\Omega_{\text{de}}}{d\Omega_{\text{dm}}} &= \frac{\Omega_{\text{de}} H \left[2\Omega_{\text{r}} + \Omega_{\text{bm}} + \Omega_{\text{dm}} + \Omega_{\text{de}}\left(1+3\omega_{\text{de}}\right) - 1 - 3\omega_{\text{de}}\right] - \frac{8\pi G}{3H^2}\left(\delta H \rho_{\text{de}}\right)}{\Omega_{\text{dm}} H \left[2\Omega_{\text{r}} + \Omega_{\text{bm}} + \Omega_{\text{dm}} + \Omega_{\text{de}}\left(1+3\omega_{\text{de}}\right) - 1\right] + \frac{8\pi G}{3H^2}\left(\delta H \rho_{\text{de}}\right)} \\ &= \frac{\Omega_{\text{de}}\left[2\Omega_{\text{r}} + \Omega_{\text{bm}} + \Omega_{\text{dm}} + \Omega_{\text{de}}\left(1+3\omega_{\text{de}}\right) - 1 - 3\omega_{\text{de}} - \delta\right]}{\Omega_{\text{dm}}\left[2\Omega_{\text{r}} + \Omega_{\text{bm}} + \Omega_{\text{dm}} + \Omega_{\text{de}}\left(1+3\omega_{\text{de}}\right) - 1\right] + \delta\Omega_{\text{de}}},\end{aligned} \tag{3.69}$$

where we have used the fact that $\frac{8\pi G}{3H^2}\rho_{\text{de}} = \Omega_{\text{de}}$. Since this coupling is not proportional to the dark matter density, it may be seen from (3.22) that the evolution of baryonic matter and dark matter may be grouped together:

$$\begin{aligned}\dot{\Omega}_m &= \dot{\Omega}_{\text{dm}} + \dot{\Omega}_{\text{bm}} \\ &= \left(\Omega_{\text{dm}} + \Omega_{\text{bm}}\right) H \left[2\Omega_{\text{r}} + \left(\Omega_{\text{bm}} + \Omega_{\text{dm}}\right) + \Omega_{\text{de}}\left(1+3\omega_{\text{de}}\right) - 1\right] + \delta\Omega_{\text{de}} \\ &= \Omega_m H \left[2\Omega_{\text{r}} + \Omega_m + \Omega_{\text{de}}\left(1+3\omega_{\text{de}}\right) - 1\right] + \delta\Omega_{\text{de}}.\end{aligned} \tag{3.70}$$

It should be noted that baryonic matter is still separately conserved here and experiences no new interaction. Thus, investigating the case where dark matter is grouped with baryonic matter and radiation is negligible ($\Omega_r = 0$), (3.69) becomes:

$$\frac{d\Omega_{\text{de}}}{d\Omega_m} = \frac{\Omega_{\text{de}}\left[\Omega_m + \Omega_{\text{de}}\left(1+3\omega_{\text{de}}\right) - 1 - 3\omega_{\text{de}} - \delta\right]}{\Omega_m\left[\Omega_m + \Omega_{\text{de}}\left(1+3\omega_{\text{de}}\right) - 1\right] + \delta\Omega_{\text{de}}}. \tag{3.71}$$

Using (3.71), the evolution of matter and dark energy may now be expressed with a phase portrait in the $(\Omega_m, \Omega_{\rm de})$-plane:

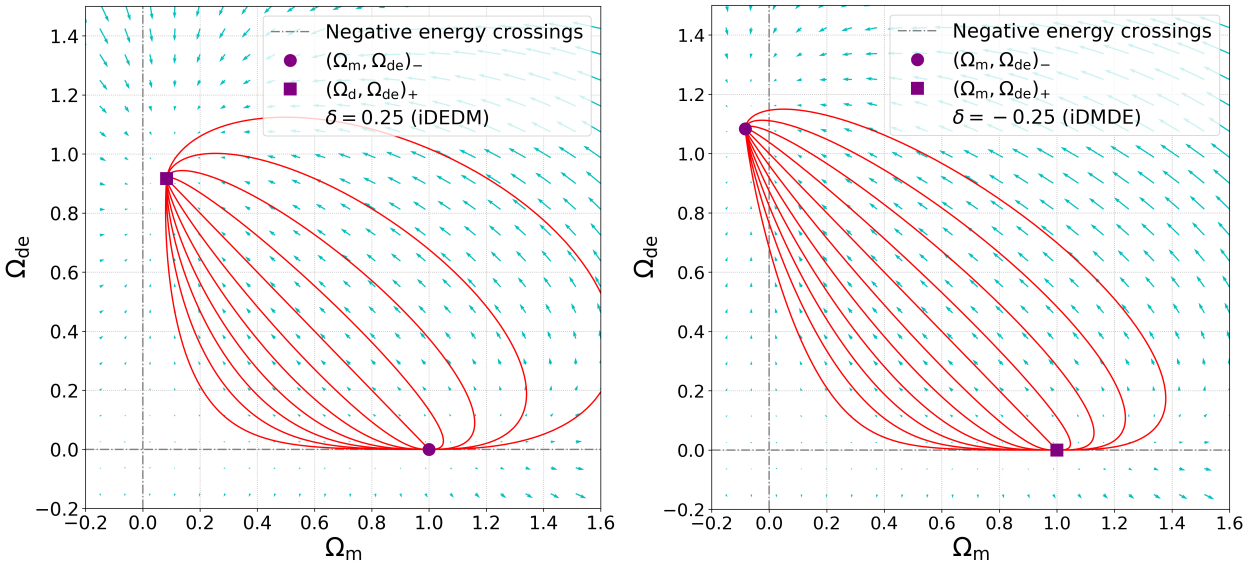

Figure 3.11: *Phase portraits for* $\Omega_{\rm dm}$ *and* $\Omega_{\rm de}$ *(*$Q_2 = \delta H \rho_{\rm de}$*)*

In Figure 3.11, the left panel shows the phase portrait of a positive δ (iDEDM), while the right panel shows a negative δ (iDMDE). The equilibrium points are calculated in Appendix B.3 to be:

$$(\Omega_m, \Omega_{\rm de})_- = (1, 0) \qquad ; \qquad (\Omega_m, \Omega_{\rm de})_+ = \left(-\frac{\delta}{3\omega}, 1 + \frac{\delta}{3\omega}\right). \tag{3.72}$$

In contrast to the previous $Q \propto \rho_{\rm dm}$ model (Figure 3.2) where the repulsor point moved, here the repulsor point is similar to the ΛCDM case (Figure 3.1), but the attractor point is instead shifted by the dark coupling. This highlights the point that the effect of the coupling is more dominant in the matter dominated past for $Q \propto \rho_{\rm dm}$, while being more dominant during later dark energy dominance for $Q \propto \rho_{\rm de}$ (due to the behaviour of $\omega_{\rm dm}^{\rm eff}$ (3.55) and $\omega_{\rm de}^{\rm eff}$ (3.96)). Therefore, this model will not solve the coincidence problem in the past as r_- does in (3.32), but will instead stabilise r in the future r_+, thereby solving the coincidence problem for future expansion:

$$r_- = \frac{\Omega_{(\rm m,-)}}{\Omega_{(de,-)}} = \frac{1}{0} \to \infty \qquad ; \qquad r_+ = \frac{\Omega_{(\rm dm,+)}}{\Omega_{(de,+)}} \approx \frac{\Omega_{(\rm m,+)}}{\Omega_{(de,+)}} = \frac{-\frac{\delta}{3\omega}}{1 + \frac{\delta}{3\omega}} \to -\frac{\delta}{\delta + 3\omega}. \tag{3.73}$$

The same point holds as discussed with regards to (3.32), where positive $\delta > 0$ (iDEDM) solves the coincidence problem, but $\delta < 0$ (iDMDE) causes negative energy densities. This brings us to the often overlooked problem of the iDMDE regime for this model. It is clear from (3.72) that $\Omega_{dm,+} \approx \Omega_{m,+} = -\frac{\delta}{3\omega}$, alongside $(\omega < 0)$, must imply that $\delta <$ (iDMDE) leads to a negative energy attractor solution for $\Omega_{\rm dm}$. We should also note that baryonic matter is grouped with dark matter, but in the distant future it dilutes as in the ΛCDM model and its contribution in the distant future should become negligible, validating the approximation $\Omega_{dm,+} \approx \Omega_{m,+}$.

3.4.2 Background analytical equations - $Q_2 = \delta H \rho_{\text{de}}$

This model will have the conservation equations obtained by substituting the coupling $Q = \delta H \rho_{\text{de}}$ into (3.3), which gives:

$$\dot{\rho}_{\text{dm}} + 3H\rho_{\text{dm}} = \delta H \rho_{\text{de}} \quad ; \quad \dot{\rho}_{\text{de}} + 3H\rho_{\text{de}}(1+\omega) = -\delta H \rho_{\text{de}}. \tag{3.74}$$

The analytical expressions for both ρ_{dm} and ρ_{de} are derived in Appendix C.2 by solving the differential equations in (3.74), yielding the following expressions:

$$\rho_{\text{dm}} = \left(\rho_{(\text{dm},0)} + \rho_{(\text{de},0)} \frac{\delta}{\delta + 3\omega}\left[1 - a^{-(\delta+3\omega)}\right]\right) a^{-3}, \tag{3.75}$$

$$\rho_{\text{de}} = a^{-(\delta+3\omega+3)}. \tag{3.76}$$

Here (3.75) and (3.76) match with the energy densities found in [84, 103, 106, 108]. The effective equation of states for this model can be obtained by substituting the coupling equation $Q = \delta H \rho_{\text{de}}$ into (3.7) and (3.9). The dark matter effective equation of state is then:

$$\omega_{\text{dm}}^{\text{eff}} = -\frac{Q}{3H\rho_{\text{de}}} = -\frac{\delta H \rho_m}{3H\rho_{\text{dm}}} = -\frac{\delta}{3}\frac{\rho_{\text{de}}}{\rho_{\text{dm}}}. \tag{3.77}$$

Similarly, for dark energy we have the effective equation of state:

$$\omega_{\text{de}}^{\text{eff}} = \omega + \frac{Q}{3H\rho_{\text{de}}} = \omega + \frac{\delta H \rho_{\text{de}}}{3H\rho_{\text{de}}} = \omega + \frac{\delta}{3}. \tag{3.78}$$

which matches with [84, 103, 106, 108]. In contrast to $Q_1 = \delta H \rho_{\text{dm}}$; $\omega_{\text{dm}}^{\text{eff}}$ is dynamical with a dependence on r, while, in contrast $\omega_{\text{de}}^{\text{eff}}$ is constant. Equations (3.75), (3.76), (3.77) and (3.78) also reduce back to the ΛCDM model when $\delta = 0$ and $\omega = -1$. Using the relation $\rho_{(\text{x},0)} = \frac{3H_0^2}{8\pi G}\Omega_{(\text{x},0)}$ from (1.32) as well as the scalefactor redshift relation $a = (1+z)^{-1}$, we obtain useful relations for ρ_{dm} and ρ_{de} from (3.75) and (3.76) as:

$$\rho_{\text{dm}} = \frac{3H_0^2}{8\pi G}\left(\Omega_{(\text{dm},0)} + \Omega_{(\text{de},0)} \frac{\delta}{\delta + 3\omega}\left[1 - (1+z)^{(\delta+3\omega)}\right]\right)(1+z)^3, \tag{3.79}$$

$$\rho_{\text{de}} = \frac{3H_0^2}{8\pi G}\Omega_{(\text{de},0)}(1+z)^{(\delta+3\omega+3)}. \tag{3.80}$$

From the relation $\Omega_{\text{x}} = \frac{8\pi G}{3H^2}\rho_{\text{x}}$, we obtain Ω_{dm} and Ω_{de} from (3.75) and (3.76) as:

$$\Omega_{\text{dm}} = \frac{H_0^2}{H^2}\left(\Omega_{(\text{dm},0)} + \Omega_{(\text{de},0)} \frac{\delta}{\delta + 3\omega}\left[1 - (1+z)^{(\delta+3\omega)}\right]\right)(1+z)^3, \tag{3.81}$$

$$\Omega_{\text{de}} = \frac{H_0^2}{H^2}\Omega_{(\text{de},0)}(1+z)^{(\delta+3\omega+3)}. \tag{3.82}$$

As before, we first determine the exact conditions to avoid the negative energy densities which were seen in Figure 3.11 and frequently avoided in the literature.

3.4.3 Positive energy density conditions - $Q_2 = \delta H \rho_{\text{de}}$

In Positive energy conditions - $Q_1 = \delta H \rho_{\text{dm}}$, the dark matter density ρ_{dm} was always positive, while the dark energy density ρ_{de} could become negative. For this model, it can instead be seen that ρ_{de} (3.76) is always positive (since $a^{-(\delta+3\omega+3)} > 0$ or all values of δ), while ρ_{dm} (3.75) has multiple terms which could become negative. We will follow the same approach as we did in Positive energy conditions - $Q_1 = \delta H \rho_{\text{dm}}$ to find the exact condition to ensure that the ρ_{dm} is always positive in this case. We need to find out where the dark matter energy density crosses the zero energy density boundary and becomes negative so that conditions may be chosen to avoid this zero crossing. This is found when we set the dark matter energy density (3.75) equal to zero:

$$\begin{aligned}
0 = \rho_{\text{dm}} &= \left(\rho_{(\text{dm},0)} + \rho_{(\text{de},0)} \frac{\delta}{\delta + 3\omega}\left[1 - a^{-(\delta+3\omega)}\right]\right) a^{-3} \\
0 &= \rho_{(\text{dm},0)} + \rho_{(\text{de},0)} \frac{\delta}{\delta + 3\omega}\left[1 - a^{-(\delta+3\omega)}\right] \\
-\rho_{(\text{de},0)} \frac{\delta}{\delta + 3\omega}\left[1 - a^{-(\delta+3\omega)}\right] &= \rho_{(\text{dm},0)} \\
\left[-1 + a^{-(\delta+3\omega)}\right] &= \frac{\rho_{(\text{dm},0)}}{\rho_{(\text{de},0)}} \frac{\delta + 3\omega}{\delta} \\
a^{-(\delta+3\omega)} &= 1 + \frac{\rho_{(\text{dm},0)}}{\rho_{(\text{de},0)}} \frac{\delta + 3\omega}{\delta} \\
\rightarrow a^{-(\delta+3\omega)} &= 1 + r_0 \left(\frac{\delta + 3\omega}{\delta}\right).
\end{aligned} \tag{3.83}$$

Using (3.83), we can find solutions where the dark matter energy density crosses zero and becomes negative ($\rho_{\text{dm}} < 0$). Using (3.83) and the relation $a = (1+z)^{-1}$, the zero crossing ($\rho_{\text{dm}} = 0$) happens at exactly the redshift $z_{(\text{dm}=0)}$:

$$z_{(\text{dm}=0)} = \left[1 + r_0 \left(\frac{\delta + 3\omega}{\delta}\right)\right]^{\frac{1}{\delta+3\omega}} - 1. \tag{3.84}$$

Using (3.83), we may explore four scenarios, **(E)** - **(H)**, where the energy density may possibly cross zero and become negative. These scenarios will be either the iDMDE ($\delta < 0$) or iDEDM ($\delta > 0$) scenarios, for either the *past* or the *future*. This leads to:

$$a^{-(\delta+3\omega)} = 1 + r_0 \left(\frac{\delta + 3\omega}{\delta}\right) \qquad \text{where} \qquad (\delta + 3\omega < 0) \tag{3.85}$$

$$\delta < 0 \Rightarrow \begin{cases} \text{Past} & (a < 1) \rightarrow (0 < \text{L.H.S.} < 1 \;\; ; \;\; \text{R.H.S.} > 1) & \textbf{(E)} \\ \text{Future} & (a > 1) \rightarrow (\text{L.H.S.} > 1 \;\; ; \;\; \text{R.H.S.} > 1) & \textbf{(F)} \end{cases}$$

$$\delta > 0 \Rightarrow \begin{cases} \text{Past} & (a < 1) \rightarrow (0 < \text{L.H.S.} < 1 \;\; ; \;\; \text{R.H.S.} < 1) & \textbf{(G)} \\ \text{Future} & (a > 1) \rightarrow (\text{L.H.S.} > 1 \;\; ; \;\; \text{R.H.S.} < 1) & \textbf{(H)} \end{cases}$$

Here we can immediately see that for both **(E)** and **(H)** the L.H.S. and R.H.S. will never cross, which means that there will be no solution for (3.85) and thus the $\rho_{\rm dm}$ will never cross zero and become negative. Therefore, $\rho_{\rm dm}$ will always remain positive for scenerio's **(E)** (*Past* expansion with $\delta < 0$) and **(H)** (*future* expansion with $\delta > 0$). Furthermore, scenario **(F)** will always have a solution and therefore the dark energy density will always become negative in the *future*, as shown by the attractor point in Figure 3.11.

$$\begin{aligned} 1 + r_0\left(\frac{\delta + 3\omega}{\delta}\right) &< 0 \\ \delta + 3\omega &< -\delta\frac{1}{r_0} \\ \delta\left(1 + \frac{1}{r_0}\right) &< -3\omega \\ \rightarrow \delta &< -\frac{3\omega}{\left(1 + \frac{1}{r_0}\right)}. \end{aligned} \tag{3.86}$$

Thus, if condition (3.86) is met, then scenario **(G** (*Past* expansion with $\delta > 0$) will always have positive energy densities. Therefore, since both **(G)** and **(H)** will always have positve energy densities, the positive coupling $\delta > 0$ (with condition (3.86) met) may be seen as physical.

Since the condition (3.86) holds, it implies that the condition $\delta < -3\omega$ must necessarily hold as well. Taking the conditions $(\delta > 0)\,;(\delta < -3\omega)$ and $\left(\delta < -\frac{3\omega}{(1+1/r_0)}\right)$ together, a general condition is obtained to ensure positive energy densities for the IDE model $Q_2 = \delta H \rho_{\rm de}$. This condition is:

$$0 < \delta < -\frac{3\omega}{\left(1 + \frac{1}{r_0}\right)}. \tag{3.87}$$

The energy densities for all these conditions may be encapsulated in Table 3.7 below:

Conditions	$\rho_{\rm dm}$ (Past)	$\rho_{\rm dm}$ (Future)	$\rho_{\rm de}$ (Past)	$\rho_{\rm de}$ (Future)	Physical
$0 < \delta < -\frac{3\omega}{\left(1+\frac{1}{r_0}\right)}$	+	+	+	+	√
$\delta > 0\ ;\ \delta > -\frac{3\omega}{\left(1+\frac{1}{r_0}\right)}$	−	+	+	+	X
$\delta < 0$	+	-	+	+	X

Table 3.7: *Conditions for positive energy densities throughout cosmic evolution* ($Q_2 = \delta H \rho_{\rm de}$)

From positive energy conditions (3.46) and (3.87) it may be concluded that only IDE models where energy flows from dark energy to dark matter iDEDM ($\delta > 0$) should be seriously considered, as couplings where energy flows from dark matter to dark energy iDMDE ($\delta < 0$) will always lead to either negative energies in the past or the future. This only holds for the couplings $Q_1 = \delta H \rho_{\rm dm}$ and $Q_2 = \delta H \rho_{\rm de}$, and may not be the case for other coupling models.

3.4.4 Cosmic coincidence problem - $Q_2 = \delta H \rho_{\rm de}$

For this model, the coincidence problem is not solved in the past but instead in the future. This can be seen from the repulsor point $r_- = \infty$ (3.73) being the same as in the ΛCDM model (3.27). Conversely, the attractor point r_+ in (3.73) shows that this model should solve the coincidence problem in the future, at least for the iDEDM regime. We will now reproduce these results from the analytical expression for $\rho_{\rm dm}$ (3.75) and $\rho_{\rm de}$ (3.76). First, we need an expression for r:

$$\begin{aligned} r &= \frac{\rho_{\rm dm}}{\rho_{\rm de}} \\ &= \frac{\rho_{(\rm dm,0)} a^{-3} + \rho_{(\rm de,0)} \frac{\delta}{\delta+3\omega} \left[1 - a^{-(\delta+3\omega)}\right] a^{-3}}{\rho_{(\rm de,0)} a^{-(\delta+3\omega+3)}} \\ &= \frac{\left(\frac{\rho_{(\rm dm,0)}}{\rho_{(\rm de,0)}} + \frac{\delta}{\delta+3\omega}\left[1 - a^{-(\delta+3\omega)}\right]\right) \rho_{(\rm de,0)} a^{-3}}{\rho_{(\rm de,0)} a^{-(\delta+3\omega+3)}} \\ &= \left(r_0 + \frac{\delta}{\delta+3\omega}\left[1 - a^{-(\delta+3\omega)}\right]\right) a^{(\delta+3\omega)} \\ &= \left(r_0 + \frac{\delta}{\delta+3\omega}\right) a^{(\delta+3\omega)} - \frac{\delta}{\delta+3\omega}. \end{aligned} \tag{3.88}$$

In terms of redshift z this becomes:

$$r(z) = \left(r_0 + \frac{\delta}{\delta+3\omega}\right)(1+z)^{-(\delta+3\omega)} - \frac{\delta}{\delta+3\omega} \tag{3.89}$$

From (3.88), it can be seen that r has the same proportionality as (3.49), such that:

$$r \propto a^{(\delta+3\omega)} \qquad \rightarrow \qquad \zeta_{\rm Q_1} = \zeta_{\rm Q_2} = -3\omega - \delta. \tag{3.90}$$

For the ΛCDM model $\zeta_{\Lambda\rm CDM} = 3$, and for a general uncoupled model $\zeta = -3\omega$, thus from (3.90) it can be seen that:

$$\zeta_{\rm Q_2} = -3\omega - \delta \rightarrow \begin{cases} \text{if } \delta > 0 \text{ (iDEDM)} & \rightarrow \quad \zeta_{\rm Q_2} < \zeta \quad \textit{alleviates} \text{ coincidence problem} \\ \text{if } \delta < 0 \text{ (iDMDE)} & \rightarrow \quad \zeta_{\rm Q_2} > \zeta \quad \textit{worsens} \text{ coincidence problem.} \end{cases} \tag{3.91}$$

This behaviour coincides with both (3.50) and the original analysis in (3.13). Furthermore, this effect becomes more extreme in both the distant past (at large redshifts $(1+z) \rightarrow \infty$) and the distant future (at redshifts $(1+z) \rightarrow 0$). This can be seen by considering these limits for (3.48), while noting the condition $\delta + 3\omega < 0$, thus:

$$\lim_{(1+z)\rightarrow\infty} r_- \rightarrow \infty, \qquad ; \qquad \lim_{(1+z)\rightarrow 0} r_+ =\rightarrow -\frac{\delta}{\delta+3\omega}. \tag{3.92}$$

These results match what was found from the phase portrait in Figure 3.11, with the repulsor point r_- and attractor point r_+ (3.32) being the same as the $(1+z) \rightarrow \infty$ and $(1+z) \rightarrow 0$ redshift limits

found for r in (3.92), respectively. Furthermore, in the distant future r has the proportionality:

$$\lim_{(1+z)\to 0} r_+ \propto a^0 \quad \to \quad \zeta_{(\mathrm{Q}_2,-)} = 0. \tag{3.93}$$

Since r is constant and $\zeta_{(\mathrm{Q}_2,+)} = 0$, this model solves the coincidence problem for future expansion. This only holds for the $\delta > 0$ (iDEDM) regime, since $\delta < 0$ (iDMDE) will lead to a negative constant r_+ due to ρ_{dm} which becomes negative at $z_{(\mathrm{dm}=0)}$ (3.84), as shown in Table 3.7, which is unphysical. Thus, for $(1+z) \to 0$ in the future, we have:

$$\lim_{(1+z)\to 0} \zeta_{\mathrm{Q}_2} = 0 \begin{cases} \text{if } \delta > 0 \to r_- = +constant & \textit{solves} \text{ coincidence problem} \\ \text{if } \delta < 0 \to r_- = -constant & \text{negative energy densities (unphysical).} \end{cases} \tag{3.94}$$

To understand why this model differs from $Q_1 = \delta H \rho_{\mathrm{dm}}$, we can consider how the effective equations of state ω^{eff} for this model evolve. To do this, we first need the explicit relation for $\omega^{\mathrm{eff}}_{\mathrm{dm}}$, which is obtained by substituting in r from (3.89) into (3.77):

$$\omega^{\mathrm{eff}}_{\mathrm{dm}} = -\frac{\delta}{3}\frac{1}{r} = -\frac{\delta}{3}\frac{1}{\left(r_0 + \frac{\delta}{\delta+3\omega}\right)(1+z)^{-(\delta+3\omega)} - \frac{\delta}{\delta+3\omega}}. \tag{3.95}$$

In the distant past the ratio $r_- \to \infty$, while in the distant future $r_+ \to -\frac{\delta}{\delta+3\omega}$, as was independently shown in both (3.73) and (3.92). Noting that $\omega^{\mathrm{eff}}_{\mathrm{de}} = \omega + \frac{\delta}{3}$ from (3.78), we can see how the dynamical effective equation of state $\omega^{\mathrm{eff}}_{\mathrm{dm}}$ behaves in both the distant past and future:

$$\omega^{\mathrm{eff}}_{\mathrm{dm}} = -\frac{\delta}{3}\frac{1}{r} \begin{cases} \text{Distant past} \quad (r = r_-): & \omega^{\mathrm{eff}}_{\mathrm{dm}} = -\frac{\delta}{3}\frac{1}{\infty} = 0 = \omega_{\mathrm{dm}} \\ \text{Distant future} \ (r = r_+): & \omega^{\mathrm{eff}}_{\mathrm{dm}} = -\frac{\delta}{3}\left(\frac{\delta}{\delta+3\omega}\right) = \omega + \frac{\delta}{3} = \omega^{\mathrm{eff}}_{\mathrm{de}}. \end{cases} \tag{3.96}$$

The effective equations of state for dark matter and dark energy are therefore the same in the distant future ($\omega^{\mathrm{eff}}_{\mathrm{dm}} = \omega^{\mathrm{eff}}_{\mathrm{de}}$). This shows that both dark matter and dark energy redshift and dilute at the same rate in the future, which effectively solves the coincidence problem for future expansion by the mechanisms discussed with regards to (3.12) in section 3.2.2. This again shows that whenever $r = +constant \to \zeta = 0$, we also have $\omega^{\mathrm{eff}}_{\mathrm{dm}} = \omega^{\mathrm{eff}}_{\mathrm{de}}$.

Furthermore, we can also see that in the distant past $\omega^{\mathrm{eff}}_{\mathrm{de}} = \omega_{\mathrm{de}}$. The effect of the coupling on dark matter will thus become negligible for past expansion, effectively mimicking the behaviour of uncoupled dark matter. Therefore, we should expect the deviation of this model's behaviour from the ΛCDM model to be most prominent in the future while behaving similarly to the ΛCDM model in the past. This feature, where $Q_2 \propto \rho_{\mathrm{de}}$ deviates from ΛCDM in the future (3.55), while $Q_1 \propto \rho_{\mathrm{dm}}$ deviates in the past (3.96), can be seen as the largest difference between the two models.

These predictions may be confirmed by plotting r (3.89) alongside both $\omega_{\text{dm}}^{\text{eff}}$ (3.95) and $\omega_{\text{de}}^{\text{eff}}$ (3.78):

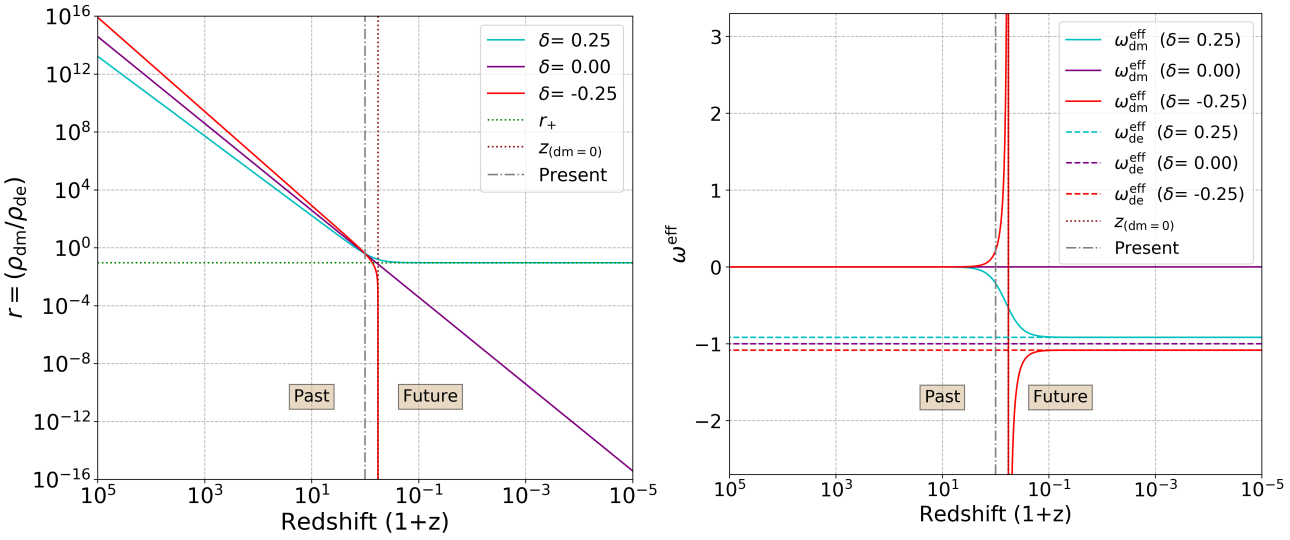

Figure 3.12: *Coincidence problem and effective equations of state ($Q_2 = \delta H \rho_{\text{de}}$)*

From the left panel in Figure 3.3 it can be seen that for the coupled model with $\delta > 0$ (iDEDM), r differs with many orders of magnitude in the past, but converges to a constant value in the future $r \to r_+$ (indicated by the dashed green line), as predicted by (3.73) and (3.92), making the present value less coincidental. The coincidence problem is thus solved for the future expansion history. This coincides with the right panel where $\omega_{\text{dm}}^{\text{eff}} = \omega_{\text{de}}^{\text{eff}}$, as shown in (3.96). The coincidence problem is also alleviated for the past expansion, since the slope of r is smaller (as predicted by (3.91)), which coincides with $\omega_{\text{de}}^{\text{eff}} > \omega_{\text{de}}$ from (3.12), causing a smaller difference in $(\omega_{\text{dm}}^{\text{eff}} - \omega_{\text{de}}^{\text{eff}})$.

Conversely, for $\delta < 0$ (iDEDM) we have $\omega_{\text{de}}^{\text{eff}} < \omega_{\text{de}}$, which worsens the coincidence problem for the past expansion history (since the slope is greater than the case $\delta = 0$). For the future expansion, it can also be seen that r becomes zero, while $\omega_{\text{de}}^{\text{eff}}$ diverges at the same point. This is due to the dark matter density ρ_{dm} which becomes zero in the future at redshift $z_{(\text{dm}=0)}$ (red dotted line) from (3.84), and then stays negative for the rest of the future expansion. Thus, the results from (3.92), (3.91), (3.94) and (3.96) can clearly be seen in Figure 3.12 and may be summarised as:

$$
\begin{aligned}
\delta > 0 \text{ (iDEDM)} \begin{cases} \text{Past expansion:} & \omega_{\text{de}}^{\text{eff}} > \omega_{\text{de}} \ (\zeta_{\text{Q}_2} < \zeta) & \textit{alleviates} \text{ coincidence problem} \\ \text{Future expansion:} & \omega_{\text{dm}}^{\text{eff}} = \omega_{\text{de}}^{\text{eff}} \ (\zeta_{\text{Q}_2} = 0) & \textit{solves} \text{ coincidence problem,} \end{cases} \\
\delta < 0 \text{ (iDMDE)} \begin{cases} \text{Past expansion:} & \omega_{\text{de}}^{\text{eff}} < \omega_{\text{de}} \ (\zeta_{\text{Q}_2} > \zeta) & \textit{worsens} \text{ coincidence problem} \\ \text{Future expansion:} & \omega_{\text{dm}}^{\text{eff}} = \omega_{\text{de}}^{\text{eff}} \ (\rho_{\text{de}} < 0) & \text{negative energy densities.} \end{cases}
\end{aligned}
\tag{3.97}
$$

These results hold due to how energy flows between the dark sectors, causing dark matter and dark energy to redshift and dilute at different rates, as discussed in section 3.2.2. To see this, we will consider the evolution of ρ_{dm} and ρ_{de}.

3.4.5 Evolution of energy densities and cosmic equalities - $Q_2 = \delta H \rho_{de}$

For Q_1 in section 3.3.5, we saw that the energy densities ρ_{dm} (3.79) and ρ_{de} (3.80) evolved with the same slope in the past, thus diluting at the same rate, which coincided with $\omega_{dm}^{eff} = \omega_{de}^{eff}$ and the coincidence problem being solved. For this model, we saw that the coincidence problem is solved for the future (3.97), thus we expect the same behaviour that was seen in Figure 3.13, but for future expansion. This can be clearly seen by plotting ρ_{dm} (3.79) and ρ_{de} (3.80) against redshift:

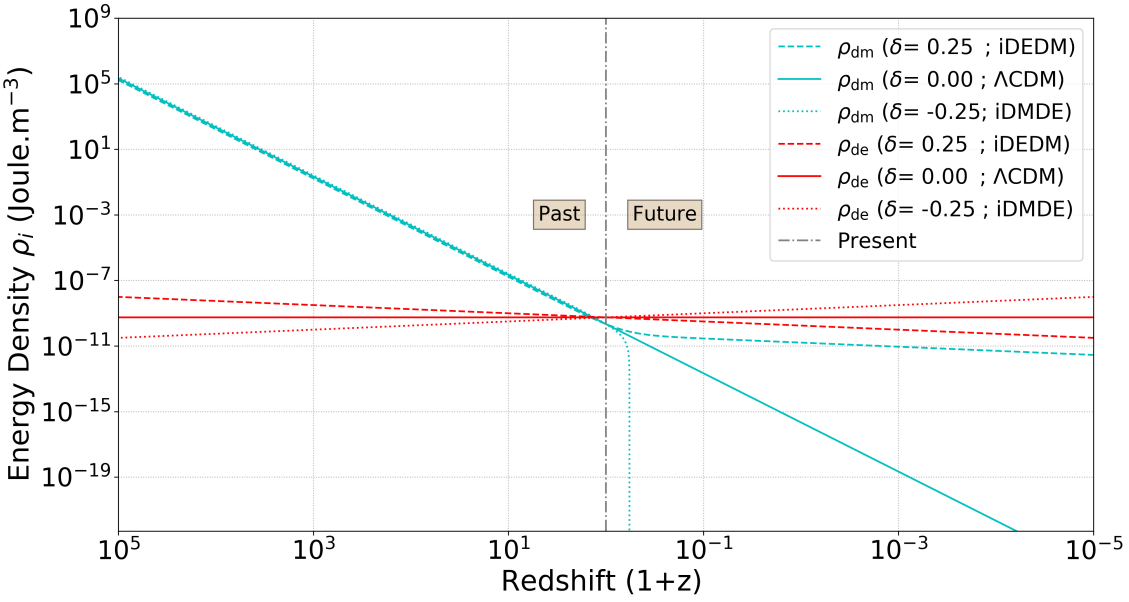

Figure 3.13: *Energy densities ρ vs redshift - ($Q_2 = \delta H \rho_{de}$)*

In Figure 3.13, we see that for $\delta > 0$ (iDEDM), dark matter receives energy from dark energy, causing ρ_{dm} to redshift slower $\omega_{dm}^{eff} < \omega_{dm}$ (smaller slope), while ρ_{de} redshifts faster (greater slope). This behaviour alleviates the coincidence problem in the past. In the future the slope at which ρ_{dm} and ρ_{de} redshift becomes the same, coinciding with $\omega_{dm}^{eff} = \omega_{de}^{eff}$ (3.96) and the coincidence problem being solved, while ρ_{dm} dilutes similar to the ΛCDM model in the past where $\omega_{dm}^{eff} = \omega_{dm}$ (3.96).

The opposite holds for $\delta < 0$ (iDMDE). Here, dark matter loses energy and redshifts faster $\omega_{dm}^{eff} > \omega_{dm}$ (greater slope), while dark energy receives this energy and redshifts slower (smaller slope). This greater difference between the slopes of ρ_{dm} and ρ_{de}, worsens the coincidence problem. There will also be a time in the future when $\rho_{dm} = 0$ at redshift $z_{(dm=0)}$ (3.84), after which $\rho_{dm} < 0$ for the rest of expansion, which is unphysical. The predicted value for $z_{(dm=0)}$ is indicated by the red marker in Figure 3.14. All these observations coincide with (3.97).

It may also be noted that $\delta > 0$ (iDEDM) ρ_{de} decreases over time, while $\delta < 0$ (iDMDE) ρ_{de} increases over time. The dark energy therefore effectively behaves like either quintessence or phantom dark energy respectively, with an equation of state $\omega_{de}^{eff} = \omega + \frac{\delta}{3}$. Since this effect continues into the future, it will have consequences for the final fate of the universe model.

We can now show that the Cosmological implications of a dark coupling hold for both coupling functions considered. This is done by plotting the density parameters of dark matter Ω_{dm} (3.81), dark energy Ω_{de} (3.82), radiation Ω_{r} (2.3) and baryonic matter Ω_{bm} (2.6):

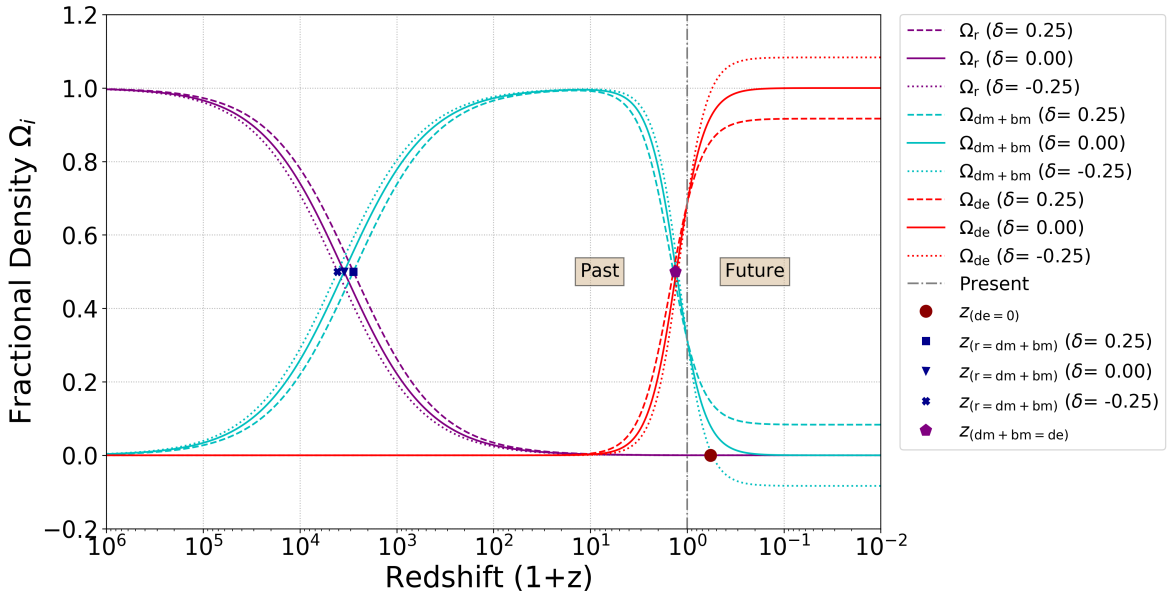

Figure 3.14: *Density parameters vs redshift - ($Q_2 = \delta H \rho_{\text{de}}$)*

From Figures 3.13 and 3.14 it is seen that for $\delta > 0$ (iDEDM), there is *less* dark matter and more dark energy in the past, and vice versa for $\delta < 0$ (iDMDE), as was previously seen in Figures 3.4 and 3.5. For $\delta > 0$ the matter-radiation equality still happens *later* and the matter-dark energy equality *earlier* in cosmic history, with the opposite holding for $\delta < 0$. Here the deviation from the ΛCDM model is significantly smaller than in Figure 3.4, with the equalities for all models happening very close to each other, as also seen in [103]. Expressions giving the exact redshift where the radiation-matter $z_{(\text{r=dm+bm})}$ (D.29) and matter-dark energy $z_{(\text{dm+bm=de})}$ (D.36) equalities happen, are derived in Appendix D.3. Equation (D.29) was numerically solved and (D.36) analytically solved, with the results shown in Tables 3.10 and 3.11. These results are indicated by the markers in Figure 3.14, matching with where the corresponding densities intersect. From these results, we once again confirm what was shown in (3.57) and in Table 3.1:

$$\begin{aligned}
&\delta > 0 \text{ (iDEDM)} \begin{cases} \text{Radiation-matter equality:} & z_{\text{IDE}} < z_{\Lambda\text{CDM}} & \text{happens } \textit{later} \text{ than } \Lambda\text{CDM} \\ \text{Matter-dark energy equality:} & z_{\text{IDE}} > z_{\Lambda\text{CDM}} & \text{happens } \textit{earlier} \text{ than } \Lambda\text{CDM}, \end{cases} \\
&\delta < 0 \text{ (iDMDE)} \begin{cases} \text{Radiation-matter equality:} & z_{\text{IDE}} > z_{\Lambda\text{CDM}} & \text{happens } \textit{earlier} \text{ than } \Lambda\text{CDM} \\ \text{Matter-dark energy equality:} & z_{\text{IDE}} < z_{\Lambda\text{CDM}} & \text{happens } \textit{later} \text{ than } \Lambda\text{CDM}, \end{cases}
\end{aligned} \tag{3.98}$$

In Figure 3.13 it may also be seen that unlike Figure 3.4, there is complete matter domination $(\Omega_{\text{dm}}, \Omega_{\text{de}})_- = (1, 0)$, as in the ΛCDM case. For this model, dark energy never completely dominates in the future, but instead dark matter and dark energy have the density parameters $(\Omega_{dm+bm}, \Omega_{\text{de}})_+ = \left(-\frac{\delta}{3\omega}, 1 + \frac{\delta}{3\omega}\right)$ from the attractor point (3.72).

3.4.6 Evolution of deceleration parameter - $Q_2 = \delta H \rho_{\text{de}}$

For this model, we have seen that the density parameters mostly deviate from the ΛCDM model during dark energy domination. We, therefore, expect this coupling function to change the behaviour of the deceleration parameter q and the effective equation of state for the fluid ω^{eff} most dramatically in the future expansion. The expressions for both q and ω^{eff} are the same for all IDE models, with only the density parameters Ω_{x} differing. Thus, for this model, we have:

$$q = \Omega_{\text{r}} + \frac{1}{2}\left(\Omega_{\text{bm}} + \Omega_{\text{dm}}\right) + \frac{1}{2}\Omega_{\text{de}}\left(1 + 3\omega\right) \qquad ; \qquad \omega^{\text{eff}} = \frac{\frac{1}{3}\Omega_{\text{r}} + \omega\Omega_{\text{de}}}{\Omega_{\text{r}} + \Omega_{\text{bm}} + \Omega_{\text{dm}} + \Omega_{\text{de}}}, \tag{3.99}$$

where the density parameters for this model are that of dark matter Ω_{dm} (3.81), dark energy Ω_{de} (3.82), radiation Ω_{r} (2.3) and baryonic matter Ω_{bm} (2.6). Plotting (3.99) with these parameters yields the following figures:

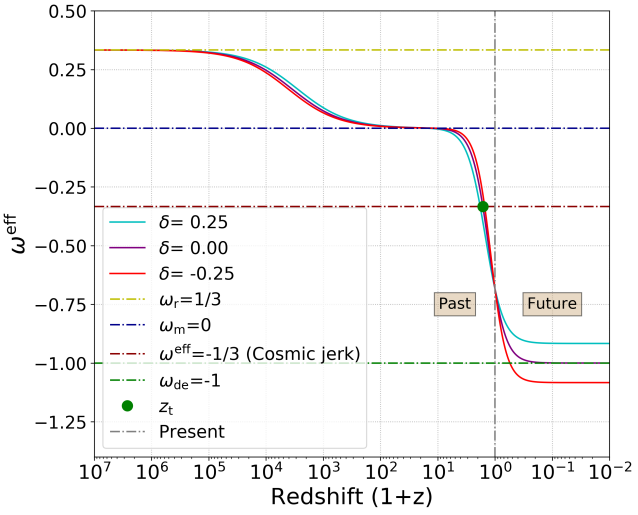

Figure 3.15: *Evolution of effective equation of state ω^{eff} with redshift ($Q_2 = \delta H \rho_{\text{de}}$)*

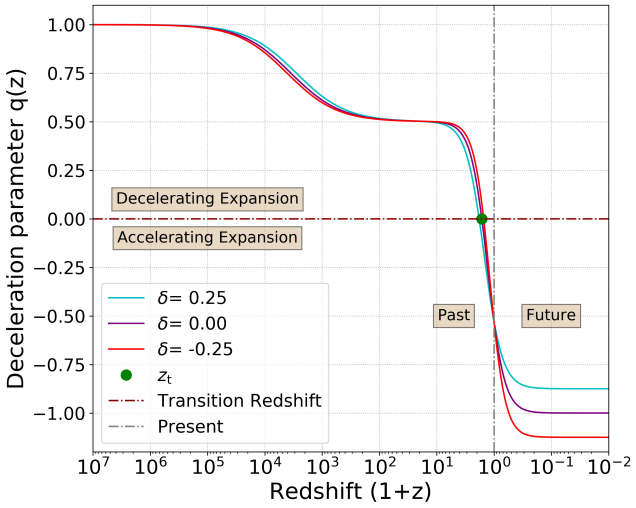

Figure 3.16: *Evolution of deceleration parameter q with redshift $(1+z)$ ($Q_2 = \delta H \rho_{\text{de}}$)*

From Figures 3.15 and 3.16 we can see that the past behaviour for the coupled models are almost identical to that of the ΛCDM model, with initial deceleration followed by acceleration from the cosmic jerk onwards. This cosmic jerk occurs at the transition redshift z_{t}, for which an analytical expression (D.36) is derived in Appendix D.3. The transition redshift for all three models are calculated from (D.36) and indicated by the marker in Figure 3.15 and 3.16, while the exact redshift for each can be found in Tables 3.10 and 3.11. Based on these results, we can again confirm the conclusions from (3.99) and Table 3.1, which state that:

$$\text{Cosmic jerk } (z_{\text{t}}) \begin{cases} \delta > 0 \text{ (iDEDM):} & z_{\text{IDE}} > z_{\Lambda\text{CDM}} \quad \text{happens } \textit{earlier} \text{ than } \Lambda\text{CDM}, \\ \delta < 0 \text{ (iDMDE):} & z_{\text{IDE}} < z_{\Lambda\text{CDM}} \quad \text{happens } \textit{later} \text{ than } \Lambda\text{CDM}. \end{cases} \tag{3.100}$$

From Figures 3.6 and 3.16 it can also be seen that similar to the ΛCDM model, these models experience complete radiation-domination $(\Omega_{\text{r}}, \Omega_{\text{dm+bm}}, \Omega_{\text{de}}) \approx (1, 0, 0) \rightarrow q = 1$; $\omega^{\text{eff}} = 1/3$, followed by complete matter-domination $(\Omega_{\text{r}}, \Omega_{\text{dm+bm}}, \Omega_{\text{de}}) \approx (0, 1, 0) \rightarrow q = 1/2$; $\omega^{\text{eff}} = 0$. As seen

in Figure 3.14, these models don't show complete dark energy domination, but instead the density parameters are obtained from the attractor point (3.72), such that we have $(\Omega_{\rm r}, \Omega_{\rm dm+bm}, \Omega_{\rm de}) \approx \left(0, -\frac{\delta}{3\omega}, 1+\frac{\delta}{3\omega}\right)$. The deceleration parameter (3.99) during dark energy domination then becomes:

$$\begin{aligned} q &= \Omega_{\rm r} + \frac{1}{2}\left(\Omega_{\rm bm} + \Omega_{\rm dm}\right) + \frac{1}{2}\Omega_{\rm de}\left(1+3\omega\right) = (0) + \frac{1}{2}\left(-\frac{\delta}{3\omega}\right) + \frac{1}{2}\left(1+\frac{\delta}{3\omega}\right)(1+3\omega) \\ &= \frac{1}{2}\left(-\frac{\delta}{3\omega} + \left[1+\frac{\delta}{3\omega} + (1+3\omega)\right]\right) = \frac{1}{2}\left(1+3\left[\omega+\frac{\delta}{3}\right]\right) = \frac{1}{2}\left(1+3\omega_{\rm de}^{\rm eff}\right). \end{aligned} \tag{3.101}$$

For the effective equation of state (3.99) we have:

$$\omega^{\rm eff} = \frac{\frac{1}{3}\Omega_{\rm r} + \omega\Omega_{\rm de}}{\Omega_{\rm r} + \Omega_{\rm bm} + \Omega_{\rm dm} + \Omega_{\rm de}} = \frac{\frac{1}{3}(0) + \omega\left(1+\frac{\delta}{3\omega}\right)}{(0) + \left(-\frac{\delta}{3\omega}\right) + \left(1+\frac{\delta}{3\omega}\right)} = \frac{\omega+\frac{\delta}{3}}{1} = \omega + \frac{\delta}{3} = \omega_{\rm de}^{\rm eff}, \tag{3.102}$$

where both (3.101) and (3.102) reduce back to the ΛCDM case when either $\delta = 0$ or $\omega_{\rm de}^{\rm eff} = \omega_{\rm de}$. We can now calculate q and $\omega^{\rm eff}$ for the parameters used in Figures 3.15 and 3.16. Thus, for $\delta = 0.25$ (iDEDM) we have $q = \frac{1}{2}\left(1+3\left[-1+\frac{0.25}{3(-1)}\right]\right) = -0.875$ and $\omega^{\rm eff} = \left(-1+\frac{0.25}{3(-1)}\right) = 0.916$, while for $\delta = -0.25$ (iDMDE) we have $q = \frac{1}{2}\left(1+3\left[-1+\frac{0.25}{3(-1)}\right]\right) = -1.125$ and $\omega^{\rm eff} = \left(-\frac{-0.25}{3}\right) = 1.083$ for dark energy-domination. These results can be seen to exactly match the values that q and $\omega^{\rm eff}$ converge to in Figures 3.15 and 3.16 during dark energy-domination.

This change in the deceleration parameter and effective equations of state can thus make the total fluid effectively behave as quintessence or phantom dark energy, without necessarily having a dark energy equation of state in that regime. Dark energy may have an equation of state $\omega < -1$, but will only have the consequences of the phantom-regime if there is a large enough negative coupling such that $\omega_{\rm de}^{\rm eff} < -1 \rightarrow \omega + \frac{\delta}{3} < -1$ [103]. Thus, dark energy may behave like quintessence if $\omega_{\rm de}^{\rm eff} > -1$ which corresponds to $\delta > 0$ (iDEDM) or phantom dark energy $\omega_{\rm de}^{\rm eff} < -1$ when $\delta < 0$ (iDMDE) as seen in Figures 3.15. This will have important consequences for the final fate of these IDE model universes, which will be discussed in section 3.4.8.

3.4.7 Hubble parameter and age of the universe - $Q_2 = \delta H \rho_{\rm de}$

The interaction Q_2 will affect the age of the universe in the same way as Q_1 in section 3.3.7. We consider the age of the universe from the evolution of the Friedmann equation from (2.13):

$$\int_0^t dt = \int_0^a \frac{1}{H(a)} da \qquad ; \qquad H^2(a) = \left(\frac{\dot{a}}{a}\right)^2 = \frac{8\pi G}{3}\left(\rho_{\rm r} + \rho_{\rm bm} + \rho_{\rm dm} + \rho_{\rm de}\right) - \frac{kc^2}{a^2}, \tag{3.103}$$

where in this model we use the energy densities $\rho_{\rm r}$ (2.3); $\rho_{\rm bm}$ (2.6); $\rho_{\rm dm}$ (3.79); $\rho_{\rm de}$ (3.80) and $k = 0$. Since both the deceleration parameter and the total effective equation of state deviates mostly during dark energy domination, we expect the expansion rate to mostly change for future

expansion. This may be seen by plotting the Hubble parameter (3.103), relative to the non-interacting case ($H/H_{\delta=0}$), against redshift. The evolution of the scale factor against time is also plotted and the age of the universe calculated, by numerically integrating (3.103) with the 4th-order Runge Kutta method, as detailed in Appendix A.4. This yields:

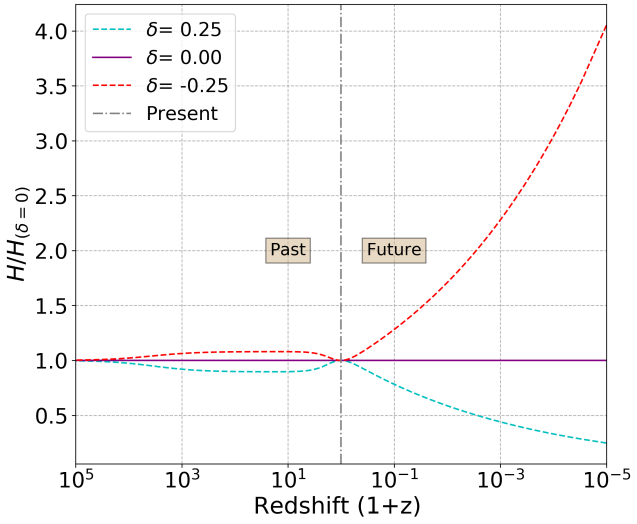

Figure 3.17: *Relative Hubble parameter ($H/H_{\delta=0}$) vs redshift ($Q_2 = \delta H \rho_{\rm de}$)*

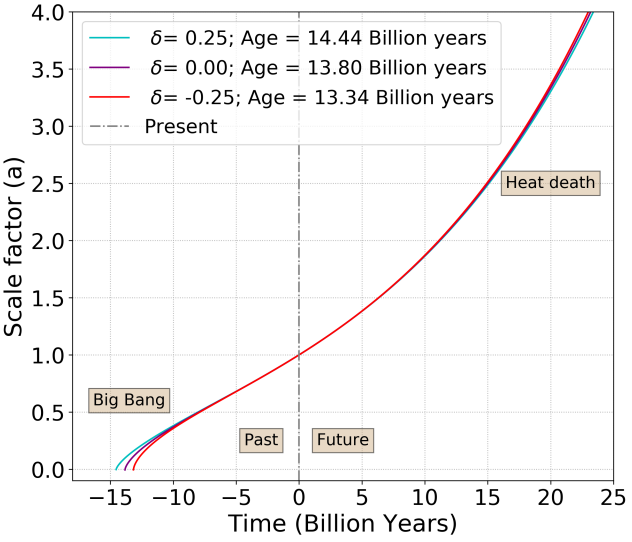

Figure 3.18: *Evolution of scale factor with time ($Q_2 = \delta H \rho_{\rm de}$)*

In Figure 3.17, $H/H_{\delta=0}$ evolves similarly to Q_1 in Figure 3.17. In both cases $H/H_{\delta=0} < 1$ for $\delta > 0$ (iDEDM) throughout most of the expansion history, indicating a faster expansion rate. This is again due to the overall suppression of dark matter seen in Figure 3.14, which causes a lower value for q and $\omega^{\rm eff}$ and therefore a slower expansion rate, as explained in section 3.3.7. This slower expansion rate in turn causes an older age for the universe as seen in Figure 3.18. The opposite of this holds for $\delta < 0$ (iDEDM). We therefore confirm the following result from (3.68) and Table 3.1:

$$\text{Age of universe } (t_0) \begin{cases} \delta > 0 \text{ (iDEDM):} & t_{(0,\text{IDE})} > t_{(0,\Lambda\text{CDM})} \quad \textit{Older} \text{ universe than } \Lambda\text{CDM}, \\ \delta < 0 \text{ (iDMDE):} & t_{(0,\text{IDE})} < t_{(0,\Lambda\text{CDM})} \quad \textit{Younger} \text{ universe than } \Lambda\text{CDM}. \end{cases} \tag{3.104}$$

In Figure 3.17, it can also be seen that $H/H_{\delta=0}$ slightly deviates from the ΛCDM model in the past, while greatly deviating for future expansion. Before considering this future expansion, we need to consider the stability of this model.

3.4.8 Doom factor and big rip - $Q_2 = \delta H \rho_{\rm de}$

As previously discussed with regard to the coupling Q_1 in section (3.3.8), an equation of state $\omega = -1$, causes gravitational instabilities [108, 109]. The stability of this model will once again be dependent on the doom factor $\mathbf{d}$ (3.14). This condition $\mathbf{d} < 0$ guarantees an a priori stable universe as discussed in section 3.2.4. Thus, for $Q_2 = \delta H \rho_{\rm de}$ we have the doom factor (3.14) [103]:

$$\mathbf{d}_2 = \frac{Q_2}{3H\rho_{\rm de}(1+\omega)} = \frac{\delta H \rho_{\rm de}}{3H\rho_{\rm de}(1+\omega)} = \frac{\delta}{3(1+\omega)}, \tag{3.105}$$

where we require $\mathbf{d} < 0$ to ensure the stability of the universe. We can see from (3.65) that similar to Q_1 in (3.66), this only occurs if δ and $(1+\omega)$ have opposite signs [87, 103, 105, 106, 108, 109]:

$$\begin{aligned}
\mathbf{d}_2 < 0 &\begin{cases} \delta < 0 \quad ; \quad \omega > -1 & \text{(Quintessence regime)} \\ \delta > 0 \quad ; \quad \omega < -1 & \text{(Phantom regime)} \end{cases} \quad \rightarrow \text{No instabilities expected} \\
\mathbf{d}_2 > 0 &\begin{cases} \delta > 0 \quad ; \quad \omega > -1 & \text{(Quintessence regime)} \\ \delta < 0 \quad ; \quad \omega < -1 & \text{(Phantom regime)} \end{cases} \quad \rightarrow \text{Instabilities can develop if } \mathbf{d} > 1.
\end{aligned} \tag{3.106}$$

Besides being stable, these models need to have positive energy throughout the entire past and future expansion to be considered viable. We therefore need to consider the positive energy condition $0 < \delta < -3\omega/(1+\frac{1}{r_0})$ in (3.87) and Table 3.7. Here it was shown that we will always have $\rho_{\text{dm}} < 0$ in the future if $\delta < 0$ (iDMDE), which is unphysical. The results from (3.106) and (3.43) can be taken together in the following table to determine the viability of the model:

δ	Energy flow	ω	Dark energy	$\mathbf{d}$	a priori stable	$\rho_{\text{dm}} > 0$	$\rho_{\text{de}} > 0$	Viable
+	DE $\rightarrow$ DM	< -1	Phantom	-	$\surd$	$\surd$	$\surd$	$\surd$
+	DE $\rightarrow$ DM	> -1	Quintessence	+	X	$\surd$	$\surd$	X
-	DM $\rightarrow$ DE	< -1	Phantom	+	X	X	$\surd$	X
-	DM $\rightarrow$ DE	> -1	Quintessence	-	$\surd$	X	$\surd$	X

Table 3.8: *Stability and positive energy criteria ($Q_2 = \delta H \rho_{\text{de}}$)*

From Table 3.8, we see that similar to Q_1, the only scenario that is free from both negative energy densities and instabilities, is phantom dark energy $\omega < -1$ in the $\delta > 0$ (iDEDM) regime. These models will thus violate the Energy conditions of general relativity; and suffer from the consequences of doing so [41]. Since $\omega_{\text{dm}}^{\text{eff}} = \omega_{\text{de}}^{\text{eff}} = \omega + \frac{\delta}{3}$ (3.96) in the future, the value of δ will determine if the universe model will experience a late time Big rip singularity. For a big rip to occur we need $\rho_{\text{de}} \rightarrow \infty$ in a finite time. This will only occur for this model if ρ_{de} (3.76) increases with scale factor as the universe expands, which only happens if the effective equation of state $\omega_{\text{de}}^{\text{eff}} = \omega + \frac{\delta}{3} < -1$:

$$\rho_{\text{de}} = \rho_{(\text{dm},0)} a^{-3(1+\omega+\frac{\delta}{3})} \quad ; \quad -3\left(1+\omega+\frac{\delta}{3}\right) > 0 \quad \text{if} \quad \omega_{\text{de}}^{\text{eff}} = \omega + \frac{\delta}{3} < -1. \tag{3.107}$$

If condition (3.107) is obeyed, the equivalent equation to (2.50) for the time of the rip t_{rip} [10, 95] can be derived for this IDE model (see Appendix E.3) as:

$$t_{rip} \approx -\frac{2}{3H_0(1+\omega+\frac{\delta}{3})\sqrt{\left(1-\frac{\delta}{\delta+3\omega}\right)\left(1-\Omega_{(\text{dm+bm},0)}\right)}}, \tag{3.108}$$

which reduces back to (2.50) if $\delta = 0$. The predicted time of the big rip (3.108) is plotted alongside the evolution of the scale factor (using the Friedmann equation (3.103) in Figure 3.19:

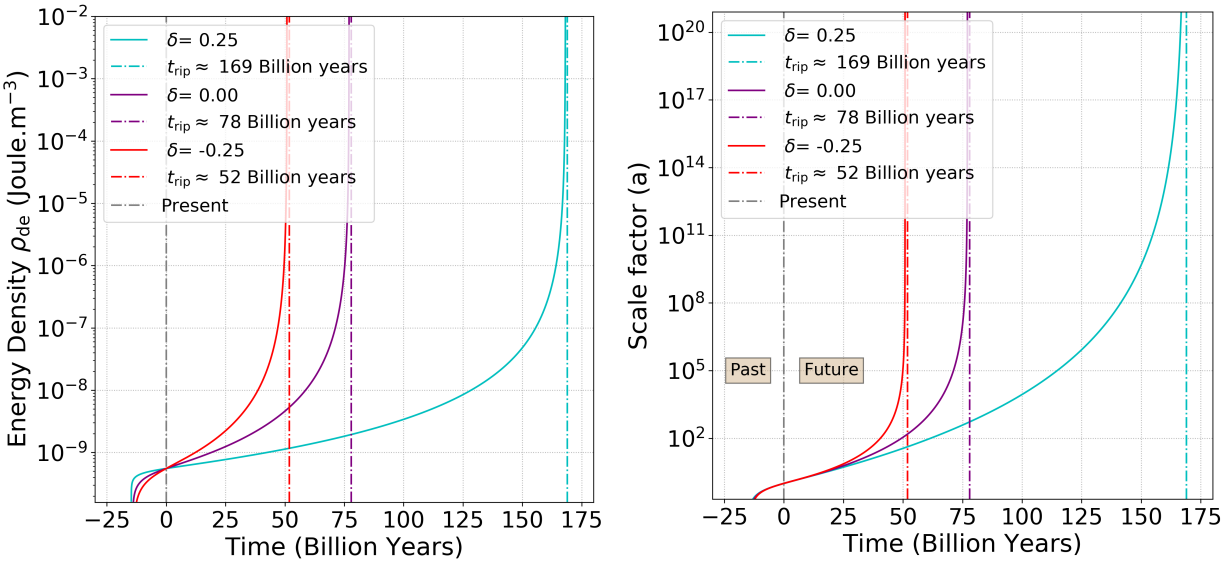

Figure 3.19: *Evolution of energy density, scale factor and the big rip for phantom ($\omega = -1.15$) IDE models - ($Q_2 = \delta H \rho_{de}$)*

In Figure 3.19, we can see that the predicted time of the big rip singularity t_{rip} (3.108) coincides with the time at which both $a \to \infty$ and $\rho_{de} \to \infty$. The time t_{rip} is significantly affected by the coupling, which coincides with what was found for Q_1 (3.68), such that:

$$\text{Big rip} \begin{cases} \delta > 0 \text{ (iDEDM):} & t_{(\text{rip,IDE})} > t_{(\text{rip},\Lambda\text{CDM})} \quad \textit{Later} \text{ big rip than } \Lambda\text{CDM}, \\ \delta < 0 \text{ (iDMDE):} & t_{(\text{rip,IDE})} < t_{(\text{rip},\Lambda\text{CDM})} \quad \textit{Earlier} \text{ big rip than } \Lambda\text{CDM}. \end{cases} \tag{3.109}$$

Unlike Q_1, these models can still be viable ($\omega < -1$ in the $\delta > 0$ (iDEDM) regime) and avoid a big rip, as long as condition (3.107) is not met, such that $\omega_{de}^{eff} = \omega + \frac{\delta}{3} > -1$, while quintessence models with $\omega > -1$ may also have a big rip if $\omega_{de}^{eff} < -1$. These scenarios are expressed in Figure 3.20:

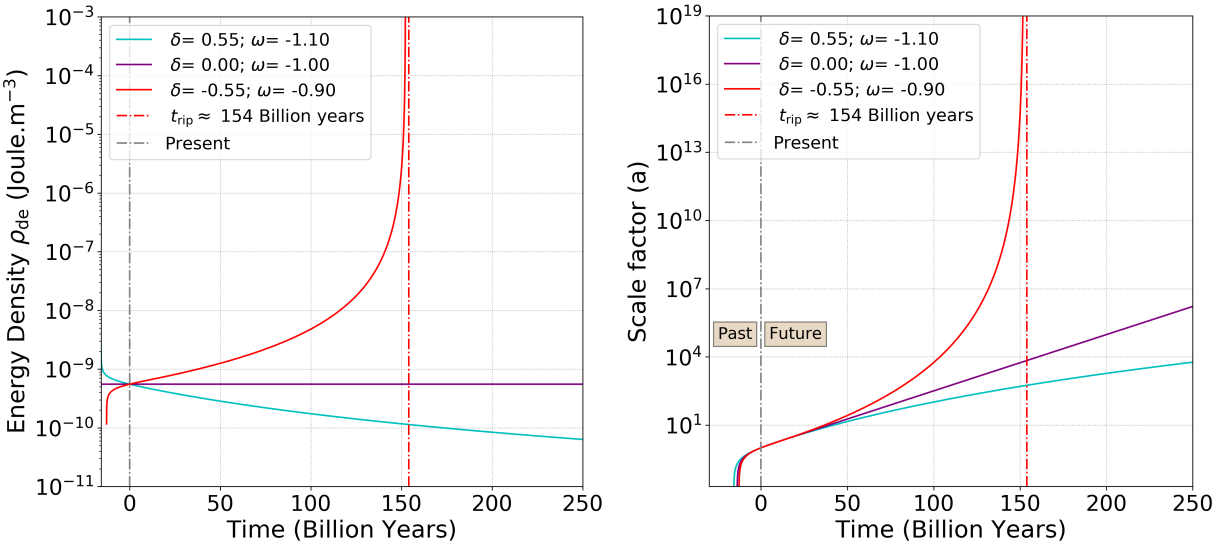

Figure 3.20: *Evolution of energy density, scale factor and the big rip for vacuum ($\omega = -1$), quintessence ($\omega = -0.9$) and phantom ($\omega = -1.1$) IDE models - ($Q_2 = \delta H \rho_{de}$)*

3.4.9 Concluding remarks on IDE model $Q_2 = \delta H \rho_{\text{de}}$

We have seen that all the Cosmological implications of a dark coupling predicted in Table 3.1 hold for both $Q_1 = \delta H \rho_{\text{dm}}$ and $Q_2 = \delta H \rho_{\text{de}}$. The results for Q_2 will be summarised below.

For this model, we have derived the often neglected positive energy condition $0 < \delta < -3\omega/(1+\frac{1}{r_0})$ (3.87), from which we note the important fact that the $\delta < 0$ (iDMDE) regime will always lead to $\rho_{\text{dm}} < 0$ in the future. This implies that the $\delta < 0$ (iDMDE) regime should not be taken seriously as a potential dark energy candidate. For the more viable $\delta > 0$ (iDMDE) regime, we saw that this model can solve the coincidence problem in the future, whilst alleviating the problem for the past (3.97). Furthermore, as seen in model Q_1, the iDMDE regime predicts a *later* radiation-matter equality, while both the matter-dark energy equality (3.98) and cosmic jerk will occur *earlier* (3.109). The age of these universe models will also be *older* (3.104). The opposite holds for $\delta < 0$ (iDMDE). These important events may be quantitatively described with cosmological parameters (2.25), for the cases $\delta = 0$ (ΛCDM), $\delta = 0.25$ (iDEDM) and $\delta = -0.25$ (iDMDE), in Tables 3.9, 3.10 and 3.11 respectively.

Table 3.9: *Important events in interacting dark energy model $\delta = 0.00$ (ΛCDM) - $Q_2 = \delta H \rho_{\text{de}}$*

Event	Redshift z	Time (Gyr)	ρ_{r}	$\rho_{\text{dm+bm}}$	ρ_Λ (J/m^3)
Big bang singularity	∞	13.80	∞	∞	∞
Radiation-matter equality	3499	13.80	10.9	10.9	5.5e-10
Cosmic jerk	0.63	6.12	5.2e-13	1.2e-9	5.5e-10
Matter-dark energy equality	0.30	3.50	2.1e-13	1.1e-9	5.5e-10

Table 3.10: *Important events in interacting dark energy model $\delta = 0.25$ (iDEDM) - $Q_2 = \delta H \rho_{\text{de}}$*

Event	Redshift z	Time (Gyr)	ρ_{r}	$\rho_{\text{dm+bm}}$	ρ_{de} (J/m^3)
Big bang singularity	∞	14.44	∞	∞	∞
Radiation-matter equality	2807	14.44	4.5	4.5	4.0e-9
Cosmic jerk	0.82	7.23	8.0e-13	1.3e-9	6.4e-10
Matter-dark energy equality	0.39	4.35	2.7e-13	6.0e-10	6.0e-10

Table 3.11: *Important events in interacting dark energy model $\delta = -0.25$ (iDMDE) - $Q_2 = \delta H \rho_{\text{de}}$*

Event	Redshift z	Time (Gyr)	ρ_{r}	ρ_{m}	ρ_{de} (J/m^3)
Big bang singularity	∞	13.34	∞	∞	∞
Radiation-matter equality	4084	13.34	20.3	20.3	6.6e-11
Cosmic jerk	0.52	5.29	7.8e-13	1.3e-9	6.4e-10
Matter-dark energy equality	0.24	2.93	1.7e-13	5.3e-10	5.3e-10

From Table 3.8, we see that the only viable regime for these models, which avoid both negative energy densities and gravitational instabilities, is phantom dark energy $\omega < -1$ in the $\delta > 0$ (iDEDM) regime. Unlike Q_1, these models will only experience a big rip future singularity at t_{rip} (3.108) if the condition $\omega_{\text{de}}^{\text{eff}} = \omega + \frac{\delta}{3} < -1$ (3.107) is met. Even if all theoretical constraints are met, any viable model should also be consistent with observational data, which we will consider next.

CHAPTER 4

Constraining interacting dark energy models with supernovae data

4.1 Observational constraints and MCMC simulations

In this chapter, we will apply some observational constraints to interacting dark energy models. There are many different cosmological data sets which include early time probes such as the CMB [4] and large scale structure constraints from baryonic acoustic oscillations (BAO) [111–113], but we will be considering Type Ia supernovae which were first used to discover Cosmic acceleration.

Utilising Type Ia supernovae, we will try to find the best Cosmological Parameters for our two IDE models (within their domain of viability), followed by a Statistical analysis to see if the predicted expansion histories of our IDE models agree with the observations from supernovae data. This will be done using a data set of 359 Type-Ia Supernovae. This data is used with a previously developed Markov Chain Monte-Carlo (MCMC) simulation for a flat FLRW universe. See [114–116] for the details of the MCMC simulation, which was originally developed to test f(R) gravity models against the ΛCDM model [115]). Once the Distance modulus for any model is specified, this simulation finds the best luminosity distance function value for different combinations of cosmological parameters. It then performs the relevant statistical analysis on these results as well. We therefore only need to specify the distance modulus equations for our IDE models, edit the MCMC code and then interpret the results obtained from the simulation. This MCMC simulation will first be used on the ΛCDM model to obtain a baseline, against which we will compare our IDE models. Once the best cosmological parameters for the interacting dark energy models have been found, the results will be statistically compared to those of the ΛCDM model. Before doing this, we will briefly discuss what Type Ia Supernovae are; and their significance as cosmological probes.

4.2 Standard candles and type Ia supernovae

Type Ia supernovae are often used as data points in cosmology since they are considered standard candles. Standard candles are objects whose absolute luminosity L are known; and thus their observed luminosity flux is only dependent on their distance from the observer and no other stellar properties [9]. This distance may be approximated with redshift z, and in an expanding universe, the distances and redshift of these objects may be used together to determine the rate of expansion at different times. These objects may therefore be used to test the Friedmann equation for any model as a description of the expansion history of the universe.

Type Ia supernovae, like all supernovae, are exploding stars. The reason type Ia supernovae may be considered standard candles is due to the process which ignites the explosion. Type Ia supernovae are formed from a white dwarf in a binary system, which accretes mass from a main sequence stellar companion [8]. White dwarfs are stellar remnants that mainly composed of carbon and oxygen. These stars are supported against gravity not by nuclear fusion but by the quantum mechanical effect known as electron degeneracy pressure, resulting from the Pauli exclusion principle. This effect can support the gravity of a white dwarf up until it reaches a maximum mass limit, known as the Chandrasekhar limit [117] which is approximately $M \approx 1.4 M_{\odot}$ [8, 118]. When the white dwarf exceeds this limit (by accreting mass from its stellar companion), the dwarf collapses and the increased density and pressure triggers a runaway nuclear fusion reaction within the star. This reaction blows the star away in a massive explosion, the brightness of which can temporarily outshine all other stars in its host galaxy [10, 119, 120]. These explosions rise to a peak brightness within a period of a few weeks, after which the brightness slowly fades over a few months, yielding a characteristic light curve [8]. Since all type Ia supernovae happen by this same mechanism and at the same critical mass, the explosions should have similar absolute luminosities and light curves. The absolute luminosity may then be used to determine the distance to the supernovae. Type Ia supernovae can therefore be regarded as standard candles.

The data used for this simulation is a set of 123 low redshift ($0.01 < z < 0.1$) and 236 intermediate redshift ($0.1 < z < 1.1$) Type-Ia Supernovae (obtained from the SDSSII/SNLS2 Joint Light-curve Analysis (JLA)), which may be found on the NASA extragalactic database (NED). The full JLA dataset will not be used due to inefficiencies of the MCMC simulation as explained in [114]. For these supernovae, the calculated absolute magnitude in the B-filter will be used (which are found in [121–123])[1]

[1] The complete supernovae dataset and the full code for the MCMC simulation, which produced all the results in this chapter, can be found in the Google drive folder https://drive.google.com/drive/folders/1Y3MhWzDrRC5v4D9jSCsAv_2X1QDwf7PW?usp=sharing

4.3 Distance modulus

To compare the supernovae data with the predictions of our models, we need a distance modulus equation which relates the difference u between the apparent magnitude m and the absolute magnitude M of an object, such that [10]:

$$u = m - M = 25 + 5 \times \log_{10}(D_{\mathrm{L}}) \tag{4.1}$$

where D_{L} is the luminosity distance. We want this quantity in terms of redshift z, so D_{L} will be related to the transverse comoving distance D_M, such that:

$$D_{\mathrm{L}} = (1+z)D_{\mathrm{M}}, \tag{4.2}$$

where D_{M} is in turn related to the curvature parameter Ω_{k}:

$$D_{\mathrm{M}} = \begin{cases} D_{\mathrm{H}} \frac{1}{\Omega_{\mathrm{k}}} \sinh\left(\sqrt{\Omega_{\mathrm{k}}} \frac{D_{\mathrm{c}}}{D_{\mathrm{H}}}\right) & \text{for} \quad \Omega_{\mathrm{k}} > 0 \\ D_{\mathrm{c}} & \text{for} \quad \Omega_{\mathrm{k}} = 0 \\ D_{\mathrm{H}} \frac{1}{|\Omega_{\mathrm{k}}|} \sinh\left(\sqrt{\Omega_{\mathrm{k}}} \frac{D_{\mathrm{c}}}{D_{\mathrm{H}}}\right) & \text{for} \quad \Omega_{\mathrm{k}} < 0; \end{cases} \tag{4.3}$$

where D_{H} is the Hubble distance and D_{c} is the line-of sight co-moving distance (LSCD). Since we are making the simplifying assumption that the universe is flat ($\Omega_{\mathrm{k}} = 0$), the transverse comoving distance will be equal to the LSCD ($D_{\mathrm{M}} = D_{\mathrm{c}}$). The LSCD D_{c} may in return be defined as [9]:

$$D_{\mathrm{c}} = \int_0^{t_0} \frac{cdt}{a} = \frac{c}{H_0} \int_0^z \frac{dz'}{jh(z')} = D_{(\mathrm{H},0)} \int_0^z \frac{dz'}{h(z')}, \tag{4.4}$$

with z' the redshift of the object you are observing and $h(z')$ the normalised Hubble parameter $h(z) = \frac{H(z)}{H_0}$. Finally, we also have the current Hubble distance $D_{(\mathrm{H},0)}$ as:

$$D_{(\mathrm{H},0)} = \frac{c}{H_0} = \frac{3 \times 10^8 \text{ m.s}^{-1}}{100\bar{h} \text{ km.s}^{-1}\text{Mpc}^{-1}} = 3000\bar{h}^{-1}\text{Mpc}, \tag{4.5}$$

with $\overline{h}$ the uncertainty in the measured value of H_0 (with $\overline{h} = 0.674$ for CMB data [4]) [11]. Taking all this together (substituting (4.5) into (4.4), substituting that result into (4.3), which is again substituted into (4.2), which is finally substituted into (4.1)) gives the distance modulus as:

$$u = m - M = 25 + 5 \times \log_{10}\left(3000\bar{h}^{-1}(1+z) \int_0^z \frac{dz'}{h(z')}\right), \tag{4.6}$$

where the corresponding normalised Hubble parameter $h(z)$ can be substituted in for each model. To do this analysis, we now need to obtain the normalised Hubble parameter $h(z)$ for the ΛCDM model, as well as the IDE models $Q_1 = \delta H \rho_{\mathrm{dm}}$ and $Q_2 = \delta H \rho_{\mathrm{de}}$.

4.3.1 Distance modulus ΛCDM

To simplify our models, we will assume a flat universe in which the radiation density is negligible (such that $\Omega_{\mathrm{k}} = \Omega_{\mathrm{r}} = 0$). For the ΛCDM model, the normalised Hubble parameter $h(z)$ is obtained from $H(z)$ (2.19):

$$\begin{aligned} h(z) = \frac{H(z)}{H_0} &= \sqrt{\Omega_{(\mathrm{r},0)}(1+z')^4 + \Omega_{(\mathrm{m},0)}(1+z')^3 + \Omega_{(\Lambda,0)} + \Omega_{(\mathrm{k},0)}(1+z')^2} \\ &= \sqrt{\Omega_{(\mathrm{m},0)}(1+z')^3 + \Omega_{(\Lambda,0)}} \\ &= \sqrt{\Omega_{(\mathrm{m},0)}(1+z')^3 + (1-\Omega_{(\mathrm{m},0)})}, \end{aligned} \tag{4.7}$$

where in the second step we assumed the universe to be flat, with a negligible contribution from radiation (such that $\Omega_{\mathrm{k}} = \Omega_{\mathrm{r}} = 0$, while noting that in a flat universe $\Omega_{(\Lambda,0)} = 1 - \Omega_{(m,0)}$ (1.33)). The distance modulus for the ΛCDM model is then obtained by substituting in the normalised Hubble parameter from (4.7) into (4.6), which gives:

$$u = m - M = 25 + 5 \times \log_{10}\left(3000\bar{h}^{-1}(1+z)\int_0^z \frac{dz'}{\sqrt{\Omega_{(\mathrm{m},0)}(1+z')^3 + (1-\Omega_{(\mathrm{m},0)})}}\right), \tag{4.8}$$

where we can see that for the ΛCDM model under these assumptions, there are only $K = 2$ free parameters: $\bar{h}$ and $\Omega_{(\mathrm{m},0)}$.

4.3.2 Distance modulus $Q_1 = \delta H \rho_{\mathrm{dm}}$

To find the normalised Hubble parameter $h(z)$ for this model, we take the corresponding Friedmann equation (3.63) with energy densities ρ_{bm} (2.6), ρ_{dm} (3.38), ρ_{de} (3.39) and $k = \rho_{\mathrm{r}} = 0$, yielding:

$$\begin{aligned} h(z) =& \sqrt{\frac{8\pi G}{3H_0^2}\left(\rho_{\mathrm{bm}} + \rho_{\mathrm{dm}} + \rho_{\mathrm{de}}\right)} \\ =& \sqrt{\left(\Omega_{(\mathrm{de},0)} + \Omega_{(\mathrm{dm},0)}\frac{\delta}{\delta+3\omega}\left[1-(1+z')^{-(\delta+3\omega)}\right]\right)(1+z)^{3(1+\omega)}} \\ & \sqrt{+\Omega_{(\mathrm{dm},0)}(1+z')^{-(\delta-3)} + \Omega_{(\mathrm{bm},0)}(1+z')^3} \\ =& \sqrt{\left(\left(1-\Omega_{(\mathrm{bm},0)} - \Omega_{(\mathrm{dm},0)}\right) + \Omega_{(\mathrm{dm},0)}\frac{\delta}{\delta+3\omega}\left[1-(1+z')^{-(\delta+3\omega)}\right]\right)(1+z)^{3(1+\omega)}} \\ & \sqrt{+\Omega_{(\mathrm{dm},0)}(1+z')^{-(\delta-3)} + \Omega_{(\mathrm{bm},0)}(1+z')^3}. \end{aligned} \tag{4.9}$$

This IDE model has at least $K = 5$ free parameters: $\bar{h}$; $\Omega_{(\mathrm{dm},0)}$; $\Omega_{(\mathrm{bm},0)}$; ω and δ. This is three more than the uncoupled ΛCDM model.

4.3.3 Distance modulus $Q_2 = \delta H \rho_{\text{de}}$

To find the normalised Hubble parameter $h(z)$ for this model, we take the corresponding Friedmann equation (3.103) with energy densities ρ_{bm} (2.6), ρ_{dm} (3.79) and ρ_{de} (3.80) and $k = \rho_{\text{r}} = 0$, thus:

$$\begin{aligned}
h(z) =& \sqrt{\frac{8\pi G}{3H_0^2}\left(\rho_{\text{bm}} + \rho_{\text{dm}} + \rho_{\text{de}}\right)} \\
=& \sqrt{\left(\Omega_{(\text{dm},0)} + \Omega_{(\text{de},0)}\frac{\delta}{\delta+3\omega}\left[1-(1+z')^{(\delta+3\omega)}\right]\right)(1+z')^3 + \Omega_{(\text{de},0)}(1+z')^{(3+3\omega+\delta)}} \\
& \sqrt{+\Omega_{(\text{bm},0)}(1+z')^3} \\
=& \sqrt{\left((1+z')^{(3\omega+\delta)} + \frac{\delta}{\delta+3\omega}\left[1-(1+z')^{(\delta+3\omega)}\right]\right)\Omega_{(\text{de},0)}(1+z')^3} \\
& \sqrt{+\left(\Omega_{(\text{dm},0)} + \Omega_{(\text{bm},0)}\right)(1+z')^3} \\
=& \sqrt{\left[\left(1-\frac{\delta}{\delta+3\omega}\right)(1+z')^{(3\omega+\delta)} + \frac{\delta}{\delta+3\omega}\right]\Omega_{(\text{de},0)}(1+z')^3 + \left(\Omega_{(\text{dm},0)} + \Omega_{(\text{bm},0)}\right)(1+z')^3} \\
=& \sqrt{\left[\left(1-\frac{\delta}{\delta+3\omega}\right)(1+z')^{(3\omega+\delta)} + \frac{\delta}{\delta+3\omega}\right]\left(1-\Omega_{(\text{m},0)}\right)(1+z')^3 + \Omega_{(\text{m},0)}(1+z')^3}
\end{aligned} \tag{4.10}$$

This coupled model has $K = 4$ free parameters: $\bar{h}$; $\Omega_{(\text{m},0)}$; ω and δ. This is two more than the uncoupled ΛCDM model, but one less than the $Q_1 = \delta H \rho_{\text{dm}}$ coupling. This is due to the dark matter and baryonic matter that can be grouped together ($\Omega_{(\text{dm},0)} + \Omega_{(\text{bm},0)} = \Omega_{(\text{m},0)}$), as was originally done in (3.71); due to the coupling function being proportional to the dark energy density $Q_2 \propto \rho_{\text{de}}$. Conversely, in coupling Q_1, the coupling strength is proportional to only the dark matter density $Q_1 \propto \rho_{\text{dm}}$, and not the total matter density. Thus, dark matter and baryonic matter cannot be grouped together. This can be seen in the difference between the Friedmann equations (4.10) and (4.9).

4.4 Cosmological Parameters

Using the MCMC simulation, the distance modulus for each model can be fitted to the supernovae data from which it can determine the most probable set of free parameter values for each model. From Tables 3.3 and 3.8 we saw that for both IDE models, the only viable regime (avoiding both negative energy densities and gravitational instabilities) is phantom dark energy $\omega < -1$ in the $\delta > 0$ (iDEDM) regime. These constraints on the free parameters are used to establish priors, which were chosen as:

$$0 < \Omega_{\text{m/dm}} < 1 \quad ; \quad 0 < \bar{h} < 1 \quad ; \quad -1.5 < \omega < -1 \quad ; \quad 0 < \delta < 1 \quad ; \quad 0 < \Omega_{\text{bm}} < 0.1 \tag{4.11}$$

These constraints are used for the ΛCDM, Q_1 and Q_2 models, with the applicable set of parameters for each model. These priors ensure that we have matter in the universe ($0 < \Omega_{\mathrm{m/dm}} < 1$), that the universe is expanding ($0 < \bar{h} < 1$); all energy densities remain positive throughout past and future evolution $0 < \delta < 1$, while avoiding the presence of any early time instabilities $-1.5 < \omega < -1$. In the MCMC simulation, we used 100 random walkers, each taking 10000 steps. These parameters were chosen by trial and error to produce meaningful results while constrained by available computational power. We may now consider the results for the baseline ΛCDM model.

4.4.1 Cosmological parameters - ΛCDM

For the ΛCDM model, we only have two free parameters, which are $\bar{h}$ and $\Omega_{(\mathrm{m},0)}$ in (4.8). Therefore, only the first two constraints $0 < \Omega_{\mathrm{m}} < 1$; $0 < \bar{h} < 1$ in (4.11) will apply, with the other parameters fixed such that $\omega = -1$ and $\delta = 0$. Running the MCMC simulation [114] produces Figure 4.1:

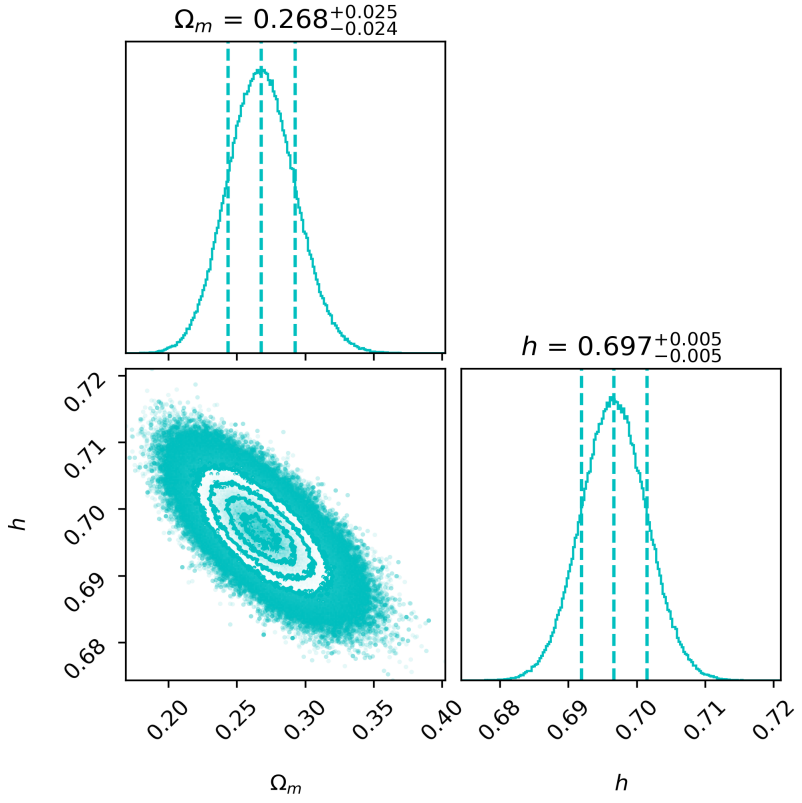

Figure 4.1: *MCMC simulation results - (ΛCDM)*

In Figure 4.1, the most probable parameter value is indicated by the middle dashed line for each parameter, assuming a Gaussian distribution [114]. The other two dashed lines on either side of the best value indicate a single standard deviation σ error on this calculated value. Thus, from Figure 4.1 we obtain the parameters $\Omega_{\mathrm{m}} = 0.268^{+0.0268}_{-0.024}$ and $\bar{h} = 0.697^{+0.005}_{-0.005}$. Comparing these results with the Planck CMB parameters (2.25), we find that our analysis yields a slightly lower value for Ω_{m}, which in turn may cause the larger obtained value of $\bar{h}$ (as discussed in sections 3.3.7 and 3.4.7). This larger value of $\bar{h}$ is characteristic of analysis using type Ia supernovae data, as discussed in

The Hubble tension. It should be noted that the value of $\bar{h} = 0.697$ is also lower than the value found of $\bar{h} = 0.743$ by [90, 91] who also used type Ia supernovae data. This may be due to the limited capabilities of our MCMC simulation. We should therefore expect this MCMC simulation to predict slightly lower values of $\bar{h}$ than other more sophisticated models.

Using the parameters from Figure 4.1 alongside the distance modulus (4.8), the ΛCDM model may be fitted to the supernovae data. This yields Figure 4.2

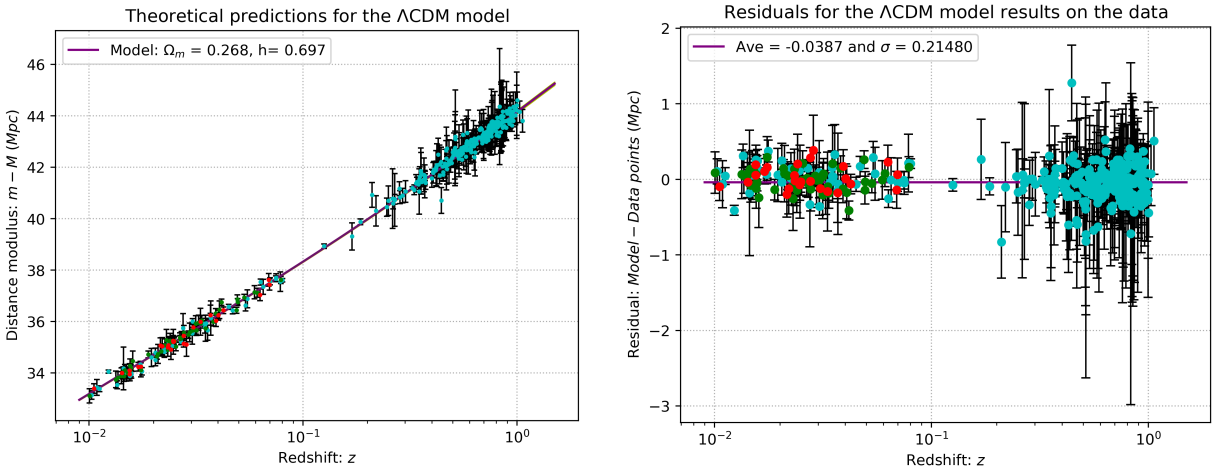

Figure 4.2: *ΛCDM model fitted with supernovae data*

The predicted distance modulus for the ΛCDM model (4.8) is indicated by the purple line in the left panel of Figure 4.2, with its error margins indicated by the barely visible green lines on either side of the purple line. The different coloured data points correspond to the absolute magnitudes calculated in [121] (cyan), [122] (red) and [123] (green). It can immediately be seen that the ΛCDM model is a good fit, as the predicted values fit the data points well. On the right panel, we have also plotted the residual distance between the predicted distance modulus (4.8) and the distance from data at any given redshift. This average residual distance from all points can be seen to be calculated as $\bar{x}_{\text{res}} = -0.0387$, with a standard deviation of $\sigma_{\text{res}} = 0.21480$, matching what was found in [114, 115]. These values are very small and indicative of how well the ΛCDM model with the parameters from Figure 4.1 fit the data. We will now move on to the first IDE model.

4.4.2 Cosmological parameters - $Q_1 = \delta H \rho_{\text{dm}}$

For IDE model $Q_1 = \delta H \rho_{\text{dm}}$, we have 5 free parameters, which are $\bar{h}$; $\Omega_{(\text{dm},0)}$; $\Omega_{(\text{bm},0)}$; ω and δ from (4.9), thus all the constraints in (4.11) will apply for this model. We use the results from Figure 4.1 as priors for the MCMC simulation, such that $\bar{h} = 0.697$, $\delta = 0$ and $\omega = -1$. For dark and baryonic matter, we use $\Omega_{\text{dm}} = 0.266$ and $\Omega_{\text{bm}} = 0.049$ from the Planck CMB parameters (2.25). Running the MCMC simulation [114] with distance modulus (4.9) produces Figure 4.4:

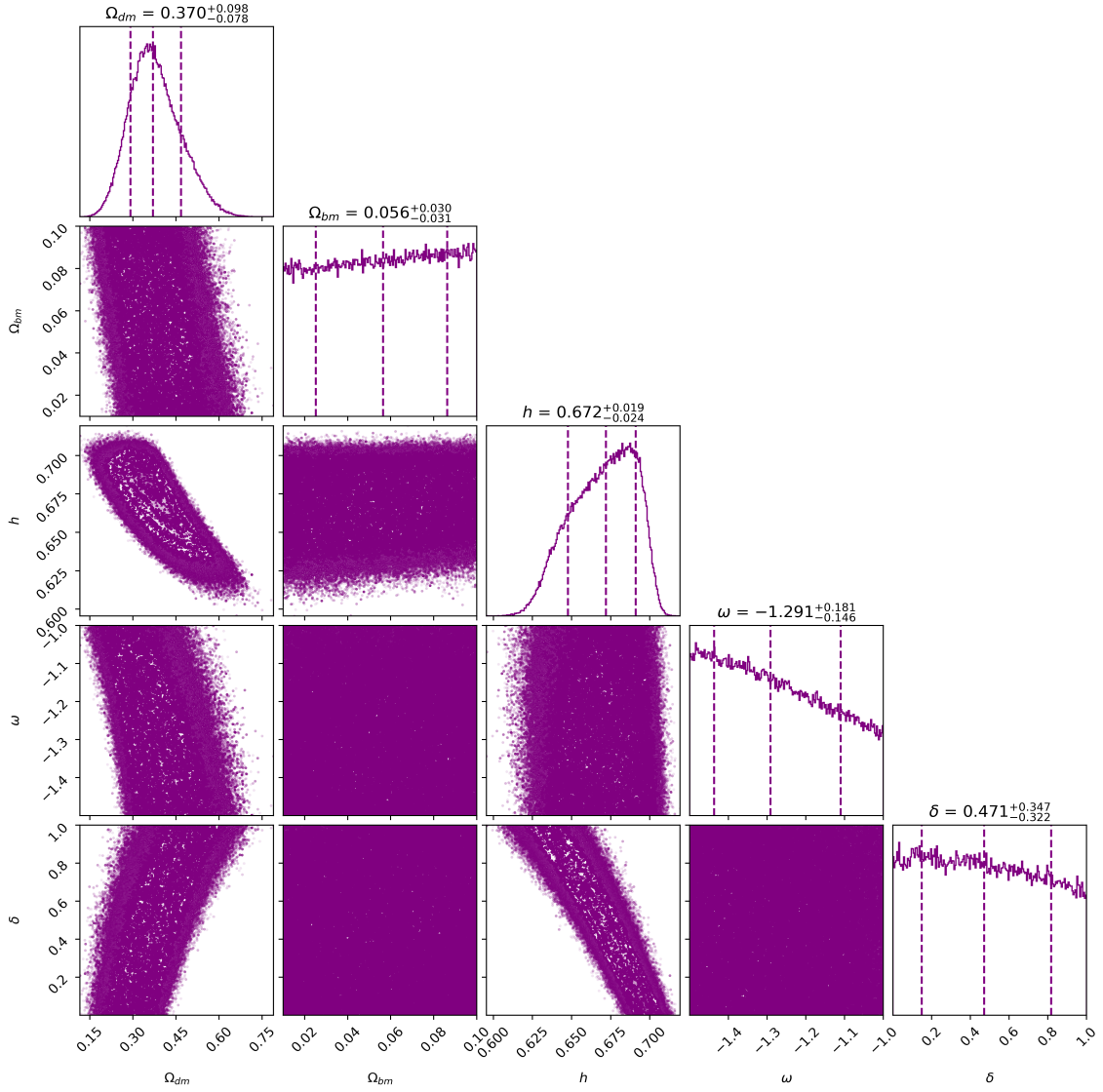

Figure 4.3: *MCMC simulation results - ($Q_1 = \delta H \rho_{dm}$)*

From Figure 4.3 we can see that $\Omega_{\text{dm}} = 0.370^{+0.098}_{-0.078}$ and $\bar{h} = 0.672^{+0.019}_{-0.029}$ have a Gaussian distribution and can be seen to be well constrained, Ω_{dm} more so than $\bar{h}$. Here Ω_{dm} is much larger than the ΛCDM model, which corresponds to a slower expansion rate and therefore a lower value of $\bar{h}$. Conversely, the parameters Ω_{dm}, ω and δ show a more uniform distribution, indicating that all the previous parameter values in the range considered have an almost equal probability of occurring [114]. This implies that these parameters are unconstrained with the present MCMC simulation and dataset. These parameters do show a tendency for a one-sided tail, which indicates that some parameter values did fit the data better than others [114], but this effect is small for this model. To constrain these parameters satisfactorily, we need to consider more datasets or use a more sophisticated MCMC simulation.

Despite the parameters being unconstrained, we can still use the distance modulus (4.9) to fit the $Q_1 = \delta H \rho_{\text{dm}}$ model to the supernovae data, which yields Figure 4.4:

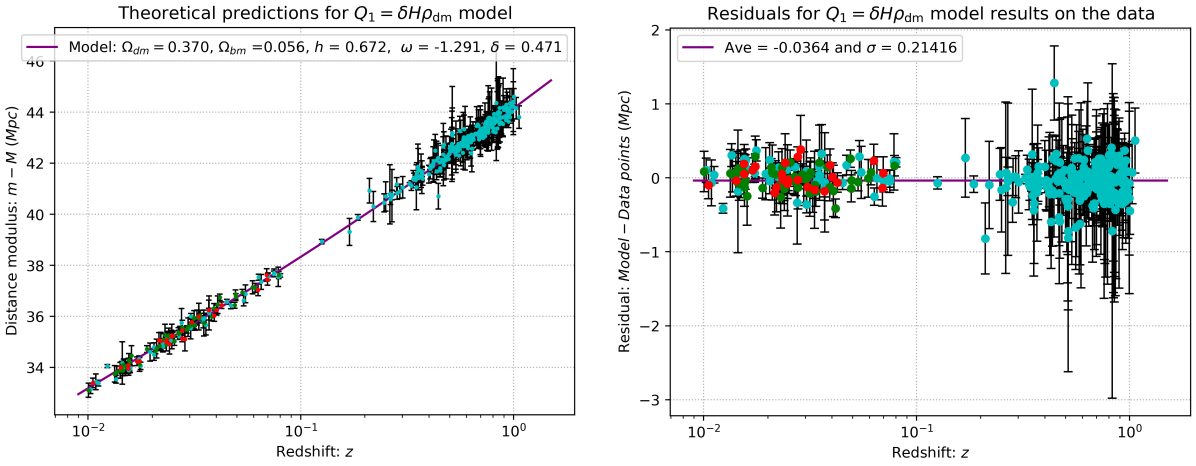

Figure 4.4: *$Q_1 = \delta H \rho_{\rm dm}$ model fitted with supernovae data*

In Figure 4.4 we can see that this model fits the supernovae data well, as the predicted distance modulus corresponds with the data points. This can be also be seen by the small average residual distance of $\bar{x}_{\rm res} = -0.0364$ and standard deviation of $\sigma_{\rm res} = 0.21460$, both smaller than the results found for the ΛCDM model in Figure 4.2. This observation will be discussed in the next section.

4.4.3 Cosmological parameters - $Q_2 = \delta H \rho_{\rm de}$

For IDE model $Q_2 = \delta H \rho_{\rm de}$, we have 4 free parameters, which are $\bar{h}$; $\Omega_{(\rm m,0)}$; ω and δ from (4.10). The first four constraints in (4.11) will thus apply. The results from Figure 4.1 is used as priors for the MCMC simulation. The MCMC simulation with distance modulus (4.9) produces Figure 4.5:

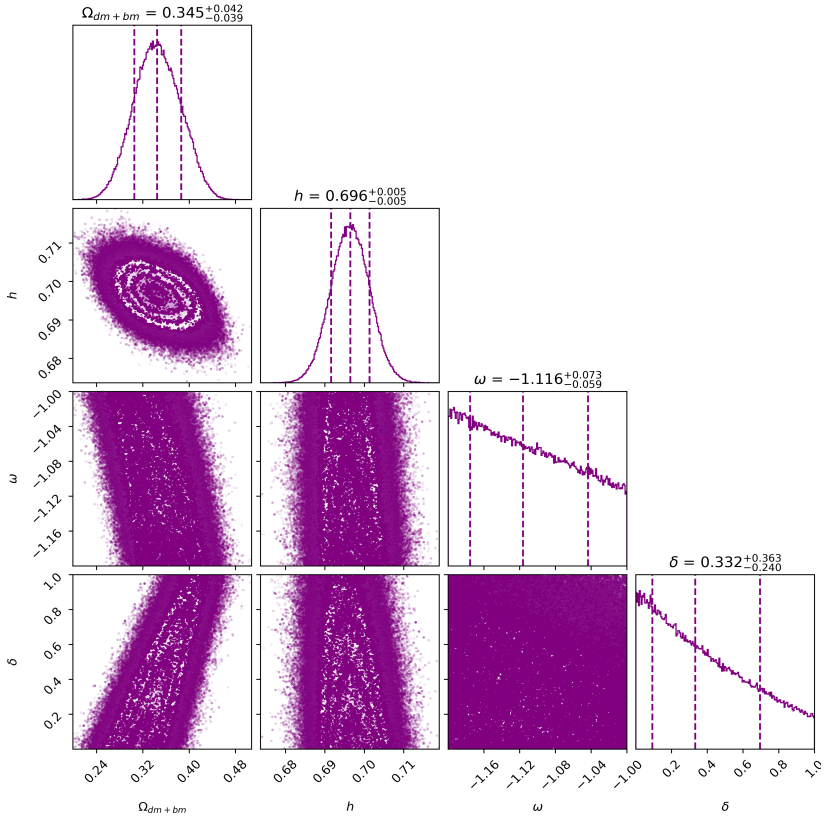

Figure 4.5: *MCMC simulation results - ($Q_2 = \delta H \rho_{de}$)*

From Figure 4.5 we can see that once again $\Omega_{\text{dm}} = 0.345^{+0.042}_{-0.039}$ and $\bar{h} = 0.696^{+0.005}_{-0.005}$ have a Gaussian distribution and are constrained, with $\bar{h}$ being far better constrained than for Q_1 in Figure 4.3. Similarly, the parameters ω and δ are not well constrained, but show a more prominent one-sided tail than Q_1. Even though ω and δ are not well constrained, it may be interesting to note that these parameters yield a dark energy effective equation of state (3.78) of $\omega^{\text{eff}}_{\text{de}} = \omega + \frac{\delta}{3} = -1.116 + \frac{0.332}{3} = -1.005$, which effectively mimics a cosmological constant. One should therefore expect this model to fit the data in a similar manner to the ΛCDM model. Thus, using the distance modulus (4.10) to fit the $Q_2 = \delta H \rho_{\text{de}}$ model to the supernovae data yields Figure 4.6:

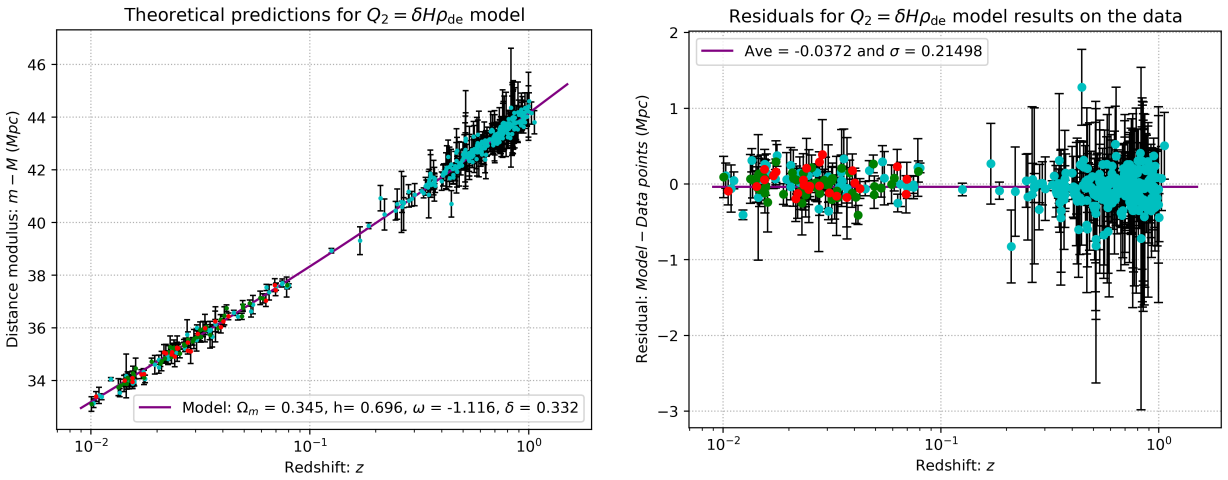

Figure 4.6: *$Q_2 = \delta H \rho_{de}$ model fitted with supernovae data*

As expected, this model shows a good fit to the supernovae data, as the predicted values are consistent with the data points. This is again reflected by the small average residual distance of $\bar{x}_{\text{res}} = -0.0372$ and standard deviation of $\sigma_{\text{res}} = 0.21498$. It should be noted that there are more free parameters for both Q_1 and Q_2, which makes it easier to fit a data set without necessarily implying that the underlying physics of these models are a better description of the data considered. To clarify how well the IDE models fit the data in comparison to the ΛCDM model, we will need to do a Statistical analysis that takes the number of free parameters into account.

4.4.4 Implications of observational parameters

We have used a MCMC simulation to produce the results in Figures 4.1, 4.3 and 4.5. The best set of cosmological parameters obtained for each model is summed up in Table 4.2 below:

Model	$\Omega_{(\text{m},0)}$	$\Omega_{(\text{dm},0)}$	$\Omega_{(\text{bm},0)}$	$\bar{h}$	ω	δ
ΛCDM	$0.268^{+0.025}_{-0.024}$	-	-	$0.697^{+0.005}_{-0.005}$	$-1.000^{+0.000}_{-0.000}$	$0.000^{+0.000}_{-0.000}$
$Q_1 = \delta H \rho_{\text{dm}}$	-	$0.370^{+0.098}_{-0.078}$	$0.056^{+0.030}_{-0.031}$	$0.672^{+0.019}_{-0.029}$	$-1.291^{+0.181}_{-0.146}$	$0.471^{+0.347}_{-0.322}$
$Q_2 = \delta H \rho_{\text{de}}$	$0.345^{+0.042}_{-0.039}$	-	-	$0.696^{+0.005}_{-0.005}$	$-1.116^{+0.073}_{-0.059}$	$0.332^{+0.363}_{-0.240}$

Table 4.1: *Cosmological parameters from MCMC simulation with type Ia supernovae data*

In Table 4.2 we can see that dark matter and baryonic matter may be grouped together ($\Omega_{(\mathrm{dm},0)} + \Omega_{(\mathrm{bm},0)} = \Omega_{(\mathrm{m},0)}$) for the ΛCDM and $Q_2 = \delta H \rho_{\mathrm{de}}$ models, while being separately constrained for $Q_1 = \delta H \rho_{\mathrm{dm}}$, due to the coupling strength being proportional to only the dark matter density $Q_1 \propto \rho_{\mathrm{dm}}$, and not the total matter density. It may again be noted that both IDE models were theoretically constrained to have phantom dark energy ($\omega < -1$), with an interaction in the iDEDM regime ($\delta > 0$). Furthermore, Q_2 was found to have a dark energy effective equation of state (3.78) of $\omega_{\mathrm{de}}^{\mathrm{eff}} = \omega + \frac{\delta}{3} = -1.116 + \frac{0.332}{3} = -1.005$, which mimics a cosmological constant.

For both IDE models, we see a supposed non-zero detection of an interaction between dark matter and dark energy within the error bars. This result, $\delta > 0$, physically implies energy flow from dark energy to dark matter (iDEDM regime). This result should not be taken too seriously since the parameters in Figures 4.3 and 4.5 were not reliably constrained and suffer from degeneracies. More data sets and more sophisticated MCMC models will be needed to provide reliable cosmological constraints. For a recent discussion on 'fake' interacting dark energy detections and how to address this problem, see [124].

Besides this fake detection of δ, we can see that the IDE models predict more matter $\Omega_{\mathrm{dm/m}}$ in the universe, which coincides with a slower expansion rate and a thus smaller value of $\bar{h}$, especially in the case of Q_1. In this case, the lower value of $\bar{h} = 0.672$ is closer to the measured value of $\bar{h} = 0.674$ from the CMB by the Planck collaboration [4]. This may seem to alleviate the The Hubble tension greatly, but this would be a premature conclusion as the calculated value of $\bar{h}$ is model dependent. We would thus need to constrain $\bar{h}$ for a single model, using both CMB and supernovae datasets. The potential of these IDE models to solve the Hubble tension has shown great promise, as seen in [87, 105, 106, 108, 109]. Here the general conclusion seems to be that iDMDE ($\delta < 0$) alleviates, while iDEDM ($\delta > 0$) worsens the Hubble tension. This is an active area of research, and for us to contribute to this discussion, we will need to consider additional sets of cosmological data and use more developed MCMC simulations.

4.5 Statistical analysis

4.5.1 AIC and BIC values

A statistical analysis of the viability of IDE models will now be done, using the Akaike information criterion (AIC) as well as the Bayesian/Schwarz information criterion (BIC or SIC), as was done by [114, 115] who developed the MCMC simulation. Both the AIC and BIC selection need a prior 'true' model with which the new model will be compared. For this "true" model, the ΛCDM model

is chosen. The AIC and BIC values are obtained from their definitions:

$$AIC = -2\ln\left(\mathcal{L}\left(\hat{\theta}|data\right)\right) + 2K, \tag{4.12}$$

$$BIC = -2\ln\left(\mathcal{L}\left(\hat{\theta}|data\right)\right) + K\log(n), \tag{4.13}$$

with $\mathcal{L}\left(\hat{\theta}|data\right)$ the likelihood function of a model, K the number of free parameters and n the amount of data points. The likelihood function is obtained by assuming a Gaussian distribution, which has a distribution function:

$$\mathcal{L}\left(\hat{\theta}|data\right) = \exp\left(-\frac{1}{2}\sum_n\left[\frac{(\mu_{data} - \mu_{theoretical})}{\sigma^2}\right]\right), \tag{4.14}$$

with σ the standard deviation, u_{data} the distance modulus for each supernova data point and $\mu_{theoretical}$ the distance modulus predicted for each model using (4.6). Substituting (4.14) into (4.12) and (4.13) gives:

$$AIC = \sum_n\left[\frac{(\mu_{data} - \mu_{theoretical})}{\sigma^2}\right] + 2K, \tag{4.15}$$

$$BIC = \sum_n\left[\frac{(\mu_{data} - \mu_{theoretical})}{\sigma^2}\right] + K\log(n). \tag{4.16}$$

The AIC and BIC values only gain significance when compared with the 'true' model. This is done by working out the difference between AIC and BIC values for the coupled models and the ΛCDM model, thus:

$$|\Delta AIC| = AIC_{model} - AIC_{\text{true}} \tag{4.17}$$

$$|\Delta BIC| = BIC_{model} - BIC_{\text{true}}. \tag{4.18}$$

These values tell you whether your model can be seen as valid with regard to the 'true' model. A useful scale that was previously adopted for the MCMC simulation [114], is the Jeffrey's scale:

$$\begin{aligned} |\Delta IC| \leq 2 \quad &\rightarrow \quad \text{well supported} \\ 4 \leq |\Delta IC| \leq 7 \quad &\rightarrow \quad \text{less supported} \\ |\Delta IC| > 10 \quad &\rightarrow \quad \text{not supported.} \end{aligned} \tag{4.19}$$

It should be noted that this is 'supported' with regard to the 'true' (ΛCDM) model. The Jeffrey's scale is not the only scale for this type of analysis and should be handled cautiously. It should therefore not be seen as a final verdict, but as a rule of thumb to the validity of these models [125].

This statistical analysis was built into the MCMC simulation we have used [114, 115]. Besides determining the likelihood function $\mathcal{L}\left(\hat{\theta}|data\right)$ (4.14), AIC (4.12), BIC (4.14), $|\Delta AIC|$ (4.17) and $|\Delta BIC|$ (4.18) values for a given cosmological model, the simulation also calculates the χ^2 and reduced χ^2 values. The results from the analysis will be discussed next.

4.5.2 Results from the statistical analysis

It should be noted that the $\mathcal{L}\left(\hat{\theta}|data\right)$, χ^2 and reduced χ^2 will tell us if the model fits the supernovae data. In general, a reduced χ^2 value of $0.5 < \chi^2 < 3$ indicates a good fit, while the largest likelihood function $\mathcal{L}\left(\hat{\theta}|data\right)$ value has the highest likelihood of being viable [114, 115].

To do this analysis we need the average residual deviation $\bar{x}_{\text{res}}$ and standard deviation σ_{res} for each model, which were found in Figures 4.2, 4.4 and 4.6 and summarised in Table 4.2 below.

Model	$\bar{x}_{\text{res}}$	σ_{res}
ΛCDM	-0.0387	0.21480
$Q_1 = \delta H \rho_{\text{dm}}$	-0.0364	0.21416
$Q_2 = \delta H \rho_{\text{de}}$	-0.0372	0.21498

Table 4.2: *Average residual deviation $\bar{x}_{\text{res}}$ and standard deviation with type Ia supernovae data*

Taking the above into consideration, the statistical analysis for our models yielded Table 4.3:

Model	$\mathcal{L}\left(\hat{\theta}|data\right)$	χ^2	Reduced χ^2	AIC	$\lvert\Delta AIC\rvert$	BIC	$\lvert\Delta BIC\rvert$
$Q_2 = \delta H \rho_{\text{de}}$	-120.6976	241.3953	0.6799	249.3953	3.9787	264.9286	11.7454
ΛCDM	-120.7083	241.4166	0.6762	245.4166	0	253.1832	0
$Q_1 = \delta H \rho_{\text{dm}}$	-121.9973	243.9946	0.6892	253.9946	8.5780	273.4112	20.2280

Table 4.3: *Statistical analysis results of each model against type Ia supernovae data*

In Table (4.3), we have listed the models in the order of the largest $\mathcal{L}\left(\hat{\theta}|data\right)$ (most viable) to the smallest (least viable). Here we see that model $Q_2 = \delta H \rho_{\text{de}}$ fits the data even better than the ΛCDM model. We also see from the reduced χ^2 results that all three models fit the data well, as they are close to the lower bound of the criteria $0.5 < \chi^2 < 3$. When we consider the $|\Delta AIC|$ and $|\Delta BIC|$ results, these models start performing worse.

Using the Jeffrey's scale (4.19), the IDE model $Q_1 = \delta H \rho_{\text{dm}}$ has little to no support, even though the average residual distance $\bar{x}_{\text{res}}$ and standard deviation σ_{res} of this model was smaller than that of the ΛCDM model. This may be due to the AIC and BIC values taking into account the amount of free parameters, which caused this model to suffer. Conversely, the coupling function $Q_2 = \delta H \rho_{\text{de}}$ can be seen to be within the criteria to have observational support for $|\Delta AIC|$, while being rejected using $|\Delta BIC|$ criteria.

The $Q_1 = \delta H \rho_{\text{dm}}$ model may therefore be observationally **rejected** from this criteria, while the $Q_2 = \delta H \rho_{\text{de}}$ model performed better and **may still be viable**. This motivates future research with additional cosmological datasets.

CHAPTER 5

Conclusions

In this dissertation, we have explored the theoretical and observational viability, as well as the cosmological implications of interacting dark energy models.

To do this, we first needed to understand why there is a need for new exotic cosmological models. Therefore, we looked at the historical development of cosmology to understand how we got to the present standard ΛCDM model, as well as its limitations and the need for developments beyond this standard model. Our study began with the foundations of modern cosmology, General relativity and the cosmological field equations, where we saw that what we experience as the force of gravity can be explained by the The Einstein field equations which, relates the curvature of spacetime to its stress-energy content. These field equations can, in turn, be applied to the universe as a whole, relating its total energy content to its curvature and subsequent evolution. This was done in our Derivation of the cosmological field equations, where we assumed an isotropic and homogeneous universe (as described by the The Friedmann-Lemaître-Robertson-Walker metric). This yielded the two most essential equations in cosmology, the two Friedmann equations, which can be used to determine the origin, evolution and fate of the universe from its energy content (which is intimately related to the Geometry of the universe). Determining the density and properties of the Components of the universe should thus determine the nature of a cosmological model.

Once we had these foundational tools for our study, we considered the ΛCDM and other non-interacting models, these are cosmological models that contain Radiation, Matter and Dark energy, of which the total energy of each component is separately conserved. The first modern cosmological model we examined was Einstein's static universe. This model first introduced dark energy in the

form of a cosmological constant Λ, but was discarded due to being unstable, as well as contradicting the discovery of the Hubble-Lemaître law, which indicated an expanding universe. Our study then moved on to early expanding universe models, the Friedmann and Lemaître cosmological models. For these models, we could analytically solve the Friedmann equations to determine each model's entire expansion history and age. Here we also saw that the density of radiation, matter and dark energy determines whether the universe experiences a big bang or a big bounce origin; and either a big crunch or a big chill (heat death) end. These models were informative but had to be discarded due to the discovery of Cosmic acceleration in 1998, which paved the way to the present standard model of cosmology, the ΛCDM model. From the Cosmological parameters, obtained from the Planck telescope in 2018, it was shown that the ΛCDM model predicts a universe that presently consists of approximately 5% baryonic matter, 26% dark matter and 69% dark energy (in the form of vacuum energy or a cosmological constant Λ). Thus 95% of the energy density in the universe is distributed between the dark sectors, of which very little is known. Using these parameters, the ΛCDM model was shown to have a big bang origin 13.8 billion years ago, followed by Radiation, matter and dark energy dominated epochs. The universe was initially decelerating before entering an epoch (about 6 billion years ago) of indefinite accelerating expansion, in which the universe ends with a slow heat death. The predictions of this model agree remarkably well with observations, but Problems with the ΛCDM model remain.

These problems include the The cosmological constant problem, in which the measured energy density of the vacuum is over 120 orders of magnitude smaller than the theoretical prediction. This casts doubt on dark energy being a cosmological constant, thus motivating research into alternative dark energy models. The second problem is The cosmic coincidence problem, which refers to the coincidence that the dark matter and dark energy densities are the same order of magnitude at the present, when we happen to observe the universe, but differ with many orders of magnitude in the past and the predicted future. This motivates research into dark matter and dark energy models that maintain a small or constant ratio in the past or future expansion. Finally, The Hubble tension concerns the 4.4σ level discrepancy between the value of the Hubble constant H_0 predicted by the ΛCDM model, using data either from the CMB or Type Ia supernovae. Therefore, any model which can alleviate this discrepancy may be a viable candidate for dark energy. Due to the problems associated with a cosmological constant, we took a brief look at Quintessence and phantom dark energy models, showing how phantom dark energy leads to a future Big rip singularity.

To address these problems, we introduced Interacting dark energy models (IDE), where dark matter and dark energy are coupled and may have non-gravitational interactions. Since 95% of the universe's energy density is located in the dark sectors, and since the properties of both dark matter and dark energy are not well constrained, there may be undiscovered interactions in the largest sector of the universe. These dark interactions were grouped into two regimes where energy flows from dark energy to dark matter, as the interacting Dark Energy Dark Matter regime (iDEDM) and

vice versa as the interacting Dark Matter Dark Energy regime (iDMDE). There are many different IDE models (specified by a coupling function Q), but some general Properties of interacting dark energy models were found to hold. The most important of these, and the reason these models were introduced, is their potential for Addressing the coincidence problem. Here we saw that if energy flows from dark energy to dark matter (iDEDM), then dark matter and dark energy may redshift and dilute with cosmic expansion at a more similar rate, alleviating the coincidence problem. This effect may even cause dark matter and dark energy to redshift at the exact same rate (when $\omega_{\text{dm}}^{\text{eff}} = \omega_{\text{de}}^{\text{eff}}$), which will completely stabilise the ratio of dark matter to dark energy throughout expansion. This would mean that the presently observed ratio of dark matter to dark energy is not coincidental, but a general property of the universe, thus solving the coincidence problem. The opposite holds for the iDMDE regime, which worsens the magnitude of the coincidence problem. Besides addressing the coincidence problem, there are other Cosmological implications of a dark coupling. It was shown that relative to the ΛCDM model, in the iDEDM regime, we find that the radiation-matter equality happens at a *later* time. In contrast, both the matter-dark energy equality and the cosmic jerk happen earlier. The age of these universe models will also be older. The opposite holds for the iDMDE case. These results are summarised in Table 3.1.

Due to the potential for these models to solve the coincidence problem, IDE models may be seen as an attractive alternative to the ΛCDM model. To be a valid alternative, these models need to be free of theoretical problems such as predicted negative energy densities and instabilities while also meeting observational constraints. Due to the energy flow between dark matter and dark energy, these models may easily suffer from negative energy densities, which we considered unphysical. We, therefore, derived general expressions which may be used to find the Evolution of energy densities and phase portraits for IDE models with any coupling function Q. These phase portraits may be used to see whether there are repulsor or attractor solutions with negative energy densities, thus ruling out the model considered. Furthermore, to ensure that these models are a priori stable, we considered the Instabilities and the doom factor for IDE models. Thus, to avoid negative energy densities and instabilities, the combination of cosmological parameters must be carefully chosen.

To explicitly show that these properties hold, we considered two IDE case studies that have linear coupling functions, Interaction model 1: $Q_1 = \delta H \rho_{\text{dm}}$ and Interaction model 2: $Q_2 = \delta H \rho_{\text{de}}$. The central difference between the two models was that the effect of the coupling is most prominent in the past expansion for $Q_1 = \delta H \rho_{\text{dm}}$, while being more prominent in the future for $Q_2 = \delta H \rho_{\text{de}}$. This can be seen by the fact that both models alleviate the coincidence problem in the iDEDM ($\delta > 0$) regime, but $Q_1 = \delta H \rho_{\text{dm}}$ completely solves the problem for past expansion (see Figure 3.3), while $Q_2 = \delta H \rho_{\text{de}}$ solves the problem for future expansion (see Figure 3.12). Furthermore, for both models we derived explicit equations for the redshift at which Important events in cosmic history occur, this includes radiation-matter equality, matter-dark energy equality and the cosmic jerk. From these results, we found that all the predictions in Table 3.1 hold for both models.

To ensure that these models are theoretically viable, we derived the Positive energy conditions - $Q_1 = \delta H \rho_{\mathrm{dm}}$: $0 < \delta < -\frac{3\omega}{(1+r_0)}$; and Positive energy density conditions - $Q_2 = \delta H \rho_{\mathrm{de}}$: $0 < \delta < -\frac{3\omega}{1+\frac{1}{r_0}}$. From these conditions we find that the iDMDE regime $\delta < 0$ always leads to negative energies. For $Q_1 = \delta H \rho_{\mathrm{dm}}$, the iDMDE regime always leads to negative dark energy densities in the past, while for $Q_2 = \delta H \rho_{\mathrm{de}}$ the iDMDE regime causes negative dark matter densities in the future expansions. This fact may also be directly observed from the repulsor and attractor points in the phase portraits for both models (Figures 3.2 and 3.11). Since negative energy densities are unphysical (even those predicted to occur in the future), the **iDMDE regime should not be taken seriously as a potential dark energy candidate**. This fact is often neglected in literature, where $Q_2 = \delta H \rho_{\mathrm{de}}$ in the iDMDE regime is regularly used, without any reference to the negative dark matter density in the future. It should be made clear that this point only holds for the couplings $Q_1 = \delta H \rho_{\mathrm{dm}}$ and $Q_2 = \delta H \rho_{\mathrm{de}}$, and may not be the case for other IDE models.

From the doom factor analysis for both IDE models, we saw that the only way to ensure a priori stable universes is if the coupling constant δ and the dark energy equation of state $(1 + \omega)$ have opposite signs, as often noted in literature. Combining this with the positive energy conditions, we find that the only viable scenario, which is free of negative energy densities and a priori stable, is phantom dark energy $\omega < -1$ in the iDEDM regime (see Tables 3.3 and 3.8). For both IDE models, the dark energy will thus violate the Energy conditions of general relativity associated with phantom dark energy. This immediately makes both IDE models less attractive from a theoretical viewpoint. For $Q_1 = \delta H \rho_{\mathrm{dm}}$, the phantom dark energy will have the consequence that the universe will end in a future big rip singularity (see Figure 3.10). For $Q_2 = \delta H \rho_{\mathrm{de}}$, the big rip may still be avoided as long as the dark energy effective equation of state $\omega_{\mathrm{de}}^{\mathrm{eff}} = \omega + \frac{\delta}{3} < -1$ (which can be seen in Figures 3.19 and 3.20). For both models, we derived expressions for The time of the big rip.

Finally, we used Standard candles and type Ia supernovae to see if the predicted expansion history from our IDE models (within their domain of viability $\delta > 0$; $\omega < -1$) could meet observational constraints. This was done using a data set of 359 Type-Ia supernovae with a previously developed MCMC simulation. The MCMC simulation used the Distance modulus for a model, to determine the best combination of Cosmological Parameters for that model. For $Q_1 = \delta H \rho_{\mathrm{dm}}$, this analysis resulted in the parameters $\Omega_{(\mathrm{dm},0)} = 0.370^{+0.098}_{-0.078}$; $\Omega_{(\mathrm{bm},0)} = 0.056^{+0.030}_{-0.031}$; $\bar{h} = 0.672^{+0.019}_{-0.029}$; $\omega = -1.291^{+0.181}_{-0.146}$ and $\delta = 0.471^{+0.347}_{-0.322}$. For $Q_2 = \delta H \rho_{\mathrm{de}}$ we obtained the parameters $\Omega_{(\mathrm{m},0)} = 0.345^{+0.042}_{-0.039}$; $\bar{h} = 0.696^{+0.005}_{-0.005}$; $\omega = -1.116^{+0.073}_{-0.059}$ and $\delta = 0.332^{+0.363}_{-0.240}$. Here ω and δ were unreliably constrained for both models (see Figures 4.3 and 4.5), thus any indication of a non-zero detection of δ should not be taken seriously. Furthermore, both IDE models indicated a lower Hubble constant than what the ΛCDM model found with the same supernovae data. These lower values are closer to the Hubble constant measured from the CMB and may seem to relieve the The Hubble tension. This conclusion can unfortunately not be made, since these results are model dependent and our parameters were unreliably constrained.

Using the cosmological parameters obtained from the MCMC simulation, we fitted the distance modulus of both IDE models to the supernovae data to see whether the predicted expansion histories of our models coincide with observations. For both models we found a good fit, with $Q_1 = \delta H \rho_{\rm dm}$ having an average residual distance of $\bar{x}_{\rm res} = -0.0364$ and a standard deviation of $\sigma_{\rm res} = 0.21460$ (see Figure 4.4), which was even smaller than the results obtained from the ΛCDM model. Similarly, $Q_2 = \delta H \rho_{\rm de}$ had a small average residual distance of $\bar{x}_{\rm res} = -0.0372$ and a standard deviation of $\sigma_{\rm res} = 0.21498$. These results may be attributed to the larger amount of free parameters causing degeneracies, making it easier to fit the data. We therefore applied a larger Statistical analysis to the IDE models, which takes the number of free parameters into account. The Results from the statistical analysis can be seen in Table 4.3. Here it was found that $Q_2 = \delta H \rho_{\rm de}$ had the highest likelihood function, indicating that this model fits the supernovae data even better than the ΛCDM model. In terms of the likelihood function $Q_1 = \delta H \rho_{\rm dm}$ did slightly worse, but showed an overall good fit as well. When the $|\Delta AIC|$ and $|\Delta BIC|$ results were considered, it was found that $Q_1 = \delta H \rho_{\rm dm}$ was completely rejected, while $Q_2 = \delta H \rho_{\rm de}$ showed some observational support. The $|\Delta AIC|$ and $|\Delta BIC|$ shows how well a model is 'supported' with regard to the 'true' (ΛCDM) model. Thus, $Q_2 = \delta H \rho_{\rm de}$ may have performed better since the dark energy in this model has an effective equation of state $\omega_{\rm de}^{\rm eff} = \omega + \frac{\delta}{3} = -1.116 + \frac{0.332}{3} = -1.005$, mimicking a cosmological constant.

To make any sound conclusions on the potential of IDE models, to address the Hubble tension and determine if observations rule out or support our models, we will need to consider more data sets from different cosmological probes. These may include constraints from the CMB and large-scale structure. This may be seen as a departure point for future work. Furthermore, the research on the theoretical viability of IDE models should be expanded. A complete perturbation analysis of these models, to move beyond the doom factor, is also recommended; and a more in-depth study of instabilities should be considered. A further expansion on this research, to include additional IDE models and investigate their strengths and weaknesses, is also proposed.

In conclusion, we find that interacting dark energy models may alleviate and even solve the cosmic coincidence problem by stabilising the ratio of dark matter to dark energy in both the past and future. For both models considered, we find that negative energy densities are inevitable if energy flows from dark matter to dark energy and that consequently we should only seriously consider models where energy flows from dark energy to dark matter. To additionally ensure models free from early time instabilities, we need to ensure that dark energy is in the phantom regime. This has the consequence that model $Q_1 = \delta H \rho_{\rm dm}$ will end with a future big rip singularity, while $Q_2 = \delta H \rho_{\rm de}$ may avoid this fate with the right choice of cosmological parameters. When the predicted expansion history from these models are statistically compared to supernovae data and the ΛCDM model, we find that $Q_1 = \delta H \rho_{\rm dm}$ is statistically rejected, while $Q_2 = \delta H \rho_{\rm de}$ may be considered viable. Thus, IDE models have shortcomings but show potential to address long-standing issues in cosmology. It is, therefore, worthwhile to continue investigating dark interactions beyond the ΛCDM model.

Appendices

APPENDIX A

Solving the Friedmann equation

This appendix shows the detailed calculations for the solutions of the Friedmann equation (2.19) for various single fluid cosmological models. The models considered are Friedmann models, with either only radiation or matter, and Lemaître models with only a cosmological constant. To show the critical role that density plays in these models, we will also consider the flat, open and closed case for each model.

A.1 Calculations for radiation-dominated Friedmann models

radiation-dominated Friedmann models have an energy distribution such that $\Omega_{(\mathrm{r},0)} \neq 0$, while $\Omega_{(\mathrm{m},0)} = 0$ and $\Omega_{(\Lambda,0)} = 0$. Substituting this into (2.19) yields the Friedmann equation for the radiation-dominated Friedmann models:

$$\left(\frac{\dot{a}}{a}\right)^2 = H_0^2 \left[\Omega_{(\mathrm{r},0)} a^{-4} + \Omega_{(\mathrm{k},0)} a^{-2}\right]. \tag{A.1}$$

A.1.1 Calculations for a radiation-dominated flat model

For a radiation-dominated flat model, we have $\Omega_{(\mathrm{k},0)} = 0$; $\Omega_{(\mathrm{r},0)} = 1$. The Friedmann equation (A.1) thus becomes:

$$\begin{aligned}
\left(\frac{\dot{a}}{a}\right)^2 &= H_0^2(1)a^{-4} - (0)a^{-2} \\
\left(\frac{\dot{a}}{a}\right)^2 &= H_0^2 a^{-4} \\
\int_0^a a da &= H_0 \int_0^t dt \\
\frac{1}{2}a^2 &= H_0(t) \\
\rightarrow a &= \sqrt{2H_0 t}.
\end{aligned} \tag{A.2}$$

The present age for this universe model t_0 can be found by considering how much time elapsed until the scale factor reached its present value of $a_0 = 1$. This is easily obtained by solving (A.2) for t_0:

$$\begin{aligned}
a_0 = 1 &= \sqrt{2H_0 t_0} \\
\rightarrow t_0 &= \frac{1}{2H_0}.
\end{aligned} \tag{A.3}$$

A.1.2 Calculations for a radiation-dominated closed model

For a radiation-dominated closed model, we have $\Omega_{(\mathrm{k},0)} < 0$. The Friedmann equation (A.1) thus becomes:

$$\begin{aligned}
\left(\frac{\dot{a}}{a}\right)^2 &= H_0^2 \left[\Omega_{(\mathrm{r},0)} a^{-4} + \Omega_{(\mathrm{k},0)} a^{-2}\right] \\
\dot{a} &= H_0 \sqrt{-\Omega_{(\mathrm{k},0)}} \sqrt{-\frac{\Omega_{(\mathrm{r},0)}}{\Omega_{(\mathrm{k},0)}} a^{-2} - 1} \\
\dot{a} &= \frac{H_0 \sqrt{-\Omega_{(\mathrm{k},0)}}}{a} \sqrt{-\frac{\Omega_{(\mathrm{r},0)}}{\Omega_{(\mathrm{k},0)}} - a^2} \\
\int_0^a \frac{1}{\sqrt{-\frac{\Omega_{(\mathrm{r},0)}}{\Omega_{(\mathrm{k},0)}} - a^2}} da &= \frac{H_0 \sqrt{-\Omega_{(\mathrm{k},0)}}}{a} \int_0^t dt.
\end{aligned} \tag{A.4}$$

We can parametrize this equation by introducing conformal time η, given by:

$$\begin{aligned}
\eta &= \int_0^t \frac{dt}{a} \\
\int_0^t dt &= \eta a.
\end{aligned} \tag{A.5}$$

Substituting (A.5) into (A.4) gives:

$$\begin{aligned}\int_0^a \frac{1}{\sqrt{-\frac{\Omega_{(\mathrm{r},0)}}{\Omega_{(\mathrm{k},0)}} - a^2}} da &= \frac{H_0\sqrt{-\Omega_{(\mathrm{k},0)}}}{a}\eta a \\ \int_0^a \frac{1}{\sqrt{-\frac{\Omega_{(\mathrm{r},0)}}{\Omega_{(\mathrm{k},0)}} - a^2}} da &= H_0\sqrt{-\Omega_{(\mathrm{k},0)}}\eta.\end{aligned} \tag{A.6}$$

Using substituting, we let $q^2 = -\frac{\Omega_{(\mathrm{r},0)}}{\Omega_{(\mathrm{k},0)}} \rightarrow q = \sqrt{-\frac{\Omega_{(\mathrm{r},0)}}{\Omega_{(\mathrm{k},0)}}}$, with $\Omega_{(\mathrm{k},0)} < 0$. We also substitute in $\theta = H_0\sqrt{-\Omega_{(\mathrm{k},0)}}\eta$ This yields:

$$\int_0^a \frac{1}{\sqrt{q^2 - a^2}} da = \theta. \tag{A.7}$$

From an integral table we may obtain [126]:

$$\int_0^a \frac{1}{\sqrt{q^2 - a^2}} da = \sin^{-1}\left(\frac{a}{q}\right). \tag{A.8}$$

Substituting (A.8) into (A.7) gives:

$$\begin{aligned}\sin^{-1}\left(\frac{a}{q}\right) &= \theta \\ \left(\frac{a}{q}\right) &= \sin(\theta) \\ a\sqrt{-\frac{\Omega_{(\mathrm{k},0)}}{\Omega_{(\mathrm{r},0)}}} &= \sin(\theta) \\ a &= \sqrt{-\frac{\Omega_{(\mathrm{r},0)}}{\Omega_{(\mathrm{k},0)}}}\sin(\theta) \\ \rightarrow a &= \sqrt{\frac{\Omega_{(\mathrm{r},0)}}{\Omega_{(\mathrm{r},0)} - 1}}\sin(\theta).\end{aligned} \tag{A.9}$$

The time t as parameterized by the conformal time η is obtained from the relation:

$$\begin{aligned}\int_0^t dt &= \eta a \\ \int_0^t dt &= \int_0^\eta a d\eta \\ t - 0 &= \sqrt{-\frac{\Omega_{(\mathrm{r},0)}}{\Omega_{(\mathrm{k},0)}}}\int_0^\eta \sin(\theta) d\eta.\end{aligned} \tag{A.10}$$

Since $\theta = H_0\sqrt{-\Omega_{(\mathrm{k},0)}}\eta$, thus $\eta = \frac{\theta}{H_0\sqrt{-\Omega_{(\mathrm{k},0)}}}$ and $d\eta = \frac{1}{H_0\sqrt{-\Omega_{(\mathrm{k},0)}}}d\theta$. Doing this substitution, we obtain:

$$
\begin{aligned}
t - 0 &= \sqrt{-\frac{\Omega_{(\mathrm{r},0)}}{\Omega_{(\mathrm{k},0)}}} \int_0^\theta \sin(\theta) \frac{1}{H_0 \sqrt{-\Omega_{(\mathrm{k},0)}}} d\theta \\
t &= \frac{\sqrt{\Omega_{(\mathrm{r},0)}}}{-H_0 \Omega_{(\mathrm{k},0)}} \left[-\cos(\theta)\right]_0^\theta \\
t &= \frac{\sqrt{\Omega_{(\mathrm{r},0)}}}{-H_0 \Omega_{(\mathrm{k},0)}} \left[1 - \cos(\theta)\right] \\
t &= \frac{\sqrt{\Omega_{(\mathrm{r},0)}}}{H_0 (\Omega_{(\mathrm{r},0)} - 1)} \left[1 - \cos(\theta)\right].
\end{aligned} \tag{A.11}
$$

The age of this model is found by setting $a = a_0 = 1$ in (A.9) to obtain the present value for θ_0:

$$
\begin{aligned}
a_0 = 1 &= \sqrt{\frac{\Omega_{(\mathrm{r},0)}}{\Omega_{(\mathrm{r},0)} - 1}} \sin(\theta_0) \\
\theta_0 &= \sin^{-1} \sqrt{\frac{\Omega_{(\mathrm{r},0)} - 1}{\Omega_{(\mathrm{r},0)}}}.
\end{aligned} \tag{A.12}
$$

Substituting this back into the time t (A.11) gives the age t_0 of the universe model:

$$
\rightarrow t_0 = \frac{\sqrt{\Omega_{(\mathrm{r},0)}}}{H_0 (\Omega_{(\mathrm{r},0)} - 1)} \left[1 - \cos\left(\sin^{-1} \sqrt{\frac{\Omega_{(\mathrm{r},0)} - 1}{\Omega_{(\mathrm{r},0)}}}\right)\right]. \tag{A.13}
$$

From the solution it may be seen that this model has a cyclic nature with a big bang at $\theta = 0$ and a big crunch at $\theta = \pi$ (making half a circle). This can be seen in Figure 2.3. Thus, these models should have a lifetime t_l and can be found by the difference between $\theta = \pi$ and $\theta = 0$ in t (A.11, giving:

$$
\begin{aligned}
t_l &= \frac{\sqrt{\Omega_{(\mathrm{r},0)}}}{H_0 (\Omega_{(\mathrm{r},0)} - 1)} \left[1 - \cos(\theta)\right]_0^\pi \\
t_l &= \frac{\sqrt{\Omega_{(\mathrm{r},0)}}}{H_0 (\Omega_{(\mathrm{r},0)} - 1)} \left[(1 - (-1)) - (1 - (1))\right] \\
\rightarrow t_l &= \frac{2\sqrt{\Omega_{(\mathrm{r},0)}}}{H_0 (\Omega_{(\mathrm{r},0)} - 1)}.
\end{aligned} \tag{A.14}
$$

The amount of time until the big crunch t_c can therefore be calculated by the difference between the lifetime of the universe t_l (A.14) and the current age t_0 (A.55):

$$\begin{aligned} t_c &= t_l - t_0 \\ t_c &= \left(\frac{2\sqrt{\Omega_{(\mathrm{r},0)}}}{H_0(\Omega_{(\mathrm{r},0)}-1)}\right) - \left(\frac{\sqrt{\Omega_{(\mathrm{r},0)}}}{H_0(\Omega_{(\mathrm{r},0)}-1)}\left[1-\cos\left(\sin^{-1}\sqrt{\frac{\Omega_{(\mathrm{r},0)}-1}{\Omega_{(\mathrm{r},0)}}}\right)\right]\right) \\ \rightarrow t_c &= \frac{\sqrt{\Omega_{(\mathrm{r},0)}}}{H_0(\Omega_{(\mathrm{r},0)}-1)}\left[1+\cos\left(\sin^{-1}\sqrt{\frac{\Omega_{(\mathrm{r},0)}-1}{\Omega_{(\mathrm{r},0)}}}\right)\right]. \end{aligned} \tag{A.15}$$

A.1.3 Calculations for a radiation-dominated open model

For a radiation-dominated closed model, we have $\Omega_{(\mathrm{k},0)} > 0$. The Friedmann equation (A.1) thus becomes:

$$\begin{aligned} \left(\frac{\dot{a}}{a}\right)^2 &= H_0^2\left[\Omega_{(\mathrm{m},0)}a^{-4} + \Omega_{(\mathrm{k},0)}a^{-2}\right] \\ \dot{a} &= H_0\sqrt{\Omega_{(\mathrm{r},0)}}\sqrt{a^2 + \frac{\Omega_{(\mathrm{k},0)}}{\Omega_{(\mathrm{r},0)}}} \\ \dot{a} &= \frac{H_0\sqrt{\Omega_{(\mathrm{r},0)}}}{a}\sqrt{1 + \frac{\Omega_{(\mathrm{k},0)}}{\Omega_{(\mathrm{m},0)}}a^2} \\ \int_0^a \frac{1}{\sqrt{1+\frac{\Omega_{(\mathrm{k},0)}}{\Omega_{(\mathrm{r},0)}}a^2}}da &= \frac{H_0\sqrt{\Omega_{(\mathrm{r},0)}}}{a}\int_0^t dt. \end{aligned} \tag{A.16}$$

We can parametrize this equation by using conformal time η. Substituting (A.5) into (A.16) gives:

$$\begin{aligned} \int_0^a \frac{1}{\sqrt{1+\frac{\Omega_{(\mathrm{k},0)}}{\Omega_{(\mathrm{r},0)}}a^2}}da &= \frac{H_0\sqrt{\Omega_{(\mathrm{r},0)}}}{a}\eta a \\ \int_0^a \frac{1}{\sqrt{1+\frac{\Omega_{(\mathrm{k},0)}}{\Omega_{(\mathrm{r},0)}}a^2}}da &= H_0\sqrt{\Omega_{(\mathrm{r},0)}}\eta. \end{aligned} \tag{A.17}$$

Using substituting, we let $q^2 = \frac{\Omega_{(\mathrm{k},0)}}{\Omega_{(\mathrm{r},0)}}a^2 \rightarrow q = a\sqrt{\frac{\Omega_{(\mathrm{k},0)}}{\Omega_{(\mathrm{r},0)}}}$ and $dq = \sqrt{\frac{\Omega_{(\mathrm{k},0)}}{\Omega_{(\mathrm{r},0)}}}da \rightarrow da = \sqrt{\frac{\Omega_{(\mathrm{r},0)}}{\Omega_{(\mathrm{k},0)}}}dq$. This yields:

$$\begin{aligned} \int_0^q \frac{1}{\sqrt{1+q^2}}\sqrt{\frac{\Omega_{(\mathrm{r},0)}}{\Omega_{(\mathrm{k},0)}}}dq &= H_0\sqrt{\Omega_{(\mathrm{r},0)}}\eta \\ \int_0^q \frac{1}{\sqrt{1+q^2}}dq &= H_0\sqrt{\Omega_{(\mathrm{k},0)}}\eta \\ \int_0^q \frac{1}{\sqrt{1+q^2}}dq &= \phi, \end{aligned} \tag{A.18}$$

where we introduced $\phi = H_0\sqrt{\Omega_{(\mathrm{k},0)}}\eta$. From an integral table we may obtain [126]:

$$\begin{aligned}\int_0^q \frac{1}{\sqrt{u^2+q^2}}dq &= \ln(q+\sqrt{q^2+u^2}) \\ \int_0^q \frac{1}{\sqrt{1+q^2}}dq &= \ln(q+\sqrt{q^2+1}),\end{aligned} \tag{A.19}$$

where for the current case, $u = 1$. Substituting (A.19) into (A.18) gives:

$$\ln(q+\sqrt{q^2+1}) = \phi. \tag{A.20}$$

We consider the special trigonometric function [126]:

$$\sinh^{-1}(q) = \ln(q+\sqrt{q^2+1}). \tag{A.21}$$

Substituting (A.21) into (A.20) gives:

$$\begin{aligned}\sinh^{-1}(q) &= \phi \\ (q) &= \sinh(\phi) \\ a\sqrt{\frac{\Omega_{(\mathrm{k},0)}}{\Omega_{(\mathrm{r},0)}}} &= \sinh(\phi) \\ a &= \sqrt{\frac{\Omega_{(\mathrm{r},0)}}{\Omega_{(\mathrm{k},0)}}}\sinh(\phi) \\ \rightarrow a &= \sqrt{\frac{\Omega_{(\mathrm{r},0)}}{1-\Omega_{(\mathrm{r},0)}}}\sinh(\phi).\end{aligned} \tag{A.22}$$

The time t as parameterized by the conformal time η is:

$$\begin{aligned}\int_0^t dt &= \eta a \\ \int_0^t dt &= \int_0^\eta a d\eta \\ t-0 &= \sqrt{\frac{\Omega_{(\mathrm{r},0)}}{\Omega_{(\mathrm{k},0)}}}\int_0^\eta \sinh(\phi)d\eta.\end{aligned} \tag{A.23}$$

Since $\phi = H_0\sqrt{\Omega_{(\mathrm{k},0)}}\eta$, thus $\eta = \frac{\phi}{H_0\sqrt{\Omega_{(\mathrm{k},0)}}}$ and $d\eta = \frac{1}{H_0\sqrt{\Omega_{(\mathrm{k},0)}}}d\phi$. Doing this substituting, we obtain:

$$\begin{aligned} t - 0 &= \sqrt{\frac{\Omega_{(\mathrm{r},0)}}{\Omega_{(\mathrm{k},0)}}}\int_0^{\phi}\sinh(\phi)\left(\frac{1}{H_0\sqrt{\Omega_{(\mathrm{k},0)}}}d\phi\right) \\ t &= \frac{\sqrt{\Omega_{(\mathrm{r},0)}}}{-H_0\Omega_{(\mathrm{k},0)}}\left[\cosh(\phi)\right]_0^{\phi} \\ t &= \frac{\sqrt{\Omega_{(\mathrm{r},0)}}}{-H_0\Omega_{(\mathrm{k},0)}}\left[\cosh(\phi) - 1\right] \\ \rightarrow t &= \frac{\sqrt{\Omega_{(\mathrm{r},0)}}}{H_0(1-\Omega_{(\mathrm{r},0)})}\left[\cosh(\phi) - 1\right]. \end{aligned} \tag{A.24}$$

The age of this model is found by setting $a = a_0 = 1$ in (A.22) to obtain the present value for ϕ_0:

$$\begin{aligned} a_0 = 1 &= \sqrt{\frac{\Omega_{(\mathrm{r},0)}}{1-\Omega_{(\mathrm{r},0)}}}\sinh(\phi) \\ \phi_0 &= \sinh^{-1}\sqrt{\frac{1-\Omega_{(\mathrm{r},0)}}{\Omega_{(\mathrm{r},0)}}}. \end{aligned} \tag{A.25}$$

Substituting this back into the time t (A.24) gives the age t_0 of the universe model:

$$\rightarrow t_0 = \frac{\sqrt{\Omega_{(\mathrm{r},0)}}}{H_0(1-\Omega_{(\mathrm{r},0)})}\left[\cosh\left(\sinh^{-1}\sqrt{\frac{1-\Omega_{(\mathrm{r},0)}}{\Omega_{(\mathrm{r},0)}}}\right) - 1\right]. \tag{A.26}$$

A.2 Calculations for matter-dominated Friedmann models

matter-dominated Friedmann models have an energy distribution such that $\Omega_{(\mathrm{m},0)} \neq 0$, while $\Omega_{(\mathrm{r},0)} = 0$ and $\Omega_{(\Lambda,0)} = 0$. Substituting this into (2.19) yields the Friedmann equation for matter-dominated Friedmann models:

$$\left(\frac{\dot{a}}{a}\right)^2 = H_0^2\left[\Omega_{(\mathrm{m},0)}a^{-3} + \Omega_{(\mathrm{k},0)}a^{-2}\right]. \tag{A.27}$$

A.2.1 Calculations for a matter-dominated flat model

For a matter-dominated flat model, we have $\Omega_{(\mathrm{k},0)} = 0$; $\Omega_{(\mathrm{m},0)} = 1$. The Friedmann equation (A.27) thus becomes:

$$\begin{aligned}
\left(\frac{\dot{a}}{a}\right)^2 &= H_0^2(1)a^{-3} + (0)a^{-2} \\
a\dot{a}^2 &= H_0^2 \\
\int_0^a a^{\frac{1}{2}} da &= H_0 \int_0^t dt \\
\frac{2}{3}a^{\frac{3}{2}} &= H_0 t \\
a &= \left(\frac{3}{2}H_0 t\right)^{\frac{2}{3}}.
\end{aligned} \tag{A.28}$$

The present age for this universe model t_0 can be found by setting $a = a_0 = 1$. This is easily obtained by solving (A.28) for t_0:

$$\begin{aligned}
a_0 = 1 &= \left(\frac{3}{2}H_0 t\right)^{\frac{2}{3}} \\
\rightarrow t_0 &= \frac{2}{3H_0}.
\end{aligned} \tag{A.29}$$

A.2.2 Calculations for a matter-dominated closed model

For a matter-dominated closed model, we have $\Omega_{(\mathrm{k},0)} < 0$. The Friedmann equation (A.27) thus becomes:

$$\begin{aligned}
\left(\frac{\dot{a}}{a}\right)^2 &= H_0^2\left[\Omega_{(\mathrm{m},0)}a^{-3} + \Omega_{(\mathrm{k},0)}a^{-2}\right] \\
\dot{a} &= H_0\sqrt{-\Omega_{(\mathrm{k},0)}}\sqrt{-\frac{\Omega_{(\mathrm{m},0)}}{\Omega_{(\mathrm{k},0)}}a^{-1} - 1} \\
\dot{a} &= \frac{H_0\sqrt{-\Omega_{(\mathrm{k},0)}}}{\sqrt{a}}\sqrt{-\frac{\Omega_{(\mathrm{m},0)}}{\Omega_{(\mathrm{k},0)}} - a} \\
\int_0^a \frac{1}{\sqrt{-\frac{\Omega_{(\mathrm{m},0)}}{\Omega_{(\mathrm{k},0)}} - a}} da &= \frac{H_0\sqrt{-\Omega_{(\mathrm{k},0)}}}{\sqrt{a}} \int_0^t dt.
\end{aligned} \tag{A.30}$$

We can parametrize this equation by using conformal time η. Substituting (A.5) into (A.30) gives:

$$\begin{aligned}\int_0^a \frac{1}{\sqrt{-\frac{\Omega_{(\mathrm{m},0)}}{\Omega_{(\mathrm{k},0)}}-a}}da &= \frac{H_0\sqrt{-\Omega_{(\mathrm{k},0)}}}{\sqrt{a}}\eta a \\ \int_0^a \frac{1}{\sqrt{a}}\frac{1}{\sqrt{-\frac{\Omega_{(\mathrm{m},0)}}{\Omega_{(\mathrm{k},0)}}-a}}da &= H_0\sqrt{-\Omega_{(\mathrm{k},0)}}\eta.\end{aligned} \tag{A.31}$$

Using substituting, we let $q^2 = a \rightarrow q = \sqrt{a}$ and $dq = \frac{1}{2}\frac{1}{\sqrt{a}}da \rightarrow da = 2\sqrt{a}dq$. We also substitute $\theta = H_0\sqrt{-\Omega_{(\mathrm{k},0)}}\eta$. This yields:

$$\begin{aligned}\int_0^q \frac{1}{\sqrt{a}}\frac{1}{\sqrt{-\frac{\Omega_{(\mathrm{m},0)}}{\Omega_{(\mathrm{k},0)}}-q^2}}2\sqrt{a}dq &= \theta \\ \int_0^q \frac{1}{\sqrt{-\frac{\Omega_{(\mathrm{m},0)}}{\Omega_{(\mathrm{k},0)}}-q^2}}dq &= \frac{1}{2}\theta.\end{aligned} \tag{A.32}$$

Once again, substitute $b^2 = -\frac{\Omega_{(\mathrm{m},0)}}{\Omega_{(\mathrm{k},0)}} \rightarrow b = \sqrt{-\frac{\Omega_{(\mathrm{m},0)}}{\Omega_{(\mathrm{k},0)}}}$ with $\Omega_{(\mathrm{k},0)} < 0$. This gives:

$$\int_0^q \frac{1}{\sqrt{b^2-q^2}}dq = \frac{1}{2}\theta. \tag{A.33}$$

From an integral table we may obtain [126]:

$$\int_0^q \frac{1}{\sqrt{b^2-q^2}}dq = \sin^{-1}\left(\frac{q}{b}\right). \tag{A.34}$$

Substituting (A.34) into (A.33) gives:

$$\begin{aligned}\sin^{-1}\left(\frac{q}{b}\right) &= \frac{1}{2}\theta \\ q\left(\frac{1}{b}\right) &= \sin(\frac{1}{2}\theta) \\ \sqrt{a}\sqrt{-\frac{\Omega_{(\mathrm{k},0)}}{\Omega_{(\mathrm{m},0)}}} &= \sin(\frac{1}{2}\theta) \\ a &= \left(-\frac{\Omega_{(\mathrm{m},0)}}{\Omega_{(\mathrm{k},0)}}\right)\sin^2(\frac{1}{2}\theta).\end{aligned} \tag{A.35}$$

We consider the trigonometric identity [126]:

$$\sin^2(x) = \frac{1}{2}(1-\cos(2x)), \tag{A.36}$$

where for the current case $x = (\frac{1}{2}\theta)$. Substituting (A.36) into (A.35) gives:

$$\begin{aligned} a &= \left(-\frac{\Omega_{(\mathrm{m},0)}}{2\Omega_{(\mathrm{k},0)}}\right)(1-\cos(\theta)) \\ \rightarrow a &= \frac{\Omega_{(\mathrm{m},0)}}{2\left(\Omega_{(\mathrm{m},0)}-1\right)}(1-\cos(\theta)). \end{aligned} \tag{A.37}$$

The time t as parameterized by the conformal time η is:

$$\begin{aligned} \int_0^t dt &= \eta a \\ \int_0^t dt &= \int_0^\eta a d\eta \\ t-0 &= \left(-\frac{\Omega_{(\mathrm{m},0)}}{2\Omega_{(\mathrm{k},0)}}\right)\int_0^\eta (1-\cos(\theta))d\eta. \end{aligned} \tag{A.38}$$

Since $\theta = H_0\sqrt{-\Omega_{(\mathrm{k},0)}}\eta$, thus $\eta = \frac{\theta}{H_0\sqrt{-\Omega_{(\mathrm{k},0)}}}$ and $d\eta = \frac{1}{H_0\sqrt{-\Omega_{(\mathrm{k},0)}}}d\theta$. Doing this substituting, we obtain:

$$\begin{aligned} t-0 &= \left(-\frac{\Omega_{(\mathrm{m},0)}}{2\Omega_{(\mathrm{k},0)}}\right)\int_0^\theta (1-\cos(\theta))\left(\frac{1}{H_0\sqrt{-\Omega_{(\mathrm{k},0)}}}d\theta\right) \\ t &= \left(\frac{\Omega_{(\mathrm{m},0)}}{2H_0\left(-\Omega_{(\mathrm{k},0)}\right)^{3/2}}\right)\left(\int_0^\theta 1 d\eta - \int_0^\theta \cos(\theta)d\theta\right) \\ t &= \left(\frac{\Omega_{(\mathrm{m},0)}}{2H_0\left(-\Omega_{(\mathrm{k},0)}\right)^{3/2}}\right)[\theta-\sin(\theta)]_0^\theta \\ t &= \frac{\Omega_{(\mathrm{m},0)}}{2H_0\left(-\Omega_{(\mathrm{k},0)}\right)^{3/2}}[\theta-\sin(\theta)] \\ \rightarrow t &= \frac{\Omega_{(\mathrm{m},0)}}{2H_0\left(\Omega_{(\mathrm{m},0)}-1\right)^{3/2}}[\theta-\sin(\theta)], \end{aligned} \tag{A.39}$$

with $\theta = H_0\sqrt{-\Omega_{(\mathrm{k},0)}}\eta$.

From the solution it may be seen that this solution is a cycloid as shown in Figure 2.4. This universe model therefore has an infinite age, which consists of sequential big bounces and big crunches. The time that elapsed since the last bounce may be obtained by setting $a = a_0 = 1$ in (A.37) to obtain the present value for θ_0:

$$\begin{aligned} a_0 = 1 &= \frac{\Omega_{(\mathrm{m},0)}}{2\left(\Omega_{(\mathrm{m},0)}-1\right)}(1-\cos(\theta_0)) \\ \theta_0 &= \cos^{-1}\left(1-\frac{2\left(\Omega_{(\mathrm{m},0)}-1\right)}{\Omega_{(\mathrm{m},0)}}\right). \end{aligned} \tag{A.40}$$

Substituting this back into the time t (A.39) gives the time since the previous bounce t_{Pb}:

$$\rightarrow t_{Pb} = \frac{\Omega_{(\mathrm{m},0)}}{2H_0\left(\Omega_{(\mathrm{m},0)}-1\right)^{3/2}}\left[\left(\cos^{-1}\left(1-\frac{2\left(\Omega_{(\mathrm{m},0)}-1\right)}{\Omega_{(\mathrm{m},0)}}\right)\right)-\sin\left(\cos^{-1}\left(1-\frac{2\left(\Omega_{(\mathrm{m},0)}-1\right)}{\Omega_{(\mathrm{m},0)}}\right)\right)\right]. \tag{A.41}$$

Since this model is cyclical with a big bang at $\theta = 0$ and big crunch at $\theta = 2\pi$, the time per bounce cycle t_b and can be found by the difference between $\theta = 2\pi$ and $\theta = 0$ in t (A.39), giving:

$$\begin{aligned} t_b &= \frac{\Omega_{(\mathrm{m},0)}}{2H_0\left(\Omega_{(\mathrm{m},0)}-1\right)^{3/2}}\left[\theta-\sin(\theta)\right]_0^{2\pi} \\ t_b &= \frac{\Omega_{(\mathrm{m},0)}}{2H_0\left(\Omega_{(\mathrm{m},0)}-1\right)^{3/2}}\left[(2\pi-\sin(2\pi))-(0-\sin(0))\right] \\ \rightarrow t_b &= \frac{\pi}{H_0}\frac{\Omega_{(\mathrm{m},0)}}{\left(\Omega_{(\mathrm{m},0)}-1\right)^{3/2}}. \end{aligned} \tag{A.42}$$

This matches with [10]. The amount of time until the next bounce t_{Nb} can therefore be calculated by the difference in time between one bounce cycle t_b (A.42) and the time since the previous bounce t_{Pb} (A.41):

$$\begin{aligned} t_{Nb} =& t_b - t_{Pb} \\ t_{Nb} =& \frac{\pi}{H_0}\frac{\Omega_{(\mathrm{m},0)}}{\left(\Omega_{(\mathrm{m},0)}-1\right)^{3/2}} - \\ & \frac{\Omega_{(\mathrm{m},0)}}{2H_0\left(\Omega_{(\mathrm{m},0)}-1\right)^{3/2}}\left[\cos^{-1}\left(1-\frac{2\left(\Omega_{(\mathrm{m},0)}-1\right)}{\Omega_{(\mathrm{m},0)}}\right)-\sin\left(\cos^{-1}\left(1-\frac{2\left(\Omega_{(\mathrm{m},0)}-1\right)}{\Omega_{(\mathrm{m},0)}}\right)\right)\right] \\ t_{Nb} =& \frac{\Omega_{(\mathrm{m},0)}}{2H_0\left(\Omega_{(\mathrm{m},0)}-1\right)^{3/2}}\left[2\pi-\cos^{-1}\left(1-\frac{2\left(\Omega_{(\mathrm{m},0)}-1\right)}{\Omega_{(\mathrm{m},0)}}\right)+\sin\left(\cos^{-1}\left(1-\frac{2\left(\Omega_{(\mathrm{m},0)}-1\right)}{\Omega_{(\mathrm{m},0)}}\right)\right)\right]. \end{aligned} \tag{A.43}$$

It may also be noted that the scale factor reaches a maximum size $a_{\max}$ at$\theta = \pi$, thus from (A.37) we have:

$$\begin{aligned} a_{\max} &= \left(-\frac{\Omega_{(\mathrm{m},0)}}{2\Omega_{(\mathrm{k},0)}}\right)(1-\cos(\pi)) \\ a_{\max} &= \frac{\Omega_{(\mathrm{m},0)}}{\left(\Omega_{(\mathrm{m},0)}-1\right)}, \end{aligned} \tag{A.44}$$

which also matches with [10].

A.2.3 Calculations for a matter-dominated open model

For a matter-dominated open model, we have $\Omega_{(\mathrm{k},0)} > 0$. The Friedmann equation (A.1) thus becomes:

$$\begin{aligned}\left(\frac{\dot{a}}{a}\right)^2 &= H_0^2\left[\Omega_{(\mathrm{m},0)}a^{-3} + \Omega_{(\mathrm{k},0)}a^{-2}\right] \\ \dot{a} &= H_0\sqrt{\Omega_{(\mathrm{m},0)}}\sqrt{1+\frac{\Omega_{(\mathrm{k},0)}}{\Omega_{(\mathrm{m},0)}}a^{-1}} \\ \dot{a} &= \frac{H_0\sqrt{\Omega_{(\mathrm{m},0)}}}{\sqrt{a}}\sqrt{1+\frac{\Omega_{(\mathrm{k},0)}}{\Omega_{(\mathrm{m},0)}}a} \\ \frac{\sqrt{a}}{H_0\sqrt{\Omega_{(\mathrm{m},0)}}}\int_0^a \frac{1}{\sqrt{1+\frac{\Omega_{(\mathrm{k},0)}}{\Omega_{(\mathrm{m},0)}}a}}da &= \int_0^t dt.\end{aligned} \tag{A.45}$$

We can parametrize this equation by using conformal time η. Substituting (A.5) into (A.45) gives:

$$\begin{aligned}\frac{\sqrt{a}}{H_0\sqrt{\Omega_{(\mathrm{m},0)}}}\int_0^a \frac{1}{\sqrt{1+\frac{\Omega_{(\mathrm{k},0)}}{\Omega_{(\mathrm{m},0)}}a}}da &= \eta a \\ \frac{1}{H_0\sqrt{\Omega_{(\mathrm{m},0)}a}}\int_0^a \frac{1}{\sqrt{1+\frac{\Omega_{(\mathrm{k},0)}}{\Omega_{(\mathrm{m},0)}}a}}da &= \eta.\end{aligned} \tag{A.46}$$

Using substituting, we let $q^2 = \frac{\Omega_{(\mathrm{k},0)}a}{\Omega_{(\mathrm{m},0)}} \rightarrow q = \sqrt{\frac{\Omega_{(\mathrm{k},0)}a}{\Omega_{(\mathrm{m},0)}}}$ (with $\Omega_{(\mathrm{k},0)} > 0$) and $dq = \frac{1}{2}\sqrt{\frac{\Omega_{(\mathrm{k},0)}}{\Omega_{(\mathrm{m},0)}a}}da \rightarrow da = 2\sqrt{\frac{\Omega_{(\mathrm{m},0)}a}{\Omega_{(\mathrm{k},0)}}}dq$. This yields:

$$\begin{aligned}\frac{1}{H_0\sqrt{\Omega_{(\mathrm{m},0)}a}}\int_0^q \frac{1}{\sqrt{1+q^2}}(2)\sqrt{\frac{\Omega_{(\mathrm{m},0)}a}{\Omega_{(\mathrm{k},0)}}}dq &= \eta \\ \int_0^q \frac{1}{\sqrt{1+q^2}}dq &= \frac{1}{2}H_0\sqrt{\Omega_{(\mathrm{k},0)}}\eta \\ \int_0^q \frac{1}{\sqrt{1+q^2}}dq &= \frac{1}{2}\phi,\end{aligned} \tag{A.47}$$

where we reintroduced $\phi = H_0\sqrt{\Omega_{(\mathrm{k},0)}}\eta$. Where we introduced $\phi = H_0\sqrt{\Omega_{(\mathrm{k},0)}}\eta$. From an integral table we can again substitute (A.19) into (A.47) gives [126]:

$$\ln(q+\sqrt{q^2+1}) = \frac{1}{2}\phi. \tag{A.48}$$

We again substitute the special trigonometric function given in (A.21) into (A.48):

$$\begin{aligned} \sinh^{-1}(q) &= \frac{1}{2}\phi \\ (q) &= \sinh(\phi) \\ \sqrt{\frac{\Omega_{(\mathrm{k},0)}a}{\Omega_{(\mathrm{m},0)}}} &= \sinh\left(\frac{1}{2}\phi\right) \\ a &= \left(\frac{\Omega_{(\mathrm{m},0)}}{\Omega_{(\mathrm{k},0)}}\right)\sinh^2\left(\frac{1}{2}\phi\right). \end{aligned} \tag{A.49}$$

We consider the trigonometric identity [126]:

$$\sinh^2(x) = \frac{1}{2}(\cosh(2x) - 1), \tag{A.50}$$

where for the current case $x = (\frac{1}{2}\phi)$. Substituting (A.50) into (A.49) gives:

$$\begin{aligned} a &= \left(\frac{\Omega_{(\mathrm{m},0)}}{2\Omega_{(\mathrm{k},0)}}\right)(\cosh(\phi) - 1) \\ \rightarrow a &= \left(\frac{\Omega_{(\mathrm{m},0)}}{2\left(1 - \Omega_{(\mathrm{m},0)}\right)}\right)(\cosh(\phi) - 1), \end{aligned} \tag{A.51}$$

The time t as parameterized by the conformal time η is:

$$\begin{aligned} \int_0^t dt &= \eta a \\ \int_0^t dt &= \int_0^\eta a d\eta \\ t - 0 &= \int_0^\eta \left(\frac{\Omega_{(\mathrm{m},0)}}{2\Omega_{(\mathrm{k},0)}}\right)(\cosh(\phi) - 1)d\eta. \end{aligned} \tag{A.52}$$

Since $\phi = H_0\sqrt{\Omega_{(\mathrm{k},0)}}\eta$, thus $\eta = \frac{\phi}{H_0\sqrt{\Omega_{(\mathrm{k},0)}}}$ and $d\eta = \frac{1}{H_0\sqrt{\Omega_{(\mathrm{k},0)}}}d\phi$. Doing this substituting, we obtain:

$$\begin{aligned}
t - 0 &= \int_0^{\eta} \left(\frac{\Omega_{(\mathrm{m},0)}}{2\Omega_{(\mathrm{k},0)}}\right)(\cosh(\phi) - 1)\left(\frac{1}{H_0\sqrt{\Omega_{(\mathrm{k},0)}}}d\phi\right) \\
t &= \left(\frac{\Omega_{(\mathrm{m},0)}}{2H_0\left(\Omega_{(\mathrm{k},0)}\right)^{3/2}}\right)\left(\int_0^{\phi}\cosh(\phi)d\phi - \int_0^{\phi} 1 d\phi\right) \\
t &= \left(\frac{\Omega_{(\mathrm{m},0)}}{2H_0\left(\Omega_{(\mathrm{k},0)}\right)^{3/2}}\right)[\sinh(\phi) - \phi]_0^{\phi} \\
t &= \left(\frac{\Omega_{(\mathrm{m},0)}}{2H_0\left(\Omega_{(\mathrm{k},0)}\right)^{3/2}}\right)[\sinh(\phi) - \phi] \\
\rightarrow t &= \left(\frac{\Omega_{(\mathrm{m},0)}}{2H_0\left(1 - \Omega_{(\mathrm{m},0)}\right)^{3/2}}\right)[\sinh(\phi) - \phi]\,,
\end{aligned} \tag{A.53}$$

with $\phi = H_0\sqrt{\Omega_{(\mathrm{k},0)}}\eta = H_0\sqrt{1 - \Omega_{(\mathrm{m},0)}}\eta$.

The age of this model is found by setting $a = a_0 = 1$ in (A.51) to obtain the present value for ϕ_0:

$$\begin{aligned}
a_0 = 1 &= \left(\frac{\Omega_{(\mathrm{m},0)}}{2\left(1 - \Omega_{(\mathrm{m},0)}\right)}\right)(\cosh(\phi_0) - 1) \\
\phi_0 &= \cosh^{-1}\left(1 + \frac{2\left(1 - \Omega_{(\mathrm{m},0)}\right)}{\Omega_{(\mathrm{m},0)}}\right).
\end{aligned} \tag{A.54}$$

Substituting this back into the time t (A.24) gives the age t_0 of the universe model:

$$\rightarrow t_0 = \left(\frac{\Omega_{(\mathrm{m},0)}}{2H_0\left(1 - \Omega_{(\mathrm{m},0)}\right)^{3/2}}\right)\left[\sinh\left(\cosh^{-1}\left(1 + \frac{2\left(1 - \Omega_{(\mathrm{m},0)}\right)}{\Omega_{(\mathrm{m},0)}}\right)\right) - \cosh^{-1}\left(1 + \frac{2\left(1 - \Omega_{(\mathrm{m},0)}\right)}{\Omega_{(\mathrm{m},0)}}\right)\right]. \tag{A.55}$$

A.3 Calculations for cosmological constant dominated Lemaître models

Cosmological constant dominated Lemaître models have an energy distribution such that $\Omega_{(\Lambda,0)} \neq 0$, while $\Omega_{(\mathrm{r},0)} = 0$ and $\Omega_{(\mathrm{m},0)} = 0$. Substituting this into (2.19) yields the Friedmann equation for

cosmological constant dominated Lemaître models:

$$\begin{aligned}\left(\frac{\dot{a}}{a}\right)^2 &= H_0^2\left[\Omega_{(\Lambda,0)}a^{-3(1+(-1))} + \Omega_{(\mathrm{k},0)}a^{-2}\right] \\ \left(\frac{\dot{a}}{a}\right)^2 &= H_0^2\left[\Omega_{(\Lambda,0)} + \Omega_{(\mathrm{k},0)}a^{-2}\right].\end{aligned} \tag{A.56}$$

A.3.1 Calculations for a cosmological constant-dominated flat model

For a cosmological constant-dominated flat model, we have $\Omega_{(\mathrm{k},0)} = 0$; $\Omega_{(\Lambda,0)} = 1$. The Friedmann equation (A.56) thus becomes:

$$\begin{aligned}\left(\frac{\dot{a}}{a}\right)^2 &= H_0^2\left[(1) + (0)a^{-2}\right] \\ \left(\frac{\dot{a}}{a}\right)^2 &= H_0^2 \\ \int_0^a \frac{1}{a}da &= H_0\int_0^t dt \\ a &= e^{H_0 t}.\end{aligned} \tag{A.57}$$

Due to this exponential nature of the solution, it can be inferred that the size of the universe will decrease in the past but will have no big bang singularity. The model, therefore, has an infinite age. This may be seen in Figure 2.5.

A.3.2 Calculations for a cosmological constant-dominated closed model

For a cosmological constant-dominated closed model, we have $\Omega_{(\mathrm{k},0)} < 0$. The Friedmann equation (A.56) thus becomes:

$$\begin{aligned}\left(\frac{\dot{a}}{a}\right)^2 &= H_0^2\left[\Omega_{(\Lambda,0)} + \Omega_{(\mathrm{k},0)}a^{-2}\right] \\ \dot{a} &= H_0\sqrt{\Omega_{(\Lambda,0)}a^2 + \Omega_{(\mathrm{k},0)}} \\ \dot{a} &= H_0\sqrt{-\Omega_{(\mathrm{k},0)}}\sqrt{\frac{\Omega_{(\Lambda,0)}a^2}{-\Omega_{(\mathrm{k},0)}} - 1} \\ \int_0^a \frac{1}{\sqrt{\frac{\Omega_{(\Lambda,0)}a^2}{-\Omega_{(\mathrm{k},0)}} - 1}}da &= H_0\sqrt{-\Omega_{(\mathrm{k},0)}}\int_0^t dt.\end{aligned} \tag{A.58}$$

Using substituting, we let $q^2 = \frac{\Omega_{(\Lambda,0)}a^2}{-\Omega_{(\mathrm{k},0)}} \rightarrow q = a\sqrt{\frac{\Omega_{(\Lambda,0)}}{-\Omega_{(\mathrm{k},0)}}}$ and $dq = \sqrt{\frac{\Omega_{(\Lambda,0)}}{-\Omega_{(\mathrm{k},0)}}}da \rightarrow da = \sqrt{\frac{-\Omega_{(\mathrm{k},0)}}{\Omega_{(\Lambda,0)}}}dq$, with $\Omega_{(\mathrm{k},0)} < 0$. This yields:

$$\begin{aligned}\int_0^q \frac{1}{\sqrt{q^2-1}}\sqrt{\frac{\Omega_{(\mathrm{k},0)}}{\Omega_{(\Lambda,0)}}}dq &= H_0\sqrt{-\Omega_{(\mathrm{k},0)}}\int_0^t dt \\ \int_0^q \frac{1}{\sqrt{q^2-1}}dq &= H_0\sqrt{-\Omega_{(\mathrm{k},0)}}t \\ \int_0^q \frac{1}{\sqrt{q^2-1}}dq &= \psi,\end{aligned} \tag{A.59}$$

where $\psi = H_0\sqrt{-\Omega_{(\mathrm{k},0)}}t$. From an integral table we may obtain [126]:

$$\begin{aligned}\int_0^q \frac{1}{\sqrt{q^2 \pm u^2}}dq &= \ln(q + \sqrt{q^2 \pm u^2}) \\ \int_0^q \frac{1}{\sqrt{q^2-1}}dq &= \ln(q + \sqrt{q^2-1}),\end{aligned} \tag{A.60}$$

where for the current case, $\pm u = -1$. Substituting (A.60) into (A.59) gives:

$$\ln(q + \sqrt{q^2-1}) = \psi. \tag{A.61}$$

We consider the special trigonometric function [126]:

$$\cosh^{-1}(q) = \ln(q + \sqrt{q^2-1}). \tag{A.62}$$

Substituting (A.62) into (A.61) gives:

$$\begin{aligned}\cosh^{-1}(q) &= \psi \\ (q) &= \cosh(\psi) \\ a\sqrt{\frac{\Omega_{(\Lambda,0)}}{-\Omega_{(\mathrm{k},0)}}} &= \cosh(\psi) \\ a &= \sqrt{\frac{-\Omega_{(\mathrm{k},0)}}{\Omega_{(\Lambda,0)}}}\cosh(\psi) \\ \rightarrow a &= \sqrt{\frac{\Omega_{(\Lambda,0)}-1}{\Omega_{(\Lambda,0)}}}\cosh(\psi),\end{aligned} \tag{A.63}$$

where $\psi = H_0\sqrt{-\Omega_{(\mathrm{k},0)}}t = H_0\sqrt{\Omega_{(\Lambda,0)}-1}t$.

From this solution it may be seen that the expansion has a parabolic nature, and will therefore have no big bang, but instead have a non-singular big bounce at some finite time in the past. This

bounce will occur at $\psi = 0$, from (A.63) this happens when the universe has a scale factor a_b

$$a_b = \sqrt{\frac{\Omega_{(\Lambda,0)} - 1}{\Omega_{(\Lambda,0)}}}. \tag{A.64}$$

The time since the bounce t_b will be the amount of time elapsed for the universe to grow from a size a_b to a size $a_0 = 1$. Thus, after a time t_b the universe will be size a_0. Solving (A.63) for t_b with $a_0 = 1$ and $\psi = H_0\sqrt{\Omega_{(\Lambda,0)} - 1}t$ gives:

$$\begin{aligned} a_0 = 1 &= \sqrt{\frac{\Omega_{(\Lambda,0)} - 1}{\Omega_{(\Lambda,0)}}} \cosh\left(H_0\sqrt{\Omega_{(\Lambda,0)} - 1}t_b\right) \\ \rightarrow t_b &= \frac{1}{H_0\sqrt{\Omega_{(\Lambda,0)} - 1}} \cosh^{-1}\left(\sqrt{\frac{\Omega_{(\Lambda,0)}}{\Omega_{(\Lambda,0)} - 1}}\right). \end{aligned} \tag{A.65}$$

A.3.3 Calculations for a cosmological constant-dominated open model

For a cosmological constant-dominated open model, we have $\Omega_{(\mathrm{k},0)} > 0$. The Friedmann equation (A.56) thus becomes:

$$\begin{aligned} \left(\frac{\dot{a}}{a}\right)^2 &= H_0^2\left[\Omega_{(\Lambda,0)} + \Omega_{(\mathrm{k},0)}a^{-2}\right] \\ \dot{a} &= H_0\sqrt{\Omega_{(\Lambda,0)}a^2 + \Omega_{(\mathrm{k},0)}} \\ \dot{a} &= H_0\sqrt{\Omega_{(\mathrm{k},0)}}\sqrt{\frac{\Omega_{(\Lambda,0)}a^2}{\Omega_{(\mathrm{k},0)}} + 1} \\ \int_0^a \frac{1}{\sqrt{\frac{\Omega_{(\Lambda,0)}a^2}{\Omega_{(\mathrm{k},0)}} + 1}} da &= H_0\sqrt{\Omega_{(\mathrm{k},0)}}\int_0^t dt. \end{aligned} \tag{A.66}$$

Using substituting, we let $q^2 = \frac{\Omega_{(\Lambda,0)}a^2}{\Omega_{(\mathrm{k},0)}} \rightarrow q = a\sqrt{\frac{\Omega_{(\Lambda,0)}}{\Omega_{(\mathrm{k},0)}}}$ and $dq = \sqrt{\frac{\Omega_{(\Lambda,0)}}{\Omega_{(\mathrm{k},0)}}}da \rightarrow da = \sqrt{\frac{\Omega_{(\mathrm{k},0)}}{\Omega_{(\Lambda,0)}}}dq$, with $\Omega_{(\mathrm{k},0)} > 0$. This yields:

$$\begin{aligned} \int_0^q \frac{1}{\sqrt{q^2+1}}\sqrt{\frac{\Omega_{(\mathrm{k},0)}}{\Omega_{(\Lambda,0)}}}dq &= H_0\sqrt{\Omega_{(\mathrm{k},0)}}\int_0^t dt \\ \int_0^q \frac{1}{\sqrt{q^2+1}}dq &= H_0\sqrt{\Omega_{(\mathrm{k},0)}}t \\ \int_0^q \frac{1}{\sqrt{q^2-1}}dq &= \varphi, \end{aligned} \tag{A.67}$$

where $\varphi = H_0\sqrt{\Omega_{(\mathrm{k},0)}}t$. From an integral table [126] we can again substitute (A.19) into (A.67) gives:

$$\ln(q + \sqrt{q^2+1}) = \varphi. \tag{A.68}$$

We again substitute the special trigonometric function given in (A.21) into (A.68):

$$\begin{aligned} \sinh^{-1}(q) &= \varphi \\ (q) &= \sinh(\varphi) \\ a\sqrt{\frac{\Omega_{(\Lambda,0)}}{\Omega_{(\mathrm{k},0)}}} &= \sinh(\varphi) \\ a &= \sqrt{\frac{\Omega_{(\mathrm{k},0)}}{\Omega_{(\Lambda,0)}}}\sinh(\varphi) \\ \rightarrow a &= \sqrt{\frac{1-\Omega_{(\Lambda,0)}}{\Omega_{(\Lambda,0)}}}\sinh(\varphi), \end{aligned} \tag{A.69}$$

where $\varphi = H_0\sqrt{\Omega_{(\mathrm{k},0)}}t = H_0\sqrt{1-\Omega_{(\Lambda,0)}}t$. The age of this model t_0 is found by setting $a = a_0 = 1$ in (A.69) to obtain the present value for t_0:

$$\begin{aligned} a_0 = 1 &= \sqrt{\frac{1-\Omega_{(\Lambda,0)}}{\Omega_{(\Lambda,0)}}}\sinh\left(H_0\sqrt{1-\Omega_{(\Lambda,0)}}t_0\right) \\ \rightarrow t_0 &= \frac{1}{H_0\sqrt{1-\Omega_{(\Lambda,0)}}}\sinh^{-1}\left(\sqrt{\frac{\Omega_{(\Lambda,0)}}{1-\Omega_{(\Lambda,0)}}}\right). \end{aligned} \tag{A.70}$$

A.4 Solving the Friedmann Equation with 4th-order Runge-Kutta Method

To numerically solve the differential equation (2.19), the Friedmann equation can be written as:

$$\begin{aligned} \dot{a} &= aH_0\sqrt{(\Omega_{(\mathrm{r},0)}a^{-4} + \Omega_{(\mathrm{m},0)}a^{-3} + \Omega_{(\Lambda,0)} + \Omega_{(\mathrm{k},0)}a^{-2})} \\ \frac{da}{dt} &= aH_0\sqrt{(\Omega_{(\mathrm{r},0)}a^{-4} + \Omega_{(\mathrm{m},0)}a^{-3} + \Omega_{(\Lambda,0)} + \Omega_{(\mathrm{k},0)}a^{-2})} = f(t, a(t)). \end{aligned} \tag{A.71}$$

Since this study will be quantitative, it should be noted that the scale factor a and the density parameters Ω are unitless. The only units are determined by the Hubble constant H_0, whose units has been converted to per billion years such that H_0 =67.4 km s^{-1}Mpc^{-1} = 0.069 Gyr^{-1}.

The 4th order Runge-Kutta Method can now be used to determine the scale factor a_n at various time intervals t_n for n intervals. The initial condition was chosen such that $a_0 = 1$ at $t = 0$, and the Runge-Kutta method could then be used to calculate the scale factor in the past and future. For a time step of h, the next time interval will be given by:

$$t_{n+1} = t_\mathrm{n} + h. \tag{A.72}$$

The formula used to determine the next scale factor a_{n+1} from the previous scale factor a_n will now be considered. For each interval, the following four increments on the slope will need to be calculated:

$$\begin{aligned} K_1 &= hf(t_\mathrm{n}, a_\mathrm{n}) \\ K_2 &= hf(t_\mathrm{n} + \frac{h}{2}, a_\mathrm{n} + \frac{K_1}{2}) \\ K_3 &= hf(t_\mathrm{n} + \frac{h}{2}, a_\mathrm{n} + \frac{K_2}{2}) \\ K_4 &= hf(t_\mathrm{n} + h, a_\mathrm{n} + K_3), \end{aligned} \tag{A.73}$$

where K_1, K_2, K_3 and K_4 are increments based on the slope at the beginning, midpoint (both K_1 and K_2) and end of each interval respectively. Using the weighted average of these four increments, the next scale factor at next increment a_{n+1} can now be calculated:

$$a_{n+1} = a_\mathrm{n} + \frac{K_1}{6} + \frac{K_2}{3} + \frac{K_3}{3} + \frac{K_4}{6}. \tag{A.74}$$

APPENDIX B

Phase portrait equilibrium points

In this appendix the equilibrium points of the phase portraits (Figures 3.1, 3.2 3.11) are calculated for the ΛCDM, $Q_1 = \delta H \rho_{\rm dm}$ and $Q_2 = \delta H \rho_{\rm de}$ models. This is done by setting the derivative of the energy densities to zero in (3.22) and obtaining the coordinates for the equilibria points.

B.1 Calculations for equilibrium points - ΛCDM

The equilibria points for the ΛCDM model is obtained by setting $\dot{\Omega}_m = 0$ and $\dot{\Omega}_\Lambda = 0$ in (3.25) such that:

$$\dot{\Omega}_\Lambda = \Omega_\Lambda H \left[\Omega_{\rm m} - 2\Omega_\Lambda + 2\right] = 0, \tag{B.1}$$

$$\dot{\Omega}_{\rm m} = \Omega_{\rm m} H \left[\Omega_{\rm m} - 2\Omega_\Lambda - 1\right] = 0. \tag{B.2}$$

The non-trivial solutions can be obtained by taking the solution $\Omega_\Lambda = 0$ in (B.1), then substituting in (B.2) gives:

$$\begin{aligned} \left[\Omega_{\rm m} - 2(0) - 1\right] &= 0 \\ \Omega_m &= 1. \end{aligned} \tag{B.3}$$

Thus the first equilibrium point is at the coordinates $(\Omega_{\rm m},\, \Omega_\Lambda)_1 = (1, 0)$. The second equilibrium point is obtained similarly by the solution $\Omega_{\rm m} = 0$ in (B.2), then (B.1) becomes:

$$\begin{aligned} [(0) - 2\Omega_\Lambda + 2] &= 0 \\ \Omega_\Lambda &= 1. \end{aligned} \tag{B.4}$$

The second equilibrium point is then the coordinates $(\Omega_{\rm m},\, \Omega_\Lambda)_2 = (0, 1)$. These two points match with the unstable starting point $(1, 0)$ and the stable attractor $(0, 1)$ in Figure (3.1).

B.2 Calculations for equilibrium points - $Q_1 = \delta H \rho_{\rm dm}$

The equilibria points for this interacting model is obtained by setting $\dot{\Omega}_{\rm dm} = 0$ and $\dot{\Omega}_{\rm de} = 0$ in (3.30) such that:

$$\dot{\Omega}_{\rm de} = \Omega_{\rm de} H \left[\Omega_{\rm dm} + \Omega_{\rm de}\,(1 + 3\omega) - 1 - 3\omega\right] - \delta H \Omega_{\rm dm} = 0, \tag{B.5}$$

$$\dot{\Omega}_{\rm dm} = \Omega_{\rm dm} H \left[\Omega_{\rm dm} + \Omega_{\rm de}\,(1 + 3\omega) - 1 + \delta\right] = 0. \tag{B.6}$$

The first equilibrium point can be obtained from the solution $\Omega_{\rm dm} = 0$ in (B.6). Substituting this solution into (B.5) gives:

$$\begin{aligned} \Omega_{\rm de} H \left[(0) + \Omega_{\rm de}\,(1 + 3\omega) - 1 - 3\omega\right] - \delta H (0) &= 0 \\ \Omega_{\rm de}\,(1 + 3\omega) &= (1 + 3\omega) \\ \Omega_{\rm de} &= 1. \end{aligned} \tag{B.7}$$

Thus, the first equilibrium point is at $(\Omega_{\rm dm},\, \Omega_{\rm de})_1 = (0, 1)$. The second point can be obtained by taking the other solution for (B.6), such that:

$$\begin{aligned} \left[\Omega_{\rm dm} + \Omega_{\rm de}\,(1 + 3\omega) - 1 + \delta\right] &= 0 \\ \Omega_{\rm dm} &= -\Omega_{\rm de}\,(1 + 3\omega) + 1 - \delta. \end{aligned} \tag{B.8}$$

Substituting (B.8) into (B.5) gives:

$$\begin{aligned} \Omega_{\rm de} H \left[(-\Omega_{\rm de}\,(1 + 3\omega) + 1 - \delta) + \Omega_{\rm de}\,(1 + 3\omega) - 1 - 3\omega\right] - \delta H \Omega_{\rm dm} &= 0 \\ \Omega_{\rm de}\left[-\delta - 3\omega\right] &= \delta \Omega_{\rm dm}. \end{aligned} \tag{B.9}$$

Substituting (B.8) into (B.9) gives:

$$\begin{aligned}
\Omega_{\text{de}}\left[-\delta-3\omega\right] &= \delta\left(-\Omega_{\text{de}}\left(1+3\omega\right)+1-\delta\right)\\
-\delta\Omega_{\text{de}}-3\Omega_{\text{de}}\omega &= -\delta\Omega_{\text{de}}+3\delta\Omega_{\text{de}}\omega+\delta-\delta^2\\
-3\omega\Omega_{\text{de}}\left(1-\delta\right) &= \delta\left(1-\delta\right)\\
\Omega_{\text{de}} &= -\frac{\delta}{3\omega}.
\end{aligned} \tag{B.10}$$

Substituting (B.10) into (B.8) gives:

$$\begin{aligned}
\Omega_{\text{dm}} &= -\left(-\frac{\delta}{3\omega}\right)\left(1+3\omega\right)+1-\delta\\
\Omega_{\text{dm}} &= \frac{\delta}{3\omega}+\delta+1-\delta\\
\Omega_{\text{dm}} &= 1+\frac{\delta}{3\omega}.
\end{aligned} \tag{B.11}$$

The second equilibrium point is at $(\Omega_{\text{dm}}, \Omega_{\text{de}})_2 = (1+\frac{\delta}{3\omega}, -\frac{\delta}{3\omega})$. These two points match with the unstable starting point $(1+\frac{\delta}{3\omega}, -\frac{\delta}{3\omega})$ and the stable attractor $(0,1)$ in Figure 3.2, while reducing back to the ΛCDM case when $\delta = 0$ and $\omega = -1$.

B.3 Calculations for equilibrium points - $Q_2 = \delta H \rho_{\text{de}}$

The equilibrium points for this interacting model is similarly obtained by setting $\dot{\Omega}_{\text{m}} = 0$ and $\dot{\Omega}_{\text{de}} = 0$ in (3.71) such that:

$$\dot{\Omega}_{\text{de}} = \Omega_{\text{de}} H\left[\Omega_{\text{m}}+\Omega_{\text{de}}\left(1+3\omega\right)-1-3\omega-\delta\right] = 0, \tag{B.12}$$

$$\dot{\Omega}_{\text{m}} = \Omega_{\text{m}} H\left[\Omega_{\text{m}}+\Omega_{\text{de}}\left(1+3\omega\right)-1\right]+\delta H\Omega_{\text{de}} = 0. \tag{B.13}$$

The first equilibrium point can be obtained from the solution $\Omega_{\text{de}} = 0$ in (B.12). Substituting this solution into (B.12) gives:

$$\begin{aligned}
\Omega_{\text{m}}\left[\Omega_{\text{m}}+(0)\left(1+3\omega\right)-1\right]+\delta(0) &= 0\\
\Omega_{\text{m}} &= 1.
\end{aligned} \tag{B.14}$$

Thus, the first equilibrium point is at $(\Omega_{\rm m},\, \Omega_{\rm de})_1 = (1, 0)$. The second point can be obtained by taking the other solution for (B.12), such that:

$$\begin{aligned} \Omega_{\rm m} + \Omega_{\rm de}\,(1+3\omega) - 1 - 3\omega - \delta = 0 \\ \Omega_{\rm de} = \frac{-\Omega_{\rm m} + 1 + 3\omega + \delta}{(1+3\omega)}. \end{aligned} \tag{B.15}$$

Substituting (B.15) into (B.13) gives:

$$\begin{aligned} \Omega_{\rm m} H \left[\Omega_{\rm m} + \frac{-\Omega_{\rm m} + 1 + 3\omega + \delta}{(1+3\omega)}\,(1+3\omega) - 1\right] + \delta H\omega = 0 \\ \Omega_{\rm m}\,[\delta + 3\omega] = -\delta\Omega_{\rm de}. \end{aligned} \tag{B.16}$$

Substituting (B.15) into (B.16) gives:

$$\begin{aligned} \Omega_{\rm m}\,(\delta+3\omega) &= -\delta\left(\frac{-\Omega_{\rm m} + 1 + 3\omega + \delta}{(1+3\omega)}\right) \\ \Omega_{\rm m}\,(\delta+3\omega)\,(1+3\omega) &= \delta\Omega_{\rm m} - \delta\,(1+3\omega+\delta) \\ \Omega_{\rm m}\left(\delta+3\omega+9\omega^2+3\omega\delta\right) &= \delta\Omega_{\rm m} - \delta\,(1+3\omega+\delta) \\ \Omega_{\rm m}\left(3\omega+9\omega^2+3\omega\delta\right) &= -\delta\,(1+3\omega+\delta) \\ 3\omega\Omega_{\rm m}\,(1+3\omega+\delta) &= -\delta\,(1+3\omega+\delta) \\ \Omega_{\rm m} &= -\frac{\delta}{3\omega}. \end{aligned} \tag{B.17}$$

Substituting (B.17) into (B.16) gives:

$$\begin{aligned} \left(-\frac{\delta}{3\omega}\right)[\delta+3\omega] &= -\delta\Omega_{\rm de} \\ \Omega_{\rm de} &= \frac{1}{3\omega}\,[\delta+3\omega] \\ \Omega_{\rm de} &= 1 + \frac{\delta}{3\omega}. \end{aligned} \tag{B.18}$$

The second equilibrium point is at $(\Omega_{\rm m},\, \Omega_{\rm de})_2 = (-\frac{\delta}{3\omega}\ ,\ 1+\frac{\delta}{3\omega})$. These two points match with the unstable starting point $(1\ ,\ 0)$ and the stable attractor $(-\frac{\delta}{3\omega}\ ,\ 1+\frac{\delta}{3\omega})$ in Figure 3.11, while reducing back to the ΛCDM case when $\delta = 0$ and $\omega = -1$.

APPENDIX C

Solving the conservation equations

In this appendix we will solve the conservation equations for interacting dark energy models (3.3) to obtain analytical expressions for the energy density of dark matter $\rho_{\rm dm}$ and dark energy $\rho_{\rm de}$. This will be done for the interacting dark energy models with the coupling functions $Q_1 = \delta H \rho_{dm}$ and $Q_2 = \delta H \rho_{de}$.

C.1 Interacting dark energy model - $Q_1 = \delta H \rho_{dm}$

The background conservation equations obtained for this model are:

$$\dot{\rho}_{dm} + 3H\rho_{dm} = \delta H \rho_{\rm dm}; \tag{C.1}$$

$$\dot{\rho}_{\rm de} + 3H\rho_{\rm de}(1+\omega) = -\delta H \rho_{\rm dm}. \tag{C.2}$$

To see how the energy density of dark matter and dark energy evolves, we can solve the conservation equations for $\rho_{\rm dm}$ and $\rho_{\rm de}$.

C.1.1 Calculations for dark matter energy density ρ_{dm}

We now solve the conservation equation (C.1) for $\rho_{\rm dm}$:

$$\begin{aligned}
\dot{\rho}_{\rm dm} + 3H\rho_{\rm dm} &= \delta H \rho_{\rm dm} \\
\dot{\rho} &= H\rho_{\rm dm}\left(\delta - 3\right) \\
\frac{\dot{\rho_{\rm dm}}}{\rho_{\rm dm}} &= \frac{\dot{a}}{a}\left(\delta - 3\right) \\
\int \frac{1}{\rho_{\rm dm}} d\rho_{\rm dm} &= \left(\delta - 3\right) \int \frac{1}{a} da \\
\ln\left|\rho_{\rm dm}\right| &= \left(\delta - 3\right)\ln\left|a\right| + C \\
\ln\left|\rho_{\rm dm}\right| &= \ln\left|a^{(\delta-3)}\right| + C \\
\rho_{\rm dm} &= a^{(\delta-3)} e^{C} \\
\rightarrow \rho_{\rm dm} &= \rho_{({\rm dm},0)} a^{(\delta-3)},
\end{aligned} \tag{C.3}$$

where $\rho_{({\rm dm},0)}$ is an integration constant such that $e^C = \rho_{({\rm dm},0)}$. This may also be written in terms of the dark matter effective equation of state $\omega_{\rm dm}^{\rm eff} = -\frac{\delta}{3}$ (3.36), such that:

$$\rho_{\rm dm} = \rho_{({\rm dm},0)} a^{(\delta-3)} = \rho_{({\rm dm},0)} a^{-3\left(1-\frac{\delta}{3}\right)} = \rho_{({\rm dm},0)} a^{-3\left(1-\omega_{\rm dm}^{\rm eff}\right)}. \tag{C.4}$$

which reduces back to the uncoupled case if $\delta = 0$ or $\omega_{\rm dm}^{\rm eff} = \omega_{\rm dm}$.

C.1.2 Calculations for dark energy density $\rho_{\rm de}$

To obtain an analytical expression for the dark energy density, we substitute $\rho_{\rm dm}$ from (C.3) into (C.1):

$$\begin{aligned}
\dot{\rho}_{\rm de} + 3H\rho_{\rm de}(1+\omega) &= -\delta H \rho_{({\rm dm},0)} a^{(\delta-3)} \\
\dot{\rho}_{\rm de} + 3\left(\frac{\dot{a}}{a}\right)\rho_{\rm de}(1+\omega) &= -\delta\left(\frac{\dot{a}}{a}\right)\rho_{({\rm dm},0)} a^{(\delta-3)} \\
\dot{\rho}_{\rm de} + 3\frac{1}{a}\dot{a}\rho_{\rm de}(1+\omega) &= -\delta\rho_{({\rm dm},0)} a^{(\delta-4)}\dot{a} \\
\frac{\dot{\rho}_{\rm de}}{\dot{a}} + \left[3(1+\omega)\frac{1}{a}\right]\rho_{\rm de} &= \left[-\delta\rho_{({\rm dm},0)} a^{(\delta-4)}\right].
\end{aligned} \tag{C.5}$$

We may now notice that equation (C.5) is a first order linear differential equation, and that if we let $\rho_{\rm de} = y$ and $a = x$, we have the general form:

$$\frac{dy}{dx} + p(x)y = f(x), \tag{C.6}$$

where $p(x) = \left[3(1+\omega)\frac{1}{x}\right]$ and $f(x) = \left[-\delta\rho_{(\mathrm{dm},0)}x^{(\delta-4)}\right]$. To solve a first order linear differential equation, we invent two new functions u and v, such that $y = uv$ and therefore $\frac{dy}{dx} = u\frac{dv}{dx} + v\frac{du}{dv}$. Rewriting the differential equation (C.6) in terms of u and v gives:

$$\begin{aligned} u\frac{dv}{dx} + v\frac{du}{dv} + 3(1+\omega)\frac{uv}{x} &= -\delta\rho_{(\mathrm{dm},0)}x^{(\delta-4)} \\ u\frac{dv}{dx} + v\left[\frac{du}{dv} + 3(1+\omega)\frac{u}{x}\right] &= -\delta\rho_{(\mathrm{dm},0)}x^{(\delta-4)}. \end{aligned} \tag{C.7}$$

We now set the term which includes v (the second term in (C.7)) to zero and solve for u:

$$\begin{aligned} \left[\frac{du}{dv} + 3(1+\omega)\frac{u}{x}\right] &= 0 \\ \frac{du}{dx} &= -3(1+\omega)\frac{u}{x} \\ \int\frac{1}{u}du &= -3(1+\omega)\int\frac{1}{x}dx \\ \ln|u| &= \ln|x^{-3(1+\omega)}| + C \\ u &= \rho_{(\mathrm{de},0)}x^{-3(1+\omega)}. \end{aligned} \tag{C.8}$$

We can now substitute u from (C.8) back into equation (C.7) and solve to find v (keeping in mind that the second term was set to zero):

$$\begin{aligned} u\frac{dv}{dx} &= -\delta\rho_{(\mathrm{dm},0)}x^{(\delta-4)} \\ \left(\rho_{(\mathrm{de},0)}x^{-3(1+\omega)}\right)\frac{dv}{dx} &= -\delta\rho_{(\mathrm{dm},0)}x^{(\delta-4)} \\ \frac{dv}{dx} &= -\delta\frac{\rho_{(\mathrm{dm},0)}}{\rho_{(\mathrm{de},0)}}\frac{x^{(\delta-4)}}{x^{-3(1+\omega)}} \\ \int dv &= -\delta\frac{\rho_{(\mathrm{dm},0)}}{\rho_{(\mathrm{de},0)}}\int x^{\delta+3\omega-1}dx \\ v + D &= -\frac{\rho_{(\mathrm{dm},0)}}{\rho_{(\mathrm{de},0)}}\frac{\delta}{\delta+3\omega}\left[x^{\delta+3\omega} + C\right] \\ v &= -\frac{\rho_{(\mathrm{dm},0)}}{\rho_{(\mathrm{de},0)}}\frac{\delta}{\delta+3\omega}\left[x^{\delta+3\omega} + C\right] + D. \end{aligned} \tag{C.9}$$

Now we substitute u (C.8) and v (C.9) into $y = uv$, which gives:

$$\begin{aligned} y &= uv \\ y &= \rho_{(\mathrm{de},0)}x^{-3(1+\omega)}\left[-\frac{\rho_{(\mathrm{dm},0)}}{\rho_{(\mathrm{de},0)}}\frac{\delta}{\delta+3\omega}\left[x^{\delta+3\omega} + C\right] + D\right] \\ y &= x^{-3(1+\omega)}\left[-\rho_{(\mathrm{dm},0)}\frac{\delta}{\delta+3\omega}\left[x^{\delta+3\omega} + C\right] + D\rho_{(\mathrm{de},0)}\right] \\ y &= \left[D\rho_{(\mathrm{de},0)} + \rho_{(\mathrm{dm},0)}\frac{\delta}{\delta+3\omega}\left[C - x^{\delta+3\omega}\right]\right]x^{-3(1+\omega)}. \end{aligned} \tag{C.10}$$

Now we let $y = \rho_{\rm de}$ and $x = a$, this becomes:

$$\rho_{\rm de} = \left[D\rho_{\rm (de,0)} + \rho_{\rm (dm,0)} \frac{\delta}{\delta + 3\omega} \left[C - a^{\delta+3\omega} \right] \right] a^{-3(1+\omega)}. \tag{C.11}$$

Finally, defining new integration constants $\rho_{\rm (de,0)} = D\rho_{\rm (de,0)}$ and $\rho_{\rm (dm,0)} = C\rho_{\rm (dm,0)}$, we have:

$$\rightarrow \rho_{\rm de} = \left(\rho_{\rm (de,0)} + \rho_{\rm (dm,0)} \frac{\delta}{\delta + 3\omega} \left[1 - a^{\delta+3\omega} \right] \right) a^{-3(1+\omega)}, \tag{C.12}$$

which matches with [84, 101, 103].

C.2 Interacting dark energy model - $Q_2 = \delta H \rho_{\rm de}$

The background conservation equations obtained for this model are:

$$\dot{\rho}_{\rm dm} + 3H\rho_{\rm dm} = \delta H \rho_{\rm de}; \tag{C.13}$$

$$\dot{\rho}_{\rm de} + 3H\rho_{\rm de}(1+\omega) = -\delta H . \rho_{\rm de} \tag{C.14}$$

To see how the energy density of dark matter and dark energy evolves, we can solve the conservation equations for $\rho_{\rm dm}$ and $\rho_{\rm de}$.

C.2.1 Calculations for dark energy density $\rho_{\rm de}$

We now solve the conservation equation (C.14) for $\rho_{\rm de}$:

$$\begin{aligned}
\dot{\rho}_{\rm de} + 3H\rho_{\rm de}(1+\omega) &= -\delta H \rho_{\rm de} \\
\dot{\rho}_{\rm de} &= -3H\rho_{\rm de}\left(1 + \omega + \frac{\delta}{3}\right) \\
\frac{\dot{\rho_{\rm de}}}{\rho_{\rm de}} &= -3\frac{\dot{a}}{a}\left(1 + \omega + \frac{\delta}{3}\right) \\
\int \frac{1}{\rho_{\rm de}} d\rho_{\rm de} &= -3\left(1 + \omega + \frac{\delta}{3}\right) \int \frac{1}{a} da \\
\ln|\rho_{\rm de}| &= -3\left(1 + \omega + \frac{\delta}{3}\right) \ln|a| + C \\
\ln|\rho_{\rm de}| &= \ln|a^{-3\left(1+\omega+\frac{\delta}{3}\right)}| + C \\
\rho_{\rm de} &= a^{-3\left(1+\omega+\frac{\delta}{3}\right)} e^{C} \\
\rho_{\rm de} &= \rho_{\rm (de,0)} a^{-3\left(1+\omega+\frac{\delta}{3}\right)} \\
\rightarrow \rho_{\rm de} &= \rho_{\rm (de,0)} a^{-(\delta+3\omega+3)},
\end{aligned} \tag{C.15}$$

where $\rho_{(\mathrm{de},0)}$ is an integration constant such that $e^C = \rho_{(\mathrm{de},0)}$. We may also substitute in the effective equation of state for dark energy $\omega_{\mathrm{de}}^{\mathrm{eff}} = \omega + \frac{\delta}{3}$ (3.78) into (C.15), giving:

$$\rightarrow \rho_{\mathrm{de}} = \rho_{(\mathrm{de},0)} a^{-3\left(1+\omega+\frac{\delta}{3}\right)} = \rho_{(\mathrm{de},0)} a^{-3\left(1+\omega_{\mathrm{de}}^{\mathrm{eff}}\right)}, \tag{C.16}$$

which reduces back to the uncoupled case if $\delta = 0$ or $\omega_{\mathrm{de}}^{\mathrm{eff}} = \omega_{\mathrm{de}}$.

C.2.2 Calculations for dark matter energy density ρ_{dm}

To obtain an analytical expression for the dark matter density, we first substitute ρ_{de} from (C.15) into (C.13), which gives:

$$\begin{aligned}
\dot{\rho}_{\mathrm{dm}} + 3H\rho_{\mathrm{dm}} &= \delta H \rho_{(\mathrm{de},0)} a^{-3\left(1+\omega+\frac{\delta}{3}\right)} \\
\dot{\rho}_{\mathrm{dm}} + 3\left(\frac{\dot{a}}{a}\right)\rho_{\mathrm{dm}} &= \delta\left(\frac{\dot{a}}{a}\right)\rho_{(\mathrm{de},0)} a^{-3\left(1+\omega+\frac{\delta}{3}\right)} \\
\frac{\dot{\rho}_{\mathrm{dm}}}{\dot{a}} + \left[3\frac{1}{a}\right]\rho_{\mathrm{dm}} &= \left[\delta\rho_{(\mathrm{de},0)} a^{-4-3\omega-\delta}\right].
\end{aligned} \tag{C.17}$$

If we let $\rho_{\mathrm{dm}} = y$ and $a = x$, Equation (C.5) is a first order linear differential equation, which has the general form:

$$\frac{dy}{dx} + p(x)y = f(x), \tag{C.18}$$

where $p(x) = \left[3\frac{1}{x}\right]$ and $f(x) = \left[\delta\rho_{(\mathrm{de},0)} x^{-4-3\omega-\delta}\right]$. As in Appendix A, we let $y = uv$ and therefore $\frac{dy}{dx} = u\frac{dv}{dx} + v\frac{du}{dv}$. Rewriting the differential equation (C.18) in terms of u and v gives:

$$\begin{aligned}
u\frac{dv}{dx} + v\frac{du}{dv} + 3\frac{uv}{x} &= \delta\rho_{(\mathrm{de},0)} x^{-4-3\omega-\delta} \\
u\frac{dv}{dx} + v\left[\frac{du}{dv} + 3\frac{u}{x}\right] &= \delta\rho_{(\mathrm{de},0)} x^{-4-3\omega-\delta}.
\end{aligned} \tag{C.19}$$

We now set the term which includes v (the second term in (C.19)) to zero and solve for u, which gives:

$$\begin{aligned}
\left[\frac{du}{dv} + 3\frac{u}{x}\right] &= 0 \\
\frac{du}{dx} &= -3\frac{u}{x} \\
\int \frac{1}{u} du &= -3\int \frac{1}{x} dx \\
\ln|u| &= \ln|x^{-3}| + C \\
u &= \rho_{(\mathrm{dm},0)} x^{-3}.
\end{aligned} \tag{C.20}$$

We can now substitute u from (C.20) back into equation (C.19) and solve to find v (keeping in mind that the second term was set to zero):

$$\begin{aligned}
u\frac{dv}{dx} &= \delta\rho_{(\mathrm{de},0)}x^{-4-3\omega-\delta} \\
\left(\rho_{(\mathrm{dm},0)}x^{-3}\right)\frac{dv}{dx} &= \delta\rho_{(\mathrm{de},0)}x^{-4-3\omega-\delta} \\
\frac{dv}{dx} &= \delta\frac{\rho_{(\mathrm{de},0)}}{\rho_{(\mathrm{dm},0)}}\frac{x^{-4-3\omega-\delta}}{x^{-3}} \\
\int dv &= \delta\frac{\rho_{(\mathrm{de},0)}}{\rho_{(\mathrm{dm},0)}}\int x^{-1-3\omega-\delta}dx \\
v + D &= -\frac{\rho_{(\mathrm{de},0)}}{\rho_{(\mathrm{dm},0)}}\frac{\delta}{\delta+3\omega}\left[x^{-(\delta+3\omega)} + C\right] \\
v &= -\frac{\rho_{(\mathrm{de},0)}}{\rho_{(\mathrm{dm},0)}}\frac{\delta}{\delta+3\omega}\left[x^{-(\delta+3\omega)} + C\right] + D.
\end{aligned} \tag{C.21}$$

Now we substitute u (C.20) and v (C.21) into $y = uv$, which gives:

$$\begin{aligned}
y &= uv \\
y &= \rho_{(\mathrm{dm},0)}x^{-3}\left[-\frac{\rho_{(\mathrm{de},0)}}{\rho_{(\mathrm{dm},0)}}\frac{\delta}{3\left(\omega+\frac{\delta}{3}\right)}\left[x^{-3\left(\omega+\frac{\delta}{3}\right)} + C\right] + D\right] \\
y &= x^{-3}\left(-\rho_{(\mathrm{de},0)}\frac{\delta}{\delta+3\omega}\left[x^{-(\delta+3\omega)} + C\right] + D\rho_{(\mathrm{dm},0)}\right) \\
y &= \left(D\rho_{(\mathrm{dm},0)} + \rho_{(\mathrm{de},0)}\frac{\delta}{\delta+3\omega}\left[C - x^{-(\delta+3\omega)}\right]\right)x^{-3}.
\end{aligned} \tag{C.22}$$

Now we substitute back $y = \rho_{\mathrm{dm}}$ and $x = a$, (C.22) then becomes:

$$\rho_{\mathrm{dm}} = \left(D\rho_{(\mathrm{dm},0)} + \rho_{(\mathrm{de},0)}\frac{\delta}{\delta+3\omega}\left[C - a^{-(\delta+3\omega)}\right]\right)a^{-3}. \tag{C.23}$$

Finally, defining new integration constants $\rho_{(\mathrm{de},0)} = D\rho_{(\mathrm{de},0)}$ and $\rho_{(\mathrm{dm},0)} = C\rho_{(\mathrm{dm},0)}$, we have:

$$\rho_{\mathrm{dm}} = \left(\rho_{(\mathrm{dm},0)} + \rho_{(\mathrm{de},0)}\frac{\delta}{\delta+3\omega}\left[1 - a^{-(\delta+3\omega)}\right]\right)a^{-3}, \tag{C.24}$$

which matches with [84, 103, 106, 108]

APPENDIX D

Important events in cosmic history

In this appendix, explicit equations will be derived for the scale factor a and redshift z at which important events in cosmic history occurred. These events are the radiation-matter equality (which initiates the period of matter-domination), the matter-dark energy equality (starting the dark energy-dominating epoch) and the cosmic jerk; when cosmic acceleration starts. Equalities that do not have analytical solutions will be written in a simplified manner and then be solved numerically. This will be done for each of the models.

D.1 ΛCDM model

In the ΛCDM model, the universe consists of radiation r, matter (which is the sum of baryonic and dark matter, since both evolve as $\rho_{\rm bm} \propto \rho_{\rm dm} \propto a^{-3}$) $m = dm + bm$ and dark energy de.

D.1.1 Calculations for the radiation-matter equality

The radiation-matter equality occurs when:

$$\rho_{\rm m} = \rho_m. \tag{D.1}$$

Substituting in the energy densities of radiation (2.2) and matter (2.5), gives:

$$\begin{aligned} \frac{3H_0^2}{8\pi G}\Omega_{(\mathrm{r},0)}a^{-4} &= \frac{3H_0^2}{8\pi G}\Omega_{(\mathrm{m},0)}a^{-3} \\ a &= \frac{\Omega_{(\mathrm{r},0)}}{\Omega_{(\mathrm{m},0)}}. \end{aligned} \tag{D.2}$$

In redshift z, the radiation-matter equality occurs at:

$$\begin{aligned} \frac{1}{(1+z)} &= \frac{\Omega_{(\mathrm{r},0)}}{\Omega_{(\mathrm{m},0)}} \\ \rightarrow z &= \frac{\Omega_{(\mathrm{m},0)}}{\Omega_{(\mathrm{r},0)}} - 1. \end{aligned} \tag{D.3}$$

If $\Omega_{(\mathrm{m},0)} = \Omega_{(\mathrm{bm},0)}$, then (D.3) and (D.5) gives the radiation-baryonic matter equality for all of the models.

D.1.2 Calculations for the matter-dark energy equality

The matter-dark energy equality occurs when:

$$\rho_{\mathrm{m}} = \rho_{\mathrm{de}}. \tag{D.4}$$

Substituting in the energy densities of matter (2.2) and dark energy (2.8), gives:

$$\begin{aligned} \frac{3H_0^2}{8\pi G}\Omega_{(\mathrm{m},0)}a^{-3} &= \frac{3H_0^2}{8\pi G}\Omega_{(\mathrm{de},0)} \\ a &= \left(\frac{\Omega_{(\mathrm{de},0)}}{\Omega_{(\mathrm{m},0)}}\right)^{-\frac{1}{3}}. \end{aligned} \tag{D.5}$$

In redshift z, the matter-dark energy equality occurs at:

$$\begin{aligned} \frac{1}{(1+z)} &= \left(\frac{\Omega_{(\mathrm{de},0)}}{\Omega_{(\mathrm{m},0)}}\right)^{-\frac{1}{3}} \\ \rightarrow z &= \left(\frac{\Omega_{(\mathrm{de},0)}}{\Omega_{(\mathrm{dm},0)}}\right)^{\frac{1}{3}} - 1. \end{aligned} \tag{D.6}$$

D.1.3 Calculations for the cosmic jerk

The cosmic jerk occurs when the deceleration (2.17) parameter is equal to zero, such that :

$$\begin{aligned} q &= 0 \\ \Omega_{\mathrm{m}} + \frac{1}{2}\Omega_{\mathrm{dm}} - \Omega_{\mathrm{de}} &= 0. \end{aligned} \tag{D.7}$$

If we assume the contribution of radiation is negligible ($\Omega_{\mathrm{m}} \approx 0$), (D.7) may be simplified to become:

$$\begin{aligned} \frac{1}{2}\Omega_{\mathrm{dm}} - \Omega_{\mathrm{de}} &= 0 \\ \Omega_{\mathrm{dm}} &= 2\Omega_{\mathrm{de}}. \end{aligned} \tag{D.8}$$

Substituting in the density parameters of matter (2.5) and dark energy (2.8), gives:

$$\begin{aligned} \left(\frac{H_0^2}{H^2}\Omega_{(\mathrm{m},0)}a^{-3}\right) &= 2\left(\frac{H_0^2}{H^2}\Omega_{(\mathrm{de},0)}\right) \\ \Omega_{(\mathrm{m},0)}a^{-3} &= 2\Omega_{(\mathrm{de},0)} \\ a &= \left(\frac{2\Omega_{(\mathrm{de},0)}}{\Omega_{(\mathrm{m},0)}}\right)^{-\frac{1}{3}}. \end{aligned} \tag{D.9}$$

In redshift z, the cosmic jerk occurs at:

$$\begin{aligned} \frac{1}{1+z} &= \left(\frac{2\Omega_{(\mathrm{de},0)}}{\Omega_{(\mathrm{m},0)}}\right)^{-\frac{1}{3}} \\ \rightarrow z &= \left(\frac{2\Omega_{(\mathrm{de},0)}}{\Omega_{(\mathrm{m},0)}}\right)^{\frac{1}{3}} - 1. \end{aligned} \tag{D.10}$$

D.2 Interacting dark energy model - $Q_1 = \delta H \rho_{\mathrm{dm}}$

In the interacting dark energy model $Q_1 = \delta H \rho_{\mathrm{dm}}$, the universe consists of radiation r, baryonic matter bm, dark matter dm and dark energy de.

D.2.1 Calculations for the radiation-matter equality

The radiation-matter equality occurs when:

$$\rho_{\mathrm{m}} = \rho_{\mathrm{bm}} + \rho_{\mathrm{dm}}. \tag{D.11}$$

Substituting in the energy densities of radiation (2.2), baryonic matter (2.5) and dark matter (3.34), gives:

$$\begin{aligned} \frac{3H_0^2}{8\pi G}\Omega_{(\mathrm{r},0)}a^{-4} &= \frac{3H_0^2}{8\pi G}\left(\Omega_{(\mathrm{bm},0)}a^{-3} + \Omega_{(\mathrm{dm},0)}a^{\delta-3}\right) \\ \Omega_{(\mathrm{r},0)}a^{-4} &= \Omega_{(\mathrm{bm},0)}a^{-3} + \Omega_{(\mathrm{dm},0)}a^{\delta-3} \\ 1 &= \frac{\Omega_{(\mathrm{bm},0)}}{\Omega_{(\mathrm{r},0)}}a + \frac{\Omega_{(\mathrm{dm},0)}}{\Omega_{(\mathrm{r},0)}}a^{\delta+1}. \end{aligned} \tag{D.12}$$

In terms of redshift this becomes:

$$1 = \frac{\Omega_{(\mathrm{bm},0)}}{\Omega_{(\mathrm{r},0)}}(1+z)^{-1} + \frac{\Omega_{(\mathrm{dm},0)}}{\Omega_{(\mathrm{r},0)}}(1+z)^{-\delta-1}. \tag{D.13}$$

Equation (D.12) and (D.13) can not be simplified further and needs to be solved numerically.

An analytical solution may be obtained for models which don't contain baryonic matter ($\Omega_{\mathrm{bm}} = 0$). This may alternatively be interpreted as the radiation-dark matter equality. Equation (D.12) then becomes:

$$\begin{aligned} 1 &= \frac{\Omega_{(\mathrm{dm},0)}}{\Omega_{(\mathrm{r},0)}}a^{\delta+1} \\ a &= \left(\frac{\Omega_{(\mathrm{r},0)}}{\Omega_{(\mathrm{dm},0)}}\right)^{\frac{1}{\delta+1}}. \end{aligned} \tag{D.14}$$

In terms of redshift this becomes:

$$\begin{aligned} \frac{1}{1+z} &= \left(\frac{\Omega_{(\mathrm{r},0)}}{\Omega_{(\mathrm{dm},0)}}\right)^{\frac{1}{\delta+1}} \\ z &= \left(\frac{\Omega_{(\mathrm{dm},0)}}{\Omega_{(\mathrm{r},0)}}\right)^{\frac{1}{\delta+1}}, \end{aligned} \tag{D.15}$$

which reduces back to the ΛCDM case (D.3) when $\delta = 0$ and $\Omega_{(\mathrm{dm},0)} = \Omega_{(\mathrm{m},0)}$.

D.2.2 Calculations for the matter-dark energy equality

The matter-dark energy equality occurs when:

$$\rho_{\mathrm{bm}} + \rho_{\mathrm{dm}} = \rho_{\mathrm{de}}. \tag{D.16}$$

Substituting in the energy densities of baryonic matter (2.5), dark matter (3.34) and dark energy (3.35), gives:

$$\begin{aligned}
\frac{3H_0^2}{8\pi G}\left(\Omega_{(\mathrm{bm},0)}a^{-3} + \Omega_{(\mathrm{dm},0)}a^{\delta-3}\right) &= \frac{3H_0^2}{8\pi G}\left[\Omega_{(\mathrm{de},0)} + \Omega_{(\mathrm{dm},0)}\frac{\delta}{\delta+3\omega}\left(1 - a^{\delta+3\omega}\right)\right]a^{-3(1+\omega)} \\
\Omega_{(\mathrm{bm},0)}a^{-3} + \Omega_{(\mathrm{dm},0)}a^{\delta-3} &= \left[\Omega_{(\mathrm{de},0)} + \Omega_{(\mathrm{dm},0)}\frac{\delta}{\delta+3\omega}\left(1 - a^{\delta+3\omega}\right)\right]a^{-(3+3\omega)} \\
\Omega_{(\mathrm{bm},0)}a^{3\omega} + \Omega_{(\mathrm{dm},0)}a^{\delta+3\omega} &= \Omega_{(\mathrm{de},0)} + \Omega_{(\mathrm{dm},0)}\frac{\delta}{\delta+3\omega}\left(1 - a^{\delta+3\omega}\right) \\
\frac{\Omega_{(\mathrm{bm},0)}}{\Omega_{(\mathrm{dm},0)}}a^{3\omega} + a^{\delta+3\omega} &= \frac{\Omega_{(\mathrm{de},0)}}{\Omega_{(\mathrm{dm},0)}} + \frac{\delta}{\delta+3\omega}\left(1 - a^{\delta+3\omega}\right) \\
\frac{\Omega_{(\mathrm{bm},0)}}{\Omega_{(\mathrm{dm},0)}}a^{3\omega} + a^{\delta+3\omega} &= \frac{\Omega_{(\mathrm{de},0)}}{\Omega_{(\mathrm{dm},0)}} + \frac{\delta}{\delta+3\omega} - \frac{\delta}{\delta+3\omega}a^{\delta+3\omega} \\
\frac{\Omega_{(\mathrm{bm},0)}}{\Omega_{(\mathrm{dm},0)}}a^{3\omega} + a^{\delta+3\omega}\left(1 + \frac{\delta}{\delta+3\omega}\right) &= \frac{\Omega_{(\mathrm{de},0)}}{\Omega_{(\mathrm{dm},0)}} + \frac{\delta}{\delta+3\omega} \\
\left(\frac{\frac{\Omega_{(\mathrm{bm},0)}}{\Omega_{(\mathrm{dm},0)}}}{\left(1 + \frac{\delta}{\delta+3\omega}\right)}\right)a^{3\omega} + a^{\delta+3\omega} &= \left(\frac{\frac{\Omega_{(\mathrm{de},0)}}{\Omega_{(\mathrm{dm},0)}} + \frac{\delta}{\delta+3\omega}}{\left(1 + \frac{\delta}{\delta+3\omega}\right)}\right).
\end{aligned} \tag{D.17}$$

In terms of redshift this becomes:

$$\left(\frac{\frac{\Omega_{(\mathrm{bm},0)}}{\Omega_{(\mathrm{dm},0)}}}{\left(1 + \frac{\delta}{\delta+3\omega}\right)}\right)(1+z)^{-3\omega} + (1+z)^{-(\delta+3\omega)} = \left(\frac{\frac{\Omega_{(\mathrm{de},0)}}{\Omega_{(\mathrm{dm},0)}} + \frac{\delta}{\delta+3\omega}}{\left(1 + \frac{\delta}{\delta+3\omega}\right)}\right). \tag{D.18}$$

Equation (D.12) and (D.13) can not be simplified further and needs to be solved numerically.

An analytical solution may be obtained for models which don't contain baryonic matter ($\Omega_{\mathrm{bm}} = 0$). This may alternatively be interpreted as the dark matter-dark energy equality. Equation (D.17)

then becomes:

$$\begin{aligned} a^{\delta+3\omega} &= \left(\frac{\frac{\Omega_{(\mathrm{de},0)}}{\Omega_{(\mathrm{dm},0)}} + \frac{\delta}{\delta+3\omega}}{\left(1+\frac{\delta}{\delta+3\omega}\right)} \right) \\ a &= \left(\frac{\frac{\Omega_{(\mathrm{de},0)}}{\Omega_{(\mathrm{dm},0)}} + \frac{\delta}{\delta+3\omega}}{\left(1+\frac{\delta}{\delta+3\omega}\right)} \right)^{\left(\frac{1}{\delta+3\omega}\right)} . \end{aligned} \tag{D.19}$$

In terms of redshift this becomes:

$$\begin{aligned} \frac{1}{1+z} &= \left(\frac{\frac{\Omega_{(\mathrm{de},0)}}{\Omega_{(\mathrm{dm},0)}} + \frac{\delta}{\delta+3\omega}}{\left(1+\frac{\delta}{\delta+3\omega}\right)} \right)^{\left(\frac{1}{\delta+3\omega}\right)} \\ z &= \left(\frac{\frac{\Omega_{(\mathrm{de},0)}}{\Omega_{(\mathrm{dm},0)}} + \frac{\delta}{\delta+3\omega}}{\left(1+\frac{\delta}{\delta+3\omega}\right)} \right)^{-\left(\frac{1}{\delta+3\omega}\right)} - 1, \end{aligned} \tag{D.20}$$

which reduces back to the ΛCDM case (D.6) when $\delta = 0$, $\omega = -1$ and $\Omega_{(\mathrm{dm},0)} = \Omega_{(\mathrm{m},0)}$.

D.2.3 Calculations for the cosmic jerk

The cosmic jerk occurs when the deceleration (3.58) parameter is equal to zero, such that:

$$\begin{aligned} q &= 0 \\ \Omega_{\mathrm{m}} + \frac{1}{2}(\Omega_{\mathrm{bm}} + \Omega_{\mathrm{dm}}) + \frac{1}{2}\Omega_{\mathrm{de}}(1+3\omega) &= 0. \end{aligned} \tag{D.21}$$

If we assume the contribution of radiation is negligible ($\Omega_{\mathrm{m}} \approx 0$), (D.21) may be simplified to become:

$$\begin{aligned} \frac{1}{2}(\Omega_{\mathrm{bm}} + \Omega_{\mathrm{dm}}) + \frac{1}{2}\Omega_{\mathrm{de}}(1+3\omega) &= 0 \\ \Omega_{\mathrm{bm}} + \Omega_{\mathrm{dm}} &= -\Omega_{\mathrm{de}}(1+3\omega). \end{aligned} \tag{D.22}$$

Substituting in the density parameters of baryonic matter (2.5), dark matter (3.34) and dark energy (3.35), gives:

$$\begin{aligned}
\frac{H_0^2}{H^2}\left(\Omega_{(\mathrm{bm},0)}a^{-3}+\Omega_{(\mathrm{dm},0)}a^{\delta-3}\right) &= -\frac{H_0^2}{H^2}\left[\Omega_{(\mathrm{de},0)}+\Omega_{(\mathrm{dm},0)}\frac{\delta}{\delta+3\omega}\left(1-a^{\delta+3\omega}\right)\right]a^{-3(1+\omega)}(1+3\omega)\\
\Omega_{(\mathrm{bm},0)}a^{-3}+\Omega_{(\mathrm{dm},0)}a^{\delta-3} &= -\left[\Omega_{(\mathrm{de},0)}+\Omega_{(\mathrm{dm},0)}\frac{\delta}{\delta+3\omega}\left(1-a^{\delta+3\omega}\right)\right]a^{-(3+3\omega)}(1+3\omega)\\
\Omega_{(\mathrm{bm},0)}a^{3\omega}+\Omega_{(\mathrm{dm},0)}a^{\delta+3\omega} &= -\Omega_{(\mathrm{de},0)}(1+3\omega)-\Omega_{(\mathrm{dm},0)}\frac{\delta}{\delta+3\omega}\left(1-a^{\delta+3\omega}\right)(1+3\omega)\\
\frac{1}{(1+3\omega)}a^{\delta+3\omega} &= -\frac{\Omega_{(\mathrm{de},0)}}{\Omega_{(\mathrm{dm},0)}}-\frac{\delta}{\delta+3\omega}\left(1-a^{\delta+3\omega}\right)-\frac{\Omega_{(\mathrm{bm},0)}}{\Omega_{(\mathrm{dm},0)}(1+3\omega)}a^{3\omega}\\
\frac{1}{(1+3\omega)}a^{\delta+3\omega} &= -\frac{\Omega_{(\mathrm{de},0)}}{\Omega_{(\mathrm{dm},0)}}-\frac{\delta}{\delta+3\omega}+\frac{\delta}{\delta+3\omega}a^{\delta+3\omega}-\frac{\Omega_{(\mathrm{bm},0)}}{\Omega_{(\mathrm{dm},0)}(1+3\omega)}a^{3\omega}\\
a^{\delta+3\omega}\left(\frac{1}{(1+3\omega)}-\frac{\delta}{\delta+3\omega}\right) &= -\frac{\Omega_{(\mathrm{de},0)}}{\Omega_{(\mathrm{dm},0)}}-\frac{\delta}{\delta+3\omega}-\frac{\Omega_{(\mathrm{bm},0)}}{\Omega_{(\mathrm{dm},0)}(1+3\omega)}a^{3\omega}\\
a^{\delta+3\omega} &= -\left(\frac{\frac{\Omega_{(\mathrm{de},0)}}{\Omega_{(\mathrm{dm},0)}}+\frac{\delta}{\delta+3\omega}}{\frac{1}{(1+3\omega)}-\frac{\delta}{\delta+3\omega}}\right)-\left(\frac{\Omega_{(\mathrm{bm},0)}}{\Omega_{(\mathrm{dm},0)}\left(1-\frac{\delta(1+3\omega)}{\delta+3\omega}\right)}\right)a^{3\omega}.
\end{aligned} \tag{D.23}$$

In terms of redshift this becomes:

$$(1+z)^{-(\delta+3\omega)} = -\left(\frac{\frac{\Omega_{(\mathrm{de},0)}}{\Omega_{(\mathrm{dm},0)}}+\frac{\delta}{\delta+3\omega}}{\frac{1}{(1+3\omega)}-\frac{\delta}{\delta+3\omega}}\right)-\left(\frac{\Omega_{(\mathrm{bm},0)}}{\Omega_{(\mathrm{dm},0)}\left(1-\frac{\delta(1+3\omega)}{\delta+3\omega}\right)}\right)(1+z)^{-3\omega}. \tag{D.24}$$

Equation (D.23) and (D.24) can not be simplified further and needs to be solved numerically.

An analytical solution may be obtained for models which don't contain baryonic matter ($\Omega_{\mathrm{bm}}=0$). Equation (D.24) then becomes:

$$\begin{aligned}
a^{\delta+3\omega} &= -\left(\frac{\frac{\Omega_{(\mathrm{de},0)}}{\Omega_{(\mathrm{dm},0)}}+\frac{\delta}{\delta+3\omega}}{\frac{1}{(1+3\omega)}-\frac{\delta}{\delta+3\omega}}\right)\\
a &= -\left(\frac{\frac{\Omega_{(\mathrm{de},0)}}{\Omega_{(\mathrm{dm},0)}}+\frac{\delta}{\delta+3\omega}}{\frac{1}{(1+3\omega)}-\frac{\delta}{\delta+3\omega}}\right)^{\left(\frac{1}{\delta+3\omega}\right)}.
\end{aligned} \tag{D.25}$$

In terms of redshift this becomes:

$$\begin{aligned} \frac{1}{1+z} &= -\left(\frac{\frac{\Omega_{(\mathrm{de},0)}}{\Omega_{(\mathrm{dm},0)}}+\frac{\delta}{\delta+3\omega}}{\frac{1}{(1+3\omega)}-\frac{\delta}{\delta+3\omega}}\right)^{\left(\frac{1}{\delta+3\omega}\right)} \\ z &= -\left(\frac{\frac{\Omega_{(\mathrm{de},0)}}{\Omega_{(\mathrm{dm},0)}}+\frac{\delta}{\delta+3\omega}}{\frac{1}{(1+3\omega)}-\frac{\delta}{\delta+3\omega}}\right)^{-\left(\frac{1}{\delta+3\omega}\right)} - 1, \end{aligned} \tag{D.26}$$

which reduces back to the ΛCDM case (D.10) when $\delta = 0$, $\omega = -1$ and $\Omega_{(\mathrm{dm},0)} = \Omega_{(\mathrm{m},0)}$.

D.3 Interacting dark energy model - $Q_2 = \delta H \rho_{\mathrm{de}}$

In the interacting dark energy model $Q_2 = \delta H \rho_{\mathrm{dm}}$, the universe consists of radiation r, baryonic matter bm, dark matter dm and dark energy de.

D.3.1 Calculations for the radiation-matter equality

The radiation-matter equality occurs when:

$$\rho_{\mathrm{m}} = \rho_{\mathrm{bm}} + \rho_{\mathrm{dm}}. \tag{D.27}$$

Substituting in the energy densities of radiation (2.2), baryonic matter (2.5) and dark matter (3.75), gives:

$$\begin{aligned} \frac{3H_0^2}{8\pi G}\Omega_{(\mathrm{r},0)}a^{-4} &= \frac{3H_0^2}{8\pi G}\left(\Omega_{(\mathrm{bm},0)}a^{-3} + \Omega_{(\mathrm{dm},0)}a^{-3} + \Omega_{(\mathrm{de},0)}\frac{\delta}{\delta+3\omega}\left[1-a^{-(\delta+3\omega)}\right]a^{-3}\right) \\ a^{-1} &= \Omega_{(\mathrm{bm},0)} + \Omega_{(\mathrm{dm},0)} + \Omega_{(\mathrm{de},0)}\frac{\delta}{\delta+3\omega}\left[1-a^{-(\delta+3\omega)}\right] \\ a^{-1} &= \left(\frac{\Omega_{(\mathrm{bm},0)} + \Omega_{(\mathrm{dm},0)} + \Omega_{(\mathrm{de},0)}\frac{\delta}{\delta+3\omega}}{\Omega_{(\mathrm{r},0)}}\right) + \left(\frac{\Omega_{(\mathrm{de},0)}\frac{\delta}{\delta+3\omega}}{\Omega_{(\mathrm{r},0)}}\right)a^{-(\delta+3\omega)}. \end{aligned} \tag{D.28}$$

In terms of redshift this becomes:

$$(1+z) = \left(\frac{\Omega_{(\mathrm{bm},0)} + \Omega_{(\mathrm{dm},0)} + \Omega_{(\mathrm{de},0)}\frac{\delta}{\delta+3\omega}}{\Omega_{(\mathrm{r},0)}}\right) + \left(\frac{\Omega_{(\mathrm{de},0)}\frac{\delta}{\delta+3\omega}}{\Omega_{(\mathrm{r},0)}}\right)(1+z)^{(\delta+3\omega)}. \tag{D.29}$$

Equation (D.28) and (D.29) can not be simplified further and needs to be solved numerically. This reduces back to the ΛCDM case (D.3) when $\delta = 0$,$\omega = -1$ and $\Omega_{(\mathrm{bm},0)} + \Omega_{(\mathrm{dm},0)} = \Omega_{(\mathrm{m},0)}$.

D.3.2 Calculations for the matter-dark energy equality

The matter-dark energy equality occurs when:

$$\rho_{\text{bm}} + \rho_{\text{dm}} = \rho_{\text{de}}. \tag{D.30}$$

Substituting in the energy densities of baryonic matter (2.6), dark matter (3.75) and dark energy (3.76), gives:

$$\begin{aligned}
\frac{3H_0^2}{8\pi G}\left(\Omega_{(\text{bm},0)}a^{-3} + \left(\Omega_{(\text{dm},0)} + \Omega_{(\text{de},0)}\frac{\delta}{\delta+3\omega}\left[1-a^{-(\delta+3\omega)}\right]\right)a^{-3}\right) &= \frac{3H_0^2}{8\pi G}\Omega_{(\text{de},0)}a^{-(\delta+3\omega+3)} \\
\left(\Omega_{(\text{bm},0)} + \Omega_{(\text{dm},0)} + \Omega_{(\text{de},0)}\frac{\delta}{\delta+3\omega}\left[1-a^{-(\delta+3\omega)}\right]\right)a^{-3} &= \Omega_{(\text{de},0)}a^{-(\delta+3\omega+3)} \\
\Omega_{(\text{bm},0)} + \Omega_{(\text{dm},0)} + \Omega_{(\text{de},0)}\frac{\delta}{\delta+3\omega}\left[1-a^{-(\delta+3\omega)}\right] &= \Omega_{(\text{de},0)}a^{-(\delta+3\omega)} \\
\Omega_{(\text{de},0)}\left(-a^{-(\delta+3\omega)} + \frac{\delta}{\delta+3\omega}\left[1-a^{-(\delta+3\omega)}\right]\right) &= -\Omega_{(\text{bm},0)} - \Omega_{(\text{dm},0)} \\
\Omega_{(\text{de},0)}\left(-a^{-(\delta+3\omega)}\left(1+\frac{\delta}{\delta+3\omega}\right) + \frac{\delta}{\delta+3\omega}\right) &= -\Omega_{(\text{bm},0)} - \Omega_{(\text{dm},0)} \\
-a^{-(\delta+3\omega)}\left(1+\frac{\delta}{\delta+3\omega}\right) + \frac{\delta}{\delta+3\omega} &= -\frac{\Omega_{(\text{bm},0)} + \Omega_{(\text{dm},0)}}{\Omega_{(\text{de},0)}} \\
a^{-(\delta+3\omega)} &= \left(\frac{\frac{\Omega_{(\text{bm},0)}+\Omega_{(\text{dm},0)}}{\Omega_{(\text{de},0)}} + \frac{\delta}{\delta+3\omega}}{1+\frac{\delta}{\delta+3\omega}}\right) \\
\left(\frac{\frac{\Omega_{(\text{bm},0)}+\Omega_{(\text{dm},0)}}{\Omega_{(\text{de},0)}} + \frac{\delta}{\delta+3\omega}}{1+\frac{\delta}{\delta+3\omega}}\right)^{-\left(\frac{1}{\delta+3\omega}\right)} &= a.
\end{aligned} \tag{D.31}$$

In terms of redshift this becomes:

$$\begin{aligned}
\frac{1}{1+z} &= \left(\frac{\frac{\Omega_{(\text{bm},0)}+\Omega_{(\text{dm},0)}}{\Omega_{(\text{de},0)}} + \frac{\delta}{\delta+3\omega}}{\left(1+\frac{\delta}{\delta+3\omega}\right)}\right)^{-\left(\frac{1}{\delta+3\omega}\right)} \\
\rightarrow z &= \left(\frac{\frac{\Omega_{(\text{bm},0)}+\Omega_{(\text{dm},0)}}{\Omega_{(\text{de},0)}} + \frac{\delta}{\delta+3\omega}}{\left(1+\frac{\delta}{\delta+3\omega}\right)}\right)^{\left(\frac{1}{\delta+3\omega}\right)}, -1
\end{aligned} \tag{D.32}$$

which reduces back to the ΛCDM case (D.6) when $\delta = 0$, $\omega = -1$ and $\Omega_{(\text{bm},0)} + \Omega_{(\text{dm},0)} = \Omega_{(\text{m},0)}$.

D.3.3 Calculations for the cosmic jerk

The cosmic jerk occurs when the deceleration parameter (3.99) is equal to zero, such that :

$$\begin{aligned} q &= 0 \\ \Omega_{\mathrm{m}} + \frac{1}{2}(\Omega_{\mathrm{bm}} + \Omega_{\mathrm{dm}}) + \frac{1}{2}\Omega_{\mathrm{de}}(1+3\omega) &= 0. \end{aligned} \tag{D.33}$$

If we assume the contribution of radiation is negligible ($\Omega_{\mathrm{m}} \approx 0$), (D.33) may be simplified to become:

$$\begin{aligned} \frac{1}{2}(\Omega_{\mathrm{bm}} + \Omega_{\mathrm{dm}}) + \frac{1}{2}\Omega_{\mathrm{de}}(1+3\omega) &= 0 \\ \Omega_{\mathrm{bm}} + \Omega_{\mathrm{dm}} &= -\Omega_{\mathrm{de}}(1+3\omega). \end{aligned} \tag{D.34}$$

Substituting in the density parameters of baryonic matter (2.6), dark matter (3.75) and dark energy (3.76), gives:

$$\begin{aligned} \frac{H_0^2}{H^2}\left(\Omega_{(\mathrm{bm},0)} + \Omega_{(\mathrm{dm},0)} + \Omega_{(\mathrm{de},0)}\frac{\delta}{\delta+3\omega}\left[1 - a^{-(\delta+3\omega)}\right]\right)a^{-3} &= -\frac{H_0^2}{H^2}\Omega_{(\mathrm{de},0)}a^{-(\delta+3\omega+3)}(1+3\omega) \\ \Omega_{(\mathrm{bm},0)} + \Omega_{(\mathrm{dm},0)} + \Omega_{(\mathrm{de},0)}\frac{\delta}{\delta+3\omega}\left[1 - a^{-(\delta+3\omega)}\right] &= -\Omega_{(\mathrm{de},0)}a^{-(\delta+3\omega)}(1+3\omega) \\ \Omega_{(\mathrm{de},0)}\left(a^{-(\delta+3\omega)}(1+3\omega) + \frac{\delta}{\delta+3\omega}\left[1 - a^{-(\delta+3\omega)}\right]\right) &= -\Omega_{(\mathrm{bm},0)} - \Omega_{(\mathrm{dm},0)} \\ \Omega_{(\mathrm{de},0)}\left(a^{-(\delta+3\omega)}\left(1+3\omega - \frac{\delta}{\delta+3\omega}\right) + \frac{\delta}{\delta+3\omega}\right) &= -\Omega_{(\mathrm{bm},0)} - \Omega_{(\mathrm{dm},0)} \\ a^{-(\delta+3\omega)}\left(1+3\omega + \frac{\delta}{\delta+3\omega}\right) + \frac{\delta}{\delta+3\omega} &= -\frac{\Omega_{(\mathrm{bm},0)} + \Omega_{(\mathrm{dm},0)}}{\Omega_{(\mathrm{de},0)}} \\ a^{-(\delta+3\omega)} &= \left(-\frac{\frac{\Omega_{(\mathrm{bm},0)}+\Omega_{(\mathrm{dm},0)}}{\Omega_{(\mathrm{de},0)}} + \frac{\delta}{\delta+3\omega}}{1+3\omega+\frac{\delta}{\delta+3\omega}}\right) \\ \left(-\frac{\frac{\Omega_{(\mathrm{bm},0)}+\Omega_{(\mathrm{dm},0)}}{\Omega_{(\mathrm{de},0)}} + \frac{\delta}{\delta+3\omega}}{1+3\omega+\frac{\delta}{\delta+3\omega}}\right)^{-\left(\frac{1}{\delta+3\omega}\right)} &= a. \end{aligned} \tag{D.35}$$

In terms of redshift this becomes:

$$\begin{aligned} \frac{1}{1+z} &= \left(-\frac{\frac{\Omega_{(\mathrm{bm},0)}+\Omega_{(\mathrm{dm},0)}}{\Omega_{(\mathrm{de},0)}} + \frac{\delta}{\delta+3\omega}}{1+3\omega+\frac{\delta}{\delta+3\omega}}\right)^{-\left(\frac{1}{(\delta+3\omega)}\right)} \\ \rightarrow z &= \left(-\frac{\frac{\Omega_{(\mathrm{bm},0)}+\Omega_{(\mathrm{dm},0)}}{\Omega_{(\mathrm{de},0)}} + \frac{\delta}{\delta+3\omega}}{1+3\omega+\frac{\delta}{\delta+3\omega}}\right)^{\left(\frac{1}{\delta+3\omega}\right)} - 1. \end{aligned} \tag{D.36}$$

This reduces back to the ΛCDM case (D.10) when $\delta = 0$, $\omega = -1$ and $\Omega_{(\mathrm{bm},0)} + \Omega_{(\mathrm{dm},0)} = \Omega_{(\mathrm{m},0)}$.

APPENDIX E

The time of the big rip

E.1 Calculations for the big rip - phantom dark energy

The big rip is also characterised by the scale factor and dark energy density becoming infinite $a \to \infty$; $\rho_{\rm de} \to \infty$ in a finite amount of time $t_{\rm rip}$, which indicates a late time singularity [10, 95]. This may be seen by considering the evolution of the Friedmann equation for a flat uncoupled universe (2.19):

$$\left(\frac{\dot{a}}{a}\right) = H_0\sqrt{\Omega_{(\mathrm{r},0)}a^{-4} + \Omega_{(\mathrm{m},0)}a^{-3} + \Omega_{(\mathrm{de},0)}a^{-3(1+\omega)}}. \tag{E.1}$$

Since the big rip will only happen at late times when the universe is almost completely dominated by dark energy, we may neglect the first two terms, as well writing the current dark energy density parameter as $\Omega_{(\mathrm{de},0)} = 1 - \Omega_{(\mathrm{m},0)} - \Omega_{(r,0)} \approx 1 - \Omega_{(\mathrm{m},0)}$. The Friedmann equation (E.1) can now be integrated from the present time t_0 at $a_0 = 1$ to the the time of the big rip $t_{\rm rip}$ at $a = \infty$:

$$\begin{aligned}
\left(\frac{\dot{a}}{a}\right) &= H_0\sqrt{\left(1 - \Omega_{(\mathrm{m},0)}\right)a^{-3(1+\omega)}} \\
\frac{da}{dt} &= H_0\sqrt{1 - \Omega_{(\mathrm{m},0)}}a^{-\frac{1+3\omega}{2}} \\
\int_{t_0}^{t_{\rm rip}} dt &= \frac{1}{H_0\sqrt{1 - \Omega_{(\mathrm{m},0)}}}\int_1^\infty a^{\frac{1+3\omega}{2}}da \\
t_{\rm rip} - t_0 &= \frac{1}{H_0\sqrt{1 - \Omega_{(\mathrm{m},0)}}}\frac{2}{3(1+\omega)}a^{\frac{3(1+\omega)}{2}}\Big|_1^\infty,
\end{aligned} \tag{E.2}$$

For phantom energy $\omega < -1$ we have $3/2(1+\omega) < 0$, which will cause the integral $a^{\frac{3(1+\omega)}{2}} \approx 0$ at $a = \infty$. Thus (E.2) becomes:

$$t_{\text{rip}} - t_0 \approx \frac{2}{3H_0(1+\omega)\sqrt{1-\Omega_{(\text{m},0)}}}\left(0 - 1^{\frac{3(1+\omega)}{2}}\right) \approx -\frac{2}{3H_0(1+\omega)\sqrt{1-\Omega_{(\text{m},0)}}} \tag{E.3}$$

This coincides with the predicted time of the big rip that was found by [95].

E.2 Calculations for the big rip - $Q_1 = \delta H \rho_{\text{dm}}$

In this coupled model, the dark energy density (3.39) is proportional to:

$$\begin{aligned}\rho_{\text{de}} &\propto \left[\Omega_{(\text{de},0)} + \Omega_{(\text{dm},0)}\frac{\delta}{\delta+3\omega}\left[1 - a^{\delta+3\omega}\right]\right] a^{-3(1+\omega)} \\ &\propto \left(\Omega_{(\text{de},0)} + \Omega_{(\text{dm},0)}\frac{\delta}{\delta+3\omega}\right) a^{-3(1+\omega)} - \Omega_{(\text{dm},0)}\frac{\delta}{\delta+3\omega}a^{\delta-3}.\end{aligned} \tag{E.4}$$

In the distant future as a becomes increasingly large, the last term will become negligible (if $\delta < 3$), and so we can approximate the dark energy density to become:

$$\rho_{\text{de}} \propto \left(\Omega_{(\text{de},0)} + \Omega_{(\text{dm},0)}\frac{\delta}{\delta+3\omega}\right) a^{-3(1+\omega)}. \tag{E.5}$$

Using this approximation, the Friedmann equation for this IDE model (2.13), with the energy densities ρ_{r} (2.3), ρ_{bm} (2.6), ρ_{dm} (3.38) and ρ_{de} (3.39) and $k = 0$ becomes:

$$\left(\frac{\dot{a}}{a}\right) \approx H_0\sqrt{\Omega_{(r,0)}a^{-4} + \Omega_{(\text{bm},0)}a^{-3} + \Omega_{(\text{dm},0)}a^{(\delta-3)} + \left(\Omega_{(\text{de},0)} + \Omega_{(\text{dm},0)}\frac{\delta}{\delta+3\omega}\right)a^{-3(1+\omega)}}. \tag{E.6}$$

Since the big rip will only happen at late times when the universe is almost completely dominated by dark energy, we may neglect the first three terms, as well as writing the current dark energy density parameter as $\Omega_{(\text{de},0)} = 1 - \Omega_{(\text{dm},0)} - \Omega_{(\text{bm},0)} - \Omega_{(r,0)} \approx 1 - \Omega_{(\text{dm},0)} - \Omega_{(\text{bm},0)}$. The Friedmann equation (E.6) then becomes:

$$\begin{aligned}\left(\frac{\dot{a}}{a}\right) &= H_0\sqrt{\left(1 - \Omega_{(\text{dm},0)} - \Omega_{(\text{bm},0)} + \Omega_{(\text{dm},0)}\frac{\delta}{\delta+3\omega}\right)a^{-3(1+\omega)}} \\ &= H_0\sqrt{1 - \Omega_{(\text{bm},0)} - \left(1 - \frac{\delta}{\delta+3\omega}\right)\Omega_{(\text{dm},0)}a^{-\frac{3}{2}(1+\omega)}}.\end{aligned} \tag{E.7}$$

This can now be integrated from the present time t_0 at $a_0 = 1$ to the the time of the big rip t_{rip} at $a = \infty$:

$$\begin{aligned}
\frac{da}{dt} &= H_0\sqrt{1-\Omega_{(\text{bm},0)} - \left(1-\frac{\delta}{\delta+3\omega}\right)\Omega_{(\text{dm},0)}}a^{-\frac{1+3\omega}{2}} \\
\int_{t_0}^{t_{\text{rip}}} dt &= \frac{1}{H_0\sqrt{1-\Omega_{(\text{bm},0)} - \left(1-\frac{\delta}{\delta+3\omega}\right)\Omega_{(\text{dm},0)}}}\int_1^\infty a^{\frac{1+3\omega}{2}}da \\
t_{\text{rip}} - t_0 &= \frac{1}{H_0\sqrt{1-\Omega_{(\text{bm},0)} - \left(1-\frac{\delta}{\delta+3\omega}\right)\Omega_{(\text{dm},0)}}}\frac{2}{3(1+\omega)}a^{\frac{3(1+\omega)}{2}}\Big|_1^\infty.
\end{aligned} \tag{E.8}$$

For phantom energy $\omega < -1$ we have $3/2(1+\omega) < 0$, which will cause the integral $a^{\frac{3(1+\omega)}{2}} \approx 0$ at $a = \infty$. Thus (E.8) becomes:

$$\begin{aligned}
t_{\text{rip}} - t_0 &\approx \frac{2}{3H_0(1+\omega)\sqrt{1-\Omega_{(\text{bm},0)} - \left(1-\frac{\delta}{\delta+3\omega}\right)\Omega_{(\text{dm},0)}}}\left(0 - 1^{\frac{3(1+\omega)}{2}}\right) \\
\rightarrow t_{\text{rip}} - t_0 &\approx -\frac{2}{3H_0(1+\omega)\sqrt{1-\Omega_{(\text{bm},0)} - \left(1-\frac{\delta}{\delta+3\omega}\right)\Omega_{(\text{dm},0)}}},
\end{aligned} \tag{E.9}$$

which is the predicted time of the big rip for IDE model $Q_1 = \delta H \rho_{\text{dm}}$. This reduces back to the uncoupled case (2.50) if $\delta = 0$.

E.3 Calculations for the big rip - $Q_2 = \delta H \rho_{\text{de}}$

For this model, it is important to note that in the distant future dark energy never completely dominates the other fluids (as usually indicated by $\Omega_{\text{de}} \rightarrow 1$ in the distant future). This is due to this model solving the coincidence problem for future expansion, thereby fixing the ratio of dark matter to dark energy. Radiation and baryons may become negligible in the distant future, but some terms from the dark matter energy density should still be included. The Friedmann equation (3.103) for this coupled model with only dark matter (3.80) and dark energy (3.80) is:

$$\begin{aligned}
\left(\frac{\dot{a}}{a}\right) &\approx H_0\sqrt{\left(\Omega_{(\text{dm},0)} + \Omega_{(\text{de},0)}\frac{\delta}{\delta+3\omega}\left[1-a^{-(\delta+3\omega)}\right]\right)a^{-3} + \Omega_{(\text{de},0)}a^{-3(1+\omega+\frac{\delta}{3})}} \\
&= H_0\sqrt{\left(\Omega_{(\text{dm},0)} + \Omega_{(\text{de},0)}\frac{\delta}{\delta+3\omega}\right)a^{-3} + \left(1-\frac{\delta}{\delta+3\omega}\right)\Omega_{(\text{de},0)}a^{-3(1+\omega+\frac{\delta}{3})}}.
\end{aligned} \tag{E.10}$$

In the future, as the scale factor a grows large, the contribution from the first two terms in (E.10) becomes small relative to the other terms and may be neglected. Doing this, the Friedmann equation (E.10) becomes:

$$\left(\frac{\dot{a}}{a}\right) \approx H_0\sqrt{\left(1-\frac{\delta}{\delta+3\omega}\right)\Omega_{(\mathrm{de},0)}a^{-3(1+\omega+\frac{\delta}{3})}}. \tag{E.11}$$

The current dark energy density parameter may also be written as $\Omega_{(\mathrm{de},0)} = 1-\Omega_{(\mathrm{dm},0)}-\Omega_{(\mathrm{bm},0)}-\Omega_{(r,0)} \approx 1-\Omega_{(\mathrm{dm+bm},0)}$. The Friedmann equation (E.11) then becomes:

$$\left(\frac{\dot{a}}{a}\right) \approx H_0\sqrt{\left(1-\frac{\delta}{\delta+3\omega}\right)\left(1-\Omega_{(\mathrm{dm+bm},0)}\right)a^{-\frac{3}{2}(1+\omega+\frac{\delta}{3})}}. \tag{E.12}$$

This can now be integrated from the present time t_0 at $a_0 = 1$ to the the time of the big rip t_{rip} at $a = \infty$:

$$\begin{aligned}
\frac{da}{dt} &= H_0\sqrt{\left(1-\frac{\delta}{\delta+3\omega}\right)\left(1-\Omega_{(\mathrm{dm+bm},0)}\right)}a^{-\frac{1}{2}(1+3\omega+\delta)} \\
\int_{t_0}^{t_{\mathrm{rip}}} dt &= \frac{1}{H_0}\frac{1}{\sqrt{\left(1-\frac{\delta}{\delta+3\omega}\right)\left(1-\Omega_{(\mathrm{dm+bm},0)}\right)}}\int_1^{\infty} a^{-\frac{1}{2}(1+3\omega+\delta)}da \\
t_{\mathrm{rip}}-t_0 &= \frac{1}{H_0}\frac{1}{\sqrt{\left(1-\frac{\delta}{\delta+3\omega}\right)\left(1-\Omega_{(\mathrm{dm+bm},0)}\right)}}\frac{2}{3(1+\omega+\frac{\delta}{3})}a^{\frac{3(1+\omega+\delta/3)}{2}}\Big|_1^{\infty}.
\end{aligned} \tag{E.13}$$

For the integral on the right hand side to become zero, we need $3/2(1+\omega+\delta/3) < 0$. Phantom dark energy does not necessarily imply this. For this to hold we can need the effective equation of state for dark energy to be smaller than -1. If $\omega_{\mathrm{de}}^{\mathrm{eff}} = \omega+\delta/3 < -1$ then it follows that $3/2(1+\omega+\delta/3) < 0$ which will cause the integral $a^{\frac{3(1+\omega+\delta/3)}{2}} \approx 0$ at $a = \infty$. Thus (E.8) becomes:

$$\begin{aligned}
t_{\mathrm{rip}}-t_0 &= \frac{2}{3H_0(1+\omega+\frac{\delta}{3})\sqrt{\left(1-\frac{\delta}{\delta+3\omega}\right)\left(1-\Omega_{(\mathrm{dm+bm},0)}\right)}}\left(0-1^{\frac{3(1+\omega+\delta/3)}{2}}\right) \\
\rightarrow t_{\mathrm{rip}}-t_0 &= -\frac{2}{3H_0(1+\omega+\frac{\delta}{3})\sqrt{\left(1-\frac{\delta}{\delta+3\omega}\right)\left(1-\Omega_{(\mathrm{dm+bm},0)}\right)}},
\end{aligned} \tag{E.14}$$

which is the predicted time of the big rip for IDE model $Q_2 = \delta H\rho_{\mathrm{de}}$. This reduces back to the uncoupled case (2.50) if $\delta = 0$.

Bibliography

[1] Nobel Committee. Scientifc Background on the Nobel Prize in Physics 2019. pages 2,9,10, Oct 2019. URL https://www.nobelprize.org/uploads/2019/10/advanced-physicsprize2019-3.pdf.

[2] Katherine Garrett and Gintaras Duda. Dark matter: A primer. *Advances in Astronomy*, 2011:122, 2011. ISSN 1687-7977. doi: 10.1155/2011/968283. URL http://dx.doi.org/10.1155/2011/968283.

[3] Richard Massey, Thomas Kitching, and Johan Richard. The dark matter of gravitational lensing. *Reports on Progress in Physics*, 73(8):086901, Jul 2010. ISSN 1361-6633. doi: 10.1088/0034-4885/73/8/086901. URL http://dx.doi.org/10.1088/0034-4885/73/8/086901.

[4] N. Aghanim, Y. Akrami, M. Ashdown, J. Aumont, C. Baccigalupi, M. Ballardini, A. J. Banday, R. B. Barreiro, N. Bartolo, and et al. Planck 2018 results. *Astronomy and Astrophysics*, 641:A6, Sep 2020. ISSN 1432-0746. doi: 10.1051/0004-6361/201833910. URL http://dx.doi.org/10.1051/0004-6361/201833910.

[5] Helge Kragh. Cosmology and the Origin of the Universe: Historical and Conceptual Perspectives. *arXiv e-prints*, art. arXiv:1706.00726, June 2017. URL https://ui.adsabs.harvard.edu/abs/2017arXiv170600726K.

[6] Per Bak and Stefan Boettcher. Self-organized criticality and punctuated equilibria. *Physica D: Nonlinear Phenomena*, 107(2-4):143150, Sep 1997. ISSN 0167-2789. doi: 10.1016/s0167-2789(97)00078-x. URL http://dx.doi.org/10.1016/S0167-2789(97)00078-X.

[7] Albert Einstein. Zur allgemeinen Relativitätstheorie. (German) [Toward a General Theory of Relativity]. 1915. URL https://articles.adsabs.harvard.edu/cgi-bin/get_file?pdfs/SPAW./1917/1917SPAW.....142E.pdf.

[8] James B. Hartle. *Gravity: An Introduction to Einstein's General Relativity*. Benjamin Cummings, illustrate edition, January 2003. ISBN 0805386629.

[9] M. P. Hobson, G. P. Efstathiou, and A. N. Lasenby. *General Relativity*. 2005.

[10] B. Ryden. *Introduction to Cosmology*. Cambridge University Press, 2016. ISBN 9781316889404. URL https://books.google.co.za/books?id=k8WSDQAAQBAJ.

[11] Matts Roos. *Introduction to cosmology, 3rd ed.* Wiley, 2003.

[12] Helge Kragh. Historical aspects of post-1850 cosmology. 2014. doi: 10.1063/1.4902842. URL http://dx.doi.org/10.1063/1.4902842.

[13] Albert Einstein. Kosmologische Betrachtungen zur allgemeinen Relativitätstheorie. *Sitzungsberichte der Königlich Preußischen Akademie der Wissenschaften (Berlin*, pages 142–152, January 1917. URL https://articles.adsabs.harvard.edu/cgi-bin/get_file?pdfs/SPAW./1917/1917SPAW.....142E.pdf.

[14] George F.R Ellis. A historical review of how the cosmological constant has fared in general relativity and cosmology. *Chaos, Solitons and Fractals*, 16(4):505–512, 2003. ISSN 0960-0779. doi: https://doi.org/10.1016/S0960-0779(02)00219-9. URL https://www.sciencedirect.com/science/article/pii/S0960077902002199.

[15] Edwin Hubble. A relation between distance and radial velocity among extra-galactic nebulae. *Proceedings of the National Academy of Sciences*, 1929. ISSN 0027-8424. doi: 10.1073/pnas.15.3.168. URL https://www.pnas.org/content/15/3/168.

[16] R. A. Alpher, H. Bethe, and G. Gamow. The Origin of Chemical Elements. *Physical Review*, 73(7):803–804, April 1948. doi: 10.1103/PhysRev.73.803. URL https://journals.aps.org/pr/abstrac.

[17] Martin Bucher. Physics of the cosmic microwave background anisotropy. *International Journal of Modern Physics D*, 24(02):1530004, Feb 2015. ISSN 1793-6594. doi: 10.1142/s0218271815300049. URL http://dx.doi.org/10.1142/S0218271815300049.

[18] A. A. Penzias and R. W. Wilson. A Measurement of Excess Antenna Temperature at 4080 Mc/s. *Astrophysical Journal*, 142:419–421, July 1965. doi: 10.1086/148307. URL https://articles.adsabs.harvard.edu/pdf/1965ApJ...142..419P.

[19] Adam G. Riess, Alexei V. Filippenko, Peter Challis, Alejandro Clocchiatti, Alan Diercks, Peter M. Garnavich, Ron L. Gilliland, Craig J. Hogan, Saurabh Jha, Robert P. Kirshner, and et al. Observational evidence from supernovae for an accelerating universe and a cosmological constant. *The Astronomical Journal*, 116(3):10091038, Sep 1998. ISSN 0004-6256. doi: 10.1086/300499. URL http://dx.doi.org/10.1086/300499.

[20] Peter M. Garnavich, Saurabh Jha, Peter Challis, Alejandro Clocchiatti, Alan Diercks, Alexei V. Filippenko, Ron L. Gilliland, Craig J. Hogan, Robert P. Kirshner, Bruno Leibundgut, and et al. Supernova limits on the cosmic equation of state. *The Astrophysical Journal*, 509(1):7479, Dec 1998. ISSN 1538-4357. doi: 10.1086/306495. URL http://dx.doi.org/10.1086/306495.

[21] S. Perlmutter, G. Aldering, M. Della Valle, S. Deustua, R. S. Ellis, S. Fabbro, A. Fruchter, G. Goldhaber, D. E. Groom, I. M. Hook, and et al. Discovery of a supernova explosion at half the age of the universe. *Nature*, 391(6662):5154, Jan 1998. ISSN 1476-4687. doi: 10.1038/34124. URL http://dx.doi.org/10.1038/34124.

[22] S. Perlmutter, G. Aldering, G. Goldhaber, R. A. Knop, P. Nugent, P. G. Castro, S. Deustua, S. Fabbro, A. Goobar, D. E. Groom, and et al. Measurements of ω and λ from 42 highredshift supernovae. *The Astrophysical Journal*, 517(2):565586, Jun 1999. ISSN 1538-4357. doi: 10.1086/307221. URL http://dx.doi.org/10.1086/307221.

[23] F. Zwicky. On the Masses of Nebulae and of Clusters of Nebulae. *Astrophysical Journal*, 86: 217, October 1937. doi: 10.1086/143864. URL https://articles.adsabs.harvard.edu/pdf/1937ApJ....86..217Z.

[24] V. C. Rubin. Dark matter in spiral galaxies. *Scientific American*, 248:96–106, June 1983. doi: 10.1038/scientificamerican0683-96. URL https://www.scientificamerican.com/article/dark-matter-in-spiral-galaxies/.

[25] John Wheeler and Kenneth Ford. Geons, black holes and quantum foam: A life in physics. *American Journal of Physics*, 68, 06 2000. doi: 10.1119/1.19497.

[26] A. Friedmann. Über die Krümmung des Raumes. *Zeitschrift fur Physik*, 10:377–386, Jan 1922. doi: 10.1007/BF01332580. URL https://link.springer.com/article/10.1007%2FBF01332580.

[27] Ofer Lahav. Observational Tests for the Cosmological Principle and World Models. In Robert G. Crittenden and Neil G. Turok, editors, *Structure Formation in the Universe*, volume 565 of *NATO Advanced Study Institute (ASI) Series C*, page 131, January 2001. URL https://arxiv.org/abs/astro-ph/0001061.

[28] Nathan J. Secrest, Sebastian von Hausegger, Mohamed Rameez, Roya Mohayaee, Subir Sarkar, and Jacques Colin. A test of the cosmological principle with quasars. *The Astrophysical Journal*, 908(2):L51, Feb 2021. ISSN 2041-8213. doi: 10.3847/2041-8213/abdd40. URL http://dx.doi.org/10.3847/2041-8213/abdd40.

[29] Matthew Kleban and Leonardo Senatore. Inhomogeneous anisotropic cosmology. *Journal of Cosmology and Astroparticle Physics*, 2016(10):022022, Oct 2016. ISSN 1475-7516. doi:

10.1088/1475-7516/2016/10/022. URL http://dx.doi.org/10.1088/1475-7516/2016/10/022.

[30] Krzysztof Bolejko and Mikoaj Korzyski. Inhomogeneous cosmology and backreaction: Current status and future prospects. *International Journal of Modern Physics D*, 26(06):1730011, Feb 2017. ISSN 1793-6594. doi: 10.1142/s0218271817300117. URL http://dx.doi.org/10.1142/S0218271817300117.

[31] Juan Garcia-Bellido and Troels Haugbølle. Confronting Lemaitre Tolman Bondi models with observational cosmology. *jcap*, 2008(4):003, April 2008. doi: 10.1088/1475-7516/2008/04/003. URL https://arxiv.org/abs/0802.1523.

[32] Kari Enqvist. Lemaitretolmanbondi model and accelerating expansion. *General Relativity and Gravitation*, 40(2-3):451466, Dec 2007. ISSN 1572-9532. doi: 10.1007/s10714-007-0553-9. URL http://dx.doi.org/10.1007/s10714-007-0553-9.

[33] Abhay Ashtekar and Edward Wilson-Ewing. Loop quantum cosmology of bianchi type i models. *Physical Review D*, 79(8), Apr 2009. ISSN 1550-2368. doi: 10.1103/physrevd.79.083535. URL http://dx.doi.org/10.1103/PhysRevD.79.083535.

[34] Hossein Ghaffarnejad and Hoda Gholipour. Bianchi I cosmology and scalar vector tensor Brans Dicke gravity. *arXiv e-prints*, art. arXiv:1706.02904, June 2017. URL https://arxiv.org/abs/1706.02904.

[35] Daniel V Schroeder. *An introduction to thermal physics*. San Francisco, CA : Addison Wesley, [2000] 2000, 2000.

[36] Stephen W. Hawking and G. F. R. Ellis. *The Large Scale Structure of Space-Time (Cambridge Monographs on Mathematical Physics)*. Cambridge University Press, 1975. ISBN 0521099064. URL http://www.amazon.com/Structure-Space-Time-Cambridge-Monographs-Mathematical/dp/0521099064.

[37] J. Santos, J. S. Alcaniz, N. Pires, and M. J. Rebouas. Energy conditions and cosmic acceleration. *Physical Review D*, 75(8), Apr 2007. ISSN 1550-2368. doi: 10.1103/physrevd.75.083523. URL http://dx.doi.org/10.1103/PhysRevD.75.083523.

[38] Matt Visser and Carlos Barceló. Energy Conditions and Their Cosmological Implications. In U. Cotti, R. Jeannerot, G. Senjanovi, and A. Smirnov, editors, *COSMO-99, International Workshop on Particle Physics and the Early Universe*, page 98, January 2000. doi: 10.1142/9789812792129_0014. URL https://arxiv.org/abs/gr-qc/0001099.

[39] Prado Martín-Moruno and Matt Visser. Classical and Semi-classical Energy Conditions. *Fundamental Theories of Physics*, 189:193, January 2017. doi: 10.1007/978-3-319-55182-1_9. URL https://arxiv.org/abs/1702.05915.

[40] Sante Carloni, Peter K S Dunsby, and Deon Solomons. Bounce conditions in (r) cosmologies. *Classical and Quantum Gravity*, 23(6):19131922, Feb 2006. ISSN 1361-6382. doi: 10.1088/0264-9381/23/6/006. URL http://dx.doi.org/10.1088/0264-9381/23/6/006.

[41] Sean M. Carroll, Mark Hoffman, and Mark Trodden. Can the dark energy equation-of-state parameter w be less than -1? *Physical Review D*, 68(2):023509, jul 2003. doi: 10.1103/PhysRevD.68.023509. URL https://arxiv.org/abs/astro-ph/0301273.

[42] V A Rubakov. The null energy condition and its violation. *Physics-Uspekhi*, 57(2):128142, Feb 2014. ISSN 1468-4780. doi: 10.3367/ufne.0184.201402b.0137. URL http://dx.doi.org/10.3367/UFNe.0184.201402b.0137.

[43] Diana Battefeld and Patrick Peter. A critical review of classical bouncing cosmologies. *Physics Reports*, 571:166, Apr 2015. ISSN 0370-1573. doi: 10.1016/j.physrep.2014.12.004. URL http://dx.doi.org/10.1016/j.physrep.2014.12.004.

[44] Anna Ijjas and Paul J Steinhardt. Bouncing cosmology made simple. *Classical and Quantum Gravity*, 35(13):135004, Jun 2018. ISSN 1361-6382. doi: 10.1088/1361-6382/aac482. URL http://dx.doi.org/10.1088/1361-6382/aac482.

[45] Gianfranco Bertone and Dan Hooper. History of dark matter. *Reviews of Modern Physics*, 90(4), Oct 2018. ISSN 1539-0756. doi: 10.1103/revmodphys.90.045002. URL http://dx.doi.org/10.1103/RevModPhys.90.045002.

[46] A. Arbey and F. Mahmoudi. Dark matter and the early universe: A review. *Progress in Particle and Nuclear Physics*, page 103865, Apr 2021. ISSN 0146-6410. doi: 10.1016/j.ppnp.2021.103865. URL http://dx.doi.org/10.1016/j.ppnp.2021.103865.

[47] V. A. Rubakov. Cosmology and dark matter, 2019. URL https://arxiv.org/abs/1912.04727.

[48] K. G. Begeman. HI rotation curves of spiral galaxies. I. NGC 3198. *A&A*, 223:47–60, October 1989. URL https://articles.adsabs.harvard.edu/pdf/1989A%26A...223...47B.

[49] Debaprasad Maity and Pankaj Saha. Connecting cmb anisotropy and cold dark matter phenomenology via reheating. *Physical Review D*, 98(10), Nov 2018. ISSN 2470-0029. doi: 10.1103/physrevd.98.103525. URL http://dx.doi.org/10.1103/PhysRevD.98.103525.

[50] Douglas Clowe, Marua Brada, Anthony H. Gonzalez, Maxim Markevitch, Scott W. Randall, Christine Jones, and Dennis Zaritsky. A direct empirical proof of the existence of dark matter. *The Astrophysical Journal*, 648(2):L109L113, Aug 2006. ISSN 1538-4357. doi: 10.1086/508162. URL http://dx.doi.org/10.1086/508162.

[51] Annika H. G. Peter. Dark matter: A brief review, 2012. URL https://arxiv.org/abs/1201.3942.

[52] Leszek Roszkowski, Enrico Maria Sessolo, and Sebastian Trojanowski. Wimp dark matter candidates and searchescurrent status and future prospects. *Reports on Progress in Physics*, 81(6):066201, May 2018. ISSN 1361-6633. doi: 10.1088/1361-6633/aab913. URL http://dx.doi.org/10.1088/1361-6633/aab913.

[53] Marc Schumann. Direct detection of wimp dark matter: concepts and status. *Journal of Physics G: Nuclear and Particle Physics*, 46(10):103003, Aug 2019. ISSN 1361-6471. doi: 10.1088/1361-6471/ab2ea5. URL http://dx.doi.org/10.1088/1361-6471/ab2ea5.

[54] Stefano Profumo, Leonardo Giani, and Oliver F. Piattella. An introduction to particle dark matter, 2019. URL https://arxiv.org/abs/1910.05610.

[55] Francesca Chadha-Day, John Ellis, and David J. E. Marsh. Axion dark matter: What is it and why now?, 2021. URL https://arxiv.org/abs/2105.01406.

[56] Masahiro Kawasaki and Kazunori Nakayama. Axions: Theory and cosmological role. *Annual Review of Nuclear and Particle Science*, 63(1):6995, Oct 2013. ISSN 1545-4134. doi: 10.1146/annurev-nucl-102212-170536. URL http://dx.doi.org/10.1146/annurev-nucl-102212-170536.

[57] A. Boyarsky, M. Drewes, T. Lasserre, S. Mertens, and O. Ruchayskiy. Sterile neutrino dark matter. *Progress in Particle and Nuclear Physics*, 104:145, Jan 2019. ISSN 0146-6410. doi: 10.1016/j.ppnp.2018.07.004. URL http://dx.doi.org/10.1016/j.ppnp.2018.07.004.

[58] Pablo Villanueva-Domingo, Olga Mena, and Sergio Palomares-Ruiz. A brief review on primordial black holes as dark matter. *Frontiers in Astronomy and Space Sciences*, 8, May 2021. ISSN 2296-987X. doi: 10.3389/fspas.2021.681084. URL http://dx.doi.org/10.3389/fspas.2021.681084.

[59] Mordehai Milgrom. Mond theory. *Canadian Journal of Physics*, 93(2):107118, Feb 2015. ISSN 1208-6045. doi: 10.1139/cjp-2014-0211. URL http://dx.doi.org/10.1139/cjp-2014-0211.

[60] Mordehai Milgrom. Mond vs. dark matter in light of historical parallels. *Studies in History and Philosophy of Science Part B: Studies in History and Philosophy of Modern Physics*, 71: 170195, Aug 2020. ISSN 1355-2198. doi: 10.1016/j.shpsb.2020.02.004. URL http://dx.doi.org/10.1016/j.shpsb.2020.02.004.

[61] Joel R. Primack and Michael A. K. Gross. *Hot dark matter in cosmology*, pages 287–308. 2001. URL https://arxiv.org/abs/astro-ph/0007165.

[62] V. Motta, Miguel A. Garca-Aspeitia, A. Hernndez-Almada, J. Magaa, and Toms Verdugo. Taxonomy of dark energy models, 2021. URL https://arxiv.org/abs/2104.04642.

[63] Michael J. Mortonson, David H. Weinberg, and Martin White. Dark energy: A short review, 2013. URL https://arxiv.org/abs/1401.0046.

[64] Dragan Huterer and Daniel L Shafer. Dark energy two decades after: observables, probes, consistency tests. *Reports on Progress in Physics*, 81(1):016901, Dec 2017. ISSN 1361-6633. doi: 10.1088/1361-6633/aa997e. URL http://dx.doi.org/10.1088/1361-6633/aa997e.

[65] Eugene Oks. Brief review of recent advances in understanding dark matter and dark energy. *New Astronomy Reviews*, 93:101632, Dec 2021. ISSN 1387-6473. doi: 10.1016/j.newar.2021.101632. URL http://dx.doi.org/10.1016/j.newar.2021.101632.

[66] Noemi Frusciante and Louis Perenon. Effective field theory of dark energy: A review. *Physics Reports*, 857:163, May 2020. ISSN 0370-1573. doi: 10.1016/j.physrep.2020.02.004. URL http://dx.doi.org/10.1016/j.physrep.2020.02.004.

[67] Sean M. Carroll. The cosmological constant. *Living Reviews in Relativity*, 4(1), Feb 2001. ISSN 1433-8351. doi: 10.12942/lrr-2001-1. URL http://dx.doi.org/10.12942/lrr-2001-1.

[68] Steven Weinberg. The cosmological constant problem. *Rev. Mod. Phys.*, 61:1–23, Jan 1989. doi: 10.1103/RevModPhys.61.1. URL https://link.aps.org/doi/10.1103/RevModPhys.61.1.

[69] Cormac ORaifeartaigh and Simon Mitton. Interrogating the legend of einsteins biggest blunder. *Physics in Perspective*, 20(4):318341, Nov 2018. ISSN 1422-6960. doi: 10.1007/s00016-018-0228-9. URL http://dx.doi.org/10.1007/s00016-018-0228-9.

[70] A. Einstein and W. de Sitter. On the relation between the expansion and the mean density of the universe. *Proceedings of the National Academy of Sciences*, 18(3):213–214, 1932. ISSN 0027-8424. doi: 10.1073/pnas.18.3.213. URL https://www.pnas.org/content/18/3/213.

[71] Ofer Lahav and Andrew R Liddle. The cosmological parameters 2014, 2014. URL https://arxiv.org/abs/1401.1389.

[72] D. J. Fixsen. The temperature of the cosmic microwave background. *The Astrophysical Journal*, 707(2):916920, Nov 2009. ISSN 1538-4357. doi: 10.1088/0004-637x/707/2/916. URL http://dx.doi.org/10.1088/0004-637X/707/2/916.

[73] Ofer Lahav and Andrew R Liddle. The cosmological parameters (2019), 2019. URL https://arxiv.org/abs/1912.03687.

[74] Adam G. Riess, LouisGregory Strolger, John Tonry, Stefano Casertano, Henry C. Ferguson, Bahram Mobasher, Peter Challis, Alexei V. Filippenko, Saurabh Jha, Weidong Li, and et al. Type ia supernova discoveries atz¿ 1 from thehubble space telescope: Evidence for past deceleration and constraints on dark energy evolution. *The Astrophysical Journal*, 607(2):

665687, Jun 2004. ISSN 1538-4357. doi: 10.1086/383612. URL http://dx.doi.org/10.1086/383612.

[75] Adam G. Riess, LouisGregory Strolger, Stefano Casertano, Henry C. Ferguson, Bahram Mobasher, Ben Gold, Peter J. Challis, Alexei V. Filippenko, Saurabh Jha, Weidong Li, and et al. Newhubble space telescopediscoveries of type ia supernovae atz 1: Narrowing constraints on the early behavior of dark energy. *The Astrophysical Journal*, 659(1):98121, Apr 2007. ISSN 1538-4357. doi: 10.1086/510378. URL http://dx.doi.org/10.1086/510378.

[76] Richard L. Burden and J. Douglas Faires. *Numerical Methods, 4th edition*. Brooks/Cole, 2012.

[77] Alan H. Guth. Inflationary universe: A possible solution to the horizon and flatness problems. *Physical review D*, 23(2):347–356, January 1981. doi: 10.1103/PhysRevD.23.347. URL https://journals.aps.org/prd/abstract/10.1103/PhysRevD.23.347.

[78] Alan H. Guth. Eternal inflation and its implications. *Journal of Physics A Mathematical General*, 40(25):6811–6826, June 2007. doi: 10.1088/1751-8113/40/25/S25. URL https://arxiv.org/abs/hep-th/0702178.

[79] Andrei Linde. *Inflationary Cosmology*, volume 738, page 1. 2007. doi: 10.1007/978-3-540-74353-8_1. URL https://arxiv.org/abs/0705.0164.

[80] Andrei Linde. Inflationary Cosmology after Planck 2013. *arXiv e-prints*, art. arXiv:1402.0526, February 2014. URL https://arxiv.org/abs/1402.0526.

[81] G. B. Mainland and Bernard Mulligan. Properties of the quantum vacuum calculated from its structure. *Journal of Physics: Conference Series*, 1956(1):012016, Jul 2021. ISSN 1742-6596. doi: 10.1088/1742-6596/1956/1/012016. URL http://dx.doi.org/10.1088/1742-6596/1956/1/012016.

[82] B Wang, E Abdalla, F Atrio-Barandela, and D Pavn. Dark matter and dark energy interactions: theoretical challenges, cosmological implications and observational signatures. *Reports on Progress in Physics*, 79(9):096901, Aug 2016. ISSN 1361-6633. doi: 10.1088/0034-4885/79/9/096901. URL http://dx.doi.org/10.1088/0034-4885/79/9/096901.

[83] Sergio del Campo, Ramón Herrera, and Diego Pavón. Interacting models may be key to solve the cosmic coincidence problem. *Journal of Cosmology and Astroparticle Physics*, 2009 (01):020020, Jan 2009. ISSN 1475-7516. doi: 10.1088/1475-7516/2009/01/020. URL http://dx.doi.org/10.1088/1475-7516/2009/01/020.

[84] Yuri L. Bolotin, Alexander Kostenko, Oleg A. Lemets, and Danylo A. Yerokhin. Cosmological evolution with interaction between dark energy and dark matter. *International Journal of Modern Physics D*, 24(03):1530007, Feb 2015. ISSN 1793-6594. doi: 10.1142/s0218271815300074. URL http://dx.doi.org/10.1142/S0218271815300074.

[85] Eite Tiesinga, Peter J. Mohr, David B. Newell, and Barry N. Taylor. Codata recommended values of the fundamental physical constants: 2018. *Rev. Mod. Phys.*, 93:025010, Jun 2021. doi: 10.1103/RevModPhys.93.025010. URL https://link.aps.org/doi/10.1103/RevModPhys.93.025010.

[86] Ivaylo Zlatev, Limin Wang, and Paul J. Steinhardt. Quintessence, cosmic coincidence, and the cosmological constant. *Physical Review Letters*, 82(5):896899, Feb 1999. ISSN 1079-7114. doi: 10.1103/physrevlett.82.896. URL http://dx.doi.org/10.1103/PhysRevLett.82.896.

[87] Eleonora Di Valentino, Alessandro Melchiorri, Olga Mena, and Sunny Vagnozzi. Interacting dark energy in the early 2020s: A promising solution to the h0 and cosmic shear tensions. *Physics of the Dark Universe*, 30:100666, Dec 2020. ISSN 2212-6864. doi: 10.1016/j.dark.2020.100666. URL http://dx.doi.org/10.1016/j.dark.2020.100666.

[88] Eleonora Di Valentino, Olga Mena, Supriya Pan, Luca Visinelli, Weiqiang Yang, Alessandro Melchiorri, David F Mota, Adam G Riess, and Joseph Silk. In the realm of the hubble tensiona review of solutions *. *Classical and Quantum Gravity*, 38(15):153001, Jul 2021. ISSN 1361-6382. doi: 10.1088/1361-6382/ac086d. URL http://dx.doi.org/10.1088/1361-6382/ac086d.

[89] Francis-Yan Cyr-Racine. Cosmic expansion: A mini review of the hubble-lemaitre tension, 2021. URL https://arxiv.org/abs/2105.09409.

[90] Adam G. Riess, Stefano Casertano, Wenlong Yuan, Lucas M. Macri, and Dan Scolnic. Large magellanic cloud cepheid standards provide a 1the determination of the hubble constant and stronger evidence for physics beyond cdm. *The Astrophysical Journal*, 876(1):85, May 2019. ISSN 1538-4357. doi: 10.3847/1538-4357/ab1422. URL http://dx.doi.org/10.3847/1538-4357/ab1422.

[91] Adam G. Riess, Stefano Casertano, Wenlong Yuan, J. Bradley Bowers, Lucas Macri, Joel C. Zinn, and Dan Scolnic. Cosmic distances calibrated to 1and hubble space telescope photometry of 75 milky way cepheids confirm tension with cdm. *The Astrophysical Journal*, 908(1):L6, Feb 2021. ISSN 2041-8213. doi: 10.3847/2041-8213/abdbaf. URL http://dx.doi.org/10.3847/2041-8213/abdbaf.

[92] Sean M. Carroll. Quintessence and the rest of the world: Suppressing long-range interactions. *Physical Review Letters*, 81(15):30673070, Oct 1998. ISSN 1079-7114. doi: 10.1103/physrevlett.81.3067. URL http://dx.doi.org/10.1103/PhysRevLett.81.3067.

[93] Shinji Tsujikawa. Quintessence: a review. *Classical and Quantum Gravity*, 30(21):214003, Oct 2013. ISSN 1361-6382. doi: 10.1088/0264-9381/30/21/214003. URL http://dx.doi.org/10.1088/0264-9381/30/21/214003.

[94] R.R Caldwell. A phantom menace? cosmological consequences of a dark energy component with super-negative equation of state. *Physics Letters B*, 545(1-2):2329, Oct 2002. ISSN 0370-2693. doi: 10.1016/s0370-2693(02)02589-3. URL http://dx.doi.org/10.1016/S0370-2693(02)02589-3.

[95] Robert R. Caldwell, Marc Kamionkowski, and Nevin N. Weinberg. Phantom energy and cosmic doomsday. *Physical Review Letters*, 91(7), Aug 2003. ISSN 1079-7114. doi: 10.1103/physrevlett.91.071301. URL http://dx.doi.org/10.1103/PhysRevLett.91.071301.

[96] Kevin J. Ludwick. The viability of phantom dark energy: A review. *Modern Physics Letters A*, 32(28):1730025, Sep 2017. ISSN 1793-6632. doi: 10.1142/s0217732317300257. URL http://dx.doi.org/10.1142/S0217732317300257.

[97] Yu-Ping Teng, Wolung Lee, and Kin-Wang Ng. Constraining the dark-energy equation of state with cosmological data. *Physical Review D*, 104(8), Oct 2021. ISSN 2470-0029. doi: 10.1103/physrevd.104.083519. URL http://dx.doi.org/10.1103/PhysRevD.104.083519.

[98] Marek Demianski, Elisabeta Lusso, Maurizio Paolillo, Ester Piedipalumbo, and Guido Risaliti. Investigating dark energy equation of state with high redshift hubble diagram. *Frontiers in Astronomy and Space Sciences*, 7, Oct 2020. ISSN 2296-987X. doi: 10.3389/fspas.2020.521056. URL http://dx.doi.org/10.3389/fspas.2020.521056.

[99] Sean M. Carroll. The quantum field theory on which the everyday world supervenes, 2021. URL https://arxiv.org/abs/2101.07884.

[100] Rong-Gen Cai and Anzhong Wang. Cosmology with interaction between phantom dark energy and dark matter and the coincidence problem. *Journal of Cosmology and Astroparticle Physics*, 2005(03):002002, Mar 2005. ISSN 1475-7516. doi: 10.1088/1475-7516/2005/03/002. URL http://dx.doi.org/10.1088/1475-7516/2005/03/002.

[101] Jussi Vliviita, Elisabetta Majerotto, and Roy Maartens. Large-scale instability in interacting dark energy and dark matter fluids. *Journal of Cosmology and Astroparticle Physics*, 2008 (07):020, Jul 2008. ISSN 1475-7516. doi: 10.1088/1475-7516/2008/07/020. URL http://dx.doi.org/10.1088/1475-7516/2008/07/020.

[102] Christian G. Bhmer, Gabriela Caldera-Cabral, Ruth Lazkoz, and Roy Maartens. Dynamics of dark energy with a coupling to dark matter. *Physical Review D*, 78(2), Jul 2008. ISSN 1550-2368. doi: 10.1103/physrevd.78.023505. URL http://dx.doi.org/10.1103/PhysRevD.78.023505.

[103] M.B. Gavela, D. Hernandez, L. Lopez Honorez, O. Mena, and S. Rigolin. Dark coupling. page 029, Jan 2009. doi: 10.1088/1475-7516/2009/07/03410.1088/1475-7516/2010/05/E01. URL https://arxiv.org/abs/0901.1611v1.

[104] M.B Gavela, L. Lopez Honorez, O Mena, and S Rigolin. Dark coupling and gauge invariance. *Journal of Cosmology and Astroparticle Physics*, 2010(11):044044, Nov 2010. ISSN 1475-7516. doi: 10.1088/1475-7516/2010/11/044. URL http://dx.doi.org/10.1088/1475-7516/2010/11/044.

[105] Eleonora Di Valentino, Alessandro Melchiorri, Olga Mena, Supriya Pan, and Weiqiang Yang. Interacting dark energy in a closed universe. *Monthly Notices of the Royal Astronomical Society: Letters*, 502(1):L23L28, Jan 2021. ISSN 1745-3933. doi: 10.1093/mnrasl/slaa207. URL http://dx.doi.org/10.1093/mnrasl/slaa207.

[106] Eleonora Di Valentino, Alessandro Melchiorri, Olga Mena, and Sunny Vagnozzi. Nonminimal dark sector physics and cosmological tensions. *Physical Review D*, 101(6), Mar 2020. ISSN 2470-0029. doi: 10.1103/physrevd.101.063502. URL http://dx.doi.org/10.1103/PhysRevD.101.063502.

[107] Supriya Pan, Jaume de Haro, Weiqiang Yang, and Jaume Amors. Understanding the phenomenology of interacting dark energy scenarios and their theoretical bounds. *Physical Review D*, 101(12), Jun 2020. ISSN 2470-0029. doi: 10.1103/physrevd.101.123506. URL http://dx.doi.org/10.1103/PhysRevD.101.123506.

[108] Matteo Lucca and Deanna C. Hooper. Shedding light on dark matter-dark energy interactions. *Physical Review D*, 102(12), Dec 2020. ISSN 2470-0029. doi: 10.1103/physrevd.102.123502. URL https://arxiv.org/abs/2002.06127.

[109] Matteo Lucca. Dark energy-dark matter interactions as a solution to the s_8 tension, 2021. URL https://arxiv.org/abs/2105.09249.

[110] Supriya Pan, German S. Sharov, and Weiqiang Yang. Field theoretic interpretations of interacting dark energy scenarios and recent observations. *Physical Review D*, 101(10), May 2020. ISSN 2470-0029. doi: 10.1103/physrevd.101.103533. URL http://dx.doi.org/10.1103/PhysRevD.101.103533.

[111] Shadab Alam, Metin Ata, Stephen Bailey, Florian Beutler, Dmitry Bizyaev, Jonathan A. Blazek, Adam S. Bolton, Joel R. Brownstein, Angela Burden, Chia-Hsun Chuang, and et al. The clustering of galaxies in the completed sdss-iii baryon oscillation spectroscopic survey: cosmological analysis of the dr12 galaxy sample. *Monthly Notices of the Royal Astronomical Society*, 470(3):26172652, Mar 2017. ISSN 1365-2966. doi: 10.1093/mnras/stx721. URL http://dx.doi.org/10.1093/mnras/stx721.

[112] Ashley J. Ross, Lado Samushia, Cullan Howlett, Will J. Percival, Angela Burden, and Marc Manera. The clustering of the sdss dr7 main galaxy sample i. a 4per cent distance measure at z=0.15. *Monthly Notices of the Royal Astronomical Society*, 449(1):835847, Mar 2015. ISSN 0035-8711. doi: 10.1093/mnras/stv154. URL http://dx.doi.org/10.1093/mnras/stv154.

[113] Florian Beutler, Chris Blake, Matthew Colless, D. Heath Jones, Lister Staveley-Smith, Lachlan Campbell, Quentin Parker, Will Saunders, and Fred Watson. The 6df galaxy survey: baryon acoustic oscillations and the local hubble constant. *Monthly Notices of the Royal Astronomical Society*, 416(4):30173032, Jul 2011. ISSN 0035-8711. doi: 10.1111/j.1365-2966.2011.19250.x. URL http://dx.doi.org/10.1111/j.1365-2966.2011.19250.x.

[114] Renier Hough. Constraining modified gravity models with cosmological data, 2019. URL http://hdl.handle.net/10394/34763.

[115] R. T. Hough, A. Abebe, and S. E. S. Ferreira. Viability tests of f(R)-gravity models with Supernovae Type 1A data, August 2020. URL https://arxiv.org/abs/1911.05983.

[116] Anna mia Swart, RT Hough, Shambel Sahlu, Heba Sami, Thato Tsabone, Rubby Aworka, Maye Elmardi, and Amare Abebe. Unifying dark matter and dark energy in chaplygin gas cosmology, 2019. URL https://events.saip.org.za/event/144/papers/1359/files/776-CG_proceedings2019v3.pdf.

[117] S. Chandrasekhar. The Maximum Mass of Ideal White Dwarfs. *apj*, 74:81, July 1931. doi: 10.1086/143324. URL https://articles.adsabs.harvard.edu/pdf/1931ApJ....74...81C.

[118] Jorge Pinochet and Michael Van Sint Jan. Chandrasekhar limit: an elementary approach based on classical physics and quantum theory. *Physics Education*, 51(3):035007, apr 2016. doi: 10.1088/0031-9120/51/3/035007. URL https://doi.org/10.1088/0031-9120/51/3/035007.

[119] Wolfgang Hillebrandt and Jens C. Niemeyer. Type ia supernova explosion models. *Annual Review of Astronomy and Astrophysics*, 38(1):191230, Sep 2000. ISSN 1545-4282. doi: 10.1146/annurev.astro.38.1.191. URL http://dx.doi.org/10.1146/annurev.astro.38.1.191.

[120] D. Andrew Howell. Type ia supernovae as stellar endpoints and cosmological tools. *Nature Communications*, 2(1), Jun 2011. ISSN 2041-1723. doi: 10.1038/ncomms1344. URL http://dx.doi.org/10.1038/ncomms1344.

[121] A. Conley, J. Guy, M. Sullivan, et al. Supernova constraints and systematic uncertainties from the first three years of the Supernova Legacy Survey. *The Astrophysical Journal, Supplement series*, 192(1):1, 2010. URL https://doi.org/10.1088/0067-0049/192/1/1.

[122] J. D Neill, M. Sullivan, D. A. Howell, et al. The local hosts of Type Ia Supernovae. *The Astrophysical Journal*, 707(2):1449–1465, 2009. doi: 10.1088/0004-637X/707/2/1449. URL https://ui.adsabs.harvard.edu/abs/2009ApJ...707.1449N/abstract.

[123] CfA3: 185 Type Ia Supernova light curves from the CfA. *The Astrophysical Journal*, 700:331–357, 2009. URL https://doi.org/10.1088/0004-637X/700/1/331.

[124] Eleonora Di Valentino and Olga Mena. A fake interacting dark energy detection? *Monthly Notices of the Royal Astronomical Society: Letters*, 500(1):L22L26, Jan 2020. ISSN 1745-3933. doi: 10.1093/mnrasl/slaa175. URL http://dx.doi.org/10.1093/mnrasl/slaa175.

[125] S. Nesseris and J. García-Bellido. Is the Jeffreys' scale a reliable tool for Bayesian model comparison in cosmology? *Journal of Cosmology and Astroparticle Physics*, 2013(8):036, 2013. URL https://doi.org/10.1088/1475-7516/2013/08/036.

[126] James Stewart. *Calculus*. Brooks/Cole, 2012.